

BIBLIOGRAPHIC INFORMATION

PB95-183984

Report Nos:

Title: U.S./P.R.C. Workshop on Experimental Methods in Earthquake Engineering. Proceedings of a Workshop. Held in Shanghai, P.R.C. on November 10-12, 1992.

Date: Jul 93

Authors: H. Krawinkler and B. Zhu.

Performing Organization: Stanford Univ., CA. John A. Blume Earthquake Engineering Center.

Sponsoring Organization: *National Science Foundation, Arlington, VA.*Tongji Univ., Shanghai (China).

Contract Nos: NSF-BCS-9210034

Supplemental Notes: Also pub. as Stanford Univ., CA. John A. Blume Earthquake Engineering Center rept. no. REPT-106.

NTIS Field/Group Codes: 89D (Structural Analyses)

Price: PC A11/MF A03

Availability: Available from the National Technical Information Service, Springfield, VA. 22161

Number of Pages: 249p

Keywords: *Meetings. *Earthquake engineering. *International cooperation. *Structural analysis. Earthquake resistant structures. Deformation. Reinforced concrete. Cyclic loads. Dynamic models. Pile structures. Model tests. Displacement. Structural vibration. Dynamic response. Test facilities. Construction materials. China. United States.

Abstract: Partial Contents: Large Triaxial Shaking Table and Experimentation on Critical Structures and Equipments; Signal Reproduction Fidelity of Servohydraulic Testing Equipment; Cyclic Loading Histories for Seismic Experimentation on Components of Structures; Aseismic Test of Building Structure; The Experimental Method of Reinforced Concrete Silos; Effects of Scale and Loading Rate with Tests of Concrete and Masonry Building Structures; Study on Similitude Relationships of Reinforced Concrete Columns Based on Shaking Table Tests; Preliminary Study on Distortion and Modification Method for Model Testing of Dynamic Ultimate Strength; Dynamic Model Test Studies of Pile Supported Piers Including Effects of Bank Deformation; Research of Vibrating Period Characteristics of R/C Structure; Advances in Sensor and Data Acquisition Technology; The Parameter Identification of Seven Story Building Model made of CSGCB.



PB95-183984

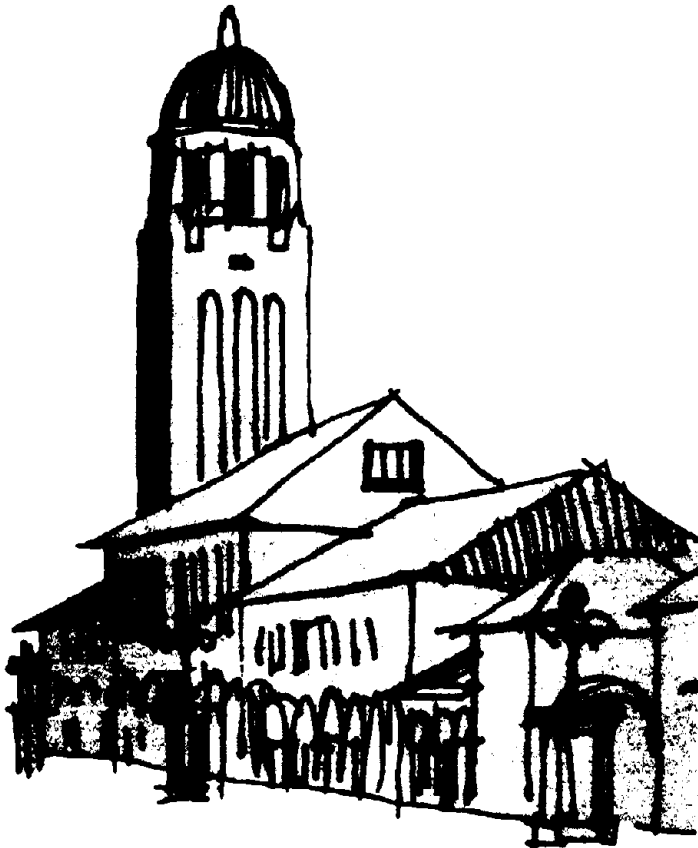
The John A. Blume Earthquake Engineering Center

Department of Civil Engineering
Stanford University

U.S./P.R.C. WORKSHOP ON EXPERIMENTAL METHODS IN EARTHQUAKE ENGINEERING

Proceedings of a
Workshop Held in
Shanghai, P.R.C.
November 10-12, 1992

Edited by
Helmut Krawinkler
and
Bolong Zhu



A report on a workshop
sponsored by the
U.S. National Science Foundation
Grant BCS-9210034
and by the
China Academy of Building Sciences
and Tongji University

Report No. 106

July 1993



PB95-183984

The John A. Blume Earthquake Engineering Center
Department of Civil Engineering, Stanford University

The State Laboratory for Disaster Reduction in Civil Engineering
Department of Civil Engineering, Tongji University

U.S./P.R.C. WORKSHOP ON EXPERIMENTAL METHODS IN EARTHQUAKE ENGINEERING

**Proceedings of a Workshop Held in Shanghai, P.R.C
November 10-12, 1992**

Edited by

Helmut KRAWINKLER and Bolong ZHU

A report on a workshop sponsored by the U.S. National Science Foundation,
Grant BCS-9210034, and by the
China Academy of Building Sciences and Tongji University

Report No. 106

July 1993

PREFACE



PE95-183984

Experimentation, which may be defined as the process of acquiring knowledge through physical observations and measurements, has been and will remain to be an essential aspect of earthquake engineering research. We resort to experiments whenever we need answers that cannot be obtained with sufficient confidence through analytical predictions. Conventionally, experiments have been utilized to study fundamental phenomena that either have escaped our attention or have been inadequately understood, or to develop or verify analytical models, or to derive empirical detailing requirements for behavior modes too difficult to model analytically.

Future issues and trends in experimental research must be driven by the demand of the public for adequate damage control and seismic safety of new and existing structures. Experimentation should support analytical modeling, seismic code developments, and the assessment of seismic performance of existing structures. In this context the need exists to take stock of (a) what information has been provided by experimental research in the past, (b) what aspects of experimental research should become the focus of future activities, and (c) what improvements are needed in testing methodologies.

As part of the U.S.-P.R.C. Protocol for Cooperative Earthquake Studies a workshop was organized to address these issues, particularly the third one. The goal was to bring together leading experts in experimental research from the U.S. and the P.R.C. to give presentations and participate in working group discussions on issues related to improvements in methods of experimental research in earthquake engineering. Topics for discussion included advances in laboratory and field testing technologies, experimental procedures and protocols, innovative testing methods, sensor and data acquisition technology, and experimental methods for specific applications. The specific objectives of the workshop were as follows:

- Assess the state-of-the-knowledge in experimental methods.
- Discuss methodologies that will improve the realism, reliability, and usefulness of experimental research on structures.
- Identify future developments needed to improve experimental methods.

The workshop was held in Shanghai, P.R.C., from November 10 to November 12, 1992. The workshop consisted of plenary presentation sessions and discussion sessions. In the plenary sessions the participants gave presentations on the state-of-the-knowledge or on new developments in experimental methods. In the working group sessions the participants focused on an assessment of the state-of-the-knowledge and future development needs in specific sub-areas of experimental methods. The conclusions of the working group sessions were discussed in a plenary session and summarized in the workshop resolutions.

These workshop proceedings document the workshop resolutions as well as the written contributions prepared for the workshop. The organizers are deeply indebted to the authors who have prepared original and thoughtful contributions for this publication. Much appreciation is expressed also to the local organizing committee of Tongji University, whose tireless efforts have contributed much to the success of this workshop.

Sponsorship for the workshop was provided by the Earthquake Hazard Mitigation Program of the U.S. National Science Foundation (Grant BCS-9210034), the China Academy of Building Sciences, and Tongji University. This support is gratefully acknowledged. The

opinions expressed in the papers and the resolutions presented herein are, however, those of the authors and participants and do not represent the official positions of the sponsoring agencies.

Co-Chairmen, P.R.C. Delegation:

Professor Bolong ZHU
Professor Lian WEI

Co-Chairmen, U.S. Delegation:

Professor Helmut KRAWINKLER
Professor Stephen A. MAHIN

Members of the Local Organizing Committee:

Weiming ZHOU, Zuhua LIU, Zhong FANG,
Shu JIA, Xiaocheng SHI, and Zhengang YAO



Participants of U.S./P.R.C. Workshop on Experimental Methods in Earthquake Engineering



TABLE OF CONTENTS

Preface	i
Photograph of Participants	iii
List of Participants	1
Technical Program	5
Workshop Resolutions	6
Papers	
Large Triaxial Shaking Table and Experimentation on Critical Structures and Equipments	9
<i>Chen Houqun and Jiang Zhichao</i>	
Development of a Three-Dimensional Earthquake Simulator at USACERL	18
<i>John R. Hayes, Jr.</i>	
Signal Reproduction Fidelity of Servohydraulic Testing Equipment	29
<i>D.A. Kusner, J.D. Rood, and G.W. Burton</i>	
Special Loading Systems for Experimental Research	40
<i>Stephen A. Mahin</i>	
An Equivalent SDOF Method of Interface Moment Simulation in Substructure PSD Test	50
<i>Guo Mingchao, Tang Daixin, and Wu Zhensheng</i>	
Cyclic Loading Histories for Seismic Experimentation on Components of Structures	59
<i>Helmuth Krawinkler</i>	
Aseismic Test of Building Structure	70
<i>Zhu Bolong</i>	
The Experimental Method of Reinforced Concrete Silos	78
<i>Zhu Bolong and Shi Weixing</i>	
Effects of Scale and Loading Rate with Tests of Concrete and Masonry Building Structures	83
<i>Daniel P. Abrams</i>	
Study on Similitude Relationships of Reinforced Concrete Columns Based on Shaking Table Tests	94
<i>Lu Xilin and Liao Guangming</i>	
Preliminary Study on Distortion and Modification Method for Model Testing of Dynamic Ultimate Strength	106
<i>Zheng Wei</i>	
Dynamic Model Test Studies of Pile Supported Piers Including Effects of Bank Deformation	114
<i>Wu Zaiguang, Han Guocheng, and Zhang Dongfeng</i>	
Simulated Rolling Loads Under Laboratory Conditions	123
<i>Frieder Seible</i>	

Generated Sequential Displacement Procedure for Seismic Testing of Stiff MDOF Systems	133
<i>Frieder Seible</i>	
Assessment and Experimental Research of Existing Walls Intensity	145
<i>Lou Yong Lin</i>	
Research of Vibrating Period Characteristics of R/C Structure	152
<i>Wu Shiyang and Liu Zhenchang</i>	
Experimental Verification of Active/Passive Control Systems	165
<i>Robert D. Hanson</i>	
Advances in Sensor and Data Acquisition Technology	172
<i>Kim D. Bennett, Le-Wu Lu, and Weiping Li</i>	
New Developments in Strong Motion Accelerographs	189
<i>John G. Diehl</i>	
Shaking Table Waveform Correction Based on Least Square System Identification	201
<i>Yin Jianhui and Bao Zhiwen</i>	
The Parameter Identification of Seven Story Building Model made of CSGCB	215
<i>Zhao Wei</i>	
Application of Curve Fitting Methods in Constructional Engineering Dynamic Parameter Identification	231
<i>Liu Lihua</i>	

LIST OF PARTICIPANTS

Participants from the P.R.C.:

Honqun CHEN
Professor
China Academy of Water Management Science
Beijing 100835

Shaoxiang DING
Vice Director
Division of Seismic Resistance
Ministry of Construction
Beijing 100835

Shu JIA
Engineer
Division of Seismic Resistance
Ministry of Construction
Beijing 100835

Zhichao JIANG
Senior Engineer
Division of Seismic Resistance
China Academy of Water Management Science
Beijing 100835

Mingsun LI
Senior Engineer
China Academy of Building Sciences
Beijing 100013

Yonglin LOU
Senior Engineer, Director
Liaoning Institute of Building Science
Shengyang 110005

Zhuqing LU
Professor and Head
Department of Structural Engineering
Shanghai College of Urban Construction
Shanghai 200092

Xiangqian NA
Professor, Programme Director
Department of Material and Engineering Sciences
National Natural Science Foundation
Beijing 100085

Mingsuen WU
Professor and President
Shanghai College of Building Materials
Shanghai 200434

Quan QIN
Professor
Department of Civil Engineering
Tsinghua University
Beijing 100084

Lin REN
Engineer
Department of Science and Technology
China Planning Committee
Beijing 100824

Jianan WANG
Associate Professor and Head
Department of Civil Engineering
Hainan University
Hainan 570028

Weiyue ZHANG
Professor and President
China Academy of Building Sciences
Beijing 100013

Wei ZHENG
Engineer
Research Division
Beijing Architectural Design Institute
Beijing 100045

Mingchao GUO
Associate Professor
Department of Civil Engineering
Harbin Institute of Architecture and Civil Engineering
Harbin 150001

Lian WEI
Director, Institute of Earthquake Engineering
ShenZhen Institute
China Academy of Building Research
ShenZhen 518028

Bolong ZHU
Professor, Vice Director
State Laboratory for Disaster Reduction in Civil Engineering
Tongji University
Shanghai 200092

Deheng YAN
Professor and Head
Department of Structural Engineering
Tongji University
Shanghai 200092

Yu ZHANG
Professor
Department of Structural Engineering
Tongji University
Shanghai 200092

Zhixin XU
Professor
Institute of Structural Theory
Vice Director
State Laboratory for Disaster Reduction in Civil Engineering
Tongji University
Shanghai 200092

Zaiyong ZHANG
Professor
Institute of Structural Theory
Tongji University
Shanghai 200092

Zhenxiang DONG
Professor
Institute of Engineering Structures
Tongji University
Shanghai 200092

Chengsong TU
Professor
Department of Structural Engineering
Tongji University
Shanghai 200092

Hunan WU
Associate Professor
Institute of Engineering Structures
Tongji University
Shanghai 200092

Kunlian ZHANG
Associate Professor
Institute of Engineering Structures
Shanghai 200092

Xiaocheng SHI
Senior Engineer
Shaking Table Division
State Laboratory for Disaster Reduction in Civil Engineering
Tongji University
Shanghai 200092

Zuhua LIU
Associate Professor
Institute of Engineering Structures
Tongji University
Shanghai 200092

Weixing SI
Lecturer
Shaking Table Division
State Laboratory for Disaster Reduction in Civil Engineering
Tongji University
Shanghai 200092

Participants from the U.S.:

Daniel P. ABRAMS
Professor of Civil Engineering
University of Illinois at Urbana-Champaign
Urbana, IL 61801-2397

Kim D. BENNETT
Assistant Professor of Electrical Engineering
Lafayette College
Easton, PA 18042-1775

John G. DIEHL
Vice President
Kinematics, Inc.
Pasadena, CA 91107

Robert D. HANSON
Professor of Civil Engineering
University of Michigan
Ann Arbor, MI 48109-2125

John R. HAYES
Supervisory Structural Engineer
U.S. Army Construction Engineering Research Laboratory
Champaign, IL 61826-9005

Helmut KRAWINKLER
Professor of Civil Engineering
Stanford University
Stanford, CA 94305-4020

Le-Wu LU
Professor of Civil Engineering
Lehigh University
Bethlehem, PA 18015-3191

Stephen A. MAHIN
Professor of Civil Engineering
University of California at Berkeley
Berkeley, CA 94720

Joel D. ROOD
Senior Application Engineer
M T S systems Corporation
Eden Prairie, MN 55344-2290

TECHNICAL PROGRAM

November 10, 1992:

9:00 - 10:00 am	Opening Session
10:00 - 10:15 am	Coffee Break
10:15 - 11:45 am	Session #1 (Presentations)
11:45 - 14:00 pm	Lunch
14:00 - 15:00 pm	Session #2 (Presentations)
15:00 - 15:15 pm	Coffee Break
15:15 - 16:45 pm	Session #2 (Presentations)
17:00 pm	Dinner

November 11, 1992

8:15 - 11:45 am	Technical Visit to Nanpu Bridge
11:45 - 14:00 pm	Lunch
14:00 - 15:00 pm	Session #3 (Discussion)
15:00 - 15:15 pm	Coffee Break
15:15 - 16:45 pm	Session #3 (Presentations)
17:00 pm	Dinner

November 12, 1992

8:30 - 10:00 am	Session #4 (Presentations)
10:00 - 10:15 am	Coffee Break
10:15 - 11:45 am	Session #4 (Discussion)
11:45 - 14:00 pm	Lunch
14:00 - 15:00 pm	Session #5 (Discussion)
15:00 - 15:15 pm	Coffee Break
15:15 - 16:45 pm	Closing Session (Summary and Conclusions)
17:00 pm	Banquet

Topics for Discussion:

1. Advances and Needs in Laboratory Testing Technology
2. Experimental Procedures and Protocol
3. Advances and Needs in Sensor and Data Acquisition Technology
4. Test Control and Loading Procedures
5. Use of System Identification Techniques
6. New and Special Purpose Facilities
7. Selection of Site for the Test Field of
Wind and Earthquake Engineering in Asian-Pacific Area
8. Workshop Summary and Conclusions

WORKSHOP RESOLUTIONS

The U.S.-P.R.C Workshop on Experimental Methods in Earthquake Engineering was implemented as part of the U.S.-P.R.C. Protocol in Cooperative Earthquake Studies, Annex 3. The participants appreciate the efforts of the organizers of the Workshop and extend their sincere appreciation for these arrangements. It was agreed that the Workshop was held with mutual respect and friendship among all participants. In the group discussions the following resolutions were concluded:

1. Advancements and refinements in experimental methods are needed in order to provide the fundamental global and detailed knowledge required to mitigate the adverse effects of earthquakes on structures. These needs exist particularly in the evaluation of existing structures, in the development and verification of innovative design concepts and structural systems, and in the study of important problems in which presently available experimental methods are found to be inadequate, such as soil-structure interaction problems.
2. In order to maximize the benefit of experimental research it is important to take full advantage of the intellectual capabilities and experimental facilities existing worldwide and to promote collaboration between countries and institutions that have complementary facilities and problems of common interest. To this end, the following actions are recommended:
 - Identify available facilities.
 - Identify important problems for which solutions are equally applicable in participating countries.
 - Identify vehicles for exchange of personnel and information.
3. The workshop participants from the P.R.C. and the U.S.A. recognize that common interests exist among researchers and practitioners of the two countries, that the workshop dialogue should be continued, and that cooperative experimental research on issues of interest to both countries should be encouraged.
4. Improvements in experimental methods, testing facilities, and instrumentation are needed particularly in the following areas:
 - Experimentation on complete structural systems.
 - Response under two- or three-directional excitation or loading.

- Experimentation on innovative structural systems and active and passive control devices and mechanisms.
 - Experimentation for damage modeling and earthquake damage assessment.
 - Experimentation for evaluation and upgrading of existing structures.
 - Real earthquake experimentation on carefully selected existing structures (instrumentation of soil [down-hole] - foundation - structure systems for the evaluation of seismic demands and capacities).
 - Structure diagnostics for detection of damage that may affect the response of structures to earthquakes.
 - Development of guidelines and criteria that assist in the selection of appropriate experimental methods, test procedures, and loading histories.
 - Improvement of existing methods and development of new methods for exciting structures in the field or laboratory.
5. Research is needed on the development of instrumentation plans, sensors, and signal processors that permit reliable measurement of all important demand (*e.g.*, ground motion) and capacity (*e.g.*, interstory drift) parameters. Full advantage should be taken of recent developments made in instrumentation technology in other fields.
6. Field experimentation needs to play a more important role in experimental research in earthquake engineering. Emphasis should be placed on instrumentation of structures in areas where severe earthquakes might occur soon, so that structural response can be recorded and evaluated in the inelastic (damage) stages. Consideration should be given to the construction and instrumentation of intentionally weak structures in a test field at a suitable location of high seismicity in order to obtain comprehensive information on the inelastic (damage) behavior of complete soil-structure systems in a realistic seismic environment. Opportunities should be sought for tests to destruction of structures scheduled for demolition.
7. A wide array of experimental methods has been developed and rapidly occurring advances in technology have provided realistic methods for simulating and recording earthquake effects. Research is needed to advance and verify these methods and to characterize the advantages and limitations of various methods. In particular, research is needed to characterize effects of
- Strain rates
 - Loading histories
 - Small, intermediate, and full scale specimens (size effects)

- **Laboratory versus field experiments**
- **Experiments on components versus complete systems.**

In addition, research is needed to improve the reliability, accuracy, control, and realism of

- **Shaking table experimentation**
- **Pseudo-dynamic experimentation**
- **Quasi-static experimentation**
- **Field experimentation.**

8. Funding is needed to improve the effectiveness and capabilities of facilities needed to perform experimental research. To this end, it is recommended that efforts be made to:

- **Upgrade the loading, instrumentation and data acquisition systems at existing laboratories**
- **Identify needed specialized test facilities (large shaking tables, reaction walls, field test sites, etc.) and carry out feasibility studies for their implementation.**

9. To enhance the utilization of experimental data in research and its application to the development of improved design and analysis methods, efforts are needed to establish minimum standards for:

- **Documentation of experiments (description of specimens, instrumentation, loading apparatus, etc.) and result (observed data, recorded data, etc.)**
- **Archiving of test information**
- **Dissemination of test information.**

Researchers and users of experimental research should convene to discuss and establish these protocols and identify technological issues to be resolved to implement these protocols.

Large Triaxial Shaking Table and Experimentation on Critical Structures and Equipments

CHEN Houqun¹ JIANG Zhichao²

(Institute of Water Conservancy and hydroelectric Power Research)

ABSTRACT



PP95-183984

State-of-the-art in major large triaxial shaking table testing facilities around the world is briefly reported. The main features of the large triaxial shaking table with six degrees of freedom installed in the Institute of Water Conservancy and Hydroelectric Power Research (IWHR) in China are presented in details.

Experimentation on critical structures and equipments both in laboratory and in field, including large arch dam, control rod system of nuclear power plant, and facilities of petrochemical industry, is described in this paper.

INTRODUCTION

Recently the progress in aseismic designing by means of advanced computer is very remarkable. Particularly, design of some critical structures and facilities, such as large dams and nuclear power plants, has incorporated progressively more sophisticated seismic analysis. Since analysis involves idealization and assumption, it is, therefore, necessary to supplement and relate analytical work to experimental results both in laboratory and in field in order to improve the mathematic model and creat greater confidence in design. Unfortunately, experimental support and confirmation has not, in general, kept pace with the rapid development of computerized analytical seismic design methods. Moreover, there are still some actual constructions that are difficult to be mathematically simulated. Obviously, improvement in design by rational experimental programs will minimize waste by

1 Professor, 2 Senior Engineer, Institute of Water Conservancy and hydroelectric Power Research, Beijing, P.R.C.

making such structures and facilities safer and more economical. This situation is particularly important for China as a developing country with high seismic activity and the settlement of large populations in those areas.

Today, special emphasis in dynamic experiments is given not only to checking and improving mathematic models and to determining the dynamic characteristics, but mainly to collapse mechanisms, optimum redundancy for stability and energy dissipation, functional failure, large deflection failure, structural repair, etc. In order to solve all those problems, a large earthquake simulator with accurately programmed acceleration inputs are increasingly desired. However, for some problems such as the dynamic interaction of dam–foundation–reservoir system with the consideration of water compressibility effects, that are sensitive to canyon and reservoir geometry as well as the reservoir bottom reflection coefficient, model test on shaking table appears inadequate and field measurements are necessary.

In this paper state-of-the-art in large earthquake simulation triaxial shaking tables is briefly introduced and experimentation on critical structures and equipments both in laboratory and in field are described.

LARGE TRIAXIAL EARTHQUAKE SIMULATION SHAKING TABLE

The present state-of-the-art in earthquake simulation testing is well defined by the ability to accurately reproduce previously recorded earthquake motions in all three directions on a large-scale table. For many critical structures, such as large dams and high-rise buildings, scaled models have to be adopted. In order to satisfy the similarity relationship a broad frequency range is required for those scaled model tests. However, because of the magnitude of capital investment and the degree of technical complexity, there are only a few large triaxial earthquake simulation tables actually in operation around the world up to now as shown in Table 1 in which their main specifications are summarized. In 1986 a large triaxial earthquake simulation shaking table was installed in Institute of Water Conservancy and hydroelectric Power Research (IWHR).

For carrying out aseismic experiments and researches on various engineering structures and equipments, in particular, on large dams including interaction of reservoir and foundation as well as on nuclear power plants. Its

Table 1 Main Specifications of Large Triaxial Shaking Table

Specification	IWHR (PRC)	TU (PRC)	ISMES (Italy)	SERC (UK)	AEDI (Russia)
Size of table(M)	5 × 5	4 × 4	4 × 4	3 × 3	6 × 6
Max. load weight(T)	20	15	30	5	50
Frequency range(Hz)	0.1–120	0.1–50	0.1–120	0.1–100	3–80
Max. acceleration(g)					
Horizontal	1.0	0.8–1.2	3.0	1.0	1.2
Vertical	0.7	0.7	2.0	1.0	1.0

main features are briefly described below.

- * In order to keep any vibration of the foundation below a level at which it might become annoying to surrounding laboratories and people, a heavy foundation with two parts was adopted. Some springs can be inserted between two parts while necessary.

- * The steel table body consists of a top plate with variable thickness, connected by vertical webs to form a square cellular system. Its fundamental frequency is 148 Hz and the weight is 23.5 T.

- * Seven actuators are used, 4 vertical for Z direction combined a preload chamber in their lower part, and 3 horizontal, among which 2 for X direction and 1 for Y direction. The hydrostatic piston rod bearings are used. Both bearing and piston are coated with special plastics, giving good sliding properties under high side loadings. The actuators are protected against overload by special plastic springs and a special hydraulic cushion on the top of upper chamber.

- * The adjustable, free of backlash universal joints coated with special plastics are used.

- * An analog control system with a broad bandwidth closed multiloop with three parameter's input and feedback together with a digital control system of ITFC software (Iterative Transfer Function Compensation) are used. The digital control system is supported by an array processor to make the performance of computations much faster than that in standard configuration.

A special designed programmable supervisory controller is used to maximum simplify the operation of the system and to protect it from various kinds of failure and breakdown cases.

A programmable PCM data acquisition system up to 100 channels and a specially developed data processing software DSP based on PC/XT, PC/AT, 286, 386, 486 computer are provided.

The shaking table has been in operating with success for more than 6 years and contributes well to aseismic designing and safety confirmation of various kinds of structures and equipments.

EXPERIMENTATION ON CRITICAL STRUCTURES AND EQUIPMENTS

China is a country of high seismicity. The regions where earthquake had occurred almost cover the whole territory. So the critical structures and equipments have more probability to experience strong earthquakes. As the accident caused by damages of critical structures and equipments can inflict grave catastrophe upon surrounding communities, great efforts have been devoted to confirming the safety and reliability of critical structures and equipments in order to minimize risks of catastrophe. It is unanimously agreed among professionals in earthquake engineering that the most important factor in aseismic designing of important objects is its successful precedent, evaluated and projected through scientific discipline with the help from experimental tests whenever necessary.

As the shaking table in IWHR is the largest and most advanced one in China, various kinds of critical structures and equipments have been carried out on the table. Some representative examples can be listed as follows:

- * Models of high arch dam of 240 M with reservoir and foundation, high reservoir intake tower and ship-lift guide tower for large hydroelectric projects;
- * Control rod system, reactor containment, high pressure safety injection pump of nuclear power plants.
- * Models of different unchored oil-storage tanks with floating roof and ring foundation;

- * Models of high-rise buildings, frame work, television tower, and structures with various kinds of isolation and energy dispersion devices;

- * High-voltage electrical equipments of different types.

As space is limited, in this paper only some examples of typical results are illustrated.

1. A seismic verification test of the control rod system of a pressurized water reactor of a nuclear power plant was carried out to confirm its scramability. The test system was supported on a special designed frame of 5.3 M to simulating the boundary condition of the cover of reactor pressure vessel. Some artificial waves were generated according to the floor response spectra at the support point. An Objective Digital Compensation technique was used for controlling table motion to minimize the error between the desired and achieved motions at the point. The dynamic behaviors and seismic responses of various elements as well as the dropping characteristics of the whole system were investigated. Fig-1, Fig-2 show the typical insertion time history and displacement response trajectory at the top. The test results allowed positive conclusions on the reliability of the system to be drawn, both from the functional and safe point of view.

2. Tests for three different tank models welded from steel and aluminium sheet to represent oil-storage tanks with capacity of 3000, 5000 and 50,000 M³ in prototype respectively were accomplished on the table. Both the tank with floating roof and vapor preventer and their reinforced concrete ring foundation with filled-in soil were modeled to meet the simulation requirements within elastic range. The models were carefully manufactured to limit the initial deviations from their specified radius by as less as 0.005. Instrumentation was installed to measure the most significant features of the tank response around the tank, such as acceleration, hydrodynamic pressure, membrane and bending strain, uplift displacement of the bottom. Also, wave height of the liquid surface at 15 points were recorded and processed directly through a microcomputer. An artificial accelerogram generated by fitting a response spectrum with sufficient long period component up to 10 second as well as the frequently used El Centro accelerograms were adopted as input test signals. Additionally, a three sine wave with sloshing resonance frequency was generated in cases for measuring movement of sloshing surface and floating roof with reference to Japanese practices.

Many meaningful conclusions were drawn from the test results and some of them were adopted by the technical regulation of earthquake resistance in petrochemical industry. As examples, in Fig-3 and Fig-4 the results of uplift and sloshing measurement are illustrated.

3. A typical example for field tests is the China-U.S. cooperation in earthquake studies on several large arch dams which began in 1981. The principal objective of the research is to obtain improved understanding of the dynamic interaction mechanisms between arch dam and its foundation rock, as well as between the dam and its compressible reservoir water; and also to develop dynamic response analysis procedures that would represent the interaction mechanism more realistically and conveniently.

In 1991 a new cooperative research program was completed successfully in Dong Jiang Dam, a 157 M high double curvature arch dam in China. In this test, in addition to the measurements of acceleration response of dam and hydrodynamic pressures along dam surface and in the reservoir, the new research program focuses on detailed field measurements of the spatial variation of three component input motion around the dam-foundation contact, the actual wave coefficient α and topography of the reservoir near the dam. For this purpose an important aspect of the test is to excite the dam and the foundation by using explosive charge placed in an array of boreholes with water stemming, as opposed to the shakers used in previous test.

The measured acceleration and hydrodynamic pressure responses were compared with analytical predictions.

F.g5 shows the measured responses at crest and their calculated accelerograms due to the measured input varying along the canyon.

Based on the past experience we look forward to a more broad foreground of cooperation in laboratory and field experimentation with both home and over-sea colleagues.

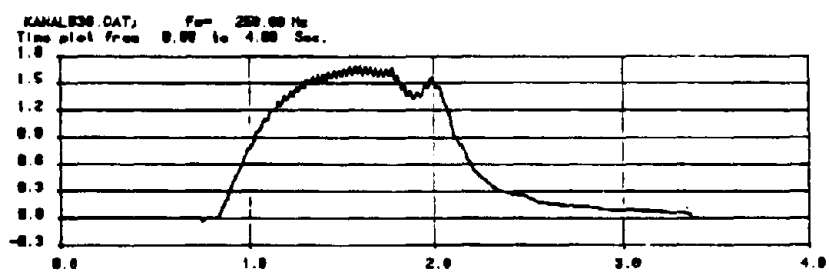


Fig-1 Insertion time history

FILE : C1213.DAT TEST-NO. 18-APR-00 10:50
 NYO.CURVE VEKTOR-ELEMENT C 1, 13

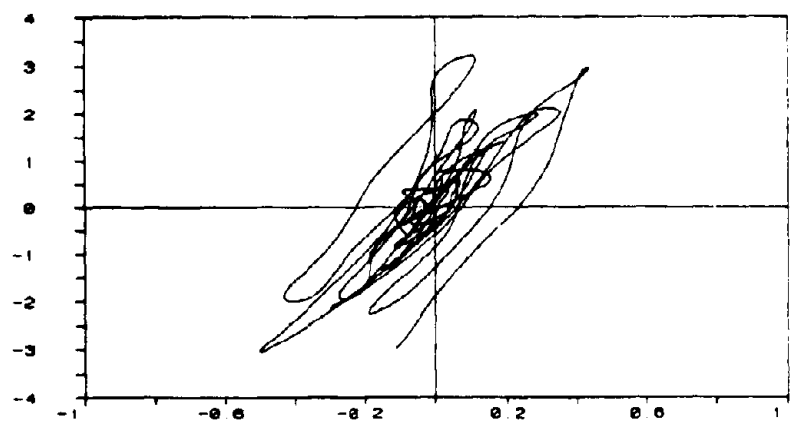


Fig-2 Displacement response trajectory at the top

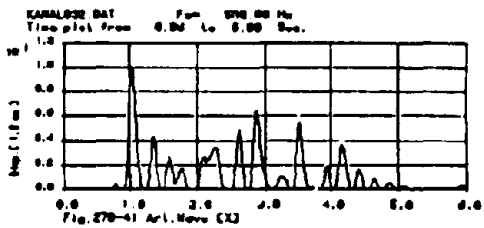


Fig.3 Time history of uplifting displacement of tank model (2.75X2.38M, Art wave Horz.0.3g)
(a) At south end of the excitation axis.

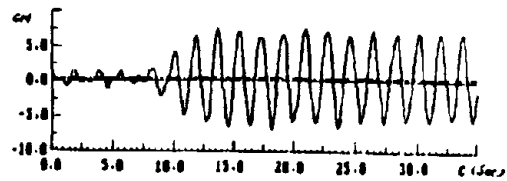


Fig.4 Sloshing wave (3 sine wave disp. input of amplitude 3.97mm)
(a) time history.

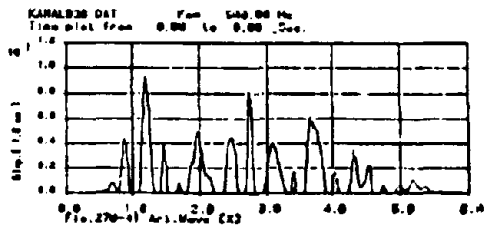


Fig.3 (b) At north end of excitation axis.

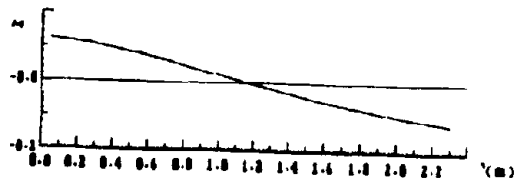


Fig.4 (b) Wave from along excitation axis.

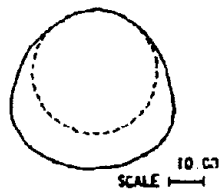


Fig.3 (c) Uplifting displacement around circumference at time 1.050 sec.

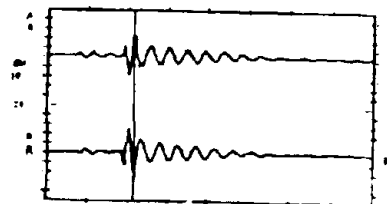


Fig.4 (c) Displacements of floating roof on excitation axis.

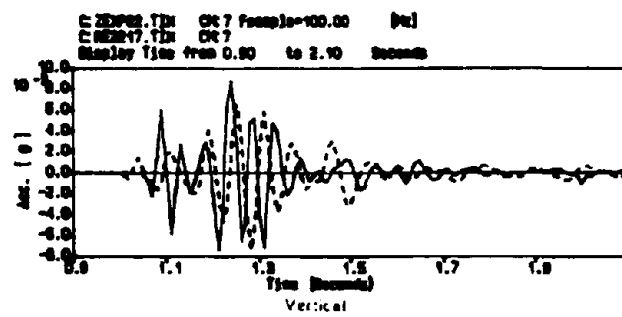
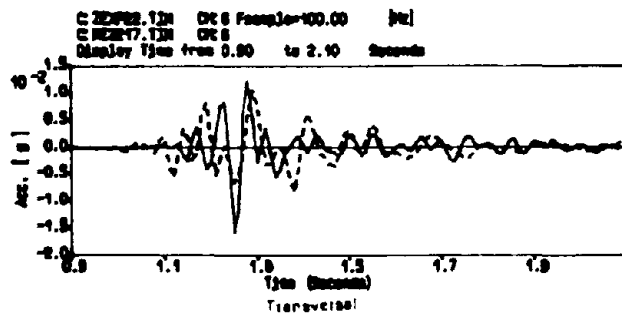
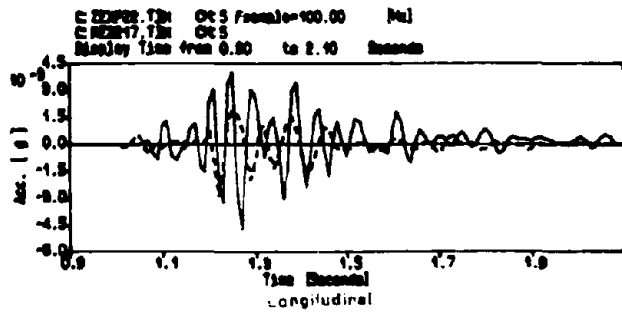


Fig. 5 Comparison of Calculated and Measured responses at crest
 ---- Calculated ——— Measured

Development of a Three-Dimensional Earthquake Simulator at USACERL

John R. Hayes, Jr.
Structural Engineering Team
Engineering and Materials Division, Infrastructure Laboratory
US Army Construction Engineering Research Laboratories
Champaign, IL 61826-9005

*Paper given at US/PRC Workshop on Experimental Methods in Earthquake Engineering
Tongji University, Shanghai, PRC, 10-14 November 1992*

INTRODUCTION

This paper outlines current efforts by the US Army Corps of Engineers Construction Engineering Research Laboratories (USACERL) and the Mid-America Consortium for Earthquake Hazard Reduction (MACEHR) to convert the USACERL Biaxial Shock Test Machine (BSTM) from its current biaxial motion capability to a fully three-dimensional (implying translational capabilities in three orthogonal directions, accompanied by appropriate rotations) earthquake simulation system. The outline will briefly comment on the need for such research capability in the US, discuss events leading to the current conversion efforts, and describe the planned facility development. The author's intent is to inform the reader of the initiative and stimulate dialog with others in the US and international research communities concerning the types of testing that should be undertaken and the partnerships that should be developed to optimize the utility of upgraded facility.

The Need for Triaxial Earthquake Motion Simulation Capability

The most compelling reason for providing triaxial motion (ie both translations along and rotations about three orthogonal axes) to simulate earthquake ground motion is that both observation and instrumentation have shown clearly that the ground moves in a random manner, with no definite correlation among orthogonal axes of motion, in major seismic events. There frequently is not a single preferred direction for significant components of ground motion at a given site. Often accompanying the random nature of the direction and magnitude of the measured motions at a site is randomness in the phasing and frequency of motions in different orthogonal directions. In the US today, there is no large or medium shaking table platform capable of producing controlled motions that can faithfully reproduce this truly random nature of ground motion for testing structural models. Experimental efforts to "replicate" actual earthquake ground motions to date have generally centered upon performing biaxial (ie translations and rotations involving the vertical axis and one orthogonal horizontal axis) tests in one of two ways: performing separate biaxial tests, one for each of two orthogonal horizontal axes of the test structure, or performing single biaxial tests in which structural models are oriented at some angle that is neither

perpendicular nor parallel to the primary horizontal axis of table motion. Both procedures have serious shortcomings. In the former, since economy of building scale dictates allowing inelastic structural behavior under severe earthquake motion input, the principle of superposition no longer applies. One cannot simply assume the results of tests conducted about a test structure's primary orthogonal horizontal axes are directly additive. In the latter, the test specimen oriented at the odd angle, while it receives motions input at an angle other than one of its two primary axes, still experiences motion input about a single axis. There is no meaningful duplication of the observed random ground motions in actual seismic events.

Of course, there is also rapidly growing worldwide analytical capability. Advances in nonlinear dynamic structural analysis techniques have made computer modelling more of a reality. However, the complexity of modelling in the nonlinear, and dynamic, regimes still presents not yet surmountable obstacles in producing practical, design-oriented tools that can provide significant insight into post-elastic structural response to earthquake motions. As stated by Professor Mete Sozen of the University of Illinois recently (Reference 1), "observation is still the essential ingredient in dealing systematically and confidently with materials and structural types having poorly understood behavior. Unlike forces related to gravity, earthquake forces act on structures very infrequently. While errors made in relation to gravity forces are almost immediately tested before accumulating a large inventory of vulnerable structures, errors made in relation to earthquake forces can be repeated hundreds or even thousands of times before experience reveals the error."

In Reference 1, Professor Sozen provides several noteworthy specific examples of structural failures in US earthquakes that have been universally attributed to shortcomings in our knowledge about three-dimensional structural response to earthquake ground motions:

1. Torsional effects were cited as primary contributions to failure of the JC Penney Department Store Building in the 1964 Anchorage, AL, earthquake, and in the Pino Suarez Building in the 1985 Mexico City earthquake.

2. The now-famous "soft-story" failure of the Olive View Medical Center in the 1971 San Fernando, CA, earthquake prompted extensive post-failure analysis. The analysis was not able to resolve completely the reasons for the large lateral displacements associated with the failure. Subsequent thought among informed researchers has been that the lack of good theoretical or analytical models that consider three-dimensional response was the major reason that analyses were not effective.

3. In the 1979 Imperial County, CA, earthquake, the Imperial County Services Building in El Centro, CA, was severely damaged. It was coincidentally well-instrumented, so good estimates of actual lateral and vertical forces were available. The calculated building resistance did not correlate distinctly with the observed failure mechanisms. As Professor Sozen has wryly pointed out, if the building had not failed, the same analyses could have been used to explain why the structure did not fail!

As a result of the lack of understanding about three-dimensional motion phenomena, earthquake-resistant structural design is negatively impacted in two ways. First, unexpected catastrophic failures can occur. Second, and more subtle and pervasive, designers and builders adopt overly conservative

construction philosophies, raising construction costs and reducing architectural and functional innovation in building design.

There is growing international endorsement of the need to study three-dimensional earthquake phenomena. Indeed, three-dimensional shaking tables are being operated around the world today. There are at least fourteen major such facilities in the People's Republic of China, Russia, Japan, the Federal Republic of Germany, Greece, Italy, Romania, and South Korea; the institution hosting this workshop, Tongji University, has a new three-dimensional shaking table. Within the US research community, there is widespread conviction about the need for three-dimensional earthquake simulation, yet no such capability is currently available. To their credit, staff members at the University of California, Berkeley, have also shown an interest in pursuing an upgrade of the excellent Berkeley shaking table to full three-dimensional capability; but, in a country the size of the US, with a number of different heavily populated areas of high seismic risk, more research than can be accommodated on a single table is needed.

A Brief Chronology

USACERL is among several laboratory organizations within the US Army Corps of Engineers; others include the US Army Waterways Experiment Station and the US Army Cold Regions Research Laboratory. USACERL performs infrastructure and environment-related research that directly supports design, construction, operations, and maintenance of US military facilities worldwide. Among many other research mission areas, USACERL performs structural engineering research. The USACERL Biaxial Shock Test Machine (BSTM) was designed and constructed by MTS Systems Corporation in 1971, as a supporting element for the structural engineering research mission. The BSTM was originally devised to perform shock tolerance testing of equipment intended for use in the old SAFEGUARD antiballistic missile program. This origin provided the impetus for many unique features in the BSTM; the features provided advantages over other shaking tables (then and now) for simulating the weapons effect-induced ground motion environment that was postulated for threats to the SAFEGUARD system, but there were also some limitations imposed on the system capabilities insofar as earthquake ground motion simulation was concerned. More will be presented on this later in the paper, but, briefly, the table has relatively high frequency and high acceleration capabilities for large payloads; these are somewhat offset in the seismic environment by relatively small displacement ("stroke") capabilities and associated velocity limitations.

In recent years, the emphasis on weapons effect research has lessened, while there has been growing concern within the US government over the potential vulnerabilities of federal and other facilities to the effects of major earthquakes. For the past three years, USACERL has had a growing Army-funded program to study the vulnerabilities of, and possible retrofit techniques for, existing military facilities in seismically active regions. The majority of these facilities are very "conventional" in their construction details; they closely resemble their non-governmental counterparts. As engineers at USACERL became more and more aware of this, it became obvious that the Army research program could benefit immensely from close cooperation with the US university community, principally the University of Illinois at Urbana-Champaign (UIUC), and, to a lesser extent, the private sector. USACERL was originally sited in Champaign largely because of its close proximity to the UIUC and its world-renowned civil engineering research talents.

USACERL engineers opened dialog with UIUC researchers about renewed seismic research cooperation in 1988-1989 (there had been close cooperation in the 1970's). It was clear at the outset that USACERL could gain much from close partnership with UIUC in this area; UIUC researchers were in turn interested in the applied perspective of the USACERL program and the mutual development of the BSTM, with associated research programs. Professors Mete Sozen and William Hall were very supportive of the partnership and were instrumental in all subsequent initiatives that have occurred. Professor Sozen initially proposed an upgrade of the BSTM to a three-dimensional "Earthquake Simulation System" in 1986. As a result of this renewal, in July 1990, USACERL hosted a workshop to address the use and possible upgrade of the BSTM. The workshop involved federal engineers from various agencies (eg National Science Foundation, National Institute of Standards and Technology), university researchers (including the National Center for Earthquake Engineering Research), and a select number of engineers from the US private sector. The workshop panelists made a number of recommendations concerning the BSTM (Reference 2). With respect to this paper, key among them were:

1. USACERL should pursue general upgrade of BSTM system capabilities and should specifically pursue upgrading the BSTM to a triaxial configuration.
2. USACERL should develop more research partnerships with other research organizations, particularly the UIUC and other members of the university community.

The second recommendation has generated exciting activity between the university community and USACERL. In January 1991, USACERL hosted a meeting of researchers from UIUC, the University of Michigan, the University of Minnesota, and the University of Texas, Austin, to discuss the formation of a consortium of institutions located in regions of generally low to moderate seismic risk; the consortium would focus primarily upon experimental seismic structural engineering research. The initially invited institutions all had active experimental research programs, so they could form a solid nucleus. Philosophically, the tie that bound all together was the collective concern about the need for research addressing the needs of various US regions where large magnitude earthquakes are known to be infrequent, hence resulting in less stringent building code requirements than for more active regions. All of the university representatives at the initial and subsequent meetings endorsed the consortium concept and, in parallel, a pursuit of a triaxial upgrade for the BSTM, with future joint usage in cooperative research projects. Since that time, two additional institutions, Memphis State University and the University of Washington, have joined, and the consortium is now informally known as the Mid-America Consortium for Earthquake Hazard Reduction (MACEHR). It is important for the reader to note that MACEHR is an informal collective of institutions with common interests and research goals. It is not a formal organization, and "members" do not currently plan to formalize the organization or exclude others who may wish to "join."

With the support of the MACEHR, USACERL has pursued the first recommendation, that of upgrading the BSTM to a true six degree-of-freedom triaxial configuration. USACERL submitted a proposal to the US Army for fiscal year (FY) 1993 funding of a proposed upgrade for the BSTM. USACERL staff members are currently awaiting notification concerning Army support of the proposed upgrade. The proposed performance characteristics of the upgraded shaking table were developed

cooperatively by USACERL and the initial MACEHR members; the characteristics represented a consensus of practical changes that could be implemented without severe cost penalties.

Proposed Triaxial Upgrade for BSTM

A brief description of the current facility is appropriate to help establish a solid background for detailing the proposed upgrade. References 2 and 3 provide thorough overviews of the existing table's characteristics; they will be summarized here.

Figures 1 and 2 present traditional log-log "tripartite" plots of the performance envelopes of the BSTM. Figure 1 shows vertical performance, while Figure 2 shows performance for the one current horizontal axis of motion. Maximum velocity for both axes of motion is 30 inches per second (76 cm/sec). For a nominal 12,000 pound (5,450 kg) payload, the maximum rated vertical acceleration is 30 g, while the maximum rated horizontal acceleration is 20 g. The table is capable of testing larger payloads at commensurately lower peak accelerations. The 60,000 pound (27,240 kg) payload-related acceleration plotted is not the table payload limit; it is the largest payload tested to date. For smaller payloads, the BSTM has proven to be controllable over a frequency range of 0-600 hz.

The test platform is a twelve foot (3.66 m) square aluminum weldment with an internal cellular construction; the platform thus balances weight reduction and stiffness. It weighs approximately 12,000 pounds (5,450 kg) and has a first natural frequency near 200 hz. A total of 15 electrohydraulic actuators is used to drive the table. Nine vertical actuators provide a total force of 810,000 pounds (367,700 kg); six horizontal actuators provide a total force of 450,000 pounds (204,300 kg). Vertical stroke range is 2.75 inches (7 cm), while horizontal stroke range is 5.5 inches (14 cm), both measured peak-to-peak. Separate vertical and horizontal concrete reaction masses are used, with a combined weight of about 4,000,000 pounds (1,816,000 kg).

The BSTM is controlled by a predominately analog system that is original equipment. It controls each actuator individually with a separate closed-loop control circuit consisting of three integrated feedback loops. By interconnecting the control loops of the 15 actuators, five degrees of freedom are controlled: vertical translation, horizontal translation, roll, pitch, and yaw. Lateral displacement is passively restrained by spherical hydraulic bearings attached to the horizontal reaction mass. The analog system also controls several other parameters: force balancing, overshoot and ringing, stabilization, model center of gravity effects, and actuator cross-coupling.

A minicomputer-based digital system is used to generate test time-history waveforms. It is flexible and can be used to generate shock, seismic, random vibration, sine sweep, and a variety of other waveforms. The primary current data acquisition system is a 60 channel modular signal conditioning system which records to a 70 channel magnetic tape recorder. USACERL has acquired 32 channels of microcomputer-based digital data acquisition and is pursuing the acquisition of additional such channels.

Since the outset of discussions among the engineers involved in the proposed upgrade, two overriding philosophies have prevailed. First, given budgetary constraints, building a new triaxial test

facility has not been considered feasible; modifying the existing facility has been seen as the only realistic option. Second, while the goal has been to develop a capable triaxial earthquake simulation system, USACERL engineers feel the existing biaxial-mode capabilities must be maintained. As mentioned above, the first upgrade proposal was developed in 1986. In that proposal, for the Triaxial Earthquake Simulation System (TESS), the envisioned triaxial configuration had two alternatives, based on a 60,000 pound (27,240 kg) payload: 1.7 g peak acceleration, or 3.4 g peak acceleration, in each of the two horizontal axes. The existing biaxial performance envelopes would have been maintained, but manual switching of system valving would have been required in changing from biaxial to triaxial test configurations.

USACERL and other members of the MACEHR have developed a new consensus performance requirement for the now-proposed triaxial upgrade; the upgrade would provide a balance of performance and economy. The proposed upgrade will provide a triaxial capability as shown in the tripartite plot of Figure 3; the existing biaxial capability will be maintained as well. In the triaxial configuration, both axes of motion would have peak acceleration capabilities of 2.0 g, for a 120,000 pound (54,480 kg) specimen; the existing horizontal axis would still have a 5.5 inch (14 cm) stroke, while the new axis would have a twelve inch (30.5 cm) stroke, again measured peak-to-peak. Detailed performance requirements are shown in Table 1 (Reference 5). Figure 4 (Reference 5) presents a plan view of the proposed new configuration.

Key features of the proposed upgrade are discussed in References 4 and 5. A number of preliminary analyses has been performed to validate the conceptual framework of the features. Several of the more significant factors involved in the upgrade are listed briefly here.

Perhaps foremost among these factors is that, to balance economy with functionality, blowdown accumulators will provide peak forces for table motion. A study of the sustained pumping capacity needed to provide the peak performance indicated that both the initial acquisition cost and the operating (ie electricity) cost would be high. MACEHR engineers arrived at a 10 second requirement for peak force capability; for such a time period, accumulators provide an economical alternate solution (this is consistent with the current operational concept for the BSTM). Both the existing accumulators and 48 new high pressure accumulators would be needed to develop the required test forces.

The new axis of motion will require a number of major modifications to the existing table, mechanical system, and foundation. A single new horizontal actuator will be added on each appropriate side of the table (see Figure 4). The table itself will require slight structural modification; the existing slide bearing mounting plates will be used to accommodate attachment points for the new actuators. The table is essentially surrounded at table level by the horizontal reaction mass. This reaction mass is reinforced with both deformed bars and post-tensioning rods. Cutting small access boxes for the new horizontal actuators will require cutting some of the existing bars, but not the rods. The reinforcement was originally configured primarily to prevent fatigue failure of the concrete, not to accommodate high service stresses. Therefore, preliminary analysis (Reference 5) indicates reinforcing the mass to offset the loss of the bar continuities will be needed but not difficult. The swivels on all 15 existing actuators will require replacement with new swivels that can accommodate the more substantial angular movement that will be associated with the added translation.

New analog controls and new digital data acquisition systems are planned.

Several dynamic tests have been conducted with the BSTM to analyze critical performance characteristics associated with the planned triaxial configuration. The tests and analyses have focused upon the friction in the actuation and restraint systems, oil column resonant frequencies, friction and resonance effects on the acceleration waveforms producible, overturning moment restraint stiffness and capacity, and foundation response to dynamic input. While some further testing is planned to complete the analyses, there appears to be no serious impediment to the envisioned upgrade process.

Proposed Future Research Activities

Predominant thought within the MACEHR consortium is that the upgraded capability will lend itself best to proof testing of scaled models of structures and their components. USACERL and partner consortium members have considered a number of initial research thrusts for the proposed facility. USACERL's current primary focus is in the reinforced concrete and masonry structural system arena. The US military has an abundance of existing "nonductile" structures that likely will require seismic retrofit in coming years, so Army-sponsored research is likely to continue in this area. This is consistent with other MACEHR members' desires to study reinforced concrete frame-wall structures. They cite (Reference 1) recent joint US-Japan studies on a seven-story structure at Tsukuba Research Laboratory. Predicted and measured base shears in the structure differed significantly. Subsequent small-scale model tests of the same configuration at the University of California, Berkeley, and at UIUC raised many questions about dynamic behavior of the structure under imposed biaxial horizontal (+ vertical) motions. Therefore, a probable early test series would involve the Tsukuba structure at approximately 1/5 scale. Complementing such a model structure test series would be a number of component tests to study fundamental behavior. In particular, the behavior of columns under imposed biaxial horizontal motion would be a significant test initiative; both bending hysteresis and shear would be studied.

MACEHR members also propose (Reference 1) to study torsional-translational behavior of braced steel moment frames; the results of using irregularly-shaped framing systems in regions of low to moderate seismicity; torsional effects due to structural and mass eccentricities in composite steel-concrete systems; out of plane response of masonry systems, particularly unreinforced masonry in regions of low to moderate seismicity; diaphragm action in steel joist roof systems used in regions of low to moderate seismicity; connection details in precast and prestressed concrete structures, and both passive and active structural control systems.

USACERL is a federal research institution. It is important to note that the BSTM is available for use on a cost-reimbursable basis by anyone in the US, within minor limitations imposed by the US Army. USACERL staff members intend that this policy will continue in the future if the proposed upgrade is implemented. Plans outlined herein involve MACEHR member institutions because of the common interests shared by all. The USACERL staff will welcome the opportunity to work with other institutions.

References

1. Sozen, MA. "Three-Dimensional Earthquake Simulator," 28 February 1992.
2. Hayes, JR, Gambill, JB, Wilcoski, J, Brady, PA, and Al-Chaar, G, "Use and Upgrade of the USACERL Biaxial Shock Test Machine: Workshop Summary," USACERL Special Report M-91/20, May 1991.
3. Fisher, WE, Gambill, JB, "Vibration Table Shakes Flaws from Equipment," Industrial Research & Development, August 1983.
4. "USACERL Biaxial Shock Test Machine (BSTM)/Triaxial Earthquake Simulation System (TESS) Upgrade Conceptual Design Study," MTS Systems Corporation, 29 June 1992.
5. Wood, SL, "Biaxial Shock Test Machine Upgrade Design Study," University of Illinois, 3 July 1992.

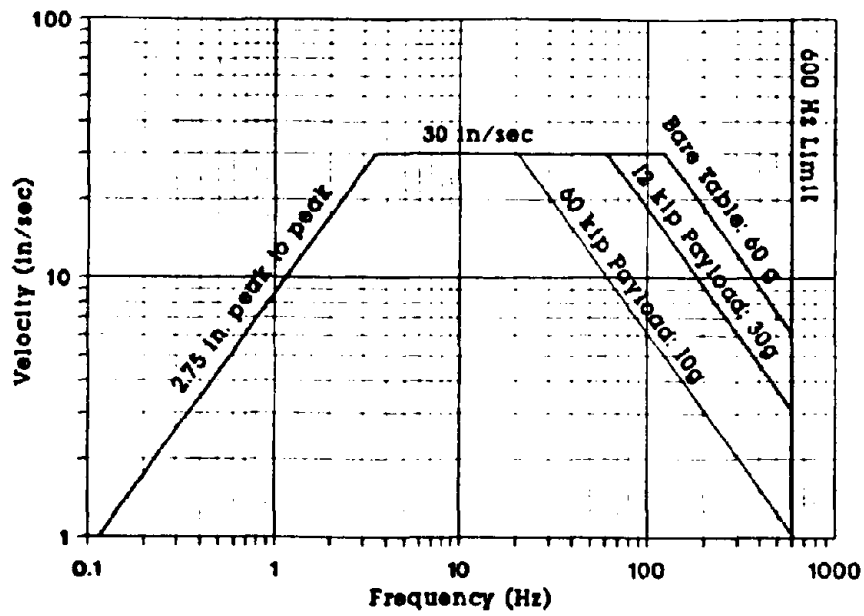


Figure 1. USACERL BSTM - Existing Vertical Performance

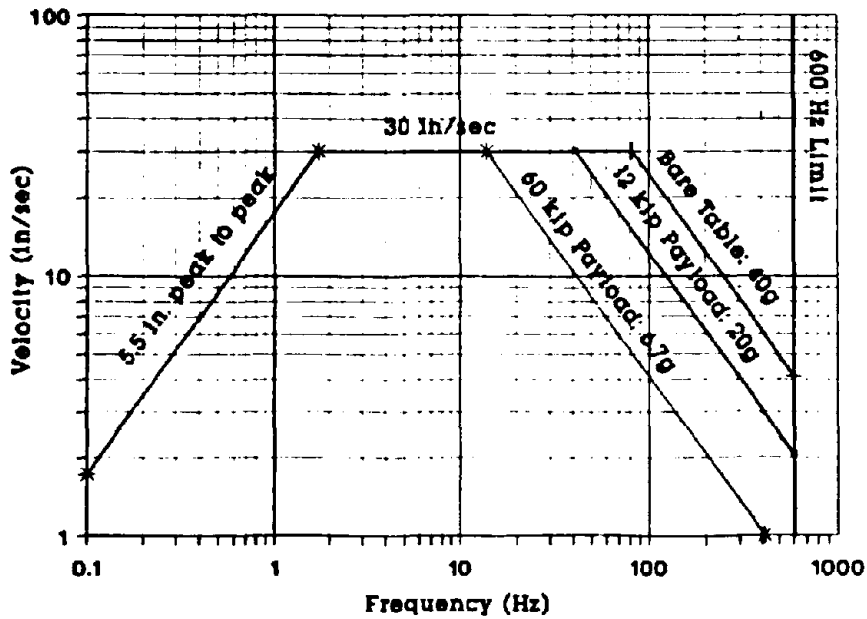


Figure 2. USACERL BSTM - Existing Horizontal Performance

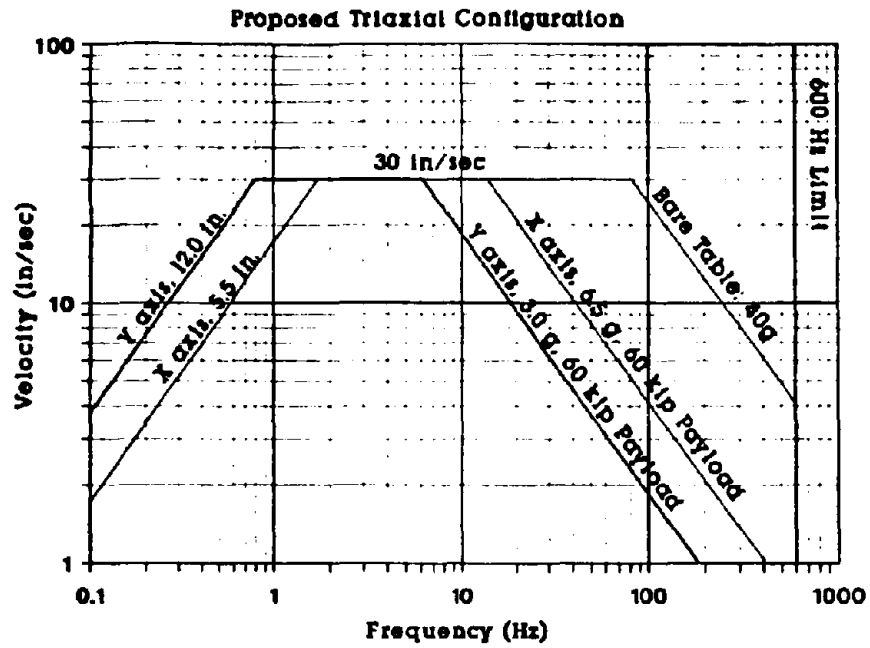


Figure 3. USACERL BSTM Upgrade - Horizontal Performance

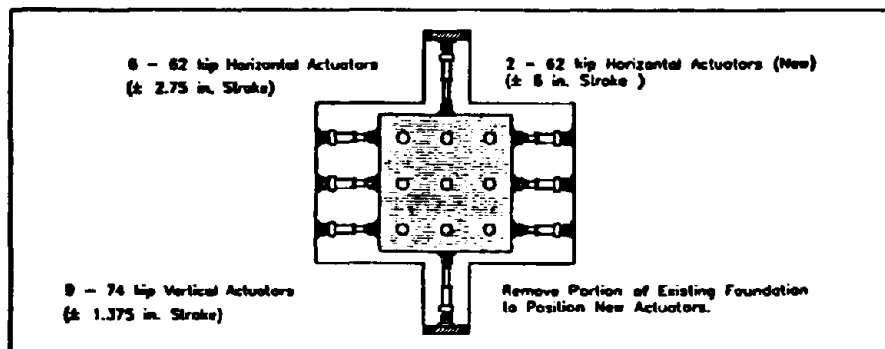


Figure 4. Plan View of Proposed Revisions to BSTM

	X direction	Y direction	Z direction
Table Weight			12 kips (existing)
Specimen Weight			120 kips
Actuators	6 - 62 kip (existing)	2 - 62 kip	9 - 74 kip (existing)
Stroke	± 2.75 in. (existing)	± 6.0 in.	± 1.38 in. (existing)
Velocity	30 in./sec	30 in./sec	20 in./sec
Acceleration	2.0 g	2.0 g	1.0 g
Base Shear	72 kips (0.6 W)	72 kips (0.6 W)	
Base Moment (including vertical eq. motion)	6000 kip-in.	6000 kip-in.	4000 kip-in.
Base Moment (without vertical eq. motion)	8500 kip-in.	8500 kip-in.	6000 kip-in.

Table 1 - Desired Performance Characteristics of 3-Dimensional Earthquake Simulator

Signal Reproduction Fidelity of Servohydraulic Testing Equipment

D. A. Kusner, J. D. Rood, G. W. Burton
MTS Systems Corporation, Eden Prairie, Minnesota, U.S.A.

ABSTRACT: Servo-hydraulic systems are often used in pseudo-dynamic, structural, and shaking table systems to simulate earthquakes, test the seismic resistance of structures and components, and to verify analytical models. High fidelity reproduction of the excitation signal is imperative to ensure that unknown or unwanted experimental errors are not introduced into the test. Knowledge of the potential sources of system wave form infidelity would greatly enhance the researcher's ability to ensure the best test results through intelligent system design. This paper provides a technical discussion of various sources and effects of wave form distortion and how to reduce them in servo-hydraulic systems.

1 Introduction

Distortion analysis is a complex issue when using multiple degree-of-freedom, closed-loop electrohydraulic servo systems. There are many potential sources of distortion, and many of them highly interdependent on each other and on various system parameters. In most cases, it is difficult to assign specific values to these sources of distortion let alone their potential effect on test results.

The best approach to system design and specification is eliminate and reduce these sources of distortion and to size the system so that the performance envelope lies outside areas of high distortion. Compromises must often be made when considering distortion, overall system performance, and cost.

The following sections describe measurement, sources, and types of distortion. In the final section, a typical performance envelope for a medium to large seismic system will be presented. The areas affected by each type of distortion will be shown.

This report provides a better understanding of the complex topic of distortion and enables the reader to make better decisions regarding operating and sizing issues.

2 Distortion Measurement

2.1 Distortion analysis

There are many types of distortion and distortion measurement methods. In seismic simulation systems, one of the principal areas of concern is the frequency response of the system. For high fidelity it is important that the system response has the same frequency content as the program signal. With other types of systems, parameters such as phase lag, system roll off, peak values, energy content, resolution, etc., may be deemed to be more important system parameters.

The most common method of distortion measurement is to measure the total harmonic distortion (THD) of the acceleration signal. With this method a representative group of pure fundamental frequencies (which span the frequency envelope of the system) is tested, one frequency at a time usually at two different programming levels. For each frequency tested the various harmonic components excited in the system are measured with respect to the magnitude of the fundamental program signal, Figure 1. The ratio of these components to the fundamental frequency is the total harmonic distortion as defined by Equation 1.

When a digital computer/analyzer is used, a fast Fourier transform can be done on the response signal. Only the significant components are counted, typically the first three to ten.

Typical values for a seismic system will be approximately 20% at 1/3 oil column frequency and dropping off to 5% at oil column higher. Depending on system mechanical resonance's, this percentage will increase again at higher frequencies.

2.2 Transducers

When measuring distortion attention should be paid to the type of transducers used, their operating characteristics, mounting locations and the parameter they will measure. For example the arcing motions of actuators, bellcranks, and linkages on some systems can introduce distortion which may not be apparent from the transducer readout.

The useful frequency range, transverse sensitivity, and the alignment of the accelerometers and mounting fixtures are important. Improper use and mounting of accelerometers can contribute significantly to distortion either directly or by contributing to control instabilities. This becomes more evident at higher frequencies.

On large seismic tables the location of the accelerometers is very important. It is important to mount accelerometers where they can measure the desired control parameter but at the same time do not pickup local structural resonance's or table deflections that would make control more difficult. Since tables cannot be perfectly rigid, it is important to realize that there will be differences and phase lags between local accelerations throughout the table.

3 Hydraulic Considerations

3.1 Servovalve Characteristics

The most important hydraulic component in terms of distortion and overall system performance is the servovalve, Figure 2. This section gives a brief overview of servovalve operation characteristics for an inertially loaded system such as a seismic system. For a more detailed analysis see Clark's paper (Clark 1983).

The servovalve is a variable orifice which, in conjunction with the external load (via the actuator piston area) and supply pressure determines the amount of oil flow through the servovalve. If there is no external load then full pressure is available across the S/V and maximum flow will be developed (open loop velocity). If the actuator piston is constrained, then there will be no flow and the pressure drop across the servovalve will be zero allowing for full pressure to be developed across the piston.

Figure 3 shows a range of servovalve spool openings plotted as a function of force (piston area X pressure) and velocity (flow/ piston area). The ellipse represents the plot of a simple sinusoidal inertial load (maximum force 90° out of phase with maximum velocity). Any number of ellipses are permissible provided they lie within the spool opening for this model. The ellipse shown is the worst case sizing condition which occurs at the intersection of the acceleration and velocity limits.

Some important points to notice are that the servovalve limits the performance only in the first and third quadrants, and that this limitation occurs just past the peak force point in the cycle. Any hydraulic constraints will affect this part of the operating cycle first.

There is a severe non-linearity in the spool opening as the system passes through peak force. During the same interval of the cycle the spool must move much faster during A than during B. This point is often referred to as the 'turnaround' point. The discontinuity at this point can be very large and is often referred to as 'pressure switching'. Operation in this region will cause the acceleration waveform to be flattened and to have a 'cusp' shape.

Field experience has shown that to minimize this servovalve non-linearity, and to allow for some design margin for the control system, the 'load' ellipse should be within the 80% spool openings and the peak force is limited to 95% of the available maximum. These margins are based on experience and are frequency dependent; at lower frequencies they can be decreased.

On system performance envelopes, this ellipse represents the intersection of the velocity limit and the acceleration limit. This is the most difficult point to attain and determines the sizing of most of the system components.

At frequencies higher than the oil column the same 'pressure switching' phenomena can occur at the intersection of the compressibility flow limit and acceleration limit. At these higher frequencies the distortion is dominated by mechanical resonant frequencies and 'pressure switching' is not as noticeable.

3.2 Servovalve Spool Lap

Much effort by researchers has been spent analyzing the effect of spool lap and metering edge shapes on signal fidelity and cavitation (Royle 1958).

A small amount of valve overlap is desired in standard grade servovalves. The principal reasons are to minimize internal leakage within the valve and to reduce the need for tight tolerances. The problem with this type of valve is that there is a dead band where a slight motion of the spool results in little change in flow. This will result in a slight indent in the acceleration curve and cause distortion.

This problem has been eliminated in single servovalve applications by the careful grinding of the spool valves using the actual measured flow characteristics of the valve to set the amount of grinding.

Studies on the potential benefits of servovalve under lap show that there is no benefit and that a definite increase in distortion exists at low frequencies and high load conditions due to the increased internal leakage.

3.3 Oil Column

A systems' oil column is an important system parameter and will directly affect distortion and upper frequency performance. Distortion arises from the natural resonance of specimen/table mass on the oil column spring of the actuators. Typically, on most inertially loaded systems the natural frequency of the oil column is well within the operating range of the system.

Operation at the oil column frequency may result in problems with gain but the distortion effects may be minimal. However, operation at frequencies of approximately 1/3 of the oil column will result in frequency components that can excite the oil column frequency and cause significant distortion. These frequency components are mainly due to the non-linearity of the servovalves.

Figure 4 shows a wave form with a third harmonic component.

In general, if the oil column frequency is fairly constant, this type of distortion can be minimized by careful tuning, use of valve linearization circuits or computer compensation.

The problem arises when the oil column frequency changes due to changes in the effective mass of the specimen. This will occur if the specimen mass or the location of the specimen on the table changes. The oil column frequency might then be moved into an area where there is slightly greater gain resulting in increased distortion. Fortunately in most cases the variance of typical test specimens is not that great.

This type of distortion primarily occurs at specific frequencies and tends to be greater at larger program values, although it can occur at lower values. It is one of the dominant distortion components.

3.4 Servo valve linearization

Servovalves are inherently non-linear devices where the flow output is proportional to the square root of the pressure drop across them. Servovalve linearization is a method using analog electronics to increase the servovalve signal at higher levels to help linearize the flow characteristics of the S/V. This has been shown (using analog computer simulation studies) to be of great benefit in regard to distortion.

Recent field experience has verified these simulation studies and resulted in a distortion reduction of one half at system frequencies at 1/3 oil column and under high load conditions.

This type of compensation technique is useful when iterative computer compensation techniques are inappropriate.

3.5 Flow limits

This type of distortion occurs whenever there is any type of flow limit. In an extreme case, where there is an absolute flow limit and the acceleration loads are relatively small, the displacement wave form will 'triangulate', with the slope of the wave form equal to the velocity limit, see Figure 5. Flow limits can arise from several sources; pump, servovalves, or accumulators.

Flow limits cause increased distortion predominantly at the velocity limits of the performance curve. The solution is to size the system conservatively and to be aware of any system parameters which may limit peak flow or the available pressure drop across the servovalve at peak velocities.

3.6 Force limits

A system can become force limited in two ways. There may be insufficient force due to compressibility flow limits, or excessive load demands due to system or specimen resonant frequencies (See 5.4).

At higher frequencies, the compressibility flow requirements (flow required to compress the trapped oil volume within the actuator) becomes significant. Compressibility flow is proportional to frequency and the stroke capacity of the actuator. This flow requirement in combination with the servovalve roll off limits the force capacity of actuators at frequencies at the high end of the performance envelope.

This compressibility flow limit in itself will not cause distortion but will limit the systems capability to react to perturbations such as those due to cross coupling from other axes. The solution is to use higher response servovalves or multiple valves to get the required upper frequency performance.

3.7 Hydraulic piping

The ideal supply for a servovalve system would be an infinite volume, constant pressure source with zero internal impedance using a fluid which is incompressible, had zero viscosity but good lubricity properties, infinite heat capacity (no cooling required), homogenous (perfectly clean), and low density (some mass is required for a S/V to work).

In reality, this fluid is not available. However with careful sizing of components and good system design, the more important limitations can be met. The main issues (in regard to distortion) are pressure loss in the piping distribution, inertial pressure spikes, cross talk through the hydraulic system, oil cleanliness and dissolved gases.

Flow losses are minimized by conservative sizing of the hydraulic lines and appropriate use of accumulators. Separate pilot supplies are used to limit the fluctuations to the servovalves.

Inertial pressure spikes occur at high operating frequencies due to the inertia of the fluid itself and the increased compressibility flow requirements. These spikes can cause noise and cross-talk problems resulting in increased distortion. Appropriate line sizes and the use of close-coupled accumulators can largely eliminate these problems.

Spool friction is due primarily to silting, a phenomena where particles within the oil tend to accumulate in front of the spool edge resulting in a large value of static friction. This leads to resolution problems and increased distortion at low programming levels. Clean oil and the use of dither will alleviate this.

Dissolved gases can have an effect at return and drain line operating pressures. Servovalve 'rumble' and other hydraulic noise are caused by dissolved gases coming out of solution downstream from the metering orifices within the servovalve. This will set a lower limit for background noise level.

4 Mechanical Considerations

4.1 Friction

Friction can arise from a number of sources within a testing system. The actuators contain a number of friction sources: seals on the actuator, rod bearings and swivels. In addition, the table may contain a number of sources (depending on the design and layout). Slide bearings, static supports and mechanical linkages are a few potential table friction sources.

Frictional loads are not large and typically account for a few percentage points of maximum system capability. The problem occurs during turnaround where there is a reversal in the direction of motion. The oil pressure must overcome this static friction before motion can begin. This causes a discontinuity in the motion. In addition, due to the compliance within the load path, a certain amount of energy is stored within the load train. Once the system starts moving, any difference between the static and dynamic friction values results in a proportion of this energy being released instantaneously. This tends to excite any mechanical resonant frequencies until the energy has been dissipated as may be seen in Figure 6.

At peak force (acceleration) operating values, the noise or distortion from friction is small. However the magnitude of this disturbance is constant so that as the program signal level is reduced it becomes an objectionable component. At low programming levels it can result in acceleration spikes much greater than the program signal.

Due to the high frequency content and short time duration of each pulse, friction has little effect on the THD value. But its effect nevertheless can be large on the wave form shape.

In general, this type of distortion is a percentage of maximum system capability so that it is critical that the system is not oversized if good low level performance is required. An example of where this is frequently a problem is in the vertical axis of seismic systems. Often the vertical actuators are sized by the overturning moment (OTM) requirement. The actual vertical axis requirements may be much less but the actuators used will be sized greater due to the OTM. This will result in greater friction (as compared to a system where smaller vertical actuators were supplied).

Friction from the rod bearings may be significant enough to justify the use of hydrostatic bearings in some cases. The use of these bearings adds system cost, complexity and pump requirements. Hydrostatic bearings require longer actuators which in some cases can make foundation design more difficult/expensive. They can also adversely affect the lateral natural frequency of the actuator due to the increased mass and length of this type of actuator.

4.2 Mechanical resonant frequencies

Within any mechanical system there are numerous resonant frequencies which might be excited. A good design philosophy with seismic systems is to keep these resonant frequencies well beyond (2 or 3 times) the maximum operating frequency. There is less chance that they will become excited and frequently, the system gain is low enough at these higher frequencies that they will not be picked up and be amplified. (These resonant frequencies usually occur in modes where the system could not control them even if it had the power to do so.) In practice there are always some components of these resonant frequencies at the upper operating frequencies of the system. Figure 7. shows a signal with higher frequency component due to a mechanical resonance.

The main table modes which can cause problems are the 'warp' and 'oil canning' modes. Careful design is required to keep these modes as high as possible. The specimen configuration and mounting can aggravate these modes especially the oil can. A change in the mounting method can extend the frequency testing range.

Local structural panel frequencies from within the table are another source of potential disturbance. The panel frequency resonant frequencies are quite high (relative to the operating range) and are more of an acoustic nuisance. Occasionally they can interact with the servovalves and add significant high frequency components to the feedback signal.

4.3 Foundation interface

A significant source of distortion can arise from the foundation and the actuator attachment to the foundation. Attention to the foundation design is required to avoid vibration modes of the foundation which will affect system operation.

At higher frequencies, the compliance at the actuator attachment can prevent the actuator from inputting full force capabilities into the table. This will create a force limit at higher frequencies limiting the response of the actuators.

With floating (isolated) foundations an appreciable relative foundation movement is possible typically peaking at about 1 Hz. To measure true displacement relative to the 'fixed ground' additional transducers must be mounted between the fixed and floating foundations are required. In practice with the use of large foundation/specimen mass ratios and adequate suspension system damping, the small increase in accuracy does not justify the cost and complexity.

4.4 Backlash

Backlash is similar to friction in that in itself it does not cause serious distortion problems. It does however provide a mechanism by which a force or energy impulse can set off other resonant frequencies in the system. The two main sources of backlash are bolted connections within the load train and the actuator swivels. Proper design and maintenance of these mechanical components are required for system fidelity.

5 Miscellaneous

5.1 Electrical noise

Noise within circuit boards has been greatly reduced in recent years with improved components. The long transducer cables used on seismic systems do offer an opportunity for noise pickup in the feedback loop. Through careful grounding design this can be attenuated to low levels.

Line noise in the operating environment and from within the consoles can be a major problem. Line noise typically is in the operating range of most seismic systems making it difficult to remove or filter.

Careful attention must be paid to grounds used both for the console and pumping system. A separate instrument ground is a necessity.

5.2 Cross coupling

Cross coupling occurs whenever actuators in one axis must react loads due to motions in another axis. The most obvious is the Over Turning Moment (TOM) loads imposed on the vertical actuators due to horizontal motion. The moment arises since the horizontal actuators do not act through the center of mass of the table/specimen.

The transducers on the table must sense these unwanted motions in order for the actuators to respond. The relative program signals in these axes may be quite low so that any components from another axis can appear to be quite significant.

Control methods using feed forward compensation can help to attenuate this cross talk from other axes. Computer compensation using iterative methods can help greatly assuming the dynamic properties of the specimen table do not change too much during a test.

This is one of the more difficult areas of distortion control and new control techniques are being explored.

5.3 Static weight

If no means are provided for an external static support, then the vertical actuators will be required to provide this component. Depending on the capabilities of the system this can be a significant percentage of vertical actuator capability. This static force provides a greater pressure gain in one direction and there will be an asymmetry which will show up as distortion.

This distortion source will occur when there are high demands on pressure (i.e. large velocity, maximum force or high frequency operating conditions). With the proper use of static supports, this type of distortion is largely eliminated.

5.4 Specimen compliance

One of the more difficult types of distortions to control is that due to specimen compliance. This compliance can come from the method used to mount the specimen to the table or from within the specimen itself. The specimen's dynamic properties may be; non-linear, they may change with load history, and have complex damping properties.

These characteristics cause a number of issues. For example, a lot of the tuning of the system is based on the assumption of a fixed coupled mass, since this determines what the oil column frequencies will be. With a complex specimen these frequencies may be load and time dependent making optimum tuning difficult.

A resonant specimen with low damping can easily overload the capacity of a system. As a simple example, a cantilever beam with no internal damping when excited in bending at its natural frequency requires an infinite moment to restrain it and yet the actual acceleration at the base is minimal.

6 Typical Performance Envelope

Figure 8 shows a typical performance plot of a medium to large seismic system. The predominant sources of distortion are listed along with the approximate regions where they occur. It is very difficult to assign specific values to the various sources. An effort has been made to rank the severity of the various sources.

The most significant are; friction sources which mainly affect low acceleration performance, oil column resonant frequencies which tend to cause problems in the mid-range, servovalve limits which result in distortion problems at the intersection of the velocity and force limits, and mechanical resonant frequencies which occurs at the higher end of the frequency range of the system.

7 Conclusion

Sources of wave form infidelity while performing experimental tests with servo-hydraulic systems have been identified and some methods of reducing distortion errors have been presented. This paper serves as a benchmark for future study and research in minimizing experimental errors with servo-hydraulic systems.

References

Clark, A. 1983. Sinusoidal and Random Motion Analysis of Mass Loaded Actuators and Valves. *Proc Nat Conf Fluid Power Vol 37: 168-171 1983*

Clark, A. and Cross, D. 1984. The effect of specimen resonances on accurate control of multiple degree-of-freedom servo-hydraulic shaking tables. *Proc 8th World Con on Earthquake Engineering*. San Francisco: U.S.A.

Royle, J. 1959. Inherent non-linear effects in hydraulic control systems with inertia loading. *Proc Instn Mech Engrs Vol 173 No 9 1959*

$$THD = \frac{\sqrt{\sum (\text{harmonics})^2}}{\text{fundamental}} \quad \text{eq (1)}$$

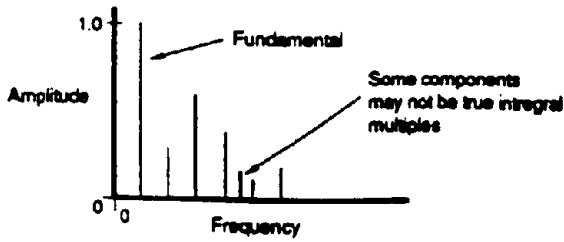


Figure 1. Frequency domain plot.

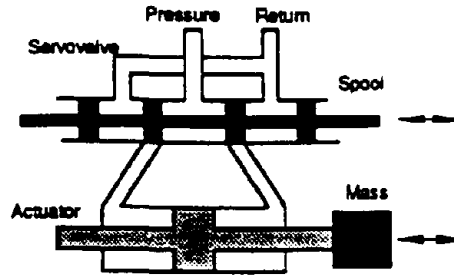


Figure 2. Functional schematic of an inertially loaded servovalve/actuator.

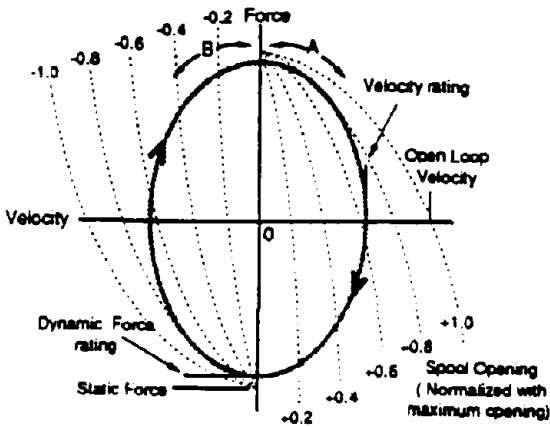


Figure 3. Force/Velocity phase plane for an inertially loaded servovalve/actuator.

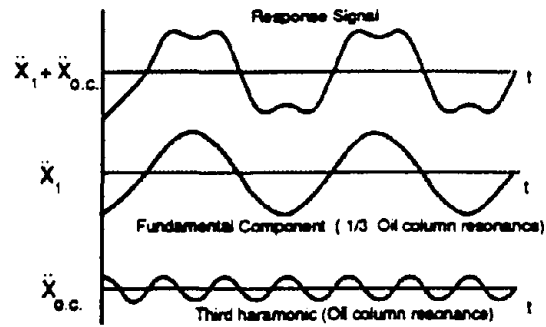


Figure 4. Third harmonic distortion due to oil column resonance.

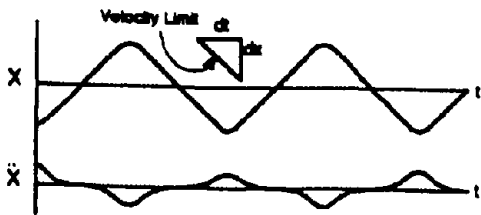


Figure 5. Triangulation of displacement wave form due to flow limits.

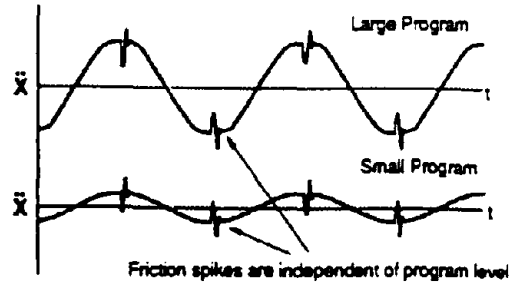


Figure 6. Effect of friction on acceleration waveform at high and low program levels.

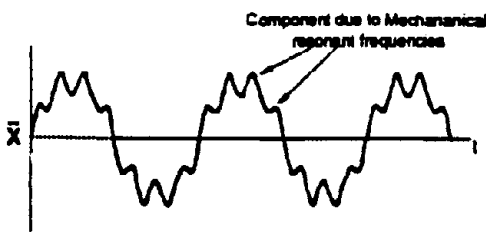


Figure 7. Distortion due to a mechanical resonant frequency

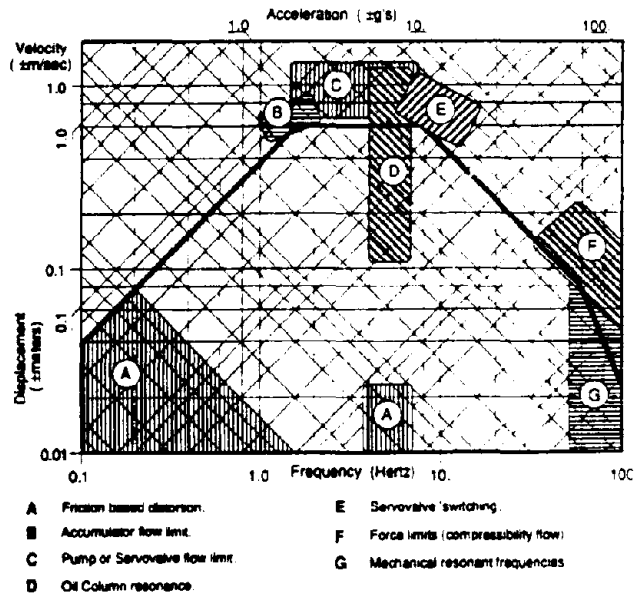


Figure 8. Performance envelope of a typical Seismic System showing regions of distortion.

SPECIAL LOADING SYSTEMS FOR EXPERIMENTAL RESEARCH

Stephen A. Mahin

**Department of Civil Engineering
Earthquake Engineering Research Center
University of California at Berkeley**

INTRODUCTION

The ease with which experimental research may be performed has improved markedly in recent years with the increased availability of electro-hydraulic actuator systems to impose forces and displacements, the greater reliability and accuracy of instrumentation, and the development of high speed, low cost data acquisitions systems. In most instances, experiments used to assess the quasi-static inelastic cyclic behavior of structures and structural components remain relatively simple. However, complications can arise due to the magnitude of the required loads and the need to test three dimensional test specimens. In other cases, quasi-static loading is not sufficient and loading histories more representative of the response of the specimen to actual earthquake ground motions are required.

In this paper, several recent examples of special testing arrangements used at Berkeley will be described. The first of these relate to simple tests of large single degree-of-freedom systems requiring the cyclic application of large lateral loads. Other tests requiring refined three dimensional control of the forces and displacements applied to a multiple degree of freedom specimen is then discussed. Extension of such on-line computer control techniques to the realistic simulation of dynamic aspects of seismic structural response are then briefly described.

CYCLIC PLANAR LOADING OF LARGE STRUCTURAL SYSTEMS

In most cases, planar tests of structural components and systems can be carried out in a simple manner. The specimen and actuator can be attached to a suitable reaction floor or frame, and the actuator can be used to impose the appropriate load or displacement history. However, in some cases the load required becomes so large that the size of the required reaction frame and actuators become excessive. While it is possible to build larger reaction and loading facilities, structural test demands can become correspondingly larger as well.

A special case requiring the test of a large and strong structure arose following the 1989 Loma Prieta earthquake. It was desirable to test a portion of the I-880 Cypress viaduct that partially collapsed in Oakland. This two level reinforced concrete structure utilized multi-celled box girders to support the upper and lower level roadways, and a two level, single span beam-column framework to support the box girders and to provide lateral resistance in the transverse direction. Tests were desired to assess the precise causes of the observed collapse of the upper level of the structure and to determine the efficacy of various retrofit schemes suggested for other double deck viaducts damaged in the San Francisco bay area.

Some of the methods considered for loading the viaduct are schematically illustrated in Fig. 1. These included the attachment of post-tensioning tendons to the deck

levels and using post-tensioning jacks to apply the lateral loads. Because cyclic loading was desired, tendons would have to be installed on both sides of the viaduct. Problems associated with this scheme related to the need for piles or other types of foundation to transmit the tendon force to the ground, and the need to anchor the tendons relatively far from the structure in order to minimize the vertical component of the tendon force on the structure. The congested urban setting of this structure precluded this simple approach.

Another approach considered the construction of a reaction frame as shown in the center portion of Fig. 1. This would allow the use of double acting electro-hydraulic actuators. However, the tests were estimated to require upwards of 4 million pounds of lateral force. The design of the foundations for the reaction frame in this case became very difficult. In particular, uplift forces were very large because of the desire to minimize the width of the frame. Because of the poor soil at the site, the reaction frame scheme was considered prohibitively expensive.

The strategy actually used in the tests is shown on the right hand side of Fig. 1. Because the failure occurred in the upper level, it was not viewed as essential to apply additional loads to the lower level. Similarly, it was not necessary to assess the contribution of the soil-foundation system to the lateral response. As a result it was possible to devise a self-equilibrating steel reaction frame within the structure. Large steel collars were attached around the base of the lower columns. Diagonal steel braces extended upwards from these collars (through holes punched in the lower deck) and joined just below the upper deck at a reaction block. Pairs of single acting (compression) oil jacks were installed on both sides of the reaction block. These transmitted force to loading blocks that were post-tensioned to the upper deck of the viaduct. Braces and oil jacks were installed on each side of a frame to preserve symmetry of loading of a frame. Three transverse frames were included in the test specimen, resulting in six diagonal braced bents and a total of twelve hydraulic jacks.

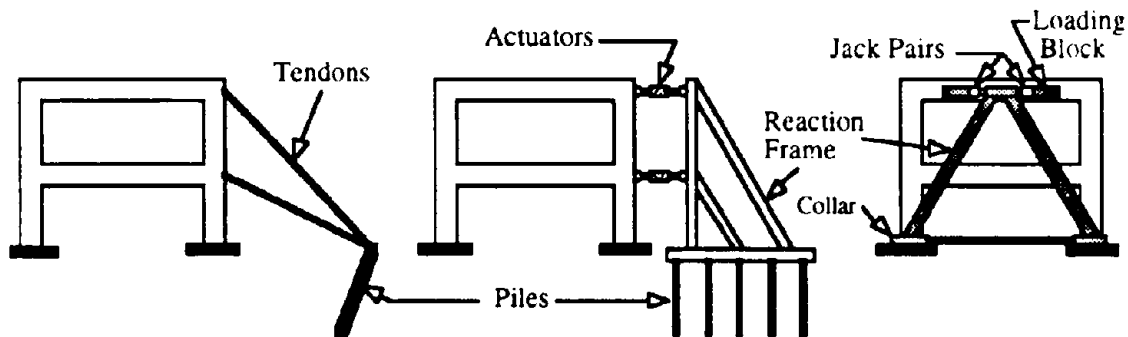


Fig. 1 Alternative Methods Considered for Field Testing of Viaduct

Simple oil jacks were utilized instead of double acting actuators in this case because of the time (and expense) required to special order the large number of relatively high capacity actuators required to develop the loads anticipated in this test. The oil jacks were easily available from local prestressing supply companies.

The oil jack arrangement could produce the cyclic loading required. For specimen motion to the left, the left jack would be extended (with the right jack retracted). For motion to the right, the jack on the right was extended. Relatively simple, manually operated hydraulic equipment was effectively employed to carry out the tests.

In another similar situation, a retrofit strategy for a building was to be evaluated. The existing structure contained a composite concrete/structural steel shear wall. A structural steel frame was provided to help carry gravity loads and seismic overturning forces, and the concrete infill and encasement was utilized to resist shear. Retrofit of the structure included thickening the concrete walls, filling in openings in the existing walls, adding shear transfer studs to the existing steel framing to enhance shear transfer between the steel frame and new concrete, and the addition of partial transverse confinement. Because of the complex stress transfer mechanism between the steel frame and the concrete and between the new and old concrete, it was desired to employ as large a scale as possible. Similarly, it was desirable to include as many bays and stories in the model as possible to minimize boundary condition effects where the specimen were attached to actuators and the reaction floor. It was, of course, not possible to test a model of the entire 15 story building. Thus, a portion of the structure was selected incorporating as many of the salient features as possible.

Several alternatives for specimen configuration and loading were considered. Ideally, a model would be constructed and attached with double acting actuators to an existing strong floor and reaction wall. This approach is shown in the left hand illustration of Fig. 2. The minimum one-third scale considered acceptable for these tests resulted in a large lateral load resistance. This load (in excess of 3,000 kips) could be developed by available laboratory actuators; however, the overturning moment developed resulted in excessively complex and expensive details for attaching the specimen to the reaction floor.

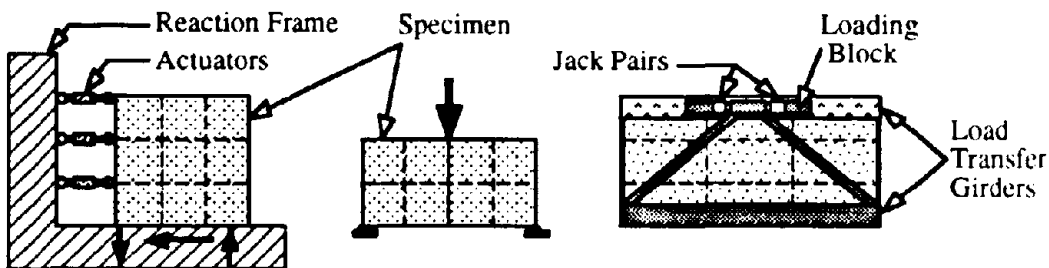


Fig. 2 Alternative Loading Arrangements Considered for Composite Wall Tests

Another option considered was to utilize a large capacity (4,000 kips) universal testing machine to load the specimen. In this case, the problem of resisting wall overturning moments could be resolved by doubling the size (height) of the specimen. In this case the wall would be tested as a simply supported beam, with its midspan representing the base of the wall in the prototype. While this option solved most of the problems encountered with the previous approach, it resulted in a specimen with twice the size without any apparent gain in useful information. In addition, for cyclic loading, it would be necessary to remove the specimen from the testing machine and invert it. Because instrumentation would have to be repetitively removed and re-installed each time the wall was flipped, the time required for testing made this option impracticable.

The option eventually employed for this test was adapted from the testing used for the Cypress viaduct (Fig. 1). A self-equilibrating frame was attached directly to the test specimen. The specimen selected was three bays wide and two stories tall, and constructed at one-third scale. Large composite steel and reinforced concrete load transfer girders were attached monolithically to the top and bottom of the test panels. Pairs of steel diagonal braces were attached to the lower transfer girder on each face of

the test specimen. Pairs of single acting oil jacks were attached to the reaction block at the top of the braces. These jacks transferred load to the specimen by means of a reaction block attached to the upper distribution beam. Operation of this test under cyclic loading was similar to that described previously for the Cypress viaduct.

CYCLIC LOAD TEST IN MULTIPLE DEGREE OF FREEDOM SPECIMENS

In multiple degree of freedom systems, additional complexity is introduced because of the need to determine the distribution of forces or displacements applied at each actuator. As a means of simplifying this problem, it is common to make the imposed loads or displacements a function of parameters measured at other locations during the test; thus, an invariant relative distribution of displacements or forces is often applied. In the case of inelastic response, it is usually preferable to control the force distribution, as localized damage to the structure could substantially alter the structure's deformed shape (e.g., the formation of weak stories). This test procedure can be implemented easily with conventional electro-hydraulic actuators by identifying one actuator as the master and setting the command signal for the other (slave) actuators to be a fraction of the force measured in the master actuator. Because of the possible instability of a structure tested into the inelastic range using force control only, most tests of this type would specify the displacement at the master actuator. The force in the master actuator would still be used to control the forces in the remaining actuators even though the master actuator is under displacement control. This arrangement is shown schematically in Fig. 3.

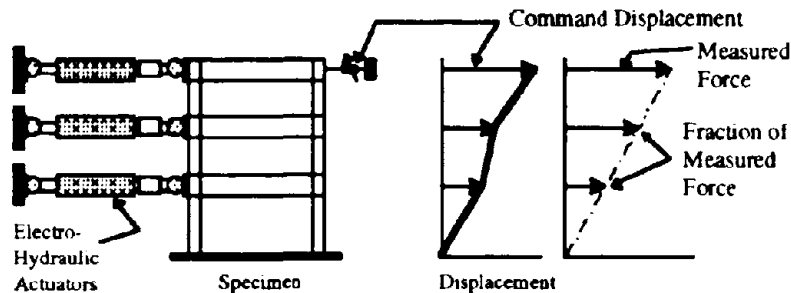


Fig. 3 Typical Planar Test of Multi-degree of Freedom System

When specimens are loaded in two or three dimensions, other complications arise. For example, consider the simple floor diaphragm in Fig. 4. Three actuators are attached to control the in-plane transverse, longitudinal and rotational motion of the diaphragm. If only longitudinal motion is required, elongation of only the longitudinal actuator will not produce the desired result. This is because of the arching action of the typically short length actuators. The in-plane rotation of the transverse actuators due to longitudinal actuator motion causes transverse motion of the specimen as shown in Fig. 4, along with transverse forces in the specimen. In addition, the displacement and forces measured in the longitudinal actuator will differ from those developed in the specimen in the undistorted longitudinal direction. These undesirable effects must be corrected for by lengthening of the transverse actuators.

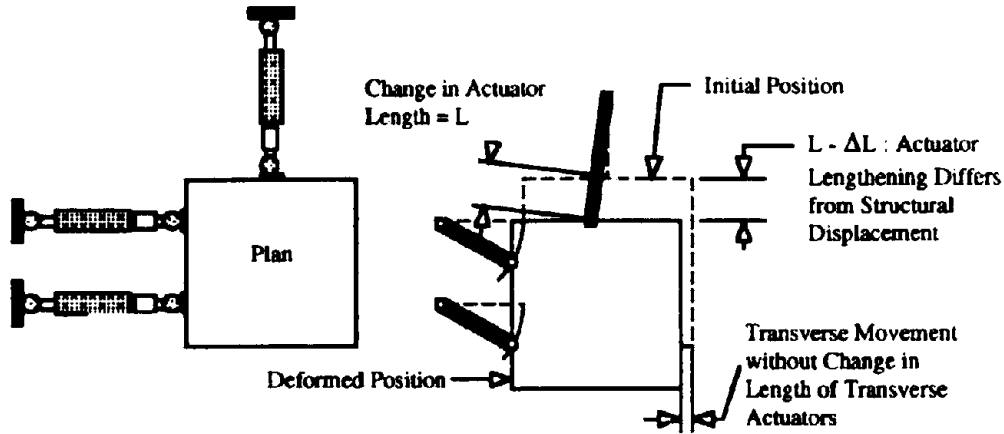


Fig. 4 Interaction of Actuator Displacements in Three Dimensional Tests

Under displacement control, the command displacement of an actuator in the above test setup should thus depend on the command displacement of the other actuators. The geometric corrections will depend on the test setup, and are usually straight forward to derive. However, they have in general a nonlinear form which is difficult to implement by simple analog manipulation of the control signals.

This nonlinearity does not introduce any special complication when the specimen will be subjected to predetermined displacement histories. Appropriate geometric manipulation of the displacement command signals can be made by digital computer (e.g., using a simple spreadsheet program) prior to the test.

Force readings in actuator load cells, must be processed similarly following a test to correct for the rotation of the actuators relative to the initial coordinate system of the specimen (see Fig. 5). The measured (or commanded) displacements are used (along with information on the actuator and structural configuration) to compute the forces along the structure's principal axes. At large displacements (and/or short actuator lengths) an actuator can induce significant forces along both of the principal axes of the specimen (P_x and P_y in the figure) and correction of the measured load cell force becomes essential.

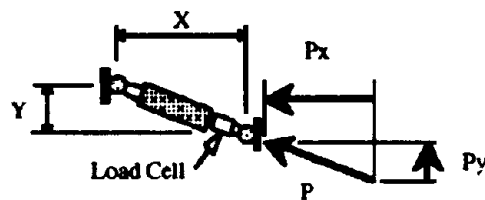


Fig. 5 Differences Between Forces Measured by Load Cell and Those Applied Along Specimen's Principal Axes

An example of such a test is that shown in Fig. 6. The prototype bridge structure supports an elevated roadway and an extended beam is required to contribute to the

transverse load resisting system through bending, shear and axial load. In the longitudinal direction of the roadway, the beam is also required to develop torsion when contributing to the lateral load resisting system. Testing of this outrigger was carried out considering horizontal motions of the deck in the transverse and longitudinal directions. The simplified test specimen used is shown in Fig. 6. A "cloverleaf" displacement pattern was specified at the tip of the column in the test specimen which results in simultaneous displacements in both principal directions. The ideal displacements were modified prior to the test to obtain command displacements corrected for geometric effects. A computer based function generator is used to send the corrected command signals (as voltages) to conventional analog servo-controllers.

An interesting feature of this test is that, in the transverse direction, the axial load in the column depends on initial gravity loads but varies due to overturning moment effects as a function of the transverse load applied. Simple considerations of statics were used to determine the appropriate axial load as a fixed fraction of the applied transverse lateral load (plus the initial gravity loading). This was implemented in the tests using simple analog summing amplifiers and analog circuitry.

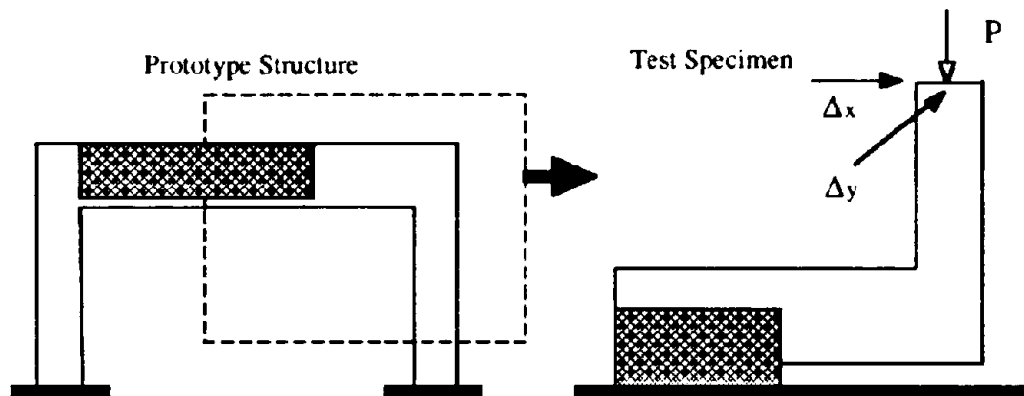


Fig. 6 Bi-directional testing of an Outrigger Bent Cap

This situation becomes more complex, if mixed force and displacement modes of actuator control are used. While the displacements in master actuators can still be pre-computed based on the desired specimen displacements at these locations, the corrections for the forces must be performed on-line during the test so that they can be used to specify the forces to be imposed at other levels. The transformation functions relating forces measured in the load cell and along the specimen's principal axes can be derived prior to the test, but they will change throughout the test as the displacements vary. More significantly, the displacements at the degrees of freedom under force control will not be known prior to the test, so measured displacements must be used during the test to determine the appropriate transformations between the desired force in a particular direction and the force measured in the load cell.

For reasonably small displacements and simple test configurations, it may be possible to utilize analog techniques to modify the loads to be applied to actuators in three dimensional tests. In other cases, the required transformations may be come sufficiently complex, and the displacements sufficiently large that digital procedures are necessary (or preferred). Relatively simple and low cost micro-computer based, control processors are available for single and multiple axis control. This may be implemented in such a manner that the digital controller makes the various transformations and carries

out the appropriate electronic control functions for the servo-control system. It can also be implemented in a more conventional analog control situation. In this case, the micro-processor repeatedly reads the displacements and forces at the actuators, makes the appropriate transformations and sends the command displacements or forces to conventional analog controllers.

PROOF TEST OF A DOUBLE LEVEL VIADUCT

An example of a test in which such digital control is used is shown in Fig. 7. In this case the lateral load resistance of a double deck viaduct was to be investigated. Earthquake-like motion in each principal plan direction was imposed quasi-statically using hydraulic actuators attached to rigid reaction frames post-tensioned to the laboratory strong floor. The columns in the prototype structure were assumed in design to be pinned at the base of the lower column and at the tip of the upper column. Considerations of asymmetry under lateral loading were used to isolate the test specimen from the remainder of the structure along the midspan of the deck in each direction. Roller supports were desired at these locations; they were implemented using vertical pin ended steel struts because of the significant uplift forces that could be developed.

A total of 10 hydraulic actuators were employed in the test. Lateral loads were applied to the top of the upper column and to the lower deck. Gravity loads were simulated in this one-third scale model using a combination of concrete and lead weights as well as vertically oriented hydraulic actuators. Because the finite length of the vertical support struts resulted in small vertical motions of the support points under lateral displacements, a specially designed vertical actuator was provided under the column to maintain the axial load in the column at a proper level. This actuator also compensated for inelastic elongation of the plastic hinge region in the lower column, and overturning moment effects due to transverse loading. A post-tensioning rod also extended up through the center of the column and was loaded with a hydraulic actuator at its top in order to maintain the column axial load at the proper level.

Because of the desire to simulate realistically the distribution of moment and shear in the transverse bent cap, two vertical actuators were used to load the bent cap at the interior webs of the box girder used for the bridge deck. In addition, to replicate the positive moment at the midspan of the bent cap due to dead load, a steel outrigger was cantilevered from the edge of the specimen and a constant vertical upward force was applied during the test.

At the lower deck level two actuators were used to impose specified displacements in the transverse direction and to limit torsion. A single displacement controlled actuator was used in the longitudinal direction at the deck level.

Two actuators were connected in a horizontal plane to the top of the column. The forces in these actuators were controlled rather than displacement as done at the lower level. If displacements were controlled at both levels, changes in deflected shape (that might occur as a result of concentrated yielding in one of the columns) could not be detected. In this case, the force in the upper level actuators was based on an assumed triangular mode shape, the ideal mass distribution at the two levels, and the column heights. For the test specimen, the force at the top level was 1.25 times the force applied at the lower level in the same direction. This actual force in the actuators were computed on-line during the test.

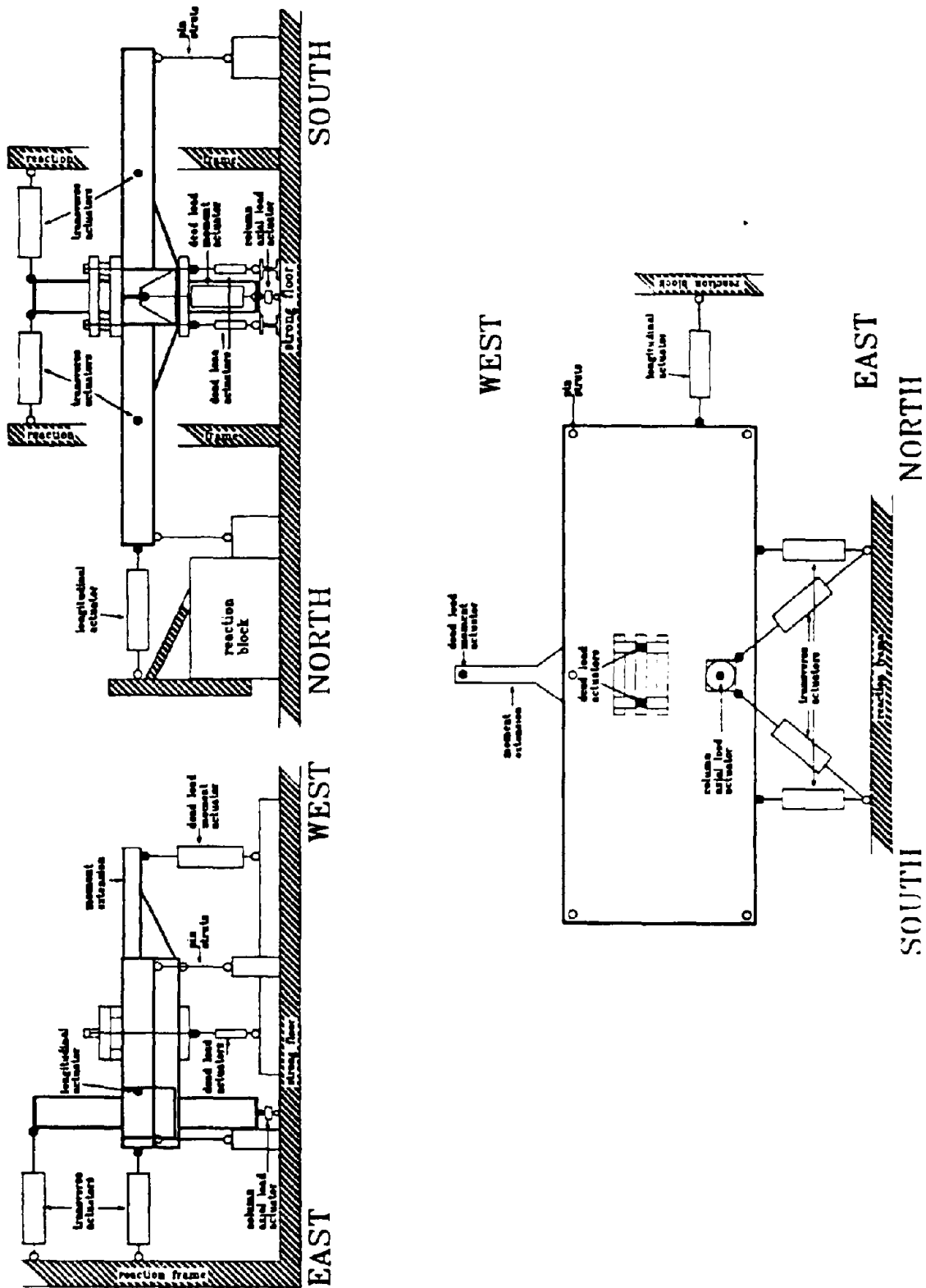


Fig. 7 Test Setup for Proof Test of Double Deck Viaduct

Because the actuators at the upper level were rotated with respect to the principal axes of the structure, a geometric correction was also applied. Since the top of the column displaces during the test, the geometric correction depended on the displaced configuration of the specimen at each step in the test. Furthermore, the forces measured in the load cells of the actuators attached to the lower deck were not oriented in the principal direction of the deck once the structure was subjected to large bi-directional motions. Thus, these forces were also corrected prior to being used to determine the lateral forces to be imposed at the top of the columns. The horizontal components of the forces imposed by the initially vertical actuators were also computed and used in the derivation of the forces to be applied at the upper level.

A dedicated high speed PC-based microprocessor was used to make these coordinate transformations and to control the specimen during the test. The microprocessor required continual input of the measured deck level actuator loads, the measured column top and deck level displacements. The control process was repeated approximately 7000 times per second. The microprocessor provided the actuator control apparatus with analog output signals for controlling the force at the top of the column.

A wide variety of loading histories were considered for the test. These included simple diagonal load paths, cloverleaf patterns and other sequences that would help identify the mechanical characteristics of the structure. The loading history selected is shown in Fig. 8.

Each step of loading was divided into three phases. In the first phase, the structure was subjected to a simple displacement cycle in the transverse direction (longitudinal displacement at the lower deck is restrained during this excursion) followed by a simple cyclic excursion in the longitudinal direction. The second phase involved two cycles of bi-directional loading in a square pattern; one clockwise and one counter clockwise. The maximum amplitude of the bi-directional excursion was the same as that for the uni-directional excursions; i.e., the projected displacement in the transverse direction was reduced to about 70% of that imposed during the unidirectional excursions. The third phase repeated the first phase so that deterioration of mechanical properties may be easily detected.

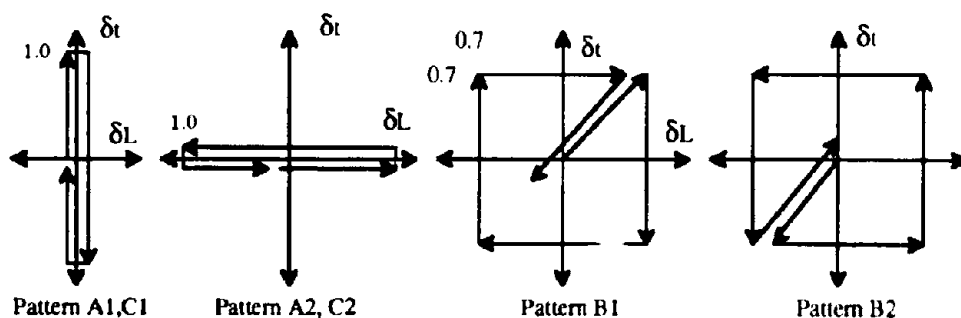


Fig. 8 Displacement History for Proof Test Specimen

The displacement history shown relates only to the lower level. The forces applied to the top of the column corresponded to those associated with the triangular mode shape and the forces required at the lower level to develop the specified displacements. Because of the complexity of bi-directional response, the upper column moved bi-directionally even under uni-directional displacements at the lower level.

PSEUDO-DYNAMIC TESTING

These on-line computer control tests can be extended to include hybrid analysis. The most common form of this form of testing in earthquake engineering is the so-called pseudo-dynamic test. In most current applications, the actuators are under displacement control. The control computer, in addition to making the various required geometric and other corrections, uses data obtained regarding the restoring force characteristics of the specimen at a particular instant in time to solve the governing equations of motion for a numerically specified ground motion. In this manner the dynamic response of the specimen can be simulated quasi-statically using conventional electro-hydraulic loading systems. Dynamic effects are simulated by the governing differential equations of motion in the computer, and the nonlinear restoring forces are determined 'continuously' from the specimen during the test.

Detailed discussion of these procedures, and their advantages and limitations, are beyond the scope of this paper. More complete description of these procedures may be found citations listed in Refs. 1 and 2.

CONCLUDING REMARKS

A wide variety of loading procedures are available for assessing the cyclic inelastic behavior of structures. Usual concerns relate to instrumentation, data acquisition and load/stroke capacity. In some tests special loading systems are required to develop and react the large forces required. In other cases, accurate measurement and control of structural response requires a variety of geometric and other corrections. Modern microprocessors make the execution of such tests simple, and allow for even more complex hybrid experimental analysis procedures, such as the pseudo-dynamic test method.

ACKNOWLEDGMENTS

The author is especially indebted to his colleagues Christopher Thewalt and Jack Moehle who participated significantly with him in the performance of the tests discussed in this paper. The author also gratefully acknowledges the financial support of the California Department of Transportation, the National Science Foundation, and EQE International. The views expressed in this paper are those of the author alone.

REFERENCES

1. Thewalt, C. and Mahin, S. " The Pseudo-dynamic Test Method: Numerical Aspects," *Experimental and Numerical Methods in Earthquake Engineering*, Ed. Donea, J. and Jones, P., Kluwer Academic Publishers, Boston, 1991.
2. Thewalt, C. and Mahin, S. " The Pseudo-dynamic Test Method: Verification and Extensions," *Experimental and Numerical Methods in Earthquake Engineering*, Ed. Donea, J. and Jones, P., Kluwer Academic Publishers, Boston, 1991.

AN EQUIVALENT SDOF METHOD OF INTERFACE MOMENT SIMULATION IN SUBSTRUCTURE PSD TEST

By Guo Mingchao¹, Tang Daixin² and Wu Zhensheng³

ABSTRACT

In this paper, an equivalent SDOF method of interface moment simulation in substructure PSD test is developed and verified by numerical test, and the summary and comment of other existing methods are also given.

INTRODUCTION

The pseudo dynamic (PSD) test using substructure techniques is called substructure PSD test herein. In detail, the whole structure is divided into two parts, one the part in which PSD test is performed and the other the part in which only numerical operation is performed, as shown in Fig.1. Generally, the test part is the weak part which will yield in advance under severe earthquake and its characteristics of restoring force is very complicated, while the rest belongs to the numerical operation part. This method not only can solve the basic problem of standard PSD test, but also be cheaper, especially for large scale and/or more complicated structure systems. Just like substructure calculation, however, at the interface between substructure and main structure, that is, between numerical operation part and PSD test part, the moment equilibrium and rotation compatibility must be satisfied, which is briefly called interface moment simulation in this paper. The interface moment simulation is clearly necessary for the structure coupling of

1. Lect. Dept. of Structure Engineering, Harbin Architectural and Civil Engineering Institute, China.

2. Prof. the same institute as that of No. 1.

3. Asso. Prof. the same institute as that of No. 1.

rotatory and translational interface degrees of freedom, it's also necessary for the structure of relatively simple shear type models, because the added axial forces caused by the overturning moment transferred from the upper part affect the characteristics of restoring forces of columns and walls directly. The interface moment simulation is easy for substructure calculation but very difficult for substructure PSD test, and becomes a key problem to be solved in this field.

The ideal of substructure PSD test has been existing since the standard PSD method was developed in 1970's. But there have been few examples of model test because of the difficulties of the interface moment simulation. There are some methods to simulate the interface moment, but they are too difficult to realize. In this paper, an equivalent SDOF method is developed and verified by numerical test.

SUMMARY AND COMMENT OF THE EXISTING METHODS

In all the existing methods, more than one actuators will be needed to simulate the interface moment as shown in Fig. 2. The formulae in the figures can show the principle of the methods. in which G is gravity, F_1 , F_2 are forces applied by actuators, M is overturning moment transferred from the upper part, V is lateral restoring force of the test part, and N is added axial force caused by M .

Method (a) is the most straightforward one and also the most difficult one to be realized in a real test. At present time there are some successful examples of PSD test of structural models with one or two-degree-of-freedom, but three-degree-of-freedom in method (a). In addition, the vertical or axial stiffness is very great. If the load is applied by controlling displacement, the integration time interval will be too small. If the load is applied by controlling force, the facilities and instruments could be damaged by large displacement due to structure deterioration. Method (b) is of two-degree-of-freedom and the axial load applied directly by actuators is avoided. However, the more

realistic loading method of actuator 1 is still one controlled by force, and the vertical load G have to be applied by special jacks or gravity load. Method (c) used in a column is of two-degree-of-freedom too. Actuator 1 applies load which can be either tension or compression, so the characteristic of restoring force of the whole structure can not be reflected correctly by the characteristic of a single column.

EQUIVALENT SDOF METHOD

Usually the seismic response of a structure is governed by first mode, so that many problems in earthquake engineering have been solved simply depending on the first mode, for example, in the bottom-shear-force-method to determine horizontal earthquake action, in the equivalent SDOF PSD method for MDOF systems, etc. If the distribution of magnitude of horizontal earthquake force along the height of analysed structure is given, the magnitude and position of resultant can be determined, and the lateral force can be applied at the resultant position, which can not only solve the problem mentioned above, but also simplify the problem greatly. In fact the magnitude of horizontal earthquake action at each floor changes stochastically, so that the magnitude and position of resultant is uncertain. But if the structure being analysed is looked upon as one that its vibration of seismic response is governed by first mode, the problem can be solved approximately. The corresponding method is called equivalent SDOF method in this paper. The following is a detailed introduction.

First, to determine the resultant position of horizontal earthquake action. As a discussion of basic method, only the elastic state of a structure is concerned. The height H from the interface to the resultant position is

$$H = \frac{\sum_{i=1}^n F_i H_i}{\sum_{i=1}^n F_i} = \frac{\sum_{i=1}^n m_i \omega_1^2 X_{i1} H_i}{\sum_{i=1}^n m_i \omega_1^2 X_{i1}} \quad (1)$$

where, m_i is the mass of i th floor, ω_1 the first frequency of the structure, X_{i1} the first mode vector, and H_i the height from interface to i th floor.

Formula (1) is valid for free vibration of the first mode. For forced vibration, if the structure vibration is governed by first mode, formula (1) will be an approximate expression. If the period of external force is equal or nearly equal to the first period of the structure, there will be a better approximation. For seismic response, if the predominant period of earthquake wave is equal or nearly equal to the first period of the structure, there will be a good approximation.

Second, to add part A with height of H on the test part. There are three possible methods to build this part. The first one is to build model according to the same part of prototype. The second one is to build a loading frame, which is much cheaper. The third one is to combine the two methods mentioned above, that is, partly model and partly frame.

Third, to apply lateral force at the resultant position. The lateral force is applied by controlling the lateral displacement $x(t)$ that is at the level of the interface. The resistant force $F(t)$ will be the restoring force of the test part, and the overturning moment at the interface $M(t)$ is

$$M(t) = F(t) \times H \quad (2)$$

NUMERICAL TEST

The feasibility of the equivalent SDOF method has been verified by numerical test of a two-story shear type steel frame.

The calculation skeleton of the frame is shown in Fig.4, and the natural parameters of the frame are shown in Tab.1.

The central difference method(CDM) is used, and the calculation starts as follows:

$$x(-\Delta t) = x(0) - \Delta t \dot{x}(0) + 1/2 \Delta t^2 \ddot{x}(0) \quad (3)$$

in which $\ddot{x}(0)$ can be obtained from the basic dynamic formula:

$$\ddot{x}(0) = m^{-1} (f(0) - c\dot{x}(0) - kx(0)) \quad (4)$$

where x , \dot{x} , \ddot{x} , f are vectors of displacement, velocity, acceleration and horizontal disturbing force respectively, Δt is time interval of integration, M , K , C are matrixes of mass, stiffness and damping respectively. Giving initial values of $x(0)$ and $\dot{x}(0)$, the calculation of CDM can be started.

For time-history calculation of the two-degree-of-freedom system, the formula of overturning moment at the level of inflexion points of the column of the first story is

$$M(t) = m_1 (\ddot{x}_1(t) + \ddot{x}_g(t)) \times 0.265 + m_2 (\ddot{x}_2(t) + \ddot{x}_g(t)) \times 0.975 \quad (5)$$

where, $\ddot{x}_g(t)$ is seismic ground acceleration, and the footnotes 1 and 2 are the signs of first floor and second floor respectively.

For numerical calculation of the equivalent SDOF of substructure PSD method, supposing that the first story is the test part and the second story is the numerical operation part, the formula of overturning moment at the level of inflexion points of the first story is

$$M(t) = F(t) \times 0.720 \quad (6)$$

It should be explained that in this example the formula is valid only at the level of inflexion points, not at the level of the interface between first story and second story, because the

purpose of the example is to verify the feasibility of the equivalent SDOF. If the formula is given at other level of inflexion points the results of the simulation should be the same.

The input earthquake wave is EL Centro, Calif. 1940.5.18 NS, and the predominant period of the wave is 0.245 second. The results of the numerical test are shown in Fig.5. It can be seen clearly that if the predominant period of the wave is equal to the first period of the structure, the equivalent SDOF method can give a good approximate simulation.

CONCLUSIONS

The method developed in this paper named equivalent SDOF method is a simple and effective one. The results of the numerical test show that if the predominant period of input seismic wave is equal or nearly equal to the first period of the structure, the method can give a good approximate moment simulation.

REFERENCES

1. Masayoshi Nakashima and Hidehiro Takai, Use of Substructure Techniques in Pseudo Dynamic Testing, Building Research Institute Ministry of Construction, March, 1985.
2. Stavros N. Dermitzakis and Stephen A. Mahin, Development of Substructuring Techniques for on-line Computer controlled Seismic Performance Testing, UCB/EERC-85/04, Earthquake Engineering Research Center College of Engineering University of California Berkeley, California, February, 1985.
3. Guo Mingchao and Tang Daixin, The Pseudo Dynamic Testing Method Using Substructuring Techniques, Journal of Harbin Architectural and Civil Engineering Institute, June, 1991.

Tab.1 Natural Parameters of the Frame

m_1	m_2	k_1	k_2	T_1	T_2
$\left(\frac{N}{m/s^2}\right)$	$\left(\frac{N}{m/s^2}\right)$	$\left(\frac{KN}{m}\right)$	$\left(\frac{KN}{m}\right)$	(s)	(s)
2500	2500	22×10^3	17×10^3	1.133	0.456

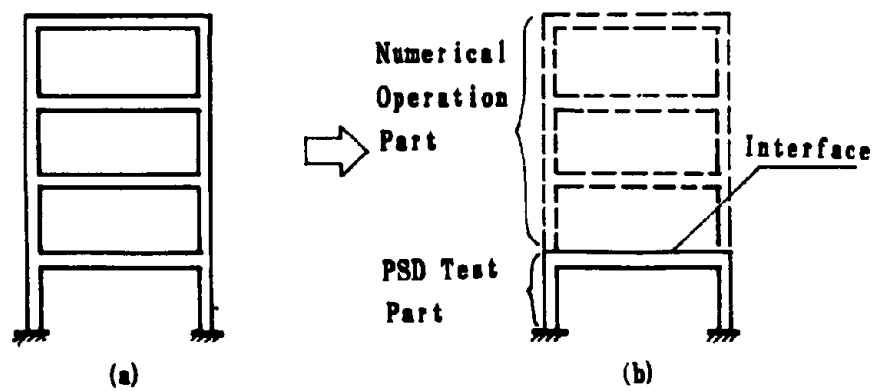


Fig.1. Idea of Substructure PSD Test

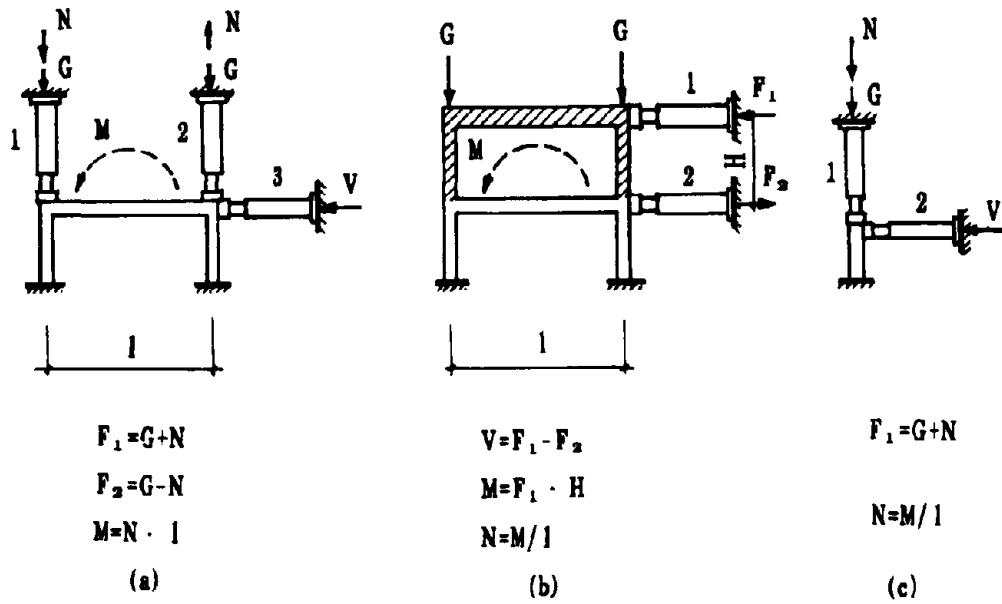


Fig. 2. Existing Methods of Interface Moment Simulation.

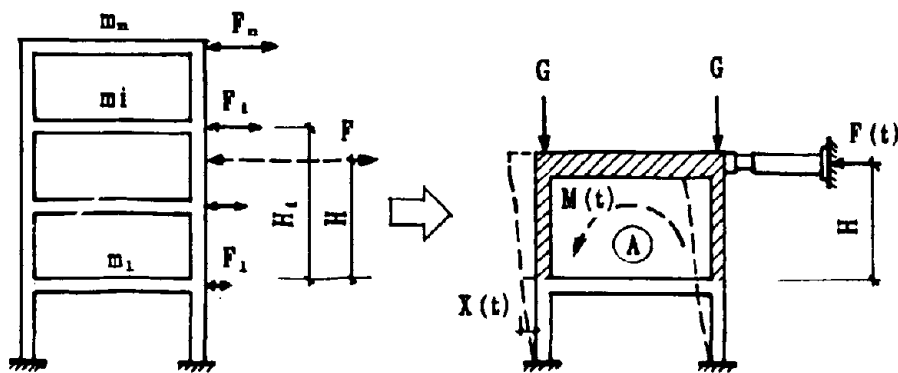


Fig. 3 Equivalent SDOF Method

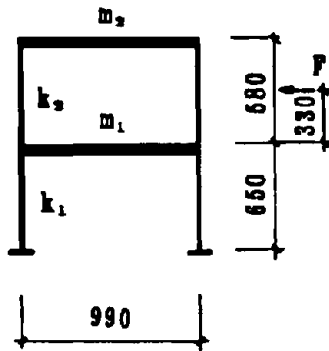
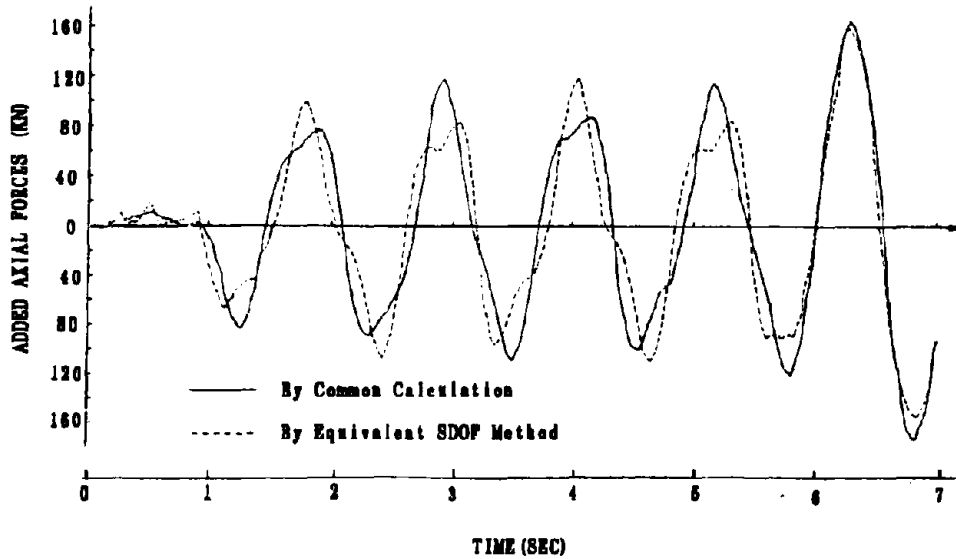
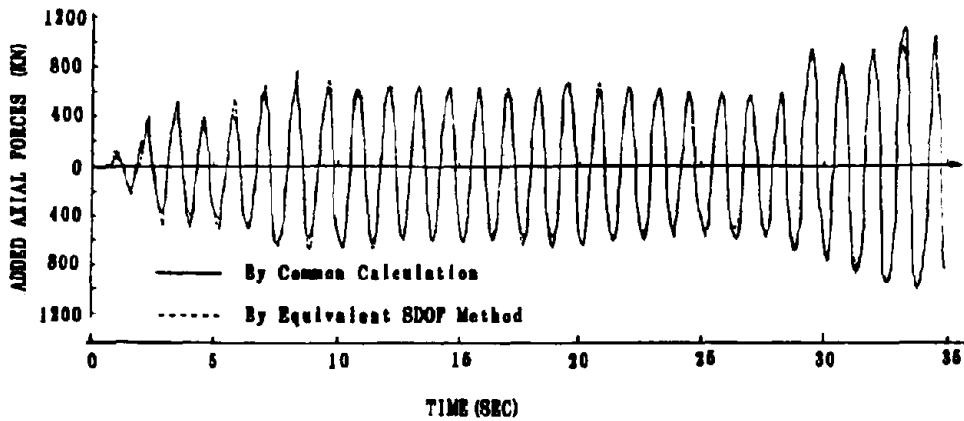


Fig. 4 Skeleton of the Frame



(a) The Predominant Period of the wave is 0.246sec.



(b) The Modified Predominant Period of the wave is 1.1sec.

Fig. 5 Added Axial Forces of the Frame

CYCLIC LOADING HISTORIES FOR SEISMIC EXPERIMENTATION ON COMPONENTS OF STRUCTURES

**Helmut Krawinkler
Department of Civil Engineering
Stanford University
Stanford, CA 94305**

INTRODUCTION

Much experimental work on structural components and subassemblies has been done in recent years in laboratories of universities, government, and industry, directed towards achieving a better understanding of the response of structures to seismic excitations. Most commonly, these experiments are performed with quasi-static cyclic load application. In these experiments the selection of loading histories and presentation of test results have always been central issues, since no general guidelines exist and decisions are made usually in a subjective manner. This has raised many questions in interpretation of experimental results and has made a consistent assessment of seismic performance of components of steel structures a difficult task.

This paper suggests guidelines for the selection of loading histories that can be employed in most quasi-static experiments whose purpose it is to assess the seismic performance of components and subassemblies as parts of structures that may be subjected to earthquake ground motions of different severities. This implies that strength and stiffness characteristics and their history dependent variation (e.g., cyclic hardening, softening, deterioration, etc.) are of primary interest. In particular, the following questions are addressed:

- How many cycles, what deformation amplitudes, and what sequence of cycles should be employed to evaluate seismic performance?
- How can the results of one experiment under a predetermined loading history be generalized so that conclusions can be drawn on the response of the same component under different loading histories?

Central to the issue of loading history and performance evaluation is the recognition that damage in a component is cumulative and the level of damage depends not only on the maximum deformation but also on the history of deformations (or loads) the component undergoes before and after the occurrence of the maximum deformation. Thus, cumulative damage concepts have to be utilized to assess performance, and loading histories in experiments must account for the history dependence of seismic performance.

CUMULATIVE DAMAGE ISSUES

The purpose of experiments is to evaluate seismic performance of components as parts of structures. Adequate performance implies that a component fulfills a set of specified performance requirements. These requirements may be based on strength and stiffness characteristics, deformation capacity, energy dissipation characteristics, or any combination thereof. For a component this implies that its role within a structure needs to be identified

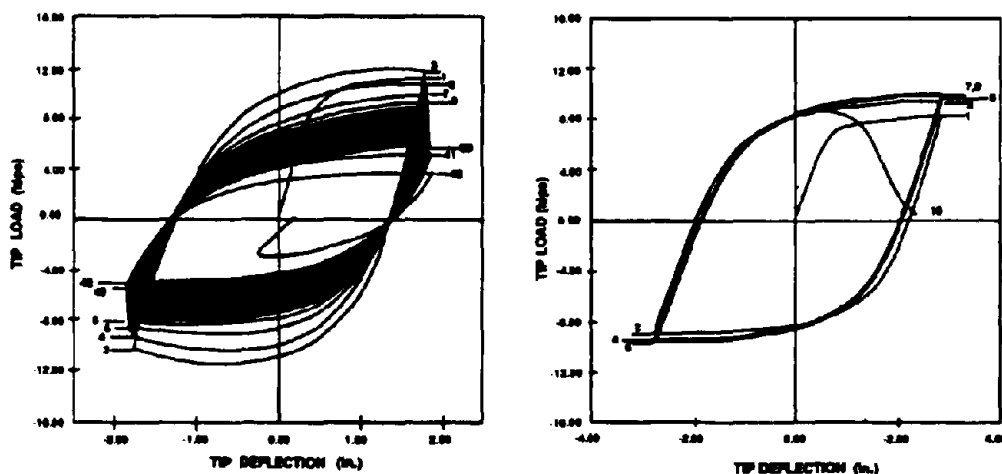
and its **capacities** (strength, deformation, and energy dissipation capacities) as well as the **demands** imposed by earthquakes need to be quantified. The emphasis here is on performance in severe earthquakes in which deterioration and safety against failure become overriding considerations, and adequate performance implies that the capacities exceed the imposed demands with an adequate margin of safety.

An experiment can provide only information on capacities, but due consideration can be given to demand issues by utilizing loading (deformation) histories that account for general demand characteristics. In seismic problems capacity and demand cannot be separated since one may strongly depend on the other. Therefore, single capacity parameters, such as maximum deformation or maximum ductility ratio, will provide inadequate descriptions of capacity unless all other important demand and capacity parameters are considered in the loading history applied to the test specimens and in the test evaluation.

Because of the randomness of the seismic demands and the dependence of the capacities on the demands, a single test or even a series of tests may not provide all the information needed for seismic performance assessment. Thus, the choice of testing programs and loading histories should be guided by the objective to maximize information and minimize complexities that will complicate test evaluation. The following summary on important issues of capacity and demand is intended to provide the background which forms the basis for selecting the testing programs and loading histories suggested in this paper..

Seismic Capacities

Basic seismic capacity parameters for a component are strength, stiffness, inelastic deformation capacity, and cumulative capacity parameters such as energy dissipation capacity. All these parameters are expected to deteriorate as the number of damaging cycles and the amplitude of cycling increases. The type of deterioration depends on the failure mode of the component. Figure 1 illustrates typical examples of deterioration for two distinctly different failure modes; **slow deterioration** (of strength and/or stiffness), typical of local buckling modes in steel structures, Fig. 1(a); and **rapid deterioration** of strength, typical of fracture modes of failure, Fig. 1(b).



(a) Slow Deterioration

(b) Rapid Deterioration

Fig. 1. Different Modes of Deterioration and Failure

Each mode of deterioration and failure has its own characteristics that may affect the choice of testing program and loading history. For instance, a failure mode exhibiting the rapid strength deterioration illustrated in Fig. 1(b) is usually caused by local imperfections that lead to material fracture. The characteristics of these imperfections may have considerable scatter and, therefore, the level at which deterioration occurs is uncertain. Thus, little confidence can be placed in the results from a single test, particularly since a clear margin of safety must be established for a failure mode with rapid strength deterioration.

Generic loading histories, which are to be applied to different specimens with different failure modes, represent a compromise that is based on important performance characteristics that are common to all specimens tested. The testing programs and loading histories recommended later are based on a general cumulative damage concept of the following characteristics:

1. Every excursion in the inelastic range causes damage in a component. Damage implies that macro- or micro-structural changes occur, which causes visible or invisible deterioration of strength and stiffness properties and brings the component closer to failure.
2. The component has a memory, i.e., the damage from inelastic excursions is cumulative.
3. Large excursions cause much larger damage than small excursions.
4. The relative amount of damage caused by an excursion depends on the plastic deformation range of the excursion, $\Delta\delta_p$, the mean deformation of the excursion (a measure of symmetry with respect to the undeformed configuration), and the sequence in which large and small excursions are applied to the component (sequence effects).
5. For a given deformation amplitude the damage is largest for a symmetric excursion since this results in the largest possible plastic deformation range.
6. The importance of sequence effects has not yet been established through research, and the sequence of large versus small excursions in a component of a structure subjected to a severe earthquake does not follow any consistent pattern. Thus, sequence effects cannot be considered in the recommended loading histories.
7. As a consequence, the number of inelastic excursions, N , and their plastic deformation ranges (or, for symmetric excursions, their deformation amplitudes), as well as the sum of the plastic deformation ranges, become the primary capacity parameters for loading histories.

Krawinkler et al. (1983) present an extensive discussion of the issues raised here and many others of interest in seismic testing and performance evaluation of structural steel components.

Seismic Demands

The demands imposed by a severe earthquake on a structural component depend on the configuration of the component within a structure, the strength and elastic as well as inelastic dynamic characteristics of the structure, and the seismic input to which the structure may be subjected. For generic components none of these variables is well defined

or narrowly bracketed. For frame structures the best mediator between component demand and seismic input appears to be the interstory drift in structures, since this parameter can usually be related to the component deformation, and the demand on this parameter can be assessed from simplified dynamic models. Although there is no definite relationship between interstory drift in multistory structures and the deformation demand in single degree of freedom (SDOF) systems, the latter is often used to estimate the former.

In the context of developing loading histories with due consideration to seismic demand, general conclusions can be drawn from studies on SDOF systems. This discussion is based on a statistical study reported by Nassar and Krawinkler (1991) on bilinear and stiffness degrading SDOF systems subjected to a set of 15 Western U.S. earthquake ground motions. The shape of the average elastic response spectrum of these records closely resembles the shape of the ATC 3-06 ground motion spectrum for $A_a = A_v$ (Applied Technology Council (1978)). This study provides, amongst others, statistical information on demand parameters for inelastic systems with ductilities of 2 to 8. This information, which in part is summarized next, forms the basis for the recommendations on loading histories given later. In the interpretation of the quantitative information presented here it must be considered that the 15 records used in this study (a) are from earthquakes whose magnitude varies from 5.7 to 7.7, (b) have strong motion durations that vary significantly, and (c) represent ground motions at stiff soil sites (soil type S_I).

Number of Inelastic Excursions, N . This parameter increases with a decrease in period T of the system; the rate of increase being very high for short period systems (exception: $T = 0.1$ sec.). The dependence of the mean value of N on T and the ductility ratio μ is illustrated in Fig. 2.

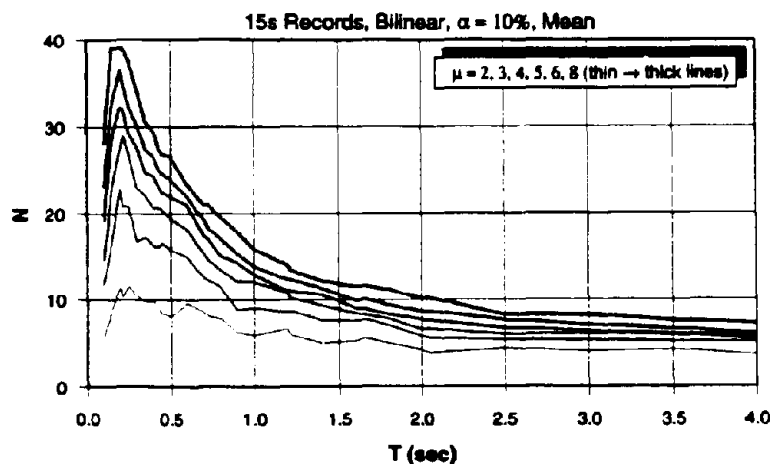


Fig. 2. Dependence of Mean Number of Inelastic Excursions on Natural Period and Ductility Ratio (Bilinear SDOF Systems with 10% Strain Hardening)

Individual Plastic Deformation Ranges, $\Delta\delta_{pl}$. The magnitudes of the plastic deformation ranges of the inelastic excursions can be represented by a lognormal distribution. Large plastic deformation ranges are rare events, and small ones are very frequent. The median of the plastic deformation ranges in an earthquake is usually less than 15% of the maximum (Hadidi-Tamjed, 1987).

Sum of Normalized Plastic Deformation Ranges, $\Sigma\Delta\delta_{pi}/\delta_y$. This parameter is used here as the basic cumulative damage parameter. For bilinear systems it is equal to the dissipated hysteretic energy normalized by $F_y\delta_y$. Similar to N , this parameter depends strongly on the period T and the ductility ratio μ . The dependence of the mean value of this parameter on T and μ is illustrated in Fig. 3.

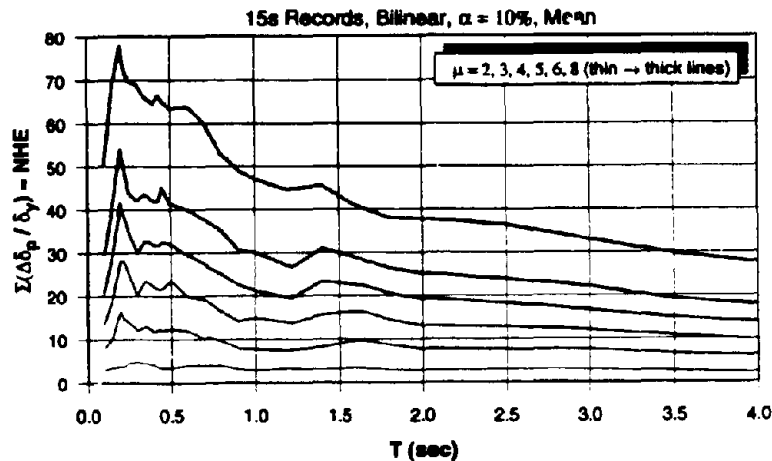


Fig. 3. Dependence of the Mean of the Sum of Normalized Plastic Deformation Ranges ($\Sigma\Delta\delta_{pi}/\delta_y$) on Natural Period and Ductility Ratio (Bilinear SDOF Systems with 10% Strain Hardening)

This brief summary shows the significant dependence of the demand parameters on the natural period of the structure of which the component is part. For generic test specimens the need exists to base these parameters on short period structures, with the understanding that their values may be very conservative for long period structures. It is to be recognized that cyclic demands for structures depend on a great number of variables, and a unique loading history will always be a compromise, but one that should be conservative for most practical cases. It also needs to be considered that the values shown in Figs. 2 and 3 may be low for earthquakes of large magnitudes (because of longer durations) and high for earthquakes in regions of lower seismicity.

The information summarized here can be utilized to develop loading histories that represent demand characteristics in "single specimen testing programs". In many cases such a testing program may be inadequate, since it does not permit an explicit assessment of cumulative damage. For the latter purpose a more comprehensive testing program is needed ("cumulative damage testing program") that permits the determination of structural performance parameters, which, together with a cumulative damage model, can be utilized to evaluate performance under arbitrary seismic excitations. Such a testing program will depend on the damage model that represents the failure mode under study. Presented next are two cumulative damage models that have been used in different studies to represent damage accumulation in steel and reinforced concrete components.

Cumulative Damage Model

Many models for cumulative damage assessment of components subjected to seismic excitations have been proposed in the literature. Most of them use either the plastic deformation range or the dissipated hysteretic energy per excursion (or cycle) as the basic demand parameter. The simplest model of this type is one that is based on the two

hypotheses of a Manson-Coffin relationship and Miner's rule (Krawinkler et al. (1983)). The first hypothesis postulates that for constant amplitude cycling the number of excursions to failure, N_f , and the plastic deformation range, $\Delta\delta_p$, (total deformation range minus elastic deformations) are related by the following equation:

$$N_f = C^{-1}(\Delta\delta_p)^{-c} \quad (1)$$

In this equation C and c are structural performance parameters that have to be determined experimentally. The equation implies that on a log-log plot the relationship between N_f and $\Delta\delta_p$ is linear.

The second hypothesis is Miner's rule of linear damage accumulation, which postulates that the damage per excursion is $1/N_f$, and that the damage from excursions with different plastic deformation ranges, $\Delta\delta_{pi}$, can be combined linearly. Thus, the total damage D is given by the equation

$$D = C \sum_{i=1}^N (\Delta\delta_{pi})^c \quad (2)$$

If this hypothesis were accurate, a total damage of $D = 1.0$ would constitute failure. Because of the known shortcomings of Miner's rule (neglect of mean deformation and sequence effects) and the scatter in the structural performance parameters C and c , the limit value of damage that constitutes failure cannot be expected to be exactly 1.0. Krawinkler et al. (1983) provide an extensive discussion of all the issues associated with this damage model.

Pilot tests (Krawinkler et al. (1983)) have shown that this model gives good predictions for various failure modes (local buckling, crack propagation and fracture at weldments) in steel structures, and that the exponent c is a rather stable parameter whereas the coefficient C exhibits considerable scatter. Provided that sufficient experimental data on the two structural performance parameters can be obtained experimentally, it becomes a matter of analysis to predict performance under various levels of ground motions which will impose different demands (N and $\Delta\delta_{pi}$)

In reinforced concrete a widely used damage model is that proposed by Park and Ang (1985). In this model damage is expressed as follows

$$D = \frac{\delta_m}{\delta_u} + \frac{\beta}{Q_y \delta_u} \int dE \quad (3)$$

in which

- D = damage index ($D > 1$ indicates excessive damage or collapse)
- δ_m = maximum deformation under earthquake
- δ_u = ultimate deformation capacity under static loading
- Q_y = calculated yield strength
- dE = incremental hysteretic energy
- β = parameter accounting for cyclic loading effect

This model also contains structural performance parameters (δ_u , β) that need to be determined experimentally.

TESTING PROGRAMS AND LOADING HISTORIES

The choice of testing program and associated loading history depend on the purpose of the experiment (research or seismic verification) and the type of anticipated failure mode (i.e., rapid or slow strength deterioration).

Single Specimen Testing Program - Multiple Step Test

This is the recommended testing program if only one specimen is available, the monotonic load-deformation response can be predicted with good confidence, the rate of strength deterioration is slow, and analytical cumulative damage modeling is not part of the investigation. This testing program should not be used if the rate of strength deterioration is rapid (see Fig. 1(b)) and the level at which this deterioration occurs may exhibit considerable scatter.

Since sequence effects cannot be evaluated in a single test, the suggested loading history consists of a series of stepwise increasing deformation cycles (**Multiple Step Test**) as illustrated in Fig. 4. In this history the cycles should be symmetric in peak deformations unless the strength is very different in the two directions. The history is divided into steps and the peak deformation of each step j is given as δ_j , a predetermined value of the "deformation" control parameter. The only exception is the first step, which should be performed in the "elastic" range and may be controlled by load rather than deformation. The number of "elastic" cycles should be large enough to obtain stable and reliable values of stiffness properties. It may be advisable to perform two steps of "elastic" cycles, at about $0.5\delta_y$ and $0.75\delta_y$, particularly for reinforced concrete components.

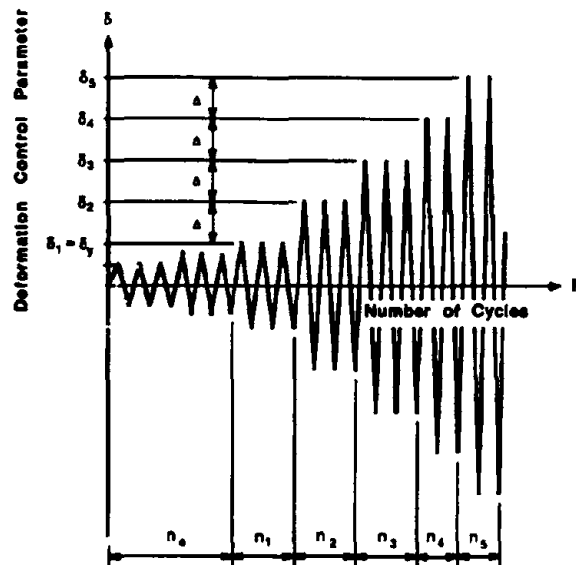


Fig. 4 Loading History for Multiple Step Test

At and beyond yielding, several cycles should be performed during each step. The step increment Δ may depend on the anticipated deformation demand, but for components whose ductility ratio is close to the story drift ductility ratio an increment of $\Delta = \delta_y$ is recommended. It may be advisable to perform small amplitude cycles after each or some of the steps in order to evaluate stiffness degradation.

In the loading history for such a test the primary parameters are the number of inelastic excursions, N , the magnitude of the plastic deformation range of each inelastic excursion, $\Delta\delta_{pi}$, the sum of the plastic deformation ranges, $\Sigma\Delta\delta_{pi}$, and the maximum ductility ratio that will be experienced in the earthquake for which performance is to be evaluated. In order to render a test useful for generic specimens, the last parameter must remain a variable to be addressed in performance evaluation, and the other three parameters should be determined so that the loading history represents the seismic demand for the full range of practical ductility ratios.

Based on these requirements and the discussion in the previous section, the following arguments are used here to establish a loading history:

1. It is assumed that the seismic demand for the interstory drift in complex structures can be represented by the response of bilinear SDOF systems.
2. The loading history should represent a "reasonable and generally conservative" demand on N , $\Delta\delta_{pi}$, and $\Sigma\Delta\delta_{pi}$ for the full range of practical story drift ductility ratios. Since both N and $\Sigma\Delta\delta_{pi}$ depend strongly on the period of the structure of which the component is part, the demands need to be established for short period structures for which the demands are high. SDOF systems with periods of 0.2 and 0.5 seconds were selected to benchmark these demands.
3. "Reasonable and generally conservative" implies that the total number of inelastic excursions, N , should be represented in average, and that the cumulative plastic deformation range, $\Sigma\Delta\delta_{pi}$, should be represented conservatively. Consideration should also be given to the fact that small inelastic excursions are much more frequent than large ones.

The loading history shown in Fig. 4 comes close to fulfilling these requirements as is illustrated in Table 1. This table shows, for three selected periods T and different ductility ratios μ , representative values of predicted SDOF seismic demands (mean values and mean plus standard deviation σ of N and $\Sigma\Delta\delta_{pi}/\delta_y$ deduced from the data given in Nassar and Krawinkler (1991)). Also shown are the corresponding values obtained from the loading history presented in Fig. 4, with the increment in peak deformation, Δ , being equal to the story yield displacement δ_y . The third part of the table illustrates how conservative the loading history is for components in long period structures.

Table 1 shows that for all periods and all ductility ratios the experimentally executed $\Sigma\Delta\delta_{pi}/\delta_y$ is greater than the predicted mean + σ , whereas the experimentally executed number of inelastic excursions in the period range from 0.2 to 0.5 seconds is smaller than the predicted mean. The reason for this disparity is that in earthquakes short period structures experience a large number of small inelastic excursions and a small number of large inelastic excursions, whereas in the recommended loading history the magnitudes of inelastic excursions are distributed more uniformly. The argument for replacing in experiments the many small excursions by a few larger excursions is that the total number of cycles that have to be performed in an experiment is reduced but the cumulative damage effect, represented by $\Sigma\Delta\delta_{pi}/\delta_y$, is still simulated conservatively. It is left to the judgment of the experimentalist to modify the loading history and simulate the expected number of inelastic excursions more accurately. It should be considered that the predicted values are from U.S. West Coast earthquakes with magnitudes between 5.7 and 7.7 and for stiff site soil conditions. For larger earthquakes with longer strong motion duration and soft soil sites the number of inelastic excursions as well as the cumulative plastic deformation ranges

may be considerably larger. On the other hand, for smaller magnitude earthquakes in regions of lower seismicity the opposite may be true. Thus, modifications to the recommended loading history may be in order if much larger or smaller seismic demands are anticipated.

Table 1. Predicted and Experimentally Executed Demands

Period T	Max. μ	N = number of inelastic excursions			$\Sigma \Delta \delta_{pi} / \delta_y$ = sum of pl. def. ranges		
		mean	mean + σ	experim.	mean	mean + σ	experim.
0.2	2	12	19	6	4	7	11
	4	28	42	16	28	41	57
	6	36	55	24	54	76	127
	8	39	59	32	78	109	229
0.5	2	8	12	6	3	5	11
	4	19	30	16	23	36	57
	6	24	35	24	41	64	127
	8	26	38	32	64	97	229
2.0	2	4	7	6	3	4	11
	4	7	10	16	13	20	57
	6	9	12	24	25	36	127
	8	10	14	32	38	52	229

More than one cyclic test is needed if performance evaluation cannot be based with confidence on the results of a single test. This is the case for specimens that exhibit the behavior shown in Fig. 1(b). The illustrated response comes from a beam specimen in which failure was caused by crack propagation and fracture at a beam flange weld (Krawinkler et al. (1983)). Although crack propagation occurred relatively early in the cyclic history, it did not lead to a noticeable deterioration until unstable crack growth occurred and the weld fractured suddenly, leading to a rapid deterioration in strength. Crack initiation and crack growth at weldments are phenomena that are greatly affected by workmanship and their characteristics may exhibit considerable scatter. For instance, in the test series from which Fig. 1(b) was obtained, three identical specimens cycled at the same deflection amplitude failed after 8, 14, and 15 cycles, respectively, and two other identical specimens cycled at a smaller deflection amplitude failed after 46 and 92 cycles, respectively. If only a single test had been performed, the performance evaluation would have led to misleading results. In such a case, several identical multiple step tests need to be performed or a cumulative damage testing program needs to be carried out.

Cumulative Damage Testing Program

A special testing program is needed if a cumulative damage model is to be developed for the purpose of assessing seismic performance of the component under arbitrary loading histories. A cumulative damage model may be utilized to evaluate the cumulative effect of inelastic cycles (or excursions) on a limit state of acceptable behavior. This limit state may be associated with excessive strength deterioration or other measures of damage tolerance. A cumulative damage model is based on a damage hypothesis and may include several structural performance parameters. The validity of the hypothesis and the values of the performance parameters have to be determined experimentally. This requires a multi-specimen testing program whose details depend on the type of damage model and failure mode to be investigated.

If the cumulative damage model given by Eq. (2) is appropriate, at least three constant amplitude tests on identical test specimens are needed in order to obtain values for the performance parameters C and c and to verify that the relationship given by Eq. (1) represents reality with sufficient accuracy. For each test a new specimen must be used since each specimen is to be tested to failure. The deformation amplitudes for the three tests should be selected so that they cover the range of interest for performance assessment.

Additional constant amplitude tests need to be performed if strength deterioration is caused by a failure mode whose characteristics may exhibit considerable scatter. In order to evaluate the scatter, tests with previously used deformation amplitudes should be repeated.

If the cumulative damage model given by Eq. (3) is appropriate, a monotonic test is needed to determine δ_u , and several more experiments are needed to evaluate β as well as the load deformation characteristics on which dE depends.

PERFORMANCE EVALUATION

Performance in general may be concerned with several limit states, ranging from serviceability to safety against failure. Although test results will provide information on all limit states, the recommendations made in this paper are put forth specifically for performance assessment at the limit state of failure.

Failure may be defined as the inability of the component to resist an imposed seismic demand without excessive deterioration in strength. This necessitated the definition of the *strength associated with failure*, Q_{min} , which must be assigned to the experiment. It is convenient to express this residual strength as a fraction α of either the measured or the predicted yield strength. The predicted yield strength appears to be more appropriate since it is used in design and in the analytical studies on which the predicted seismic demands are based. The fraction α is a matter of judgment and may depend on the rate of strength deterioration close to failure. Once Q_{min} is defined, the experiment(s) will provide all information relevant to performance evaluation.

If a cumulative damage testing program is employed, performance can be predicted directly from the damage model and analytical predictions of seismic demands. In a single specimen testing program the intent of the multiple step test is to incorporate the most important cyclic demand characteristics of N and $\Sigma \Delta \delta_{p,i}$, regardless of the maximum deformation or ductility demand imposed by an earthquake. Thus, during performance assessment only one additional primary demand parameter remains to be considered. Conventionally, this additional demand parameter is the maximum ductility ratio, which needs to be predicted from analytical studies on the structure of which the component is part.

Presuming that the component ductility demand can be evaluated with due consideration given to the uncertainty in seismic input, performance assessment can be based on the evaluation of capacity/demand ratios of ductility and other important performance parameters. The capacities to be used for this purpose are quantities associated with Q_{min} and the corresponding δ_{max} obtained from the experiment. The primary capacity/demand ratio is likely that for ductility, but other ratios, such as those for cumulative hysteretic energy dissipation and cumulative plastic deformation ranges, should also prove useful for performance evaluation.

Adequate performance implies that a margin of safety needs to be provided against failure. Thus, the required capacity/demand ratios should be larger than 1.0. How much larger depends on the degree to which input uncertainties are considered in the determination of

ductility demands and on the mode of failure of the test specimen. If the mode of failure is associated with rapid strength deterioration, the required capacity/demand ratios should be larger than for modes of failure with gradual strength deterioration.

ACKNOWLEDGMENTS

The work summarized here was carried out by the author as part of a project on the development of "Guidelines for Cyclic Seismic Testing of Components of Steel Structures" (ATC-24, 1992), which is administered by the Applied Technology Council. This project was sponsored by the American Iron and Steel Institute, the American Institute of Steel Construction, the National Science Foundation, and the National Center for Earthquake Engineering Research. The opinions expressed in the paper are those of the author and may not necessarily be those of ATC or the sponsoring agencies.

REFERENCES

- Applied Technology Council, 1978. "Tentative Provisions for the Development of Seismic Regulations for Buildings," National Bureau of Standards, Special Publication 510, Applied Technology Council, Publication ATC 3-06, June 1978.
- Applied Technology Council, 1992. "Guidelines for Cyclic Seismic Testing of Components of Steel Structures," Applied Technology Council, Publication ATC-24, 1992.
- Hadidi-Tamjed, H., 1987. "Statistical Response of Inelastic SDOF Systems Subjected to Earthquakes," Ph.D. Dissertation, Department of Civil Engineering, Stanford University, December 1987.
- Krawinkler, H., et al., 1983. "Recommendations for Experimental Studies on the Seismic Behavior of Steel Components and Materials," John A. Blume Center Report No. 61, Department of Civil Engineering, Stanford University, September 1983.
- Nassar, A.A., and Krawinkler, H., 1991. "Seismic Demands for SDOF and MDOF Systems," John A. Blume Earthquake Engineering Center Report No. 95, Department of Civil Engineering, Stanford University, June 1991.
- Park, Y.-J., and Ang, A.H.-S., 1985. "Mechanistic Seismic Damage Model for Reinforced Concrete." Journal of Structural Engineering, ASCE, Vol.111, No. 4, April 1985, pp. 722-739.

ASEISMIC TEST OF BUILDING STRUCTURE

Zhu Bolong

Professor of Civil Engineering
Tongji University

ABSTRACT

A general discussion about aseismic test is presented in this paper. It is involved the aseismic static test and aseismic dynamic test, laboratory test and field test. Besides, the aseismic behaviour and aseismic capacity are also discussed in this paper.

INTRODUCTION

It is well known that, using the aseismic test results to estimate the aseismic behaviour or aseismic capacity is very useful. So, many seismic countries pay their attention to the development of aseismic test method. On the other hand, how to use the aseismic test results to correctly evaluate the aseismic behaviour or aseismic capacity arouses the interest of every researcher in area of aseismic design of building structures.

The kinds of aseismic test methods can be summarized as follows:

Aseismic static test { *cyclic loading*
noncyclic loading—pseudo dynamic
Aseismic dynamic test { *cyclic loading—vibrator, shaking table*
noncyclic loading—shaking table, field test

It should be noted that, not any aseismic test in laboratory can reappear one actual earthquake. But, in comparison with the static test, the dynamic test is better; in comparison with cyclic loading, the noncyclic loading corresponding to seismic responses is more close to the practice; besides, in comparison with the tests in laboratory, the field dynamic test is more close to the earthquake.

Except the problem of test method, in the area of how to use the test results, the aseismic behaviour and aseismic capacity should be distinguished.

ASEISMIC STATIC TEST AND ASEISMIC DYNAMIC TEST

It is well known that the difference between static and dynamic tests is the strain rate effects, test duration and the possibility to change test program.

1. Strain Rate Effect

Cyclic loading

Fig. 1 shows the hysteresis loops of masonry walls subjected to the static and dynamic loading. The shear strength of masonry wall increases with the decrease of loading period. Such phenomenon is similar to concrete and steel, as shown in Fig. 2 and Fig. 3. According to the earthquake response of building structure, the strain rate of member has a various value within $0.01 \sim 0.025$ / sec. It means that during earthquake the dynamic strength of the ordinary material maybe increase $10 \sim 15\%$ in comparison with the static strength of that.

Noncyclic loading

The static noncyclic loading may be realized by two ways: one is the test specimen loaded by a predicted loading pattern, the other is pseudo-dynamic test. Since the pseudo dynamic test is an actuator-computer on line system, the stiffness variation of members can be reflected in the calculated process. Therefore, the latter is better than the former. But, in comparison with the shaking table noncyclic dynamic test, the static noncyclic test can not provide following two distinguishing features: strain rate effect and failure pattern. It should be mentioned that the failure pattern of test specimen or test model building depends on the test method: static or dynamic, the latter can provide acceleration. Shaking table test has verified that this problem is particularly evident in masonry test, as shown in Fig.4.

2. Test Duration

Except the preparing period, the test duration of static test is longer than that of dynamic. The duration of static test needs several hours, but that of dynamic test only needs few seconds.

3. Possibility to Change Test Program

In static test according to the loading path or loading pattern, the specimen can be experimented one stage after another, and the experiment can be temporarily stopped at any stage

to inspect the cracks and deformation. Sometimes, the original test program may be changed on the base of experimental development. But in dynamic test, the above-mentioned advantage is very few.

LABORATORY TEST AND FIELD TEST

In laboratory the static experiments and shaking table tests including cyclic and noncyclic loading can performed, but in the test field only the noncyclic dynamic test can be done.

1. Laboratory Experiment

The important advantage of laboratory experiment is that under the same condition, a group of specimens using same method can be tested. It is very useful in practice.

Static test

For the design purpose, the researchers can experiment a series of specimens to determine the available strength and reasonable constructional measures by means of static test. For example, Fig. 5 shows the shear strength of masonry walls (where: R_s —shear strength of masonry, R_j —shear strength of mortar joint, σ_0 —normal pressure), and Fig. 6 shows the relationship between number of cycle and degradation of restoring force.

On the other hand, it is well known that the restoring force model is very important for nonlinear structural analysis of earthquake response. So, based on the results of a series tests, the restoring force model of member or structure can be determined. For instance, Fig.7 shows the restoring force model of reinforced concrete flexural member with axial load, and Fig.8 shows the masonry wall subjected to the reversed shear force.

Owing to the fact that the restoring force model involves the yielding strength and deformation, the ultimate strength and deformation, the initial stiffness and the stiffness degradation, etc., the above mentioned factors are the key factors of the seismic behavior of members.

Shaking table test

On the shaking table the model structure or members can be tested. In spite of the fact that the model building tested on the shaking table is not equal to the real building excited by the natural earthquake, the damage characteristics and crack pattern are close to the actual phenomena.

With the gravitational field problem, the aseismic capacity of prototype structure can be approximately estimated by that of model building tested on the shaking table according to similitude relationship.

2. Field Test

In general, the aseismic field tests involve two main kinds: one is the testing structure tested in field by artificial earthquake, the other is the testing structure built at multiple earthquake area waiting for the actual earthquake.

Artificial earthquake

Recently, the artificial earthquakes occurred from two ways: one is the explosion earthquake, the other is by using special device exploded according to some predicting time series. Fig.9 shows the explosive generated ground motion in China, and Fig.10 shows the time history of ground motion occurred by special explosion device in China.

Natural earthquake

University of Tokyo constructed a natural earthquake testing field in the Chiba, Japan. A series of large-scale model buildings according to different test purposes are built at testing field waiting for the earthquake. Owing to the fact that in the field different magnitude earthquake frequently occurred, the control center of testing field has obtained a lot of information of earthquake responses of large-scale model buildings.

ASEISMIC BEHAVIOUR AND ASEISMIC CAPACITY

The aseismic test results are always used to determine the aseismic behaviour or aseismic capacity. It should be mentioned that both of them have some common content, and have some different objectives.

1. Common Content

The following factors of the member of building structure should be discussed for the aseismic behaviour and aseismic capacity:

- (a) **Strength:** crack and ultimate strength, degradation of strength;
- (b) **Deformation:** ductile and ductility factor, deformation and deformability;
- (c) **Energy:** energy absorption and energy dissipation;

- (d) Stiffness: initial stiffness, unloading stiffness, repeated loading stiffness, equivalent stiffness and stiffness degradation;
- (e) Hysteresis loops: pattern and area of loops, hysteretic damping, skeleton curve;
- (f) Failure mechanism.

2. Different objectives

Though both the aseismic behaviour and aseismic capacity have some common research content, from the viewpoint of the solution of the problem, they have some different objectives.

Aseismic behaviour

In order to compare the basic parameters between two different members or between two different constructional measures of one member, the aseismic behaviour of member should be studied. As shown in Fig.6, in order to compare the aseismic constructional measures, the strength, stiffness, degradation, hysteresis loops, deformation, failure mechanism, etc., all of which need to be studied. But, it should be pointed out that, for aseismic behaviour it is unnecessary to solve the problem that up to what level of earthquake the structure can resist.

Aseismic capacity

In order to solve the problem that what level of earthquake can be resisted by the structure, the aseismic capacity should be studied, and in connection with this problem, the strength, stiffness, etc. of structure should be concerned.

In general, the aseismic capacity of structure may be determined by many ways(Fig.11).

REFERENCE

- [1] Zhu Bolong, Aseismic Test of Structures, (in Chinese), 1989, E / Q publishing house.
- [2] Zhu Bolong, A review of Aseismic Test for Masonry Structure in China, 1989.
- [3] Facilities for Observation and Simulation of Earthquake Motion, University of Tokyo.

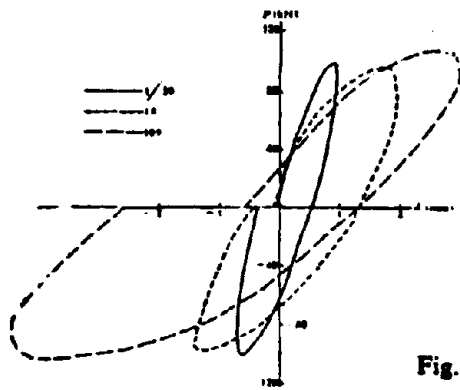


Fig.1

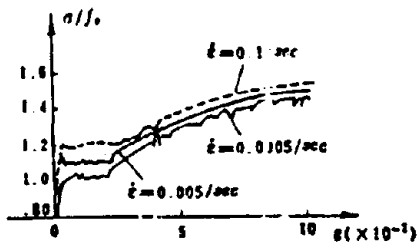


Fig.2

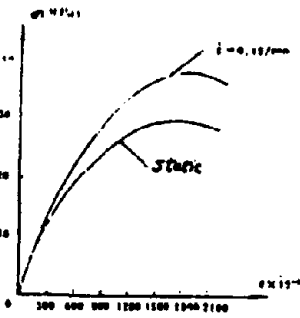


Fig.3



Fig.4

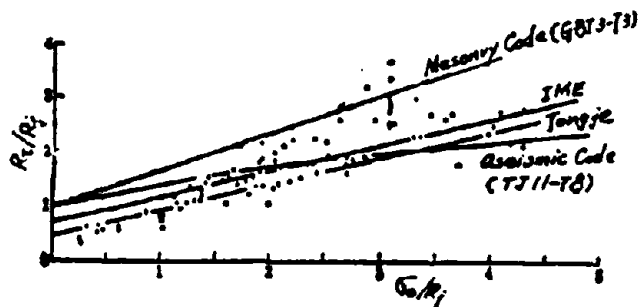


Fig.5

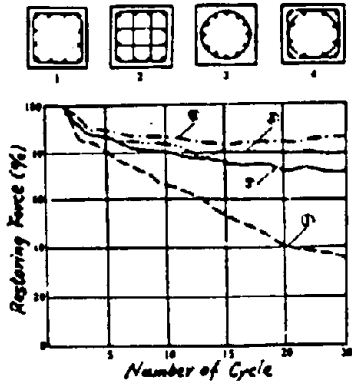


Fig.6

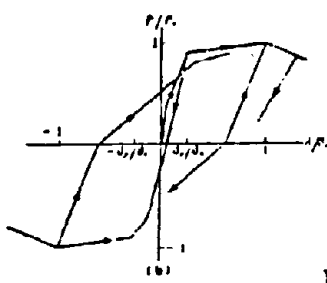


Fig.7

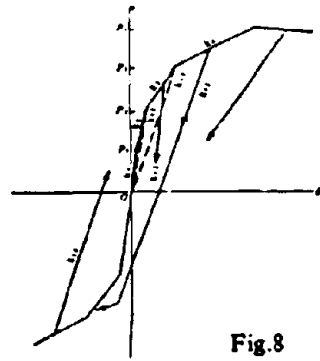


Fig.8

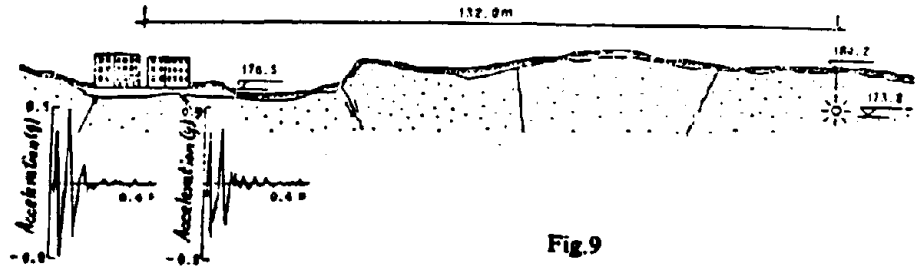


Fig.9

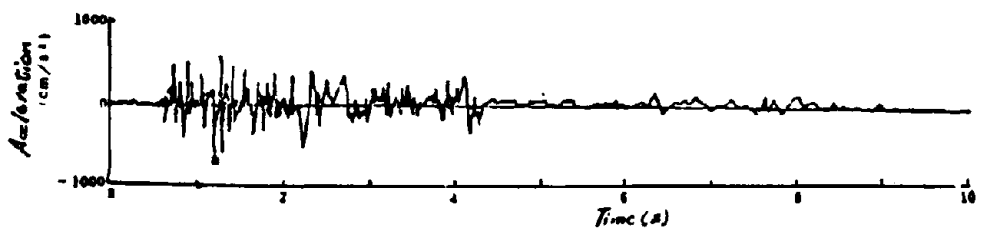


Fig.10

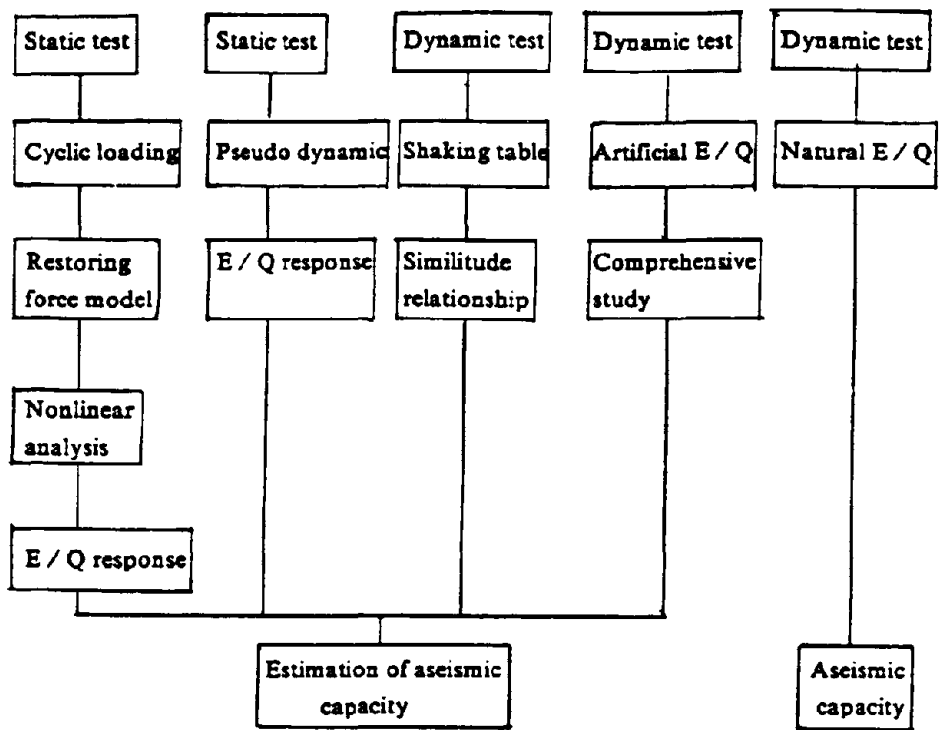


Fig.11

The Experimental Method of Reinforced Concrete Silos

Zhu Bolong Shi Weixing
(Tongji University, Shanghai, China)

Abstract

This paper discusses the similarity relationship determination, model design and construction, test method and experiment procedure etc. with the example of Huangdao Electricity Plant. The experiment result by this method is quite satisfying.

1. Preface

As a kind of modern structure, silos suffer less from earthquake, especially from intense earthquake. But their failure during earthquake has been observed. During the earthquake of March 4, 1977 in Romania, the supporting structures, top storey structures of silos, were destroyed, the roof of small top building cracked, and even collapsed.

Since 1960s, some dynamic researches on silos have been done abroad. But their research directions limit to dynamical effective mass of storage. There are few researches on the seismic responses and failure of silos. With the more and more extensive application of silos, the experiment research on the seismic resistant performances of silos becomes more and more imperative. This paper discusses the simulated seismic shaking table experiment method of reinforced concrete silo with the example of Hangdao Electricity Plant.

2. Model Design

According to the actual situation of shaking table of State Laboratory for Disaster Reduction in Civil Engineering in Tongji University and the height of structure laboratory, the size scale ratio between prototype and model of Hangdao Electricity Plant silo is taken as 10:1.

The result of previous statics research on silo shows that the friction between cylinder wall and storage has great effect on storage material pressures. In order to simulate actual friction situation better, microconcrete is selected as model storage silo's material, and steel net is used to simulate the bars in the cylinder wall of prototype. The model storage material is still coal. Therefore, the

density scale factor of storage material must be 1. Because gravity accelerate scale factor must be 1 in any experiment on the earth, silo model must be actual model. Other similarity requirements are listed in table 1.

There are still some problems in the material selection for this model made strictly according to the prototype. Grade 300 concrete is used as prototype material. According to similarity requirement, microconcrete for model can only be grade 30. Thus, such low-graded concrete will cause great inconvenience in the model construction and installation in experiment. Therefore, the strength of microconcrete should be appropriately enhanced. The grade of microconcrete in this paper is 50. It will slightly increase the tensile strength of specimen. According to the similarity requirement, the steel strength of the model should be 1/10 that of prototype. It is difficult to obtain such material. The adoption of alloyed material, such as aluminum, lead etc. will increase the cost of model and is unpractical in the present fund condition. Therefore, No. 12 steel net is used to simulate the bars in the cylinder wall of prototype. This will have little effect on the tensile strength of model silo, but have some effect on the development of crack. Model material property tested from experiment is showed as follows:

①. Microconcrete

Strength: 4.20MPa for Model A, 4.60MPa for Model B.

Elastic modulus: 4.74×10^4 MPa

②. Steel

Yield strength: $\varnothing 4$ 535MPa

$\varnothing 6$ 354MPa

$\varnothing 8$ 235MPa

Elastic modulus: 1.96×10^4 MPa

③. Coal

Density: 902kg/m³ for model A, 874kg/m³ for model B

Moisture: 8% for model A, 11% for model B

Friction angle: 37.3°

Friction factor (on microconcrete wall): 0.6

Two models, named model A and model B, are used in the paper. Model A is the actual model of second-phase coal silo of Huangdao. Model B is the improvement of model A. It eliminates inner cylinder structure. Its supporting structure consists of outer cylinder wall and inner columns. The hopper is directly supported on the outer cylinder wall and its top building is eliminated. The profile of model A and model B are showed in Fig. 1 and Fig. 2. Photo. 1 is the construction scene of model B. Photo. 2 is the appearance of model A and B.

3. Test Method

3.1 Instrument Selection

1. Sensors

Like other shaking table experiments, sensors used in the model silo experiment also include strain gauge, displacement gauge and acceleration gauge. Additionally, it is one of the objects of this experiment to measure storage material pressures. Therefore, this experiment also requires pressure sensors.

2. Data Sampling System

Storage material pressure is required to measure in this experiment. It takes as long as 2 hours to fill coal into the silo. In such a long time, test error is unavoidable because of the instrument adrift resulted from temperature and other factors. Therefore, the good performance American MTS 460 Data Sampling System of Simulated Seismic Shaking Table is used in sample data.

3.2 Measurement Point Arrangement

The symmetricity is taken advantage to reduce measurement points.

1. Strain Measurement

Strain measurement includes cylinder wall strain, supporting structure strain and openings strain. Model B also includes the joint strain of cylinder wall and hopper.

①. Cylinder Wall Strain

Strain gauges are arranged on $\sqrt{1.40}$, $\sqrt{1.80}$ and $\sqrt{2.50}$ to measure vertical and circular stress distribution in the cylinder wall. Both inner and outer strain gauge are used to account for the possible moment in the cylinder wall. Because the inner side of the silo will be impacted by the coal and cause strain gauge to be susceptibly damaged. In another way, we arrange strain gauge on the 250mm long $\varnothing 4$ bar, and burry the bar in the inner side microconcrete of the cylinder wall. Inner side strain is measured by the bond between the bar and microconcrete.

②. Supporting Structure Strain

Vertical strain gauges are arranged on $\sqrt{0.05}$ to study the effect of superstructure on foundation.

③. Openings Strain

The stress concentration at the openings is the weak area of the structure. Therefore, strain gauges are arranged at the openings.

2. Storage Material Pressures

Six pressure boxes are arranged on each model. They are numbered P-1, P-2, P-3, P-4, P-5, P-6, as showed in Fig. 3. P-1- P-4 measure the pressures on cylinder wall. P-5, P-6 measure the pressures on the inclined side of the hopper.

3. Displacement and Acceleration

The arrangement of displacement sensors and acceleration sensors is showed in Fig.4. Because seismic wave is inputed in two directions respectively during dynamic experiment, displacement sensors D-1, D-2, D

-3, D-4 and acceleration sensors A-1, A-3 are arranged in X direction when seismic wave is inputed in X direction, and they are arranged in Y direction when seismic wave is inputed in Y direction.

4. Experiment Procedure

1. Lift the model on the shaking table, as showed in Fig. 5, and install sensors and cables.

2. Test the eigenvibration characteristic of empty silo in both X direction and Y direction.

3. Adrift test: The time to fill coal in the experiment is so long that the instrument adrift resulted from the temperature change is unavoidable. It is necessary to conduct adrift test, record the relation curve between sensor signal and temperature, and find invalid sensors.

4. Build scaffold for filling coal.

5. Coal filling experiment: Carry the coal to the experiment hall by trolley, and lift it to the scaffold, then it is filled into the silo. Sample data every twenty minutes, and record the temperature and the amount of filled coal.

6. Coal flowing experiment: Disturb with iron bar in the mouth of hopper to cause the coal to flow for 30-60 seconds continuously, and sample data. Coal flowing experiment consists of coal flowing in east hopper, coal flowing in west hopper and coal flowing in both hoppers simultaneously.

7. Test the eigenvibration characteristic of full silo in X direction.

8. Test the full silo when inputed with seismic wave in X direction: 0.1g and 0.23g wave sequentially.

9. Test the eigenvibration characteristic of full silo in Y direction.

10. Test the full silo when inputed with seismic wave in Y direction: 0.1g, 0.23g, 0.45g, 0.9g, 1.48g, 1.8g and 2.0g wave sequentially.

5. Experiment Result

Experiment result indicates that storage material pressures distribution under seismic wave is large at upper and lower and little at middle pattern. There is approximately linear relation between the increment of storage material pressures and table acceleration. There is nonlinear relation between the decrement of storage material pressures and table acceleration. When silo endures seismic wave, diagonal microcrack occurs first at the wall-hopper joint. With the increase of table acceleration, cracks occur at the door opening, 'E'

shape beam, girth, window opening of the silo. These position are the weak links of the structure. According to similarity relation, when the prototype silo suffers from 7 degree earthquake, cracks will occur at the root and hopper, and part of bars yeild. But there is no danger of collapse.

6. Conclusion

Limited by the storage material, reinforced concrete silo model must be actual model. The simulated seismic shaking table experiment of elaborately designed microconcrete silo model has satisfactory result.

Reference

- (1). C. Pavel, R. Agent, and A. Pusca, ' A Seismic Design of Cereal Silos in Romania ', Eighth World Conference on Earthquake Engineering V. VI, San Francisco, 1984.
- (2). Zhu Bolong, ' Structure Seismic Resistance Experiment ', Seismic Publishing House, 1989.

Table 1

Parameter	Value
Length	0.1
Time	0.3162
Frequency	3.162
Displacement	0.1
Acceleration	1.0
Gravity Acceleration	1.0
Density	1.0
Strain	1.0
Stress	0.1
Elastic Modulus	0.1
Pressure	0.1

EFFECTS OF SCALE AND LOADING RATE WITH TESTS OF CONCRETE AND MASONRY BUILDING STRUCTURES

Daniel P. Abrams
Newmark Civil Engineering Laboratory
University of Illinois at Urbana-Champaign
Urbana, IL 61801

ABSTRACT

Static and dynamic response of reduced-scale and full-scale test structures are correlated to discern effects attributable to scale and loading rate. Three case studies are presented where large-scale building systems were represented using reduced-scale models that were subjected to dynamic excitation using a shaking table. The test structures were (a) ten-story reinforced concrete frame-wall systems, (b) three-story reinforced masonry building systems, and (c) unreinforced masonry infills in reinforced concrete frames. In addition to dynamic tests, static testing of either critical components, or of the complete structural system, has been done to examine differences attributable to the modeling method, or to the loading procedure.

INTRODUCTION

A paradox has plagued experimental earthquake engineering research since its inception. Actual buildings are massive structural systems that are excited dynamically during earthquakes. If dynamic response of these systems is to be examined in a laboratory setting, test structures must be reduced in size. If extrapolation of research results to structural engineering practice is to be made, the use of reduced-scale models may be questioned by code writing officials. Therefore, large-scale specimens must be tested as well, but at static rates, because hydraulic flow and payload capacities of present shaking tables are not suited for large-scale building systems. Whereas the question of scale is absolved by testing a large-scale structure, other questions emerge with respect to the extrapolation of static test results for estimating dynamic response. Until shaking tables emerge in our laboratories that are large enough to test full-scale building systems, these questions will continue to be asked, and the paradox will be past on to the next generation of experimental researchers.

Three separate laboratory testing programs are described that include shaking table tests of reduced-scale structures, and large-scale static tests. The presentation serves to acquaint foreign researchers with state-of-the-art testing practices used in the United States for earthquake engineering research. A second objective is to provide some insight to possible differences in seismic response attributable to specimen size or loading rate.

Reduced-scale models are generally excited dynamically on shaking tables to provide response data for examination. This category of testing is depicted as element *a* of the matrix shown in Fig. 1. Large-scale test structures are usually tested statically (element *c* of matrix). It is of obvious interest to understand relations between response of reduced-scale specimens

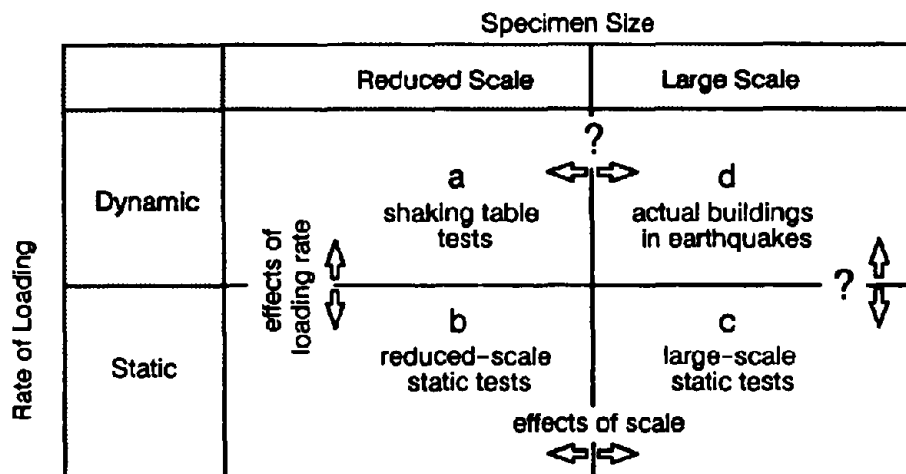


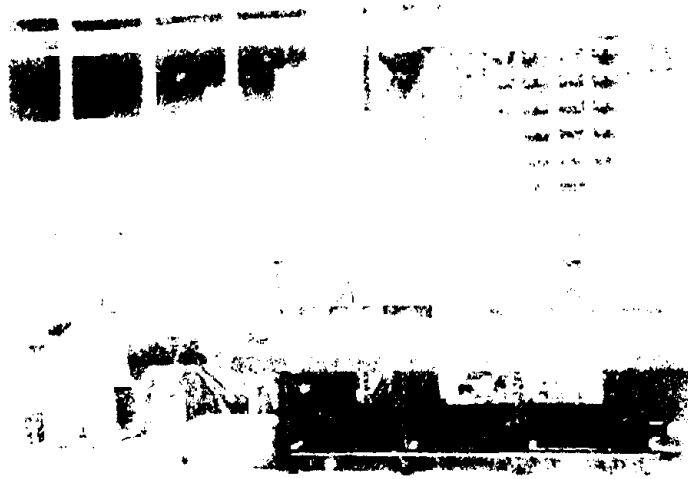
Fig. 1 General Relationships Between Scale and Loading Rate

and full-scale buildings (*a* to *d* correlation), and between static behavior of large-scale specimens and dynamic response of actual systems excited by earthquakes (*c* to *d* correlation). Unfortunately since data on dynamic response of full-scale structures is usually not available to make direct correlations with laboratory specimens, to understand these relations requires an alternate approach. If a twin reduced-scale specimen is subjected to similar response histories as its sibling on the shaking table (element *b* of matrix), then direct correlations attributable to scale (*b* to *c* correlation), and loading rate (*a* to *b* correlation) can be made. Through assimilation of these two correlations, it may be surmised how to extrapolate test data from reduced-scale dynamic tests, or large-scale static tests, to estimate dynamic response of actual building systems. Whereas this approach does not provide a direct correlation, it is the best that can be used until capacities of earthquake simulators are increased to the extent that dynamic response of full-scale systems can be measured. The three case studies given in this paper help to illustrate this testing philosophy.

TESTS OF TEN-STORY RC FRAME-WALL SYSTEMS

In the first case study, a series of ten-story reinforced concrete structures at approximately one-twelfth scale were excited to failure on the Illinois shaking table (Fig. 2). Information on these tests can be found in References 1 and 4. Replicas of beam-column joints, and base-story columns were constructed at a large scale, and were tested statically to define hysteresis relations (Refs. 8 and 9). In addition, replicas of the same components were constructed at the same reduced-scale as the ten-story test structures and again tested statically (Refs. 2 and 3).

Hypothetical differences in dynamic response for large and small structures have been compared by modeling hysteresis relations for both reduced and full-scale components in a non-linear dynamic analysis (Refs. 5 and 6). Because hysteresis relations are based only on static experiments, this hypothetical correlation is of the type *b* to *c*. A sample of the research results



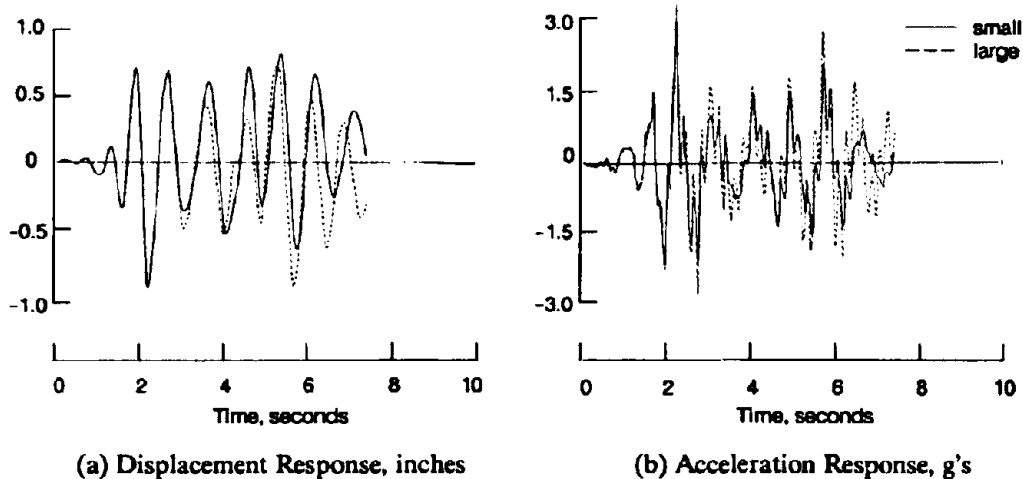


Fig. 3 Computed Top-Level Response for Large and Small Frame-Wall Systems

the Illinois shaking table (element *a*). In addition, a twin one-quarter scale system was tested statically (element *b*) with an identical sequence of deflections as its shaking table sibling.

The large-scale test structure is shown in Fig. 4. Lateral forces were applied at the top of the second-story to simulate inertial forces that would vary along the height of a three-story building in an inverted triangular pattern. A twin pair of 500 kN servohydraulic actuators were used. Since story shears would be zero above the second story for this specimen, there was no need to construct a third story. Because lateral deflections at the second-level were appreciable relative to the stroke lengths of the actuators, displacement control could be used for the pair of actuators without having significant differences in the forces for the two actuators.

Results from testing the large-scale specimen are summarized in Ref. 7. Test data provided benchmark information for calibration of code values for allowable shear and compressive stresses. In addition, test results suggested modes of failure to be included in future computational models. Nonlinear behavior of the system was governed by inelastic deformations of the central piers in shear. The system continued to resist lateral force after diagonal cracks were observed in the central piers suggesting that story shear could be redistributed to exterior piers with no loss of strength. Though the system and the loading was symmetrical, behavior of local pier elements was found to be asymmetrical as a result of alternating axial forces.

The one-quarter scale structure is shown in Fig. 5. Concrete blocks were exactly one-quarter the size of full-scale 8-inch block and were fabricated using the same casting process as used in actual manufacturing. Reduced-scale reinforcement consisted of annealed wire. Mortar and grout materials were essentially the same as full-scale materials with the exception that large-size fine aggregates were removed. Because the stress-strain properties of the wire could be made to simulate typical Grade 60 reinforcement, and the grout was closely modeled, both the tensile and compressive properties of the materials could be replicated. The demand for exact simulation of bonding between the masonry units and mortar joints was not of a great

that a reinforced masonry structure could dissipate energy through hysteresis in much the same way as does a reinforced concrete structure. Nonlinear, dynamic drifts could be estimated using the same models as proposed for reinforced concrete systems. A capacity design approach proved to be acceptable for reinforced masonry systems. Measured response suggested that a single-degree-of-freedom nonlinear spring model could be used to estimate nonlinear response histories, and that an equivalent linear model could be used to estimate nonlinear response maxima. In summary, modeling at one-quarter scale proved to be a suitable method for investigating overall response of reinforced masonry systems. Detailed descriptions of research results from the shaking table studies can be found in Refs. 12 and 13.

Direct correlations between the reduced-scale dynamic tests and the large-scale static test (*a* to *c* type correlation) cannot be made because there are two variables to consider: the scale and the loading rate. However, an attempt has been made to do this in Ref. 10. It was found that nonlinear response of a masonry building system is sensitive to the ways that it is constructed and tested. Dynamic testing resulted in a lateral force distribution which was much different than the inverted triangular distribution that was represented with the single concentrated static force. Lateral strength of the fully grouted, one-quarter scale specimen was limited by shear strength of the exterior piers. A weak sliding shear plane was developed at the top of the piers which resulted in nearly all of the story shear being attracted to a single exterior pier. The partially grouted full-scale specimen did not behave in this manner since the central piers proved to be the most vulnerable elements.

A twin of the one-quarter scale test structure was tested statically following the shaking table experiment. Cycles of lateral displacements at the third level were applied with a servohydraulic actuator in the exact same sequence as was observed from the dynamic test. Lateral forces at the first and second levels were governed so that an inverted triangular loading distribution would be maintained throughout the testing. The top-level actuator was controlled using an analog ramp function. The sequence of peaks in the top-level deflection history were pre-defined with an array of data points that were input to a personal computer. Lateral deflections at the top level relative to the test floor were continuously monitored and compared with the current target peak for a particular cycle. When the target deflection was reached, a five-volt signal was sent from the computer to the function generator which at that instant reversed the ramp function for the top-level actuator.

Sample plots that contrast the base moment-deflection relations for the shaking table specimen and its statically tested twin are presented in Fig. 6 (this is a type *a* to *b* correlation of Fig. 1). The time increments shown in the figure are expressed in terms of the duration of dynamic testing. Differences in lateral stiffness and strength were appreciable for the two test specimens. In the last and most severe test run, flexural strengths for the static specimen were 79% of strengths for the dynamic specimen. The lowest average stiffness taken from peak to peak of the largest cycle for the static specimen was 55% of that for the dynamic specimen. It was apparent that the rate of strain can have an appreciable effect on crack propagation. Observed damage for the dynamic specimen was much less than for that for the static specimen despite the fact that the dynamic specimen resisted more force. From these observations, it was concluded that static testing in a laboratory provides a more demanding environment than an actual seismic event. Thus, large-scale static testing should be a conservative approach. A summary of correlations between the static and dynamic specimens can be found in Ref. 11.

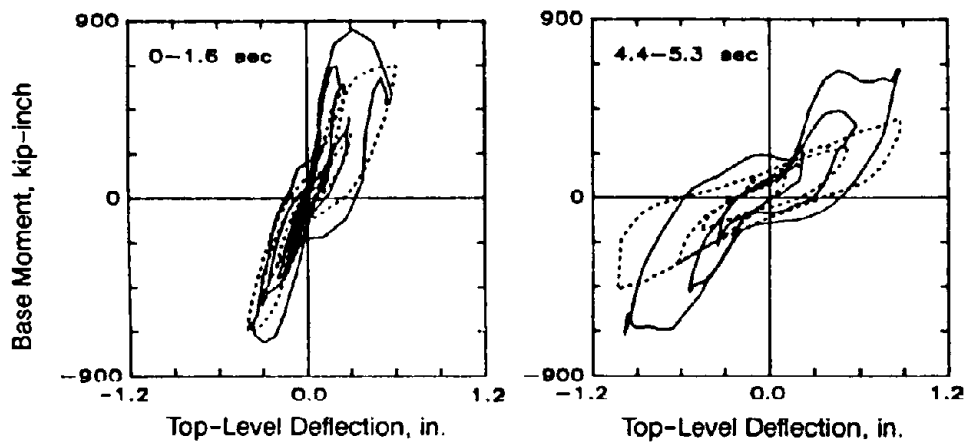


Fig. 6 Static and Dynamic Measurements for One-Quarter Scale Masonry Test Structures

TESTS OF UNREINFORCED MASONRY INFILL-FRAME SYSTEMS

The third case study is a present research project that is being done at the University of Illinois and the US Army Construction Engineering Laboratory (CERL). Large-scale reinforced concrete frames with masonry infills are being subjected to a series of in-plane static force reversals before static out-of-plane pressures are applied. The tests are being done to improve methods for evaluating out-of-plane strength of cracked masonry infills, and may be categorized as type *c* specimens in Fig. 1. At CERL, one-half scale replicas of the large-scale specimens are being subjected to simulated earthquake motions on a shaking table. These tests can be categorized as type *a* specimens in Fig. 1.

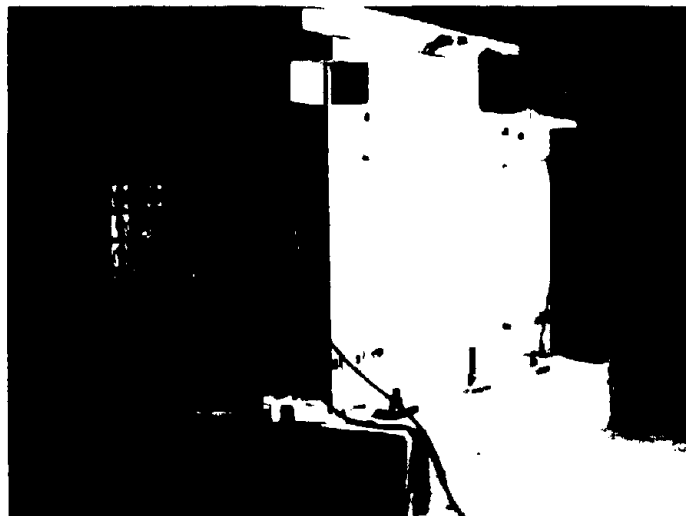


Fig. 7 Large-Scale Masonry Infill Test Specimen

A typical large-scale infill specimen is shown in Fig. 7. In-plane lateral forces are applied using a pair of servohydraulic actuators. One actuator is controlled in accordance with a series

of programmed displacements while the other actuator is controlled such that its force will be identical with the first actuator. By using this method, displacement control can be utilized making it possible for post-peak behavior to be examined in a controlled manner while torsion of the two lateral forces is kept to zero.

Out-of-plane pressures are applied with an air bag. The bag is expanded between a masonry infill panel, and a concrete reaction slab. Air is supplied to the bag at a constant flow rate making the test a volume-controlled one. Air pressure is measured with an electronic gage that is checked against a simple manometer that relates pressure to the height of a water column. In addition, the total lateral force is measured with load cells so that the true contact area between the bag and the infill can be deduced.

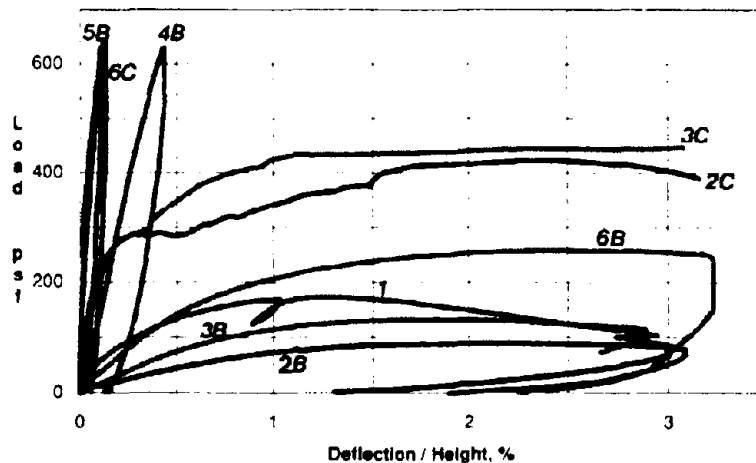


Fig. 8 Measured Out-of-Plane Behavior of Large-Scale Masonry Infills

A summary of out-of-plane behavior is shown in Fig. 8 where transverse pressure is plotted versus lateral deflection (expressed as a percentage of the height). Each curve in the figure is for a different infill specimen. Parameters of the study are the type of masonry (clay brick for specimens 1, 2B, 3B and 6B, and concrete block for specimens 4B and 5B), the infill height to thickness ratio (34 for specimens 1, 2B, and 3B, 17 for specimens 4B and 6B, and 11 for specimen 5B), and the mortar type (Type N portland cement-lime mortar for specimens 1, 2B, 4B, and 5B, and lime mortar for specimens 3B and 6B). In addition some specimens (2C, 3C and 6C) are being repaired after testing with a cement-plaster coating.

The large-scale tests done to date have shown that the out-of-plane strength of an unreinforced masonry infill can be quite high even when cracked with in-plane loads. This is a result of the substantial arching action that develops for panels with a low h/t ratio. An analytical model is being developed that accounts for inelastic behavior of a two-way plate that is subjected to arching action. Yield line analyses commonly used for reinforced concrete slabs are being adapted to include arching effects.

The half-scale specimen (Fig. 9) consists of two parallel concrete frames with masonry infills that are joined by a concrete slab. Half-scale clay masonry units are fabricated using the same

process as used for actual bricks. Mortar joints are scaled down to one-half of full-scale joints. Actual deformed rebars are used for the longitudinal reinforcement in the frame. Maximum aggregate size for the frame concrete is limited to 3/8 inch, or one-half that of conventional full-scale concrete mixes.

Test specimens are aligned on the shaking table so that the principal plane of the masonry infills are parallel with the input motion. After exciting specimens so that the masonry cracks under in-plane shear, they are rotated ninety degrees so that the masonry infills are subjected to transverse pressures resulting from their own inertial forces. For the in-plane testing, additional masses are placed on the top slab so that inertial forces will be large enough to crack infills with in-plane shears. These additional masses are removed for the out-of-plane testing. The amplitude of the base motion is scaled for the out-of-plane tests so that the inertial resulting from the mass of the masonry will be sufficient to result in significant damage.

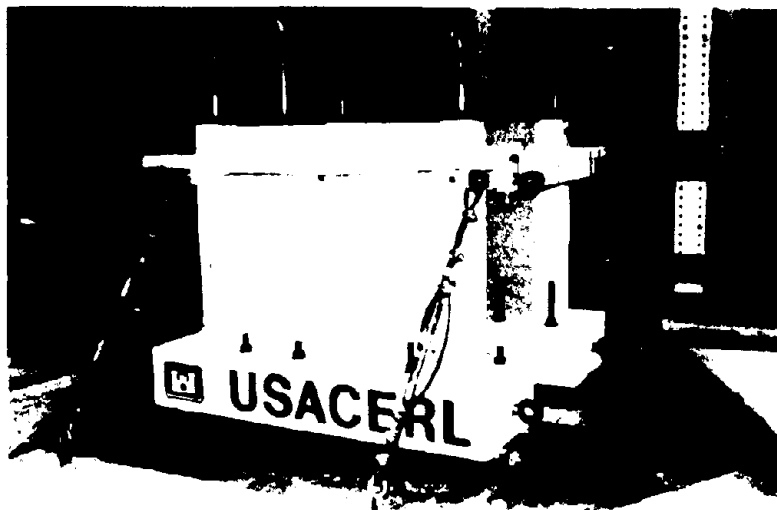


Fig. 9 Half-Scale Masonry Infill Test Specimen

Dynamic testing of the first infill specimen has recently taken place. Since test data is still being reduced, correlations with the large-scale specimens cannot be made at this time. Although a dynamically tested specimen should be stiffer and stronger than one tested statically, it is anticipated that the influence of repeated and reversed load reversals may result in a compensating deterioration of stiffness and strength. Preliminary correlations of crack patterns for specimens of each size have revealed similar extents of cracking suggesting that this tendency may be true.

CONCLUDING REMARKS

Three case studies have provided a general overview of various approaches to experimental earthquake engineering research. Shaking table experiments of ten-story reinforced concrete frame-wall systems, three-story reinforced masonry wall systems, and one-story masonry infill-concrete frame systems have each demonstrated the advantages of dynamic testing. Large-scale static tests of reinforced concrete components, a two-story reinforced masonry building, and one-story infill-frame systems have provided data on the seismic behavior of actual structures which is needed for extrapolation of dynamic test data from the reduced-scale structures.

If there is one primary commonality between the three case studies it is that tests of reduced-scale structures on shaking tables, or large-scale specimens tested statically will always be inconclusive. At best, three of the four elements of the matrix shown in Fig. 1 will be filled. Dynamic response of large-scale systems must always be surmised on the basis of the experiments done on either reduced-scale or statically tested specimens. Gaps will always exist between tests of reduced-scale and large-scale specimens because of material and loading differences making correlations difficult to make between them.

The central conclusion from this presentation is that large-scale dynamic experiments are needed. If a large shaking table were available for dynamic tests of full-scale one or two-story structures, then it may be possible for earthquake engineering research to advance to a new generation.

ACKNOWLEDGMENTS

The author wishes to acknowledge the National Science Foundation of the United States for sponsoring nearly all of the research described in this paper. The study of earthquake response for ten-story concrete buildings was done as a doctoral dissertation under the direction of Professor Mete Sozen, and supported through the NSF earthquake hazards mitigation. A follow-up study of scale relations was done as a NSF research initiation and subsequent grant while the author was at the University of Colorado. The study of three-story reinforced masonry buildings was one task of many of the NSF sponsored US-Japan masonry program that was done through the Technical Coordination Committee for Masonry Research. The study on masonry infills is part of the NSF program on Repair and Rehabilitation of Seismic Resistant Structures. The half-scale infill tests are supported by the US Army Corps of Engineers.

REFERENCES

1. Abrams, D. P. and M. A. Sozen, "Experimental Study of Frame-Wall Interaction in Reinforced Concrete Structures Subjected to Strong Earthquake Motions," *Structural Research Series No. 460*, University of Illinois at Urbana-Champaign, May 1979, 386 pp.
2. Abrams, D. P. and M. E. Kreger, "Modeling of Reinforced Concrete Members at Small Scales," *Proceedings of the Seventh World Conference on Earthquake Engineering*, Vol. 2, Istanbul, Turkey, September 1980, 191-199.
3. Gilbertsen, N.D., and J.P. Moehle, "Experimental Study of Small-Scale R/C Columns Subjected to Axial and Shear Force Reversals," *Structural Research Series No. 481*, University of Illinois at Urbana-Champaign, July 1980, 95 pp.
4. Abrams, D. P., "Behavior of Small-Scale Reinforced Concrete Model Structures," *Dynamic Modeling of Concrete Structures*, Publication SP-73, American Concrete Institute, 1982, 65-82.
5. Abrams, D. P. and S. Tangkijngamvong, "Dynamic Response of Reduced-Scale Models and Reinforced Concrete Structures," *Proceedings of the Eighth World Conference on Earthquake Engineering*, Vol. VI, San Francisco, California, July 1984, 371-378.
6. Abrams, D. P., "Dynamic Response of Models and Concrete Frame Structures," *Design of Concrete Structures: The Use of Model Analysis*, The Institution of Structural Engineers and the Building Research Establishment, Construction Press, London, 1985, 13-1 to 13-9.
7. Abrams, D. P., "Lateral Resistance of a Two-Story Reinforced Concrete Block Building," *Proceedings of Session on Advances in Analysis of Structural Masonry*, ASCE Structures Congress, New Orleans, September 1986, pp. 41-57.
8. Abrams, D. P., "Influence of Axial Force Variations on Flexural Behavior of Reinforced Concrete Columns," Title No. 84-S26, *Structural Journal of the American Concrete Institute*, Vol. 84 No. 3, May-June 1987, pp. 246-254.
9. Abrams, D. P., "Scale Relations for Reinforced Concrete Beam-Column Joints," *Structural Journal of American Concrete Institute*, Vol. 84 No. 6, Nov-Dec 1987, pp. 502-512.
10. Abrams, D.P., "Dynamic and Static Testing of Reinforced Concrete Masonry Structures," *Journal of The Masonry Society*, Vol. 7, No. 1, Jan-June 1988, pp. T18-T22. Also, in *Proceedings of the Ninth World Conference on Earthquake Engineering*, Tokyo-Kyoto, August 1988, 6pp.
11. Paulson, T.J., and D.P. Abrams, "Correlation between Static and Dynamic Response of Model Masonry Structures," *Earthquake Spectra*, Journal of the Earthquake Engineering Research Institute, Vol. 6, No. 3, August 1990, pp. 573-592.
12. Abrams, D.P., T.J. Paulson, and A. Tena-Colunga, "Aspects of Response for Masonry Building Structures," *Proceedings of Fourth U.S. National Conference on Earthquake Engineering*, Palm Springs, May 1990, 10pp.
13. Abrams, D.P., and T.J. Paulson, "Perceptions and Observations of Seismic Response for Reinforced Masonry Building Structures," *Proceedings of Fifth North American Masonry Conference*, Univ. of Illinois, June 1990, 13pp.
14. Abrams, D.P. and T.J. Paulson, "Modeling Concrete Masonry Building Structures at One-Quarter Scale," *Structural Journal of the American Concrete Institute*, Title No. 88-S50, Vol. 88, No. 4, July-August 1991, pp. 475-485.

STUDY ON SIMILITUDE RELATIONSHIPS OF REINFORCED CONCRETE COLUMNS BASED ON SHAKING TABLE TESTS

Lu Xilin¹ and Liao Guangming²

ABSTRACT

According to dynamic similitude requirements and properties of reinforced concrete structures, five sets of reinforced concrete columns were tested on shaking table to find out the similitude relationships between models and prototypes in the case of some similitude requirements are not satisfied.

INTRODUCTION

In the research of seismic resistance of engineering structures, it is necessary to carry out shaking table tests in order to investigate the dynamic behavior of structures under strong earthquake. Since the capacity and size of shaking table are limited, it is very common to do model test on shaking table instead of prototype test. Therefore the similitude relationships between model and prototype become a key problem in this kind of test, and more and more scholars pay attention to the research on dynamic similitude requirements of reinforced concrete structures. For many years the research work was limited to the theoretical analysis, and little work was done by means of shaking table tests. The work in this paper is mainly based on shaking table tests of reinforced concrete columns and system identification, then the similitude relationships and the formula were obtained to predict the response of prototype by using the model test results.

SHAKING TABLE TESTS

Five sets of 18 reinforced concrete columns were tested on shaking table to investigate the behavior of reinforced concrete with different scale factors when some of the similitude requirements are not met.

Test Design

The cross section of basic columns, which is on the 1/2 scale of prototype, is 200 mm by 300 mm with the height of 1800 mm, and the cross section of model columns is 100 mm by 150 mm with the height of 900 mm and 50 mm by 75 mm with the height of 450 mm respectively. The specimens are shown in Fig.1.

The aggregates and the reinforcements were equally scaled during the manufacture of the specimens, and the additional load was applied to the specimens to simulate the vertical load with different scale factors in order to study the effect of gravity load on the dynamic behavior. The similitude relationships are listed in table 1.

-
1. Assoc. Professor, Institute of Eng. Struct., Tongji Univ., P. R. China
 2. Engineer, Institute of Eng. Design, Chengdu Branch, Academia Sinica

Table 1 Similitude Relationships

scaling parameters *	similitude requirements
strain S_ϵ	1
stress S_σ	$S_\sigma = S_E$
modulus of elasticity S_E	$S_E = S_\sigma$
poisson's ratio S_μ	1
mass density S_ρ	$S_\rho = S_\sigma / S_L$
length S_L	S_L
displacement S_x	$S_x = S_L$
rotation S_β	1
area S_A	$S_A = S_L^2$
concentrated force S_p	$S_p = S_E S_L^2$
line load S_v	$S_v = S_\sigma S_L$
uniformly distributed force S_q	$S_q = S_\sigma$
moment S_M	$S_M = S_\sigma S_L^3$
mass S_m	$S_m = S_\rho S_L^3$
stiffness S_k	$S_k = S_E S_L$
damping S_c	$S_c = S_m / S_t$
time or period S_t	$S_t = (S_m / S_k)^{0.5}$
velocity S_v	$S_v = S_x / S_t$
acceleration S_a	$S_a = S_x / S_t^2$

* The scaling parameters refer to the ratio of units between prototype and model for a physical quantity, i. e. $S_L = L_p / L_m$ (where L_p, L_m are the length of prototype and model respectively).

According to the properties of the specimens and similitude requirements, the compressed EL-centro (N-S, 1940) earthquake record was used as input acceleration of the shaking table with sampling data of 1000 points. The peak value of the input acceleration was gradually increased to study the behavior of reinforced concrete in the different deformation stages. The acceleration and displacement of the specimens were surveyed

during excitations, and the strains of reinforcements and the surface strains of concrete were measured as well. All the data were recorded and stored in PDP 11/34 computer for further analysis.

Test Results

All the specimens underwent four stages from elasticity to failure during the whole tests.

Elastic stage When the peak value of input acceleration was very low, the deformation of the specimens was very small, and the specimens did not crack at all. The peak values of input and response are listed in table 2, and the time history of acceleration response is shown in Fig. 2.

Table 2 The test results in elastic stage

specimen No.	concrete strength (Mpa)	vertical load (kN)	input accel. (g)	response accel. (g)
Z2-1	33.7	100	0.1367	0.2793
Z2-2	37.5	136	0.1095	0.1707
Z4-1	36.2	39.86	0.1719	0.3906
Z4-2	31.2	39.86	0.1663	0.2762
Z8-1	20.0	3.40	0.3031	1.0130

Cracking stage When the input acceleration was increased, the horizontal cracks appeared in the bottom of the columns, and the deformation of the specimens was still small, and the crack width was also very small. The test results in this stage are listed in table 3, and the displacement time history is shown in Fig. 3.

Table 3 The test results in cracking stage

specimen No.	input accel. (g)	response accel. (g)
Z2-1	0.2305	0.4883
Z2-2	0.2112	0.4047
Z4-1	0.3223	0.5899
Z4-2	0.3450	0.5859
Z8-1	0.5230	1.7487

Reinforcement yielding stage When the input was increased, the cracks in the bottoms of the columns penetrated through the cross section, a portion of concrete was crushed, and the reinforcements of the columns were yielded. As a result the deformation of the specimens became very large. The test results in this stage are listed in table 4, and the time history of acceleration response is shown in Fig. 4.

Table 4 The test results in yielding stage

specimen No.	input accel. (g)	reponse accel. (g)
Z2-1	0.4414	0.7637
Z2-2	0.4028	0.6237
Z4-1	0.7810	1.0000
Z4-2	0.7470	0.9174
Z8-1	1.0609	2.2727

Failure stage When the peak value of input was over 1g, the specimens were swung severely; and the concrete in the cracking zone was crushed; and the test finally stopped. The test results in this stage are listed in table 5, and the acceleration response is shown in Fig. 5.

Table 5 The test results in failure stage

specimen No.	input accel. (g)	response accel. (g)
Z2-1	1.2110	1.6290
Z2-2	0.8036	0.9561
Z4-1	1.5800	0.8200
Z4-2	1.3320	0.8744
Z8-1	2.1434	2.7715

SIMILITUDE RELATIONSHIPS

For earthquake simulation of the structures, the dynamic similitude relationships mainly include the vibration frequencies of model and prototype, the failure mechanism of model and prototype, the restoring force characteristics of model and prototype, and the resistance capacity of model and prototype. Therefore in this research emphasis is put on the dynamic behavior of model and prototype to study their similitude relationships.

Frequency similarity between model and prototype

According to similitude relationships the frequency of prototype can be expressed as

$$f_p = S_f f_m \quad (1)$$

when the boundary condition of the model is the same as that of prototype. But sometimes, the model condition is different from that of prototype. Therefore the similitude parameter of frequency must be modified as follows:

$$S_f = \beta_f S_{f,d} \quad (2)$$

$$\beta_f = (S_{k,t} / S_{k,d})^{0.5} \quad (3)$$

where S_f — modified similitude parameter of frequency;

$S_{f,d}$ — designed similitude parameter of frequency;

β_f — coefficient concerning the stiffness difference caused by the model's boundary condition; when the condition is identical, $\beta_f = 1$; when the model stiffness is larger than it should be, $\beta_f < 1$; when the model stiffness is smaller than it should be, $\beta_f > 1$;

$S_{k,t}$ — tested similitude parameter of stiffness;

$S_{k,d}$ — designed similitude parameter of stiffness.

With expressions (1) to (3), the similitude parameter of frequency is modified. The tested results and modified results are listed in table 6.

Table 6 Frequency similitude parameters of model and prototype

specimen No.	similitude parameters			errors (%)		notices
	designed $S_{f,d}$	tested $S_{f,t}$	modified S_f	No modi. δ_n	modified δ	
Z2-1	0.366	0.436	0.448	16.055	2.752	Z2-1/Z8-1
Z2-2	0.855	0.894	0.855	4.362	4.362	Z2-2/Z4-2
Z4-1	0.893	0.864	0.893	3.356	3.356	Z2-1/Z4-1
	0.763	0.816	0.763	6.495	6.495	Z2-2/Z4-1
Z4-2	1.000	0.946	1.000	5.708	5.708	Z2-1/Z4-2
Z8-1	0.313	0.412	0.383	24.029	7.038	Z2-2/Z8-1
	0.410	0.504	0.502	18.651	0.396	Z4-1/Z8-1
	0.366	0.461	0.448	20.607	2.820	Z4-2/Z8-1

From table 6, it can be seen that the modified S_f matches the tested $S_{f,t}$ very well. With the modified S_f , we can obtain the prototype's frequency which can be used either for dynamic analysis or for seismic design of the prototype.

Failure mechanism similarity between model and prototype

The shaking table tests of five-set reinforced concrete columns show that the crack pattern and failure mechanism of the models are quite similar with that of prototype: all the reinforced concrete columns cracked from the bottom of the columns; and when the reinforcement yielded the concrete at the cracked section crushed; and finally the specimens lost their stability because of the large deformation in the plastic hinge. Therefore it is possible to predict the failure behavior of prototype with model testing.

Restoring force characteristics similarity between model and prototype

By means of system identification to the test data, it can be seen that the restoring force models of prototype and model are quite similar: before reinforcements yield the bilinear restoring force model can be used to predict the seismic response; after reinforcements yield the trilinear

model with descending branch can be used to calculate the dynamic response. The restoring force model is shown in Fig.6 and the comparison of tested and predicted acceleration time history is shown in Fig.7.

Acceleration response similarity between model and prototype

Acceleration is an important factor in the seismic design of structures, therefore it is common to use the acceleration response to evaluate the seismic resistant capacity of structures. From the above-mentioned five-set model tests the following formula for predicting the acceleration response of prototype can be obtained

$$A_p = \beta_1 \beta_2 \beta_3 \beta_4 A_{m,t} \quad (4)$$

where β_1 is the coefficient concerning the material strength of specimens and the stiffness of specimens as well as the depth of compression zone of the column section.

$$\beta_1 = 1 - (1 - \beta_R / \beta_k) \xi_1 \quad (i = 1, 2, 3, 4) \quad (5)$$

where $\beta_R = R_p / R_m$; $\beta_k = K_p / K_m$; where R_p and R_m are the material strength of prototype and model, respectively; K_p and K_m are the stiffness of prototype and model, respectively; ξ_1 is the depth coefficient of compression zone of the column section, $\xi_1 = 1, 0.77, 0.4, 0.05$ for the four deformation stages according to the above-mentioned tests.

$$\beta_2 = 1 / \beta_1 \quad (6)$$

β_2 is coefficient concerning the size effect of concrete.

$$\beta_1 = \frac{0.56 + 0.697 \frac{d_m}{0.423 V_m / h_m + h_m}}{0.56 + 0.697 \frac{d_m}{0.423 V_m S_L / h_m + h_m}} \quad (7)$$

where d_m — maximum lateral dimension of model column;

h_m — height of model column;

V_m — volume of model column;

S_L — scaling parameter of length;

$$\beta_3 = S_E S_L^2 / S_m \quad (8)$$

$$\beta_4 = 1 - \delta_1 \quad (9)$$

where δ_1 is the input error of the shaking table in percentage which can be obtained in each test run 1.

$A_{m,t}$ — tested acceleration response of the model.

With expressions (4) to (9), we have calculated the acceleration responses of prototype on the basis of model testing. The results are as follows:

Predicting the response of Z2-1 and Z2-2 with model Z8-1

In this case, all the coefficients are for Z2-1 vs. Z8-1: $\beta_1 = \{ 0.5566, 0.6586, 0.8226, 0.9772 \}$; $\beta_2 = 0.939$, $\beta_3 = 0.544$; $\beta_4 = 1 - \delta_1$; for Z2-2 vs. Z8-1: $\beta_1 = \{ 0.56, 0.6612, 0.824, 0.978 \}$; $\beta_2 = 0.939$; $\beta_3 = 0.4$; $\beta_4 = 1 - \delta_1$. The final results are listed in table 7 in which $A_{p,t}$ is the tested response of the prototype, A_p the predicted response of the prototype, and δ_o the error between tested and predicted responses.

Table 7 Predicted response of Z2-1 and Z2-2 with model Z8-1

Stages		I		II		III	
Specimens		Z2-1/Z8-1	Z2-2/Z8-1	Z2-1/Z8-1	Z2-2/Z8-1	Z2-1/Z8-1	Z2-2/Z8-1
Input (g)	$A_{m,t}$	0.3031	0.3031	0.5230	0.5230	1.0609	1.0609
	δ_1	0.2060	0.1060	0.2340	-0.009	0.3070	0.0530
Resp. (g)	$A_{m,t}$	1.0130	1.0130	1.7487	1.7487	2.2727	2.2727
	$A_{p,t}$	0.2793	0.1707	0.4883	0.4047	0.7637	0.6237
	A_p	0.2304	0.1902	0.4505	0.4300	0.6685	0.6657
	δ_o	0.1700	0.1100	0.0770	0.0620	0.1200	0.0670

Predicting the response of Z4-1 and Z4-2 with model Z8-1

In this case, all the coefficients are for Z4-1 vs. Z8-1: $\beta_1 = \{ 0.58, 0.6766, 0.8320, 0.9790 \}$; $\beta_2 = 0.9807$; $\beta_3 = 0.3491$; $\beta_4 = 1 - \delta_1$; and for Z4-2 vs. Z8-1: $\beta_1 = \{ 0.511, 0.6235, 0.8044, 0.9756 \}$; $\beta_2 = 0.9807$; $\beta_3 = 0.3491$; $\beta_4 = 1 - \delta_1$. The final results are listed in table 8.

Table 8 Predicted response of Z4-1 and Z4-2 with model Z8-1

Stages		I		II		III	
Specimens		Z4-1/Z8-1	Z4-2/Z8-1	Z4-1/Z8-1	Z4-2/Z8-1	Z4-1/Z8-1	Z4-2/Z8-1
Input (g)	$A_{m,t}$	0.3031	0.3031	0.5230	0.5230	1.0609	1.0609
	δ_1	-0.360	-0.360	-0.430	-0.470	-0.520	-0.500
Resp. (g)	$A_{m,t}$	1.0130	1.0130	1.7487	1.7487	2.2727	2.2727
	$A_{p,t}$	0.3906	0.2762	0.5899	0.5859	1.0000	0.9174
	A_p	0.2776	0.2410	0.5791	0.5486	0.9838	0.9388
	δ_o	0.2900	0.1300	0.0180	0.0640	0.0160	0.0230

Predicting the response of Z2-1 and Z2-2 with model Z4-1

In this case, all the coefficients are for Z2-1 vs. Z4-1: $\beta_1 = \{ 0.9512, 0.9624, 0.9805, 0.9976 \}$; $\beta_2 = 0.9781$; $\beta_3 = 1.5944$; $\beta_4 = 1 - \delta_1$; and for Z2-2 vs. Z4-1: $\beta_1 = \{ 1.0254, 1.0195, 1.0102, 1.0013 \}$; $\beta_2 = 0.9781$; $\beta_3 = 1.17235$; $\beta_4 = 1 - \delta_1$. The final results are listed in table 9.

Table 9 Predicted response of Z2-1 and Z2-2 with model Z4-1

Stages		I		II		III	
Specimens		Z2-1/Z4-1	Z2-2/Z4-1	Z2-1/Z4-1	Z2-2/Z4-1	Z2-1/Z4-1	Z2-2/Z4-1
Input	$A_{m, t}$	0.1719	0.1719	0.3223	0.3223	0.7810	0.7810
	(g) δ_1	0.1890	-0.046	0.1640	-0.062	0.0280	0.1390
Resp.	$A_{m, t}$	0.3906	0.3906	0.5899	0.5899	1.0000	1.0000
	$A_{p, t}$	0.4883	0.4047	0.7637	0.6237	1.6290	0.9561
	(g) A_p	0.4742	0.4189	0.7401	0.6387	1.5121	0.8697
	δ_o	0.0290	0.0350	0.0310	0.0240	0.0720	0.0900

Predicting the response of Z2-1 and Z2-2 with model Z4-2

In this situation, all the coefficients are for Z2-1 vs. Z4-2: $\beta_1 = \{ 1.05411, 1.04166, 1.02164, 1.0027 \}$; $\beta_2 = 0.9871$; $\beta_3 = 1.5944$; $\beta_4 = 1 - \delta_1$; and for Z2-2 vs. Z4-2; $\beta_1 = \{ 1.13634, 1.10498, 1.05454, 1.0068 \}$; $\beta_2 = 0.9781$; $\beta_3 = 1.17235$; $\beta_4 = 1 - \delta_1$. The final results are listed in table 10.

Table 10 Predicted response of Z2-1 and Z2-2 with model Z4-2

Stages		I		II		III	
Specimens		Z2-1/Z4-2	Z2-2/Z4-2	Z2-1/Z4-2	Z2-2/Z4-2	Z2-1/Z4-2	Z2-2/Z4-2
Input	$A_{m, t}$	0.1663	0.1663	0.3450	0.3450	0.7470	0.7470
	(g) δ_1	0.1500	-0.077	0.2460	0.0040	-0.016	0.0897
Resp.	$A_{m, t}$	0.2762	0.2762	0.5859	0.5859	0.9174	0.9174
	$A_{p, t}$	0.4883	0.4047	0.7637	0.6237	1.6290	0.9561
	(g) A_p	0.3859	0.3876	0.7176	0.6448	1.4850	1.0098
	δ_o	0.2090	0.0420	0.0600	0.0340	0.0880	0.0560

CONCLUSIONS

Based on the test results and similitude analysis as well as calculation, the following conclusions can be drawn for the dynamic model testing.

(1) The dynamic similitude relationships of prototype and model are influenced by material strength, model design and fabrication accuracy, boundary condition of model, loading techniques as well as the mass ratio of prototype and model. If these factors are effectively controlled, the model test on shaking table can be used to predict the response of prototype with acceptable accuracy.

(2) The crack and failure patterns of model and prototype are quite similar; and the dynamic restoring force characteristics of model and prototype is also similar.

(3) The vibration frequency has good similitude relationships in model and prototype. With expressions (1) to (3), the frequency of

prototype can be obtained.

(4) The acceleration response of prototype can be predicted with expressions (4) to (9) although some of the similitude requirements were ignored in the modeling. The test results show that the predicted response and tested response matched in the acceptable accuracy.

REFERENCES

- [1] G.M. Sabnis, H.G. Harris, etc., Structural Modeling and Experimental Techniques, Prentice-hall, Inc., Englewood Cliffs, 1983.
- [2] H.G. Harris, Dynamic Modeling of Concrete Structures, Publication SP-73, ACI, Detroit, 1982.
- [3] H. Krawinkler, Possibilities and Limitations of Scale Model Testing in Earthquake Engineering, Proc. of the 2nd U. S. National Conference on Earthquake Engineering, 1979.
- [4] X.L. Lu and B.L. Zhu, Shaking Table Tests of Model R.C. Columns and Their Similitude Relationships, Proc. of the 2nd Chinese National Conference on Earthquake Engineering, 1987 (in Chinese).
- [5] G.M. Liao and X.L. Lu, Study on the Dynamic Similitude Relationships of Reinforced Concrete Structures, Journal of Sichuan Building Science Research, No.3, 1989 (in Chinese).

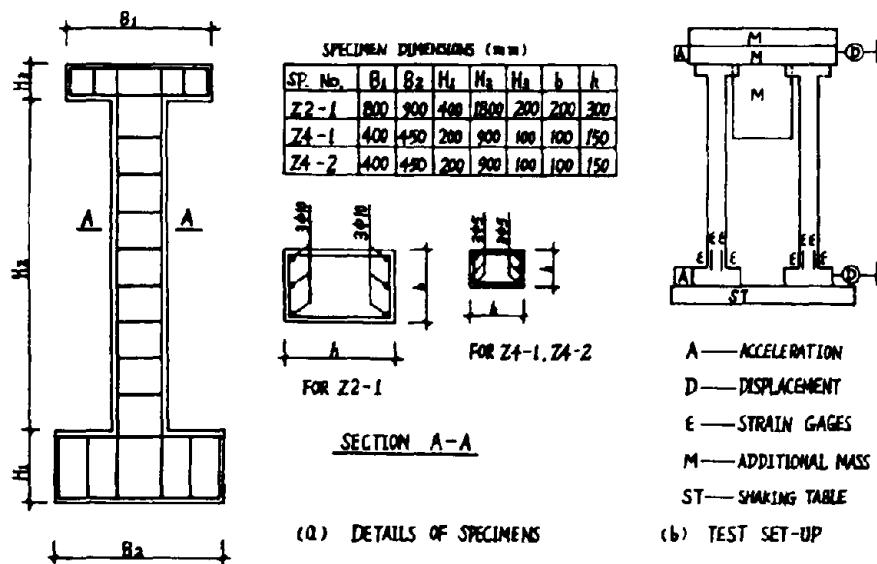


Fig.1 Details of specimens and test set-up

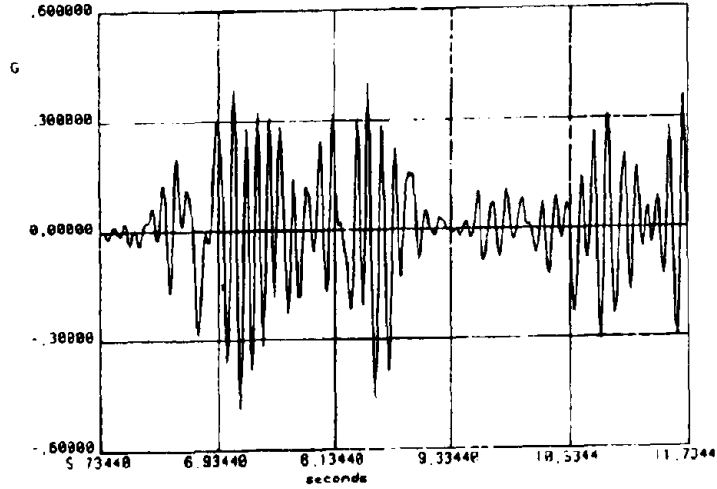


Fig.2 Time history of acceleration response
of Z2-1 (elastic stage)

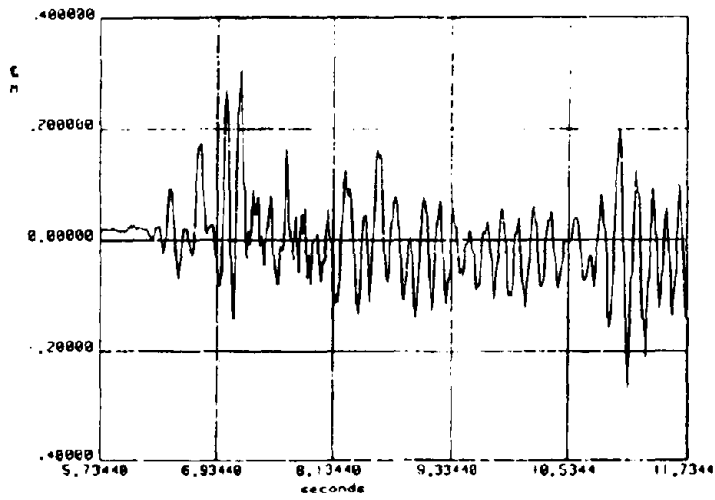


Fig.3 Time history of displacement response
of Z4-2 (cracking stage)

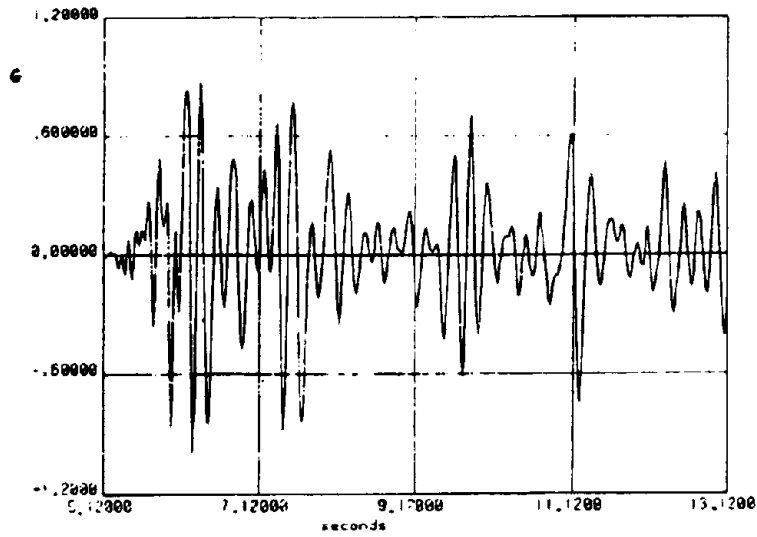


Fig.4 Time history of acceleration response of Z4-1 (yielding stage)

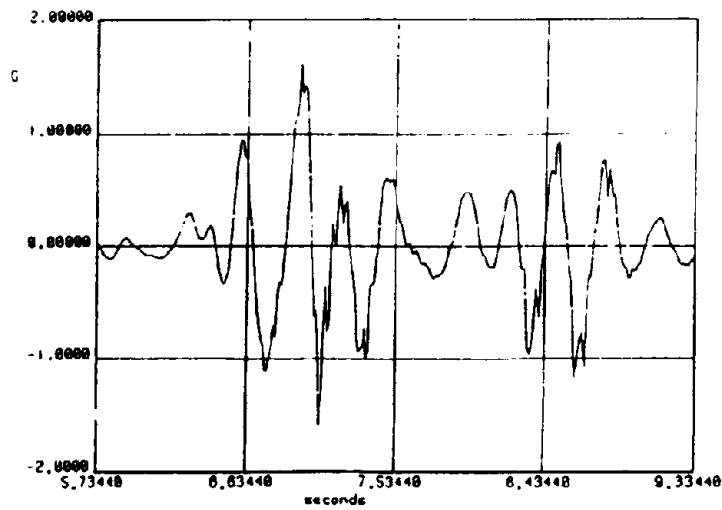


Fig.5 Time history of acceleration response of Z2-1 (failure stage)

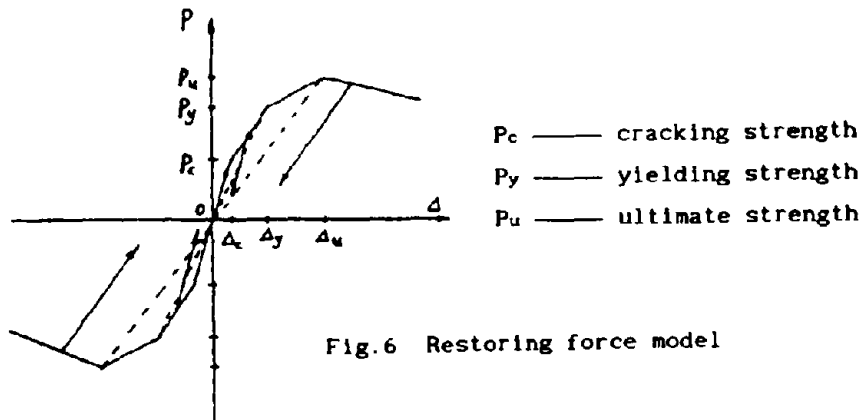


Fig. 6 Restoring force model

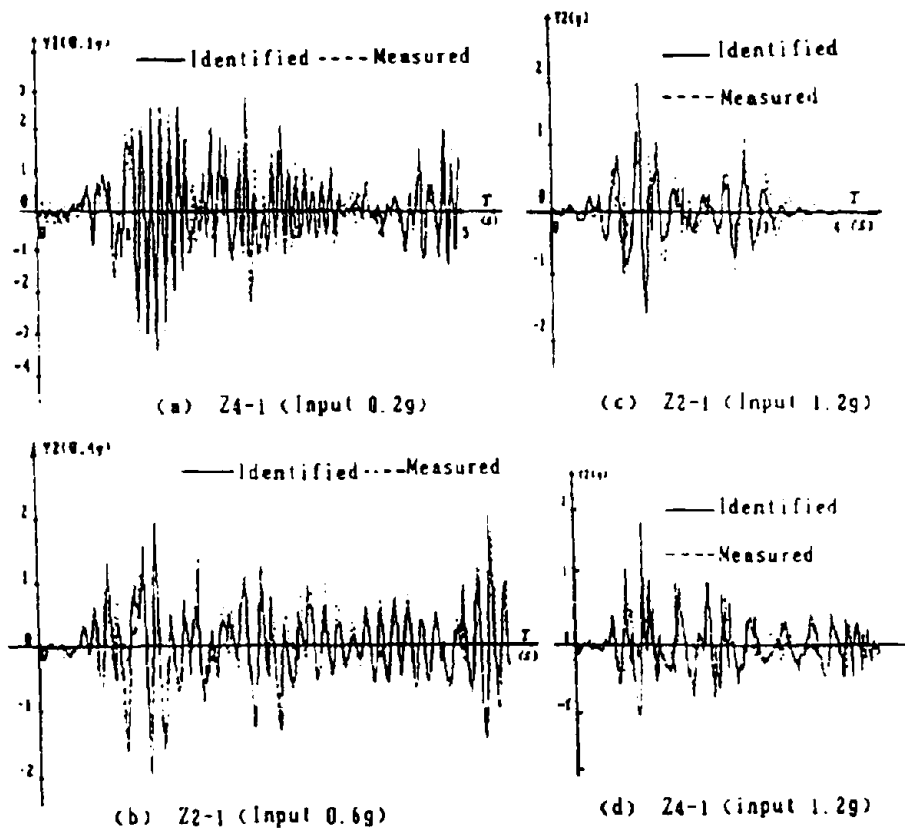


Fig. 7 Time history of measured and identified acceleration responses

PRELIMINARY STUDY ON DISTORTION AND MODIFICATION METHOD FOR MODEL TESTING OF DYNAMIC ULTIMATE STRENGTH

Zheng Wei*

ABSTRACT

Based on the concept of Ideal Model and Real Model defined in this paper, the magnitude of distortion and general modification method for model testing is presented. Particularly for example, the distortion of gravity in the masonry building model testing of dynamic ultimate strength and its magnitude is analysed and modification method is applied to modify the results of two multiple-story masonry building models, tested on the shaking table, in order to estimate the seismic capacity of the prototype buildings.

INTRODUCTION

Model testing is a practical method for realizing and predicting the response of prototype structure that is subjected to complicated loads. However, the extent to which the model represents the prototype depends on the extent to which the parameters of model comply with the resemble relationships. Although the resemble relationships deduced from the Buckingham theory^{(1) . (2)} are very clear, some difficulties will be found in making and testing the model that complies with all resemble relationships. Hence there are always distortions in the model testing, all that can be done is to control the distortion on the lowest level, estimate adequately the distortion and modify it.

In this paper, resemble relationships are not discussed in details, only distortion and modification method in model testing is concerned with.

IDEAL MODEL, REAL MODEL AND MAGNITUDE OF DISTORTIONS

In fact, the parameters, used to describe the structure, can be divided into two groups.

One group is composed of the known parameters, such as geometry size, strength of materials, loads and so on, which can be defined as Characteristic Parameters, written in

* M.Eng and structural engineer, Research Department, Beijing Institute of Architectural Design and Research, Beijing, P.R.C.

$\{P_p\}$ or P_p for the prototype, and in $\{M_m\}$ or M_m for the model;

Another group is composed of the unknown parameters, such as critical strength of structure, displace, peak value of dynamic acceleration and so on, which can be defined as Response Parameters, written in $\{P_r\}$ or P_r for the prototype, and $\{M_r\}$ or M_r for the model.

The purpose of structure testing is to obtain the Response Parameters of structure subjected to the effect of the Characteristic Parameters of structure. When it is difficult to test the prototype structure, we can translate the Characteristic Parameters of the prototype structure, $\{P_c\}$, into the Characteristic Parameters of the model structure, $\{M_c\}$. Through testing the model structure, we can obtain the Response Parameters of the model structure, $\{M_r\}$, then the Response Parameters of the model structure, $\{M_r\}$, can be translated into the Response Parameters of prototype structure, $\{P_r\}$, which we expect.

The procedure above can be simply expressed as follows.

$$\{M_c\}_i = [S_c]_{mi} \cdot \{P_c\}_i \quad (1)$$

$$\{M_r\}_i = \{F(M_c)\}_i \quad (2)$$

$$\{P_r\}_i = [S_r]_{pi}^{-1} \cdot \{M_r\}_i \quad (3)$$

Here, $[S_c]_{mi}$ or $[S_r]_{pi}$ is the translation matrix, which is determined by the resemble relationships and consists of the scaling parameters; $F(M_c)$ is the rule which both prototype and model should follow. It shows that the Response Parameters of the structure is the function of the Characteristic Parameters. This function can be explicit or implicit.

Restricted by real conditions, there is scarcely the model that complies with all resemble relationships. For the sake of discrimination, the concept of Ideal Model and Real Model is proposed as follows.

The model which complies with all resemble relationships can be defined as Ideal Model, in which Characteristic Parameters are written in $\{M_c\}$, and Response Parameter written in $\{M_r\}$;

The model which complies with several, not all, resemble relationships can be defined as Real Model, in which Characteristic Parameters are written in $\{M'_c\}$, and Response Parameters written in $\{M'_r\}$.

In Distortions of the model, there are the differences between the parameters of the Real Model and the parameters of the Ideal Model. If taking $\{\Delta M_c\} = \{M'_c\} - \{M_c\}$, then the magnitude of Distortions can be represented by $\{\Delta M_c\}$, and the parameter, $\{\Delta M_c / M'_c\}$, can be used to evaluate the precision of the Real Model.

MODIFICATION METHOD FOR THE REAL MODEL TESTING

Usually the tested model is the Real Model, which Characteristic Parameters is $\{M'_c\} = \{M_c\} + \{\Delta M_c\}$, including the Distortion, $\{\Delta M_c\}$. Through testing the Real Model,

the Response Parameters of the Real Model can be obtained as follows;

$$\{M'_r\} = \{F(M_e + \Delta M_e)\}$$

Apparently, $\{M'_r\}$ is not the Response Parameters of the Ideal Model, which should be $\{M_e\} = \{F(M_e)\}$, the influence of the Distortion is included in $\{M\}$. Fig.1 shows the relationships among Ideal Prototype, Ideal Model, Real Prototype and Real Model. So if we translate the Response Parameters of the Real model into that of prototype, what we can obtain is not correct Response Parameters of Ideal Prototype, as we have expected, but the Response Parameters of Real Prototype, which includes the influence of the Distortion.

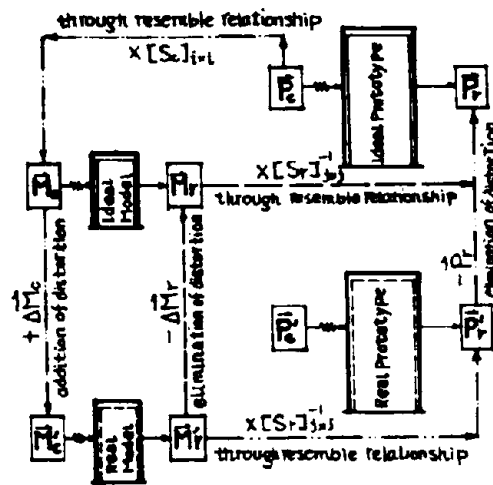


Fig.1 The relationships among Ideal Prototype, Ideal Model, Real Prototype and Real Model.

In order to obtain the Response Parameter of the Ideal Prototype on the base of testing of the Real Model, the following modification method is proposed;

The Response Parameters of the Real Model can be expressed as;

$$\{M'_r\} = \{F(M_e + \Delta M_e)\} \quad (4)$$

The Response Parameters of the Ideal Model can be expressed as;

$$\{M_e\} = \{F(M_e)\} \quad (5)$$

If the different, $\{\Delta M_e\}$, is eliminated from Formu.4, the Response Parameters of the Ideal Model, $\{M_e\}$, can be obtained. So Formu.5 can be changed as follows;

$$\begin{aligned} \{M_e\} &= \{F(M_e)\} = \{F([M_e + \Delta M_e] + [-\Delta M_e])\} = \{F([M_e] + [-\Delta M_e])\} \\ &= \{F(M'_r)\} + [\partial F(M'_r) / \partial M'_r] \cdot \{-\Delta M_e\} \\ &= \{F(M'_r)\} - [\partial F(M'_r) / \partial M'_r] \cdot \{\Delta M_e\} \end{aligned}$$

Here $[\partial F(M'_j) / \partial M_j]$ is a Jacobi Matrix, which means the changes of Response Parameters caused by the unit changes of the Characteristic Parameters. If $\{F(M'_j)\}$ is the explicit function, it is easy to obtain this Jacobi Matrix; If $\{F(M'_j)\}$ is not the explicit function, the Jacobi Matrix can be obtained through a series of testing by changing some Characteristic Parameters in some range.

In order to eluminate the concept and modification method above, the Distortion of gravity and its modification in the masonry building model tested on the shaking table will be discussed.

DISTRORTION OF GRAVITY IN THE MODEL TESTED ON THE SHAKING TABLE

In the model testing on the shaking table, the scaling parameter of the dynamic acceleration is as follows:

$$C_u = \frac{C_a}{C_p C_l} \quad (2)$$

Here, C_l is the scaling parameter of geometry size, for small scale model, $C_l > 1$; C_p is the scaling parameter of stress, for the model of non-linear ultimate strength, in order to maintain the strict resemble relationships between model and prototype at any stage, the property of materials between model and prototype should comply with the resemble relationships shown in Fig.2. For the mansory building model, it is difficult to find the substitutive materials for the model, which can comply with the resemble relationships shown in Fig.2. Usually the model materials is taken as the same as the prototype materials, so $C_p = 1$; C_p is the scaling parameter of density, it is difficult to raise the density of the model, substitutive method is to add additional mass blocks into the model, but its amounts is limited, usually $C_p > 1 / C_l$.

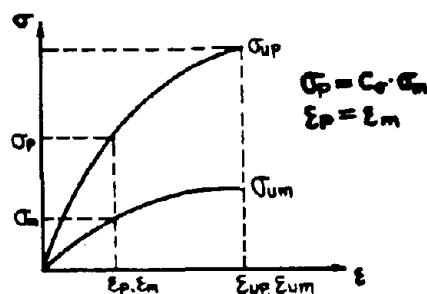


Fig.2 The resemble relationship of the property of materials between model and prototype.

Restricted by above conditions, for the masonry building model of dynamic testing, $C_a < 1$.

On the other hand, for the model of dynamic testing, the scaling parameter of gravity acceleration, C_g , should be the same as the scaling parameter of dynamic acceleration, C_a , that is $C_g = C_a$, so that the ratio of gravity to dynamic force can keep the same between model and prototype.

Hence, the gravity acceleration of the Ideal Model, g_m , should be that $g_m = g_p / C_g = g_p / C_a = g / C_a > 1$, here g_p is the gravity acceleration of prototype, and $g_p = g$;

However, the tested model usually is in the same gravity acceleration as prototype, so the tested model is a Real Model, in which gravity acceleration is that $g'_m = g_p = g$. There is gravity distortion in the model of dynamic testing. The magnitude of the distortion is that $\Delta g_m = g'_m - g_m = g - g / C_a = (1 - 1 / C_a) \cdot g$, or $\Delta g_m / g'_m = \Delta g_m / g = 1 - 1 / C_a$.

MODIFICATION OF THE GRAVITY DISTORTION IN THE MASONRY BUILDING MODEL TESTED ON THE SHAKING TABLE

Because the peak value of input acceleration at which the critical cracks occur in the masonry buildings, which is written in A_{pc} for prototype and written in A_{mc} for model, is an acceptable index of the aseismic capacity of the masonry buildings, the modification of the influence of the distortion of gravity acceleration on the value of A'_{mc} in the Real Model should be made in order to predict correctly the aseismic capacity of prototype building.

The modification procedure is as follows;

First, two assumptions are adopted;

- 1) The value of A_{pc} or A_{mc} is directly proportional to the crack-resistant strength of the masonry building;
- 2) The crack-resistant strength of the masonry building is indexed out by the strength that resists main tensile stress in the masonry walls.

According to Chinese national aseismic building code (TJ-78), the strength of main tensile stress of the Ideal Model of the masonry building is the following;

$$R_1 = R_1 \sqrt{1 + \frac{\sigma_0}{R_1}} \quad (7)$$

The strength of main tensile stress of the Real Model of the masonry building is the following;

$$R'_1 = R_1 \sqrt{1 + \frac{\sigma'_0}{R_1}} \quad (8)$$

Here σ_0 and σ'_0 is respectively the vertical stress in the Ideal Model and the vertical stress in the Real Model; R_1 is the shear strength of mortar.

Taking $\Delta\sigma_0 = \sigma'_0 - \sigma_0$, $\Delta\sigma_0$ is the magnitude of the distortion of the vertical stress in the Real Model. Because the distortion of the vertical stress is caused by the distortion of the gravity acceleration, and the vertical stress is directly proportional to the gravity acceleration, the following relationship can be obtained;

$$\frac{\Delta\sigma_0}{\sigma_0} = \frac{\Delta g}{g} \quad \text{or} \quad \Delta\sigma_0 = \frac{\Delta g}{g} \sigma'_0 = (1 - 1/Cu) \sigma'_0$$

If taking

$$R_1 = F(\sigma_0) = R_1 \sqrt{1 + \frac{\sigma_0}{R_1}}$$

$$R'_1 = F(\sigma'_0) = R_1 \sqrt{1 + \frac{\sigma'_0}{R_1}}$$

then

$$R_1 = F(\sigma_0) = F(\sigma'_0 - \Delta\sigma_0) = F(\sigma'_0) + \frac{\partial F(\sigma'_0)}{\partial \sigma'_0} (-\Delta\sigma_0) = R'_1 + \frac{\partial F(\sigma'_0)}{\partial \sigma'_0} (-\Delta\sigma_0)$$

So

$$\Delta R_1 = F(\sigma'_0) - F(\sigma_0) = \frac{\partial F(\sigma'_0)}{\partial \sigma'_0} \Delta\sigma_0 = \frac{1}{2\sqrt{1 + \frac{\sigma'_0}{R_1}}} \Delta\sigma_0$$

$$= \frac{1}{2(R_1 + \sigma'_0)} R_1 \sqrt{1 + \frac{\sigma'_0}{R_1}} \times (1 - 1/Cu) \sigma'_0 = (1 - 1/Cu) \frac{\sigma'_0}{2(R_1 + \sigma'_0)} R'_1$$

According to the assumption, Formu.6 and Formu.7, the distortion of the peak value of input acceleration, A, can be obtained as follows;

$$\Delta A_{mc} = A'_{mc} \frac{\Delta R_1}{R_1} = (1 - 1/Cu) \frac{\sigma'_0}{2(R_1 + \sigma'_0)} A'_{mc}$$

The approximate peak value of input acceleration, A, at which the critical cracks occur in the Ideal Model of masonry building, can be obtained as follows;

$$A_{mc} = A'_{mc} - \Delta A_{mc}$$

According to the resembel relationships, the peak value of input acceleration, A, at which the critical cracks occur in the prototype masonry building is obtained as follows;

$$A_{pc} = Cu A_{mc} = Cu(A'_{mc} - \Delta A_{mc})$$

$$\text{Taking } \lambda = -(1 - 1/Cu) \frac{\sigma'_0}{2(R_1 + \sigma'_0)} \quad \text{then} \quad A_{pc} = A'_{mc} - \Delta A_{mc} = (1 + \lambda) A'_{mc}$$

$$\text{So } A_{pc} = Cu A_{mc} = Cu(1 + \lambda) A'_{mc}$$

Taking the two multi-story masonry building models, tested by author on the shaking table in Tongji University⁽⁴⁾, this method is applied to predict the aseismic capacity of

prototype building.

The basic resemble and the scaling parameter of the two model are shown in Table 1;

Table 1

scaling parameter	category		
	resemble relationship	the value of Ideal Model	the value of Real Model
C_1	C_1	4.00	4.00
C_p	C_p	0.25	0.769
C_e	C_e	1.00	1.834
C_{Rj}	C_e	1.00	1.549
C_u	$C_e / C_p C_1$	1.00	0.596

The basic Characteristic Parameters and experimental results of testing on the shaking table are shown in Table 2;

Table 2

Model	category			
	C_u	R_j (kg/cm ²)	σ'_0 (kg/cm ²)	A'_{mr} (g)
I	0.596	0.602	1.620	0.336
II	0.596	0.602	0.667	0.420

The modification procedure and modified results are shown in Table 3;

Table 3

Prototype	category			
	C_u	λ	$A'_{pc} = C_u A'_{mr}$	$A_{pc} = (1+\lambda)C_u A'_{mr}$
	0.596	0.247	0.200g	0.250g
	0.596	0.178	0.250g	0.294g II

Note: A'_{pc} —the peak value of input acceleration at which critical crack occur in the prototype building, not taking distortion into accounts.

From the analysis above for the masonry building model tested on the shaking table with the distortion of gravity acceleration, the conclusion can be made that if the influence of distortion of gravity is not taken into accounts, the aseismic capacity of prototype deduced from the experimental results of the Real Model is lower and on the safe side.

REFERENCES

- (1) Wang Guangyian, The Vibration of Engineering Structure, P.R.C.

- (2) **Harry G. Harris, Dynamic Modeling of Concrete Structure, U.S.A.**
- (3) **E. Fumagalli, Statical and Geomechanical Models, Springer-Verlag / Wein 1973, Italy.**
- (4) **Zheng Wei, Identification for the Mathematical Models for the Unreinforced Concrete Block Masonry Building with R.C.Frame At the First Story and Estimation of Its Seismic Capacity, The dissertation for the degree of E.M., Tongji University, 1988, P.R.C.**

DYNAMIC MODEL TEST STUDIES OF PILE SUPPORTED PIERS INCLUDING EFFECTS OF BANK DEFORMATION

Wu Zaiguang¹, Han Guocheng² and Zhang Dongfeng³

(Dalian University of Technology)

ABSTRACT

Presented in this paper are the results of dynamic model tests of pile supported piers which are performed on the large scale shaking table. The main objects of test studies are inquire into failure feature and mechanism of the piers under different deformation of the bank slopes. Additionally, dynamic characteristics under microvibration are also measured for some piers.

INTRODUCTION

During the Tangshan earthquake of 1976, some pile supported piers located in Tianjin area suffered damage to varies extent. An earthquake damage survey shows that seismic induced bank deformation is one of significant factors which bring about failures of the piers. Since the aseismic research of pile supported pier involves the dynamic interactions of water, soil, pile structures and retaining wall, it is a very complicated subject. Up to the present, a few of research works have been done. Gao, M. [1] conducted a series of dynamic model tests of piled piers and mainly studied the dynamic characteristics under microvibration. Gao, G.Y. [2] also performed similar discusses by means of the tests of prototype piers. At the same time, other researchers [3] presented the aseismic analysis for piled piers. But summarily speaking, the studies were concentrated on linear elastic vibration of the piers. The further research for failure of the piers under strong earthquake is urgently required. In this paper, we regard the model piers as the object of studies, systematically investigate the effects of permanent deformation of the bank slope

1. Doctor, Dalian University of Technology, Dalian, P. R. China

2. Professor, Dalian University of Technology, Dalian, P. R. China

3. Master, Dalian University of Technology, Dalian, P. R. China

under macrovibration on failure of the piers, and give the relevant conclusions and propositions.

MODEL DESIGN AND CONSTRUCTION

The model tests are done by mean of the seismic-simulation shaking table which has size of 3×3 m , load carrying capacity of 10 ton , and maximum horizontal exciting acceleration of 1000 gal. The model piers are construction in a steel container ($4 \times 1 \times 1$ m), which is rigidly fixed upon the shaking table and mounted a plexiglass plate only on one lateral vertical face.

The model simulates a typical beam-slab wide-platform type pier at Tianjin port. Based on load carrying capacity of the shaking table, the geometrical proportion of model is taken as $1 / 30$. Each model pier contains 3 bents, and each bents has 2 fork piles and 12 vertical piles which is concrete squire ones with the cross-section of 17×17 mm. Four kinds of materials are selected to construct homogeneous bank slopes, i.e., plain concrete, gravel with mean grain diameter of 10 mm , beach sand and silt. The concrete bank is rigid and no bank deformation. Other three kinds of bank slopes are constructed by soil-fill in water and different bank deformations will take place under strong vibration. Two types of retaining walls, linked the platform with the heaped area, are used, i.e., gravity grain concrete wall and light steel counterforted wall. The profile of model pier is given in Fig. 1.

RESONANCE EXPERIMENTS

In order to get a clear understanding of the influence of different material bank slopes on the free vibretion characteristics of piers, we respectively performed the resonance tests for four piers. Piles, platforms, and retaining walls in these piers are same, only bank slopes are different. In the experiment, the shaking table excits the models in the form of micro-amplitude simple harmonic motion, the amplitude of which is 15 gal and frequencies change from 5 Hz to 45 Hz. The resonance curve of the model are measured and the dynamic features are obtained from the curves. The final results are given in Table 1, in which, f_1 represents the fundamental frequency of vibration, β_1 is the enlargement factor and ξ_1 is the damping ratio. From here, we can summrize following conclusions: 1). The free vibration characteristics of pile supported piers greatly change with the stiffness of bank slopes, when bank stiffness increases, the fundamental frequency of pier rises and the enlargement factor increases. 2). The foundamental frequencies of fore platform and rear plat-

form are equal, which shows that pounding between them don't occurs under microvibration. 3). Besides the concrete bank, for other three deformable banks, the fundamental frequencies of the piers are almost equal to ones of the banks. Obviously, since the most part of piles are buried in the soils, intense vibration of the piers is easily excited at the fundamental frequency of the bank slopes.

DYNAMIC FAILURE EXPERIMENTS

The objects of the tests are to investigate the basic feature of dynamic failure and to comprehend the failure mechanism. In the failure experiments, the simple harmonic vibration with linear increasing amplitude are taken as the input motions, the frequencies of which are retained at the fundamental ones of the pier and the amplitude of which increase at the rate of 80 gal per minute until the serious failures take place. Through the preparatory tests, the final loading accelerations of the shaking table are determined as: silt bank 300 gal, sand bank 350 gal, gravel bank 420 gal and concrete bank 1550 gal. In order to understand the failure cases under different loading periods, the method of the piece wise loading are used in the tests.

1. Pier Failure with Concrete Rigid Bank Slope

Obviously, no permanent deformations engender in the bank slope for this type of pier. The failures of pier prodominantly come from the action of earthquake inertia force. Fig. 2 gives the amplitude curves of response and input accelerations. From this Fig., it can be seen that in the period of initial loading, as exciting intensity of shaking table increases, the response amplitudes of the platforms increase, but when the amplitude of input motion exceeds some value, the responses gradually decrease along with the increments of input motion. The maximum response acceleration of the rear platform is 550 gal when the exciting acceleration reaches 155 gal. At this moment, the fractures are observed on the pile No. 7 and 8, the locations of which are at the fixing point on the bank surface. Continuously, when exciting intensity increases to 410 gal, the maximum response acceleration of the fore platform reaches 720 gal. Then, the fork piles begin to fracture at the location near pile caps. As the piles break one by one, the responses of platforms reduce seriously. Until the amplitude of input motion comes into 1550 gal, the platforms tend to completely collapse, and then the test stops. Based on above test phenomena, two initial conclusions may be drawn: 1). The aseismic capability of the pier with concrete rigid bank is very strong because of no bank deformations. The whole instability of the pier shouldn't happen until the earthquake force exerted on the pier achieves considerably strong value. 2). The

horizontal earthquake inertia force isn't fully supported by fork piles. The fractures firstly occur at vertical piles of rear platform, and after fork piles of fore platform broke, the platformes can also bear a number of inertia forces. These facts show that vertical piles must undertake horizontal earthquake force.

2. Pier Failure with Gravel Bank Slope

Besides earthquake inertia force, the bank deformation is also a important factor causing the failure of this type pier. Fig. 3 gives the amplitude curves of response and input accelerations. The input acceleration reflects the intensity of ground motion and the response accelerations embody the action of inertia force. Here in , it can be found that when the input amplitude comes into near 125 gal, the maximum response amplitudes of the platforms appear and are respectively 340 gal and 420 gal for fore platform and rear platform. Comparison with concrete rigid bank pier shows that at initial failure, the amplitude of input motion reduce from 155 gal to 125 gal, the response amplitude of fore platform decrease from 720 gal to 340 gal and rear platform from 550 gal to 420 gal. Obviously, the carrying capacity of the gravel bank pier reduce seriously than concrete bank pier, not only for the input motion but also for response inertia force. The reason should be the effect of bank deformation since piles, platforms, retaining walls, etc., are fully same for two types of piers. After initial failure, as the exciting intensity increases, the responses of platforms decrease gradually. Fig. 4 is the deformed pier profile when the input acceleration of shaking table reaches 250 gal. Fig. 5 gives the final deformed profile near completely collapse. At present, the input amplitude is 420 gal. Fig. 6 shows the bank horizontal displacement process along with increment of input motion amplitude. By summarized above test results, the following points can be drawn: 1). The initial fractures of rear platform piles are mainly effected by the earthquake inertia force and the most breaking locations are near 9 cm under bank surface, while ones of fore platform piles result from combined actions of bank deformation and inertia force, the breaking points mostly appear near pile caps. 2). The further failures of the pier are predominatly influenced by bank deformations, not only for fore platform but also for rear platform. 3). When there are the bank deformations in the pier, although the deformations are not intensive, it can also make the aseismic capability of pier reduce seriously. Comparing with the concrete rigid bank pier, the final carrying capacity of deformable gravel bank pier decreases from 1550 gal to 420 gal.

3. Pier Failure with Sand Bank Slope

The failures of sand bank pier are similar to gravel bank pier but it is more severe duo to larger bank deformations. The input and response acceleration amplitude curves are drawn in Fig. 7. Figs. 8-9 give the deformed pier profiles

respectively at shaking table input acceleration 250 gal and 350 gal. At the same time, the horizontal displacement curve of the bank slope is also shown in Fig. 6. In fact, at the initial failure, the pier's carrying capacity to ground motion is only about 80 gal, the maximum response accelerations are respectively 370 gal and 325 gal for fore and rear platforms. The initial breaking points of rear platform piles mainly occur about 13 cm under bank surface, which shows the action of inertia force. But the initial fractures of fore platform piles mostly appear near pile caps, which is action result of bank deformation. Continuously loading, the new fractures of rear platform piles are observed near the pile caps and under deeper soil layers, and also, the old breaking points take place stagger displacements owing to the actions of inhomogeneous soil pressures. Meanwhile, the fore platform happen similar failure. Comparison between tow displacement curves in Fig. 6 shows that the deformation of sand bank is evidently larger than gravel bank, therefor, the failure extent under same input amplitude is also more severe, which is reflected by Figs. 8-9. The final aseismic capability of sand bank pier decrease again than gravel bank pier, from 420 gal to 350 gal.

4. Pier Failure with Silt Bank Slope

Comparison with sand bank pier shows three different points: 1). The settlement of bank is larger while the horizontal sliding motion is slightly smaller. 2). The most breaking points of piles appear near the pile caps, fractures in the soil are minority. 3). The horizontal and vertical displacements of the bents are larger, which obviously reflects the weaker effects of friction and support of silt on the piles. Fig. 10 gives the input and response acceleration amplitude curves. Fig. 11 is the final deformed profile of the pier near instability. It can be found that at the initial failure the response accelerations of platforms are only 220 gal, the action of bank deformation is more notable. The final input acceleration carried by the pier already reduces to 300 gal. The aseismic capability is the lowest in the four types of piers.

SUMMARIZATIONS AND CONCLUSIONS

The practical earthquake damages of pile supported piers show that its aseismic capability needs to raise still further. But because of the complicity of this problem, it hasn't been satisfyingly solved up to the present, not only from theoretical analysis but also from model test. In this experiment, we use loose soil mediums to construct the bank slopes and build the model pile supported piers. Through the tests, we preliminarily investigate the pier's dynamic characteristics, failure mechanism, main influence factors, etc. Some new phenomena are revealed.

From the resonance experiment, we can found that the dynamic features of pile supported piers are predominately conditioned by the dynamic characteristics of bank slopes. Therefore, when we determine some pier's dynamic features, we must firstly understand the bank's dynamic characteristics.

From the failure process and mechanism analysis for above four types of piers, we can say that the main reasons causing dynamic failures of pile supported piers are combination actions of bank deformation and earthquake inertia force. For the bank with stonger stiffness and higher density, the failures of pier are prodominently caused by seismic inertia force, the carrying capacity of pier to ground motion is more intensive. On the contrary, for the bank constructed by soft soils or liquescent sands, the bank deformation is the most factor leading to the severe failure of pier, the aseismic capability of pier is lower because considerable bank deformation will occur under the action of weaker earthquake motion. As comparisons, the input and response acceleration amplitudes for four types of piers at the initial failure are summarized in Table 2. At the same time, final input acceleration amplitudes are also given in Table 2. Clearly, when the bank slopes change from rigid concrete to deformable loose soil mediums, the carrying capacity of pier to ground motion reduces by more than one-half at the initial failure, the actions of inertia force to pier failure greatly decrease, and the carrying capacity at final instability almost reduces by eighty percent. Therefore, the most effective measure raising aseismic capability of pile supported pier is to decrease bank deformation under earthquake motion.

REFERENCES

1. Gao Ming, et al., Aseismic Experimental Studies and Dynamic Analysis of Pile Supported Piers, Journal of Naning Hydraulic Research Institute, No.4, 1981.
2. Gao Guangyi, et al., Dynamic Characteristic Studies of pile supported Piers, Proceeding of the Conference on Technical Codes of Harbour Engineering, Beijing, 1987.
3. Ding Weinong, Aseismic Analysis of Pile Supported Structures Considering Soil-Pile Interaction, Proceeding of Conference on Earthquake-resistant Design of Important Engineering, Harbin, 1985.

Table 1 Dynamic Characteristics of Model Piers

Bank Forms	Fore Platform			Rear Platform			Bank slope	
	f_1 (Hz)	β_1	ξ_1	f_1 (Hz)	β_1	ξ_1	f_1 (Hz)	β_1
Silt	13	8.80	0.081	13	9.89	0.076	12	3.30
Sand	16	10.66	0.078	16	11.08	0.073	15	4.25
Gravel	17	11.07	0.065	17	13.80	0.063	18	4.21
Concrete	26	11.08	0.029	26	15.65	0.031		

Table 2 Failure Acceleration Amplitudes (gal)

Bank Forms	Initial Failure				Final Failure
	Fore Platform		Rear Platform		Shaking Table
	Shaking Table	Platform	Shaking Table	Platform	
Concrete	410	720	155	550	1550
Gravel	140	340	125	410	420
Sand	75	370	87	325	350
Silt	100	275	87	215	300

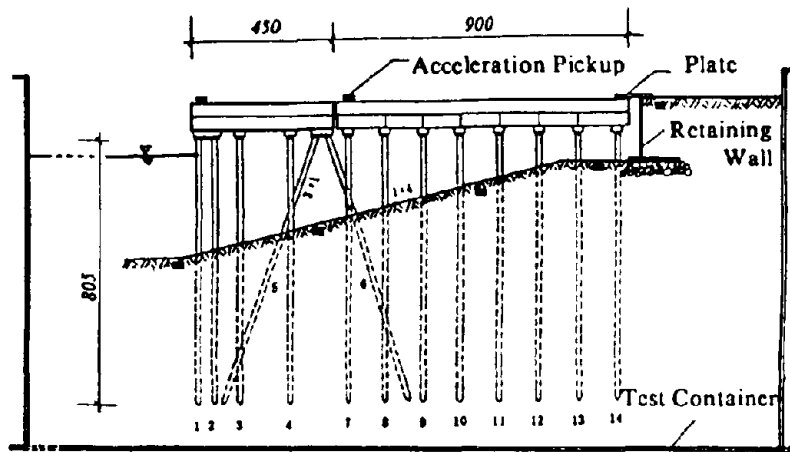


Fig.1 Model Pier Profile

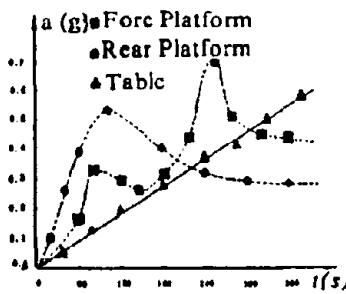


Fig.2 Amplitude Curves (Concrete Bank)

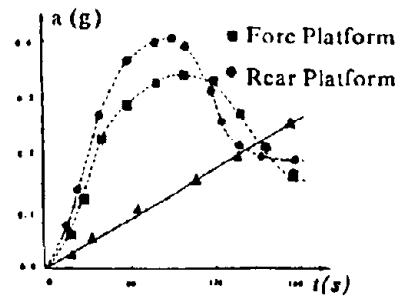


Fig.3 Amplitude Curves (Gravel Bank)

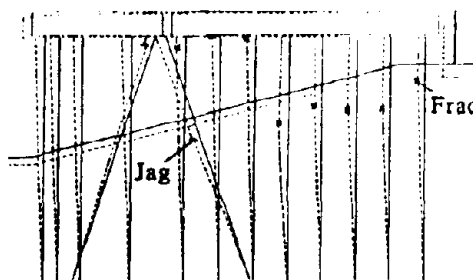


Fig.4 Deformed Profile (Gravel, 250 gal)

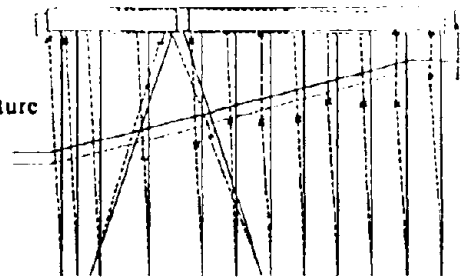


Fig.5 Deformed Profile (Gravel, 420 gal)

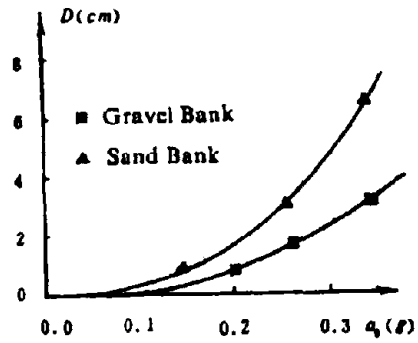


Fig. 6 Bank Displacement Curves

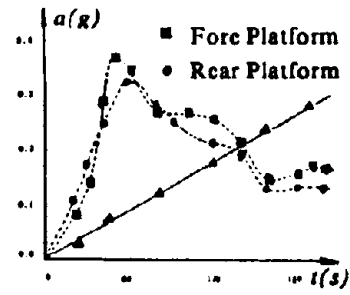


Fig. 7 Amplitude Curves (Sand Bank)

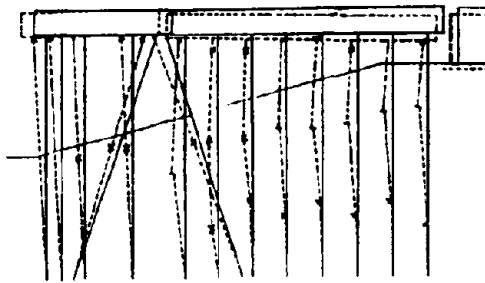


Fig. 8 Deformed Profile (Sand, 250 gal)

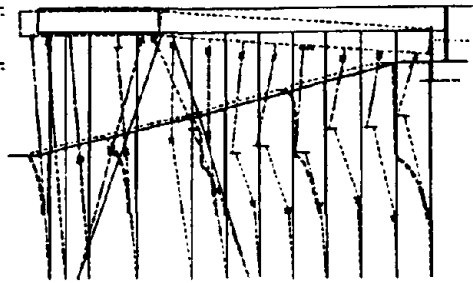


Fig. 9 Deformed Profile (Sand, 350 gal)

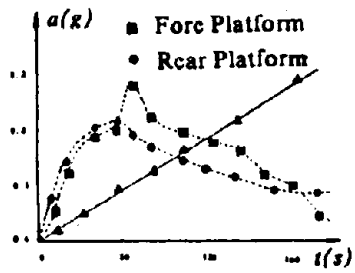


Fig. 10 Amplitude Curves (Silt Bank)

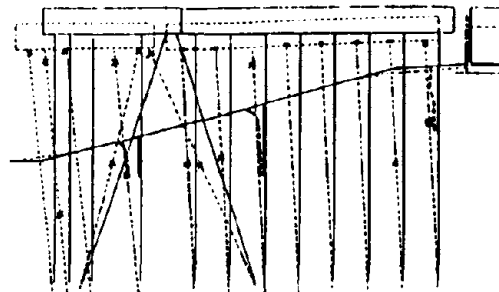


Fig. 11 Deformed Profile (Silt, 300 gal)

SIMULATED ROLLING LOADS UNDER LABORATORY CONDITIONS

by

Frieder Seible

Professor of Structural Engineering
Department of Applied Mechanics and Engineering Sciences
University of California, San Diego
La Jolla, CA 92093-0411

INTRODUCTION

Internal forces and deformations in highway bridges under moving vehicle loads can be far greater than those due to the same loads applied statically. The analysis of short and medium span structures subjected to moving loads is complicated by the uneven riding surface, large mass of the moving vehicle relative to that of the bridge structure and the interaction between the motions of the bridge and the vehicle suspension. The impact of moving loads at various speeds and their interaction with the dynamic characteristics of bridge structures are only empirically accounted for in the bridge design process. Investigations of different truck suspension systems and their influence on the structural response of a bridge are very difficult to perform experimentally and require, typically, prototype field testing with all associated environmental and ambient noise problems. On the other hand, large or full-scale testing of bridge structures or components under controlled laboratory conditions typically substitutes traffic loads by stationary point loads neglecting dynamic vehicle-structure interaction effects.

The objective of the current research program was twofold: (1) to develop a test method for the simulation of fatigue type loads such as rolling traffic load cycles experienced in an actual bridge structure, and (2) to calibrate numerical models in conjunction with experimentally obtained dynamic response data to study the behavior of bridge structures under rolling loads inclusive of vehicle-structure interaction effects.

The recently completed servo-controlled multi-actuator system at the Charles Lee Powell Structural Systems Laboratory at the University of California, San Diego (UCSD) [1] permits the simulation of rolling traffic type loads through a series of computer controlled actuators along the length of the bridge structure. In the following, the development of a test methodology and associated test method for application of rolling traffic loads under controlled laboratory conditions is described. The developed test method was extended to include vehicle-structure interaction effects by modifying the load history input forcing functions based on numerically evaluated interaction data.

As part of an ongoing research project with the California Department of Transportation, a 11 ft-6 in. wide, 56 ft long section of an existing 25 year old cast-in-place reinforced concrete T-girder bridge was brought from Fresno, California to the Charles Lee Powell Structural Systems Laboratory at the University of California, San Diego for full-scale investigation of different repair and strengthening measures [2]. The following paper discusses the simulation of rolling loads on the deck of this bridge section utilizing a time-programmed series of servo-controlled actuators and parallel and interactive numerical studies of the dynamic response to moving loads at various speeds.

EXPERIMENTAL ROLLING LOAD SIMULATION

The overall experimental test setup is shown in Fig. 1. The main components are (1) the full-scale prototype bridge test section, (2) the loading frame tensioned to the test floor, and (3) the three servo-controlled hydraulic actuators arranged in a series along the length of the bridge at midspan and the quarter points. For the rolling load simulations, the full-scale bridge section was tested as a simply supported structure. Instrumentation of the bridge specimen consisted of LVDT's for deflection measurements along the length of the bridge structure and load cells under the simply supported diaphragms. The hydraulic actuators featured feedback-controlled load cell readings and internal LVDT measurements to assess bridge structure and load frame deformations.

The fundamental dynamic response of the test specimen was determined from forced vibration tests at 10.65 Hz [2]. Frequency response functions were obtained at discrete locations in the structure from a random excitation with a 30 pound Acoustic Power System's seismic, low frequency, long stroke shaker, placed at an off-center location on the bridge deck. The excitation location and the response stations are seen in Fig. 4. Table 1 presents the dynamic response characteristics of the Gepford Overhead bridge section.

Table 1. Gepford Overhead Bridge Section – Modal Parameters (Simply Supported)

Mode	Frequency Hz	Damping %	Characteristic
1	10.65	1.59	Bending
2	21.79	1.29	Torsion
3	30.43	1.38	Bending

The load was applied using three 220 kip MTS servo-controlled actuators reacted against the four-column structural steel load frame. The three actuators were positioned to load at the south quarter, center and north quarter points of the bridge span, respectively. Each load was in the form of a single point load, applied midway between the girders representing a wheel load, using an 8 in. by 20 in. elastomeric pad. To determine the stiffness characteristics of the bridge section, the AASHTO-83 HS-20 basic maximum wheel load of $P_{20} = 16$ kips, without impact allowance, was applied independently with each of the three actuators and the corresponding deflections at the quarter points and midspan were recorded. A conditioned symmetric stiffness matrix system was obtained from the flexibility measurements of the 3 DOF system.

The initial test objective was to simulate rolling loads of constant speed which can be represented by discrete triangular loading functions in time for the three actuators as shown schematically in Fig. 2.

A preload of 1.5-2.0 kips was applied on the bridge section with each of the three actuators, and rolling load was simulated by the application of load with time as shown in Fig. 3a for a speed of 30 mph. the triangular load input ensures linear variation of



FIG 1. Rolling Load Test Setup

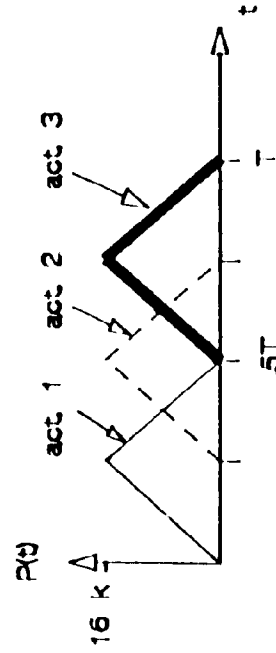
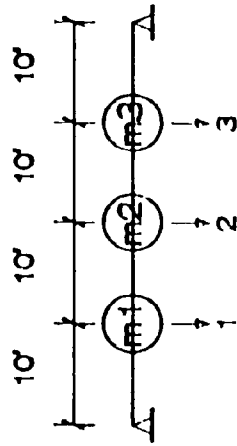
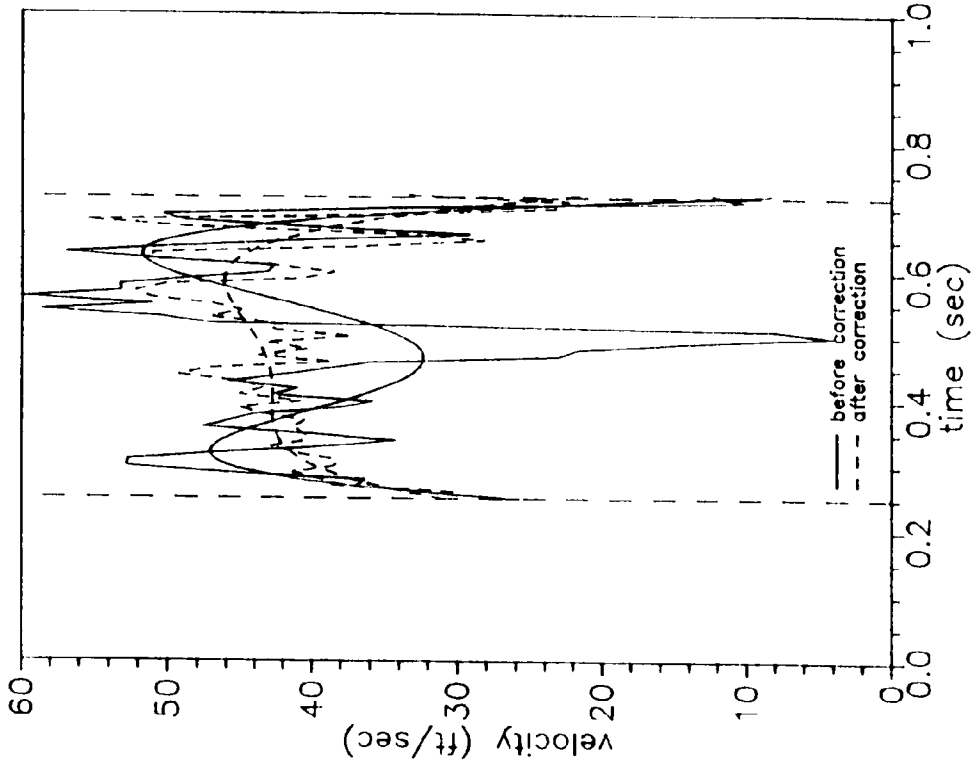
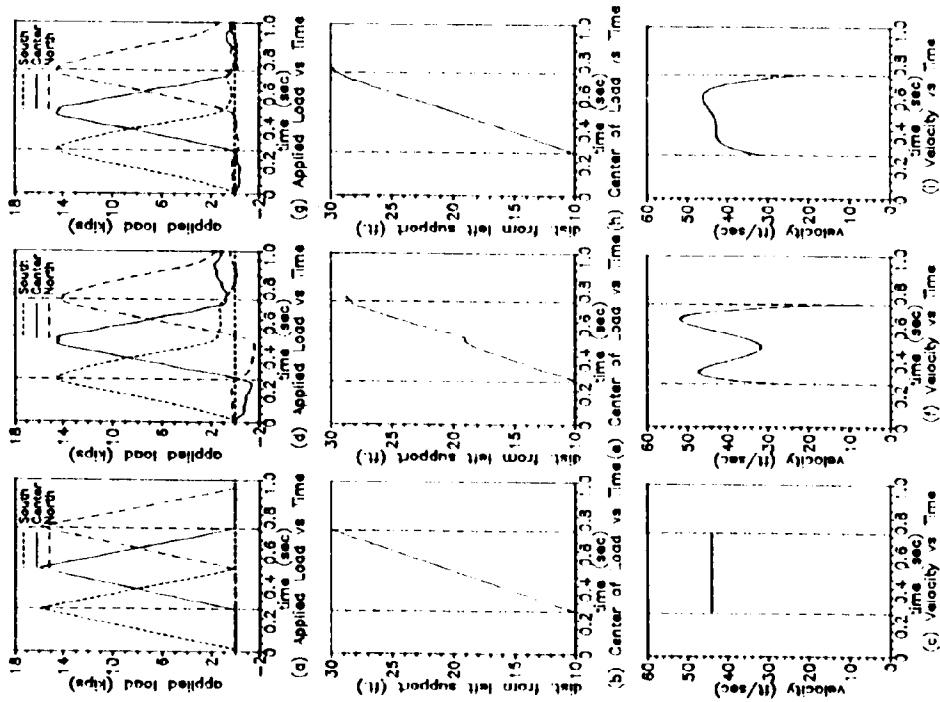


FIG 2. 3-DOF Dynamic Model



**FIG 4. Initial and Corrected Velocity Profile
(v = 30 mph)**



**FIG 3. Load and Velocity Profiles
(Truck Speed = 30 mph)**

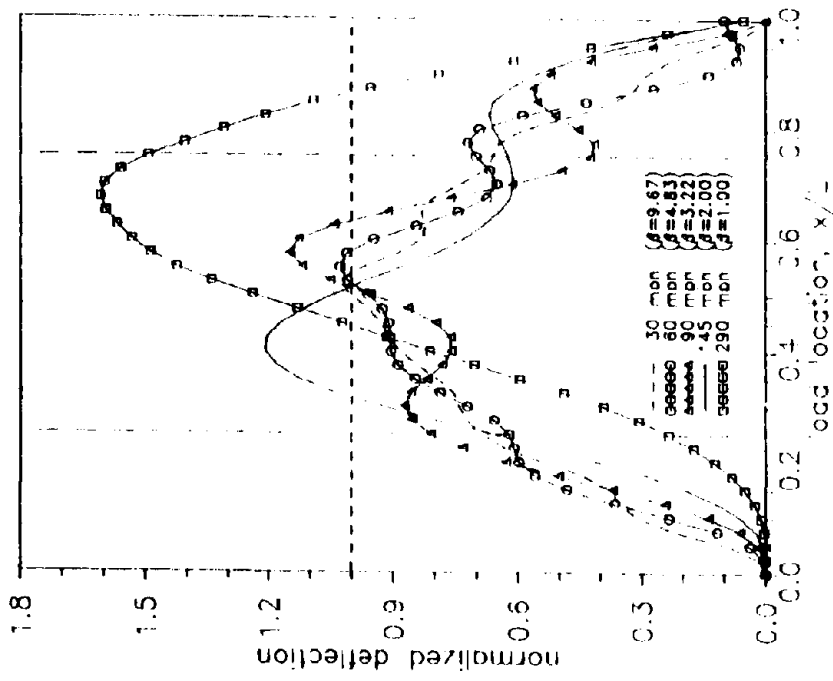


FIG 5. Numerical Normalized Midspan Deflections for Moving Loads

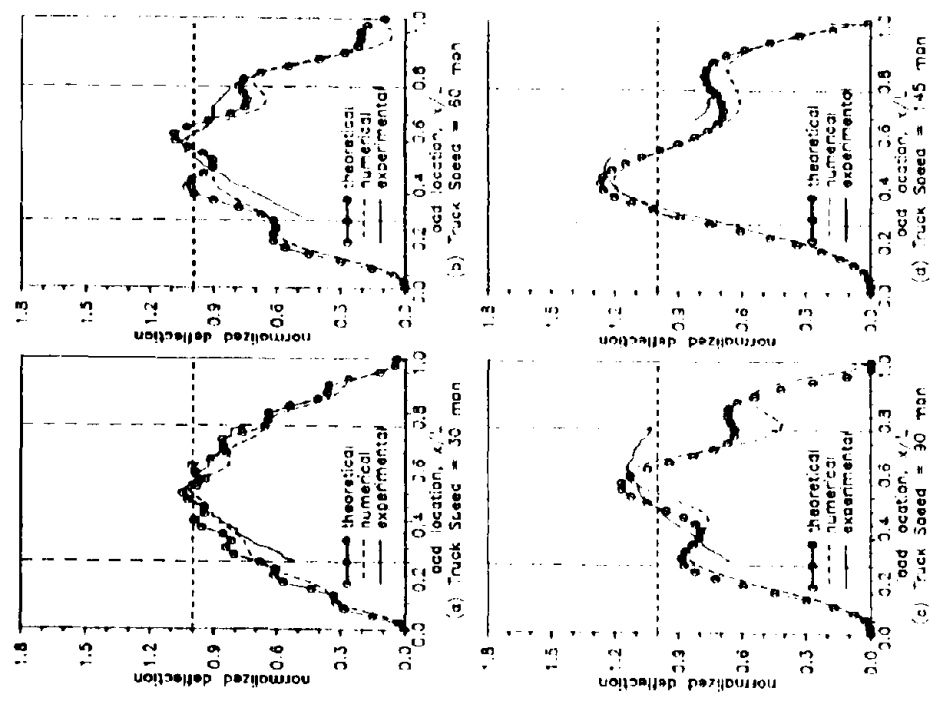


FIG 6. Comparison of Dynamic Midspan Deflection Amplification

the center of load action between the south and north quarter span points, and hence results in constant velocity between the quarter span points. On application of load at the south quarter point, there is a loss of load at the other loading locations (Fig. 3d) due to the deflection of the bridge section at those points. Hence, an iterative process is resorted to whereby a correction is applied to negate the loss of load. Figure 3 depicts the ideal input (a-c), the input without (d-f) and with the correction (g-i) for the loss of load at the three loading sections. Part of the load deviation is also caused by the flexible load frame which requires large actuator movements for small load changes. It is observed that the higher the truck speed, the more difficult it is to attain the triangular load output. This is the result of physical limitations of the hydraulic actuators to follow the input time-history for shorter time periods. It can be seen that for the region between the quarter span points of the bridge structure, a fairly uniform velocity profile can be obtained experimentally. The experimental velocity profile could be improved if (1) a larger number of actuators along the length of the bridge structure is used, and (2) a stiff load frame which can eliminate the excess actuator travel is employed. The velocity is calculated every two-hundredths of a second and a fourth degree polynomial curve fit provides a good approximation of the measured velocity profile. Figure 4 presents the actual measured velocity profile before and after correction, as well as the fourth degree polynomial curve fit for the simulated 30 mph truck speed shown in Fig. 3. The measured midspan deflection due to the loading divided by the midspan static deflection under the load concentrated at midspan yields the dimensionless normalized midspan deflections from the experimental simulation of a 16 kip wheel load moving at various speeds is shown in Fig. 6 together with analytical and numerical predictions.

For general interpretation of results, the truck speed can be related to the dynamic bridge response characteristics. Thus the ratio of the frequency of the bridge structure to the loading frequency can be expressed as

$$\beta = \frac{\omega_{\text{bridge}}}{\omega_{\text{loading}}}$$

where ω_{loading} is given by the vehicle speed V divided by the span length L . Thus truck speeds of 30, 60, 90 and 145 mph, with loading frequencies of 1.1, 2.2, 3.3 and 5.32 Hz, have β values of 9.67, 4.83, 3.22 and 2, respectively.

ANALYTICAL, NUMERICAL AND EXPERIMENTAL RESPONSE COMPARISON

To evaluate the obtained experimental rolling load amplification characteristics, the experimental results for various truck speed simulations were compared with closed form analytical response characteristics obtained using Timoshenko's simply supported beam under rolling load equations [3] and a numerical 3 DOF model, see Fig. 2, with experimentally calibrated stiffness and mass characteristics.

The 3 by 3 stiffness matrix was obtained from flexibility measurements on the bridge section. Using the first two measured fundamental frequencies and the condition of symmetry, $m_1 = m_3$, the diagonal mass matrix M is obtained by solving the equation

$$\left| K - \omega_b^2 M \right| = 0$$

The 3 DOF system was analyzed for the triangular loading (constant velocity) for various speeds using the computer program CALSD-EDSET [4]. As can be seen in Fig. 3, the load in the numerical model is at a constant velocity only over that portion of the span from the south quarter point to the north quarter point, unlike the constant velocity along the span length assumed in the Timoshenko closed form solution. In the numerical 3 DOF model, the ideal velocity profile for the actual experiment was selected as the forcing function, see Fig. 2. Thus, the numerical model corresponds closely to the experimental test and is in fact calibrated using the experimental test setup and can therefore be directly used in an interactive testing procedure. Figure 5 depicts the normalized midspan deflection due to a wheel load of 16 kip moving at speeds of 30, 60, 90, 145 and 290 mph ($\beta = 9.67, 4.83, 3.22, 2$ and 1 , respectively). Again, similar to the theoretical solution, the β ratio is evident in the normalized deflection plot.

Figure 6 compares the theoretical and numerical prediction of normalized midspan deflections with the experimental simulation of moving loads at 30, 60, 90 and 145 mph ($\beta = 9.67, 4.83, 3.22$ and 2 , respectively). For each speed it can be observed that the numerical and experimental peak deflections occur at the same span location for the wheel load, and the discrepancies in the displacement response toward the quarter span points can be attributed to the deviations in the velocity profile at those locations. Table 2 summarizes the dynamic magnification factors for the Gepford Overhead bridge section for a rolling load truck weighing 16 kips moving at speeds of 30, 60, 90 and 145 mph, respectively. Table 2 shows the variation of the dynamic displacement magnification with the frequency ratio β and compares the values obtained from the experimental simulation to those obtained from theory and numerical solutions. The close agreement in the magnification factors validates the employed experimental procedure. Small differences with respect to the theoretical deflections can be attributed to the assumption of a constant cross section for the entire bridge and the complete rolling load path over the entire bridge length.

Table 2. Comparison of Dynamic Displacement Magnification Factors

Freq. Ratio β	Truck Speed (mph)	Theoretical	Numerical	Experimental
9.67	30	1.05	1.03	1.04
4.83	60	1.09	1.03	1.06
3.22	90	1.17	1.15	1.15
2.00	145	1.27	1.21	1.25

VEHICLE STRUCTURE INTERACTION EFFECTS

Timoshenko [3] developed expressions to determine the load applied on roadways due to vibration produced by the contours of the vertical road alignment. The road contour is assumed to be represented by the equation

$$y = \frac{h}{2} \left(1 - \cos \frac{2\pi x}{l} \right)$$

where l is the wave length, h is the permanent deformation of the deck surface, and x and y are the horizontal and vertical coordinates, as shown in Fig. 7. The additional load ΔP on the road due to the vibration assuming the entire truck weight is sprung and incorporating vehicle suspension is given by the relation

$$\Delta P = -\frac{kh}{2} \frac{\tau_1^2}{\tau_2^2 - \tau_1^2} \left(\cos \frac{2\pi t}{\tau_1} - \cos \frac{2\pi t}{\tau_2} \right)$$

where

V = constant velocity of motion along the horizontal axis x

k = spring stiffness

P = truck sprung weight ($W_1 = P$, $W_2 = 0$, see Fig. 7)

$\tau_1 = 2\pi \sqrt{P/kg}$ = natural period of vibration of sprung weight

$\tau_2 = (l/V)$ = time necessary to cross the wave length l

Two cases were simulated using the experimental setup described above for a truck speed of 60 mph. The first case assumed a spring stiffness of 8 kip/in. and the permanent deflection at the center of the bridge of $h = 0.5$ in. The second case assumed a fictitious stiffness of 0.1 kip/in. and a permanent midspan deflection of $h = 20$ in. to match first mode shape of the structure. Figures 8a and b indicate the additional load applied due to the surface unevenness and truck suspension for the two cases stated above. Figure 7 compares the 3 DOF numerical prediction of normalized midspan deflections with the experimental simulation of a truck speed of 60 mph with and without any vehicle-structure interaction effects for the two cases mentioned above. Table 3 summarizes the dynamic displacement magnification factors obtained from the experimental simulation and those obtained using the numerical model prediction. It is observed that the close agreement between the magnification factors validates the employed experimental procedure. The ratio of the frequency of the bridge to the frequency of the vehicle is denoted by β^* and the ratio of the frequency of the vehicle to the loading frequency is defined as $\bar{\beta}$. Hence

$$\beta^* = \frac{\omega_b}{\omega_v}$$

and

$$\bar{\beta} = \frac{\beta}{\beta^*} = \frac{\omega_v}{\omega_l}$$

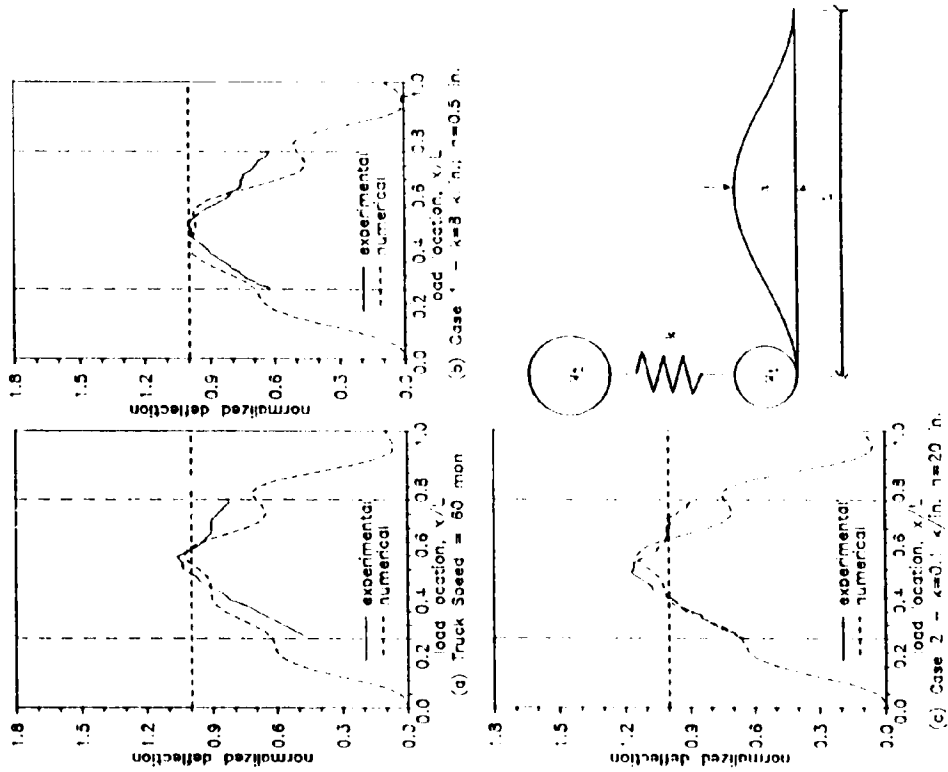


FIG 7. Normalized Midspan Deflections with Vehicle-Structure Interaction

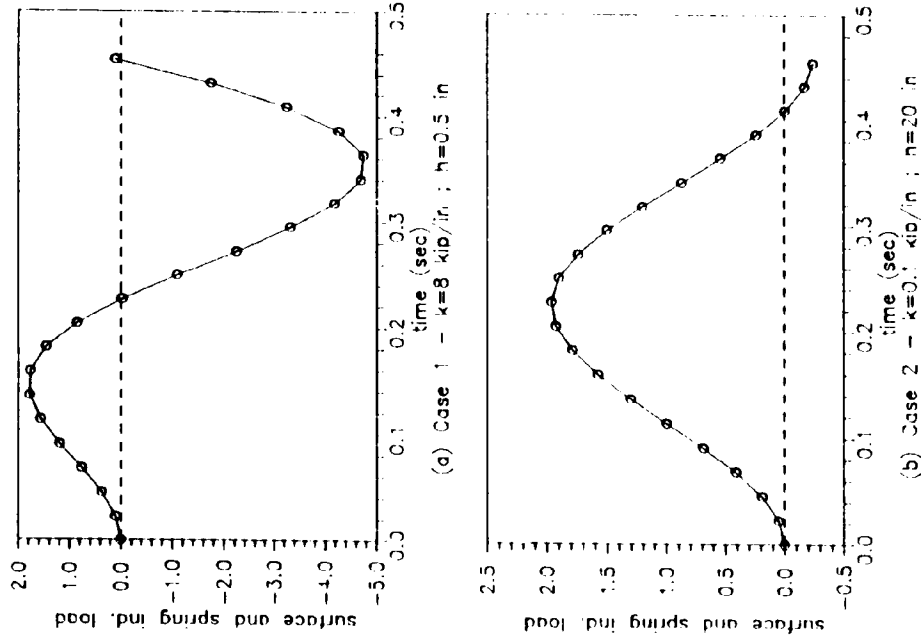


FIG 8. Load Correction for Uneven Road Profile and Vehicle-Structure Interaction

It should be noted that in case 1, the vehicle-structure interaction actually counteracts the dynamic magnification effects, while case 2, which was selected to match the fundamental mode shape of the bridge, shows the expected magnification.

Table 3. Comparison of Dynamic Displacement Magnification Factors Due to Vehicle-Structure Interaction Effects ($\beta = 4.83$)

$\bar{\beta}$	Numerical	Experimental
∞	1.040	1.060
6.32	0.997	1.001
0.71	1.150	1.175

CONCLUSIONS

This paper summarizes the experimental simulation of rolling loads with the time-programmed series of servo-controlled actuators at the UCSD Charles Lee Powell Structural Systems Laboratory. Forced vibrations tests were performed to obtain the fundamental frequency of the bridge section. The theory of moving loads on a simply supported beam developed by Timoshenko was reviewed and numerical studies using the 3 DOF model described. Close agreement was observed in comparisons of the results obtained from theory and numerical studies to those obtained from experimental simulations. Simulation of rolling loads incorporating various truck stiffness and the unevenness of the road surface and the vehicle-structure interaction is not possible using the described interactive procedure.

REFERENCES

- [1] Seible, F., "Design and Construction of the Charles Lee Powell Structural Systems Laboratory," Structural Systems Research Project, Report No. SSRP-86/01, University of California, San Diego, November 1986.
- [2] Seible, F., Latham, C. and Krishnan, K., "Structural Concrete Overlays in Bridge Deck Rehabilitation – Summary of Experimental Results, Analytical Studies and Design Recommendations," Structural Systems Research Project, Report No. SSRP-88/04, University of California, San Diego, June 1988.
- [3] Timoshenko, S., "Vibration Problems in Engineering," II edition, D. Van Nostrand Company, Inc., New York, 1937.
- [4] Seible, F., Latham, C.T. and Kürkchübasche, A.G., "CALSD – Instructional Computer Programs for Structural Engineering – User Information Manual," University of California, San Diego, February 1987.

GENERATED SEQUENTIAL DISPLACEMENT PROCEDURE FOR SEISMIC TESTING OF STIFF MDOF SYSTEMS

Frieder Seible

Professor of Structural Engineering
Department of Applied Mechanics and Engineering Sciences
University of California, San Diego
La Jolla, CA 92093-0411

INTRODUCTION

Modern design of structural systems for seismic loading relies heavily on inelastic deformations to absorb the seismic energy input by large deformations at reliable capacities rather than by large capacities at small deformation levels. Thus, earthquake resistant structural systems will experience local distress and need to accommodate large inelastic deformation cycles without deterioration of design capacity levels. Since the structure is expected to perform well beyond the proportionality or yield limit state during its lifetime, traditional analysis and design models, which relate unfactored or factored design loads and linear elastically determined demand to service or ultimate capacity levels, are no longer appropriate to capture the relevant realistic structural response. Thus, new analysis and design tools are needed which can (1) realistically capture the post-yield to ultimate deformation level state response, (2) account for realistic seismic load input and (3) determine the location and nature of local and global failure modes.

A large number of complex nonlinear analysis models and advanced capacity design models have been developed in the academic research environment but the quality and usefulness of these models depends to a large extent on their appropriate verification and calibration. Since the unpredictable and devastating nature of earthquakes allows gathering of post-yield field data only to a very limited degree the validation of these models depends largely on experimental laboratory testing. These laboratory tests need to be performed at a large or full-scale in order to capture the correct onset and development of failure modes at the local and their complex interaction at the global structural systems level. Since failure mechanisms and their nonlinear behavior are typically controlled by the structural detailing of joints, connections etc., only very limited scaling is permissible in the experimental verification. Thus, experimental techniques are needed, which can take complete full-scale structural systems under realistic seismic load input from the undamaged initial state through the yield limit state and the formation of local mechanisms all the way to the final global collapse mode. Realistic seismic load input to these full-scale models requires not only the application of mass proportional loading but also the participation of the structure in the load determination, both, in terms of stiffness degradation effects on the dynamic response characteristics and in terms of higher mode effects.

In an effort to develop new design guidelines for masonry structures in seismic zones, the TCCMAR [1] (Technical Coordinating Committee for Masonry Research) has conducted in both the U.S. and Japan extensive experimental and analytical research to provide a broad data base for design model development. The final verification of the developed procedures and models is by means of a five-story full-scale reinforced

concrete masonry building test under simulated seismic load input. A detailed description of the test procedure developed for the U.S.-TCCMAR five-story full-scale research building test is provided in the following. After a brief introduction of the theoretical basis for simulated seismic on-line testing, the GSD (Generated Sequential Displacement) test procedure is presented, starting with a general description of the test methodology and the formulation of the test method, followed by the test method implementation, verification and fine-tuning, and an interpretation of obtained test results from full-scale multi-story reinforced concrete masonry shear wall systems. It should be noted, that the primary objective of the described work was not the development of new pseudo-dynamic testing theories or techniques but rather to the application and refinement of existing procedures to allow the on-line testing of stiff multi-degree of freedom systems under seismic load input.

GSD DEVELOPMENT

General Concept

As a direct extension of the pseudo-dynamic on-line technique, the GSD procedure was developed for the full-scale seismic testing of stiff multi-degree of freedom structures. Since the method was developed in direct support of models for design guidelines, the test procedure must allow the test structure to be exposed to seismic input segments which cause structural response representative of critical design limit states. Thus, a carefully selected sequence of input segments is developed which will not only provide the structural response to one particular seismic event but rather a sequence of critical structural response states including higher mode effects which need to be considered in the design process.

An example of such a sequential load side definition is provided in Fig. 1a where the James Rd 230 component of the 1979 Imperial valley acceleration record was used to provide input segments of various response characteristics as diagnosed by the corresponding segment response spectra, see Fig. 1b. Based on the measured structural stiffness characteristics, an appropriate input segment can now be selected and scaled to produce the desired critical design limit state.

Displacements generated by these input segments through a numerical time integration scheme must now be applied to the test structure as mass proportional sequential floor loads. Thus, the four components of the GSD test method consists of (1) the selected sequence of recorded or generated seismic ground motion input segments, (2) the analytical model and the numerical time integration scheme (typically referred to as the outer loop of the control system), (3) the computer-controlled inner loop of the on-line servo-controlled actuator system, and (4) the actuator and loading system itself with ramp generator and servo-control. Since pseudo dynamic test applications and developments are reported in detail in [2 to 8], only modifications to the basic concept are reported in the following.

Hardware

The hardware components of the loading system consist of the servo controlled actuators, load distribution beams connected to the actuators and elastomeric bearing pads which transmit the load to the test specimen. As an example, the test setup, geometry and dimensions of a three-story shear wall used in the first series of GSD implementation experiments is shown schematically in Fig. 2. In this setup, the loads

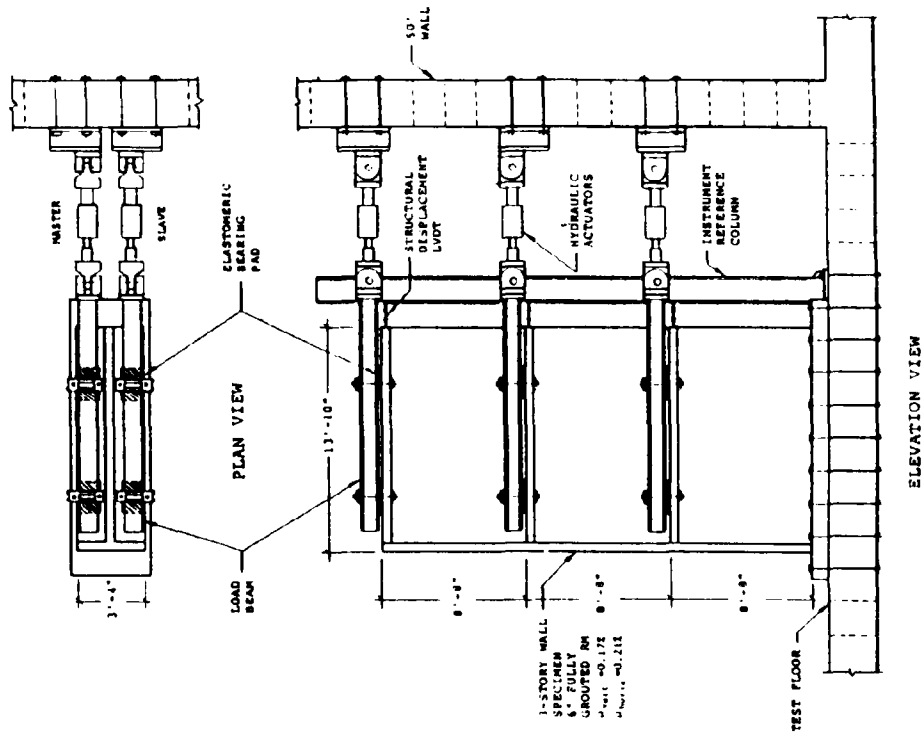


FIG 2. Three-Story Wall Test Setup

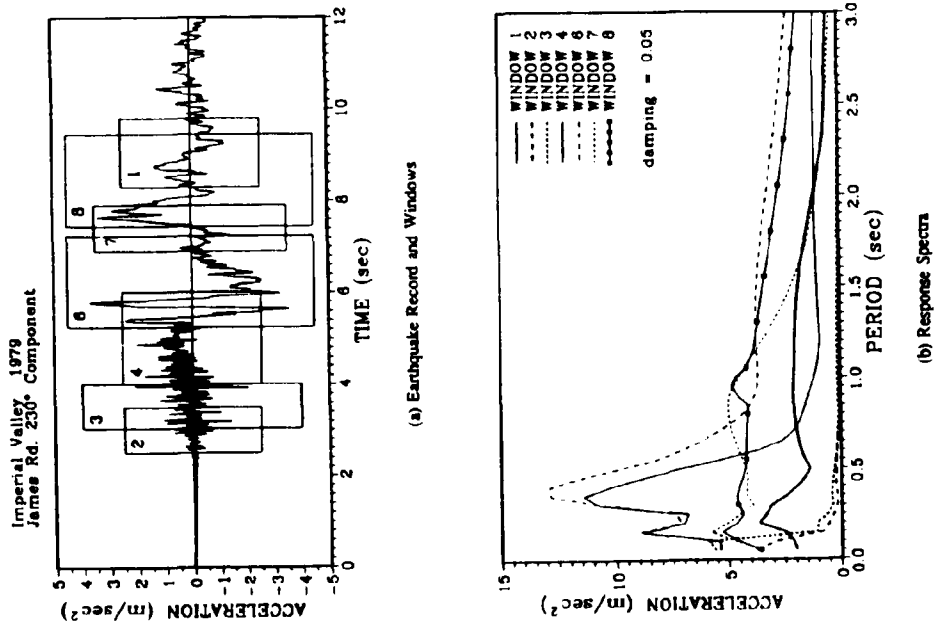


FIG 1. GSD Acceleration Input Segments

were transmitted to the structure at each floor slab through load distribution beams and two elastomeric bearing pads.

This arrangement represents a new approach in testing stiff MDOF systems. By virtue of reducing the apparent stiffness of the floor slab, this arrangement provides approximately uniform load distribution between the two points of load application. The elastomeric bearing pads have several important functions. First, the pads provide a mechanical amplification of the structural displacements to be imposed. This amplification of the displacements allows for easier control of the actuators at small structural displacement levels. It is advantageous that higher amplification is obtained at low load levels when displacements are very small, while the amplification gets lower as the load increases. Second, the pads also provide limited unconstrained structural rotations and expansions of the floor system, thus allowing structural deterioration without compromising the mass proportional loading. Third, the elastomeric pads protect the structure from actuator instabilities during shake down tests, and fourth, the coupling between structural DOFs is greatly reduced which almost eliminates higher order interaction effects during initial load stages.

Software

Because of the use of the elastomeric loading pads, as well as due to the deflections in the loading system, the actuator displacements will not be equal to the desired structural displacements. Therefore, this loading system arrangement requires an additional scheme in controlling the actuators. This procedure is performed in the software level, i.e., an extra iterative loop to impose the specified displacement to the structure.

The control algorithm developed for the GSD procedure is summarized in Fig. 3. The essential feature of the algorithm is the use of an "outer" and an "inner" software loop. The outer loop calculates the structural displacements to be imposed through the pseudo-dynamic algorithm at each time-step. These target displacements are provided to the inner loop, which calculates the necessary actuator displacements.

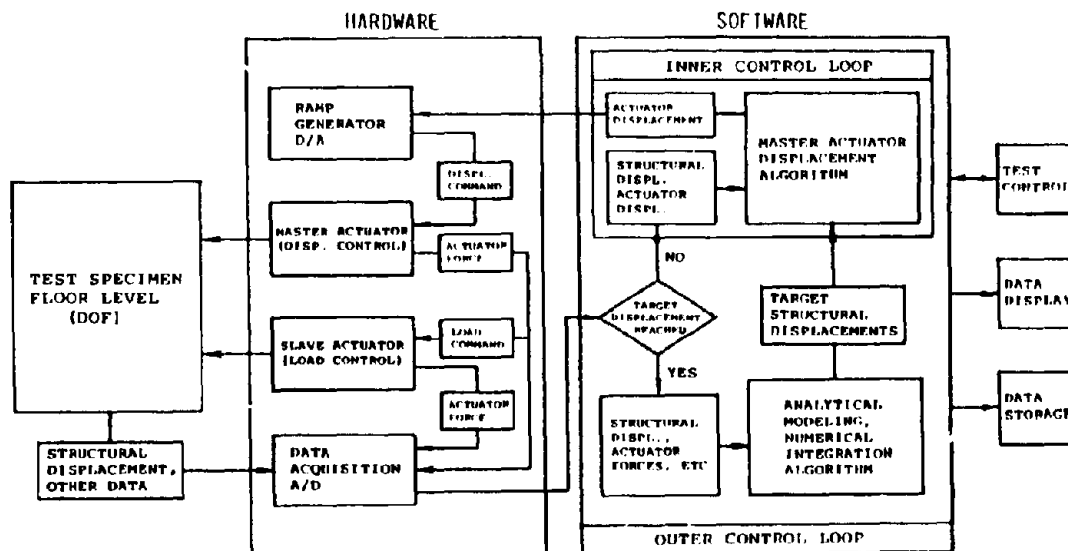


FIG 3. GSD Control Schematic per DOF

The inner loop can be described as follows: The actual structural displacements are measured, and the difference between the target and actual structural displacements is multiplied by a scale factor, resulting in an incremental actuator displacement for the next sub-iteration. This increment is added to the current actuator displacement to arrive at the next desired actuator displacement, which is subsequently applied through a ramp generator to the displacement controlled master actuator. The structure is moved and the new structural and actuator positions are measured. The process is then repeated, until the floor displacements satisfy certain convergence criteria, such as a specified displacement error tolerance (for example, 0.001 in.= 0.025 mm). It can be shown that if the value of the multiplier lies between 0 and 2, the convergence of the structural displacement to the target displacement is guaranteed. However, the most suitable value of the multiplier depends on anticipated bearing pad displacement amplification. The value of the multiplier should be chosen such that reversal of the direction of the structural displacement increments (i.e., flip flopping) be avoided.

When the desired structural displacements are reached the restoring forces are measured and are used in the outer loop to calculate the next structural target displacement. The process is repeated for all required acceleration input segments.

GSD IMPLEMENTATION

Three-Story Wall Tests

The GSD test method was implemented on three-story reinforced masonry shear walls. Two three-story wall specimen were used, and the schematic test setup is depicted in Fig. 3. The loading system of the test structure consisted of three pairs of servo-controlled hydraulic actuators, load distribution beams and elastomeric loading pads. The actuator forces were reacted against the UCSD Structural Systems Laboratory's 50 ft (15.24 m) reaction strong wall. Two 165-kip (733.9 kN) actuators with ± 6.00 inch (152.4 mm) stroke capacity were used to load the structure at each floor level through the arrangement shown in the figure. A vertical preload of up to 100 kips (444.8 kN) was applied to each of the elastomeric pads to allow friction based load transfer.

Loading System Setup. To properly simulate mass proportional floor loading, loads have to be uniformly introduced to the test structure not only along the length of the test building but also over the width. Thus, two actuators were employed per floor level, which will ultimately also allow the testing of a building under torsional response as long as the actuators are force coupled and prevent torsional response when the actuators are displacement slaved. In the three-story shear wall tests, one actuator, designated as "master", was controlled in displacement command by the software through a digital interface. The load cell output from the master actuator was then fed into the load controlled slave actuator as a command signal. Because of the tight analog coupling, the net effect is that of a single displacement controlled actuator with uniform loading on both sides of the wall.

Instrumentation. The instrumentation was designed to provide information in two specific areas: (1) test control and (2) structural response. Test control instrumentation is depicted in Fig. 3 with load cells, actuator internal and external LVDTs referenced to a separate instrumentation frame. The structural displacement and restoring force information required for the pseudo-dynamic algorithm were provided by three LVDTs measuring floor displacements (at the center of floor slabs) relative to an independent

instrumentation column placed between the specimen and the reaction wall and by six load cells attached to the hydraulic actuators. The LVDTs measuring the structural displacements had a range of ± 0.2 in. (± 5 mm) range for tests on the stiff, undamaged structure. Extended range LVDTs were used to accommodate greater floor displacements after the structure softened. The analog circuitry of the load cells was also optimized to the anticipated load levels. To further reduce measurement errors, the average of at least 25 A/D readings of each channel was used for the calculations in the outer control loop.

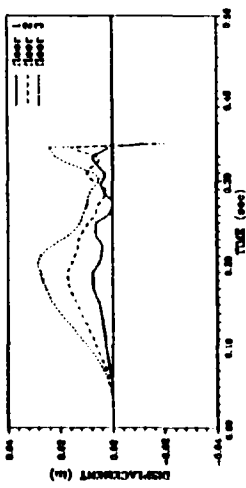
TEST DESCRIPTION

Numerical Modeling. The pseudo-dynamic algorithms and parameters chosen for the present test series reflect the issues discussed above. The three-story wall specimens were idealized as 3-DOF systems, with the masses lumped at the floor levels. The mass of the floors was adjusted in order to allow a the time integration interval of at least 0.005 seconds in the conditionally stable algorithms. The initial measured structural stiffness and the actual test specimen mass resulted in natural frequencies of 17.7, 63.1, and 117.5 Hz for the 3-DOF model. Since the El Centro 1940 NS ground motion record chosen for the Wall 1 experiments had its major source of energy below 5 Hz, and to provide for integration time steps of reasonable length, the analytical model was adjusted with contributory mass equal to 15 times the specimen mass, resulting in initial (uncracked) natural frequencies of 4.6, 16.3, and 30.3 Hz at an assumed damping of 5%. As expected, the natural frequencies were found to decrease as the test sequence proceeded, indicating the damage state of the structure.

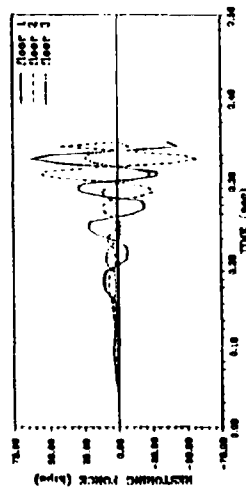
Although the Newmark explicit method was first applied with 5% modal viscous damping, cases without numerical damping were also examined for later stages of the tests. When the Modified Newmark Explicit algorithm was used, the parameters were chosen such that larger damping effects be obtained in the higher modes, while still providing realistic damping in the first mode. For Hilber's alpha method, a standard set of parameter values ($\alpha = 0$, $\beta = 0.25$ and $\gamma = 0.5$) were used, which leads to the constant-average-acceleration integration without numerical damping.

GSD Test Implementation - Wall Specimen 1. The first three-story shear wall specimen was used to implement the proposed GSD testing procedure. A scale factor of 0.5 was applied to a time window comprising $t = 1.0$ sec in the 1940 El Centro NS component acceleration record.

First, two experiments were performed using the Newmark Explicit time integration scheme with a time step of 0.005 sec, constant 5% modal damping, and structural displacement error tolerance of 0.001 in. The response obtained in Test 9 is shown in Fig. 4. Both the displacement and restoring force histories show diverging oscillatory behavior, representing the uncontrolled growth of spurious higher modes leading to unrealistic relative story shear forces in the structure, and ultimately to an instability in the loading system. This phenomena has been observed in other MDOF pseudo dynamic tests [4]. Following these tests, the time integration algorithm was changed to the Modified Newmark Explicit scheme, having frequency proportional damping to suppress the spurious higher modes. Using the pretest measured stiffness, calculated damped natural frequencies were 3.8, 15.4, and 28.0 Hz, and the integration parameters were adjusted to give 3.4, 22.8, and 59% damping for the first three modes respectively. The results of Tests 13 and 15, along with a prediction, are shown in Fig. 5. The noteworthy features of these results are the dominance of first mode response, controlled higher modes, and the good reproducibility between the two tests.



(a) Displacement Time Histories



(b) Load Time Histories
FIG 4. Test 9, NE

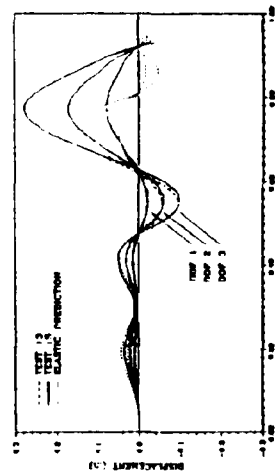


FIG 5. Tests 13 and 15, MNE

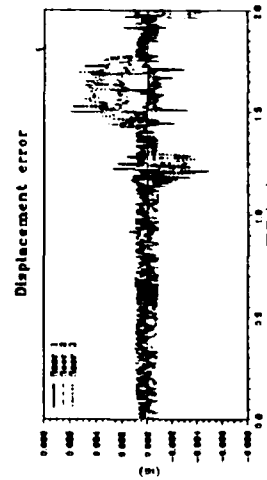
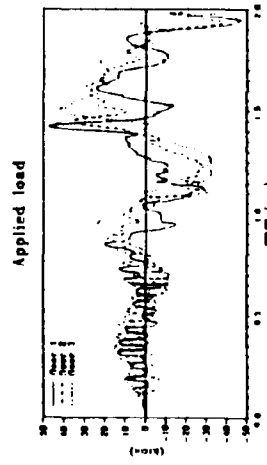
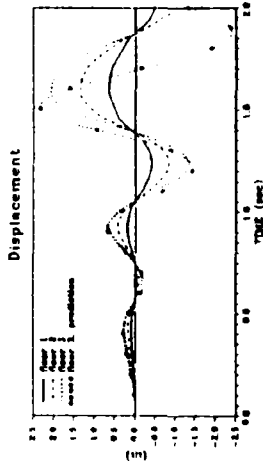


FIG 6. Test 35, MNE

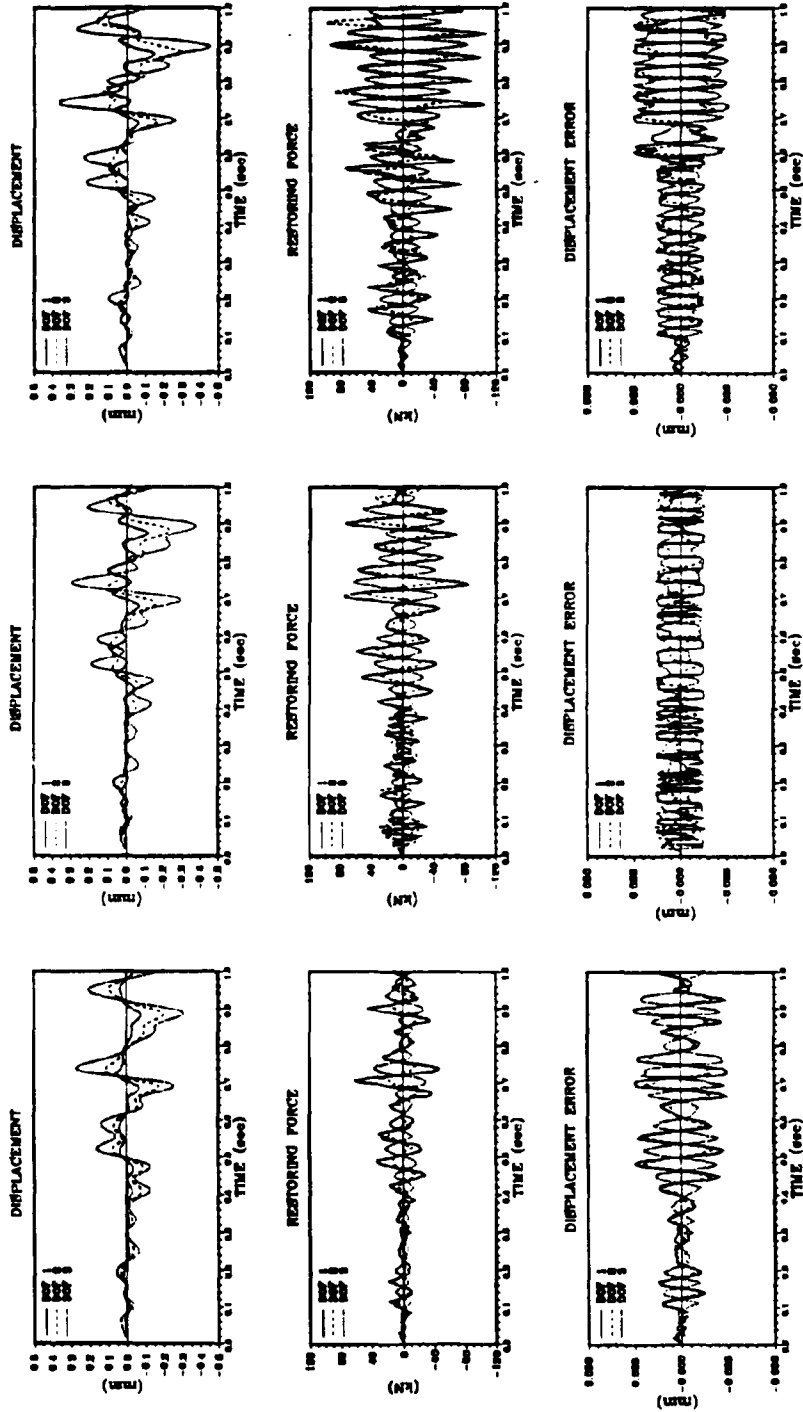
The latter feature shows stability of the structural properties at least to the end of Test 13 corresponding to top floor peak displacement of 0.1 in. with the flange in tension. The results indicate the onset of nonlinearity at about 0.45 seconds. This coincided with the first observed flexural cracking at the base, resulting in period elongation and amplitude increase over the linear elastic prediction, as expected.

During these tests elastomeric pad deflections resulted in actuator displacement amplifications of 3 to 5. The structural displacement errors were kept below the 0.001 in. error tolerance. Restoring force oscillations remained, despite the lack of significant higher modes displacement participation.

Results of Test 35 on the significantly softened structure are presented in Fig. 6. Pretest stiffness measurements gave 1.45, 8.65, and 19.81 Hz for the first three modes, a significant reduction from the undamaged values for the first two modes. The acceleration scale factor of 0.5 was retained, as were the integration algorithm, time step, and error limit. The response now is very nonlinear at all displacement levels. The top floor displacement reached 2 in. (50.8 mm) corresponding to a drift of 0.64%. Load oscillations with about the same frequency remain to about 0.8 sec of the response, but appear with a much lower frequency thereafter. The structural displacement errors also fall considerably outside of the 0.001 in. (0.0254 mm) bound after about 1.2 sec, especially for floors 2 and 3, and the deviations, in general, follow the trends in the structural restoring forces. In imposing the structural displacements, the errors were allowed to exceed the limits rather than undertake an unreasonably large number of iterations to force the displacements to converge. To stay within tight convergence tolerances may be counterproductive due to the long time required and the resulting stress relaxation effects. Significant diagonal cracking and toe crushing occurred by this time. While the Wall 1 tests showed that the developed GSD method can simulate seismic loads on stiff MDOF systems, the capture of higher mode effects and better control of errors and corresponding load oscillations were investigated in the Wall 2 test specimen.

GSD Test Refinements - Wall Specimen 2. Wall specimen 2, which was the same as specimen 1 in dimensions and properties, was used to refine the GSD procedure. The performed sequence of tests on the three-story masonry wall is summarized in Table 1, indicating, in addition to the acceleration window, also integration scheme, scale factor and change in the three natural response periods for the masonry wall prior to the associated test.

Three analytical models were used in analyzing the outer loop target story displacements, namely the Newmark Explicit (NE), the Modified Newmark Explicit (MNE) and the implicit Hilber's Alpha (HA) methods. The implicit scheme (HA) allowed constant damping for all modes without artificially suppressing higher mode effects in multi-story buildings. After testing the first of the two three-story walls with the MNE method at very slow testing rates, a displacement error correction scheme was introduced in the outer control loop. In this correction, the difference between the calculated structural target displacement and the actual measured structural displacement is multiplied by the initial structural stiffness (measured experimentally at the beginning of the test segment), yielding a restoring force correction which is added to the measured restoring force in the subsequent outer loop calculation of the next target displacement. Since the restoring force errors result in spurious higher mode effects, a correction to the restoring forces reduces spurious higher mode effects and allows for smoother structural response. With this restoring force correction, even the NE method showed stable results and was successfully implemented without any artificial



(a) Test 19 (MNE)

(b) Test 20 (IIA)

(c) Test 21 (NE)

FIG 7. Structural Displacement, Restoring Force and Displacement Error Histories for Wall 2 Tests

Table 1. GSD Tests on Three-Story Wall Specimen No. 2

TEST number	integ. runn. scheme	secc. window	scale factor	damping ζ_i/ζ_{i0} (%)	Test Length (sec)	Time (sec)	Test speed ratio	Natural Period T_i/T_0 (sec)	maximum top displacement push/pull (mm)
TEST 19	MNE	2	0.5	6.7/27/72	1.0	2575	2575	0.23/0.064/0.035	0.271/ -0.067
TEST 20	HA	2	0.5	5/5/5	1.0	9225	9225	0.23/0.061/0.034	0.300/ -0.376
TEST 21	NE	2	0.5	-	1.0	4289	4289	0.23/0.061/0.034	0.366/ -0.452
TEST 31	MNE	2	6.0	6.7/24/58	0.74	7856	10616	0.23/0.070/0.038	3.752/ -1.952
TEST 44	NE	3	2.5	-	0.92	11046	12007	0.29/0.087/0.046	3.878/ -7.684
TEST 48	NE	4	0.25	-	1.66	7622	4592	0.30/0.094/0.050	10.045/ -5.401
TEST 52	NE	6	0.4	-	0.85	5540	6518	0.31/0.098/0.051	20.501/ -22.050
TEST 56	NE	6	0.3	-	1.64	9055	5521	0.42/0.122/0.055	31.688/ -11.424
TEST 60	NE	7	1.5	-	0.75	4790	6387	0.38/0.139/0.059	35.458/ -35.141
TEST 66	NE	8	0.9	-	0.40	1405	3513	0.85/0.174/0.060	102.308/ -0.036
TEST 67	NE	8	-0.9	-	0.39	1570	4025	0.85/0.174/0.060	0.0356/ -100.83

- * MNE : Modified Newmark Explicit method
- HA : Hilber's Alpha method (implicit)
- NE : Newmark Explicit method

numerical damping, thus capturing all possible higher mode effects. Thus, for the second wall, the restoring force correction was applied to all integration schemes shown in Table 1.

The computer-controlled inner loop was modified two special features to improve testing speed. First, the actuator displacement amplification factor was applied to the difference between the target and the measured structural displacements to account for the elastomeric loading pad amplifications and for opposite direction displacements in higher mode response. Second, since the command signal and the actuator displacement relationship may be off-bias and not completely linear, the new displacement increment for individual actuator movement is added to the previous command signal rather than to the measured actuator displacement, thus reducing the flip-flop phenomena in the inner control loop convergence. A significant improvement in testing speed can be observed, see Tests 60 and 66 in Table 1.

Results from the three-story full-scale masonry wall tests are presented in the following. The pre-yield phase was used to compare the effect of the different time integration schemes, e.g., Tests 19, 20 and 21 in Table 1. Response time-histories for the three tests are depicted in Fig. 7. As can be seen, Test 19, the MNE scheme (Fig. 7a) results in a first mode response, since all higher mode effects are numerically damped out. Some higher mode effects were captured with the HA method (Test 20), with 5% damping per mode. The higher mode response is visible in Fig. 7b in the displacement time-history and in the increased restoring forces. Finally, the NE scheme, without any numerical damping, featured the largest second mode contributions, as can be seen in Fig. 7c. The displacement error can be tightly controlled by specified error tolerances (note the three different levels in Fig. 7c), where the error tolerance was adjusted in three steps.

The above discussed modifications to conventional on-line testing techniques have allowed the testing of stiff masonry wall systems with GSD using reliable integration schemes such as NE without introducing artificial numerical damping and resulted in pseudo-dynamic test rates of one to four thousand times the real seismic event, or in test durations of typically less than one hour per one second of earthquake time-history, see Table 1.

ONGOING DEVELOPMENTS

A critical factor for the application of the presented GSD method is the speed of the procedure. It was observed in the sequence of the tests up to this point, that the speed of the test depends on the number of sub-iterations needed for the inner loop algorithm to converge. Therefore, faster convergence in the inner loop iterations should be considered in order to achieve greater effectiveness of the test procedure. In the earlier tests, the restoring force time-histories indicated considerable level of higher mode response, and this probably causes very slow convergence within the inner loop iterations. The use of the restoring force correction using the initial stiffness matrix solved some of the problems encountered in the earlier tests. However, the true correction should be based on the current tangent stiffness, not the initial stiffness.

Some theoretical investigation of the inner loop algorithm reveals the following: the use of a single multiplier for all the DOFs has the least effect to reduce the displacement error in the highest mode. Figure 8 shows a conceptual simulation of the behavior of the structural displacement for a three-DOF structure. The displacement error vector can be decomposed into 3 mode-shapes (eigenvectors of the stiffness matrix), and these errors eventually converge to zero if the inner loop iteration is repeated. The y-axis in Fig. 8 represents the amplitude of each mode in the displacement error divided by the initial value (for each mode). Since the convergence rate of the third mode (i.e., the highest mode) is the smallest, the ratio for the highest mode becomes larger compared with lower modes. If the inner loop is terminated at a finite number of steps, the resulting displacement error is dominated by the highest mode. It is obvious that such displacement error produces the maximum restoring force error, with the use of the same level of displacement error tolerance. This effect will become more serious as the number of DOFs increases since the ratio of the smallest eigenvalue and the largest eigenvalue of the stiffness matrix becomes larger.

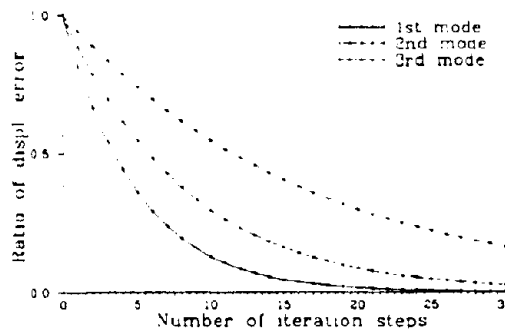


FIG 8. Structural Displacement Convergence

It can be shown that the remedy for this is to use a multiplier which ties the displacement error vector to the actuator displacement increment vector. That implies a multiplier in the form of matrix, as opposed to the use of "scalar" multiplier in the present tests. However, this will require some information on the relationship between the actuator displacement increments and structural displacement increments, which can be described by a transformation matrix. If one tries to obtain this matrix (which can be called displacement amplification matrix), a certain estimation procedure must be implemented. It is very convenient that the estimation procedure can be applied to the estimation of tangential stiffness matrix in the same manner, and the result can be used

to the refined version of the restoring force correction mentioned above. These developments are currently under investigation.

CONCLUSIONS

A new testing methodology for full-scale reinforced concrete masonry structures subjected to simulated seismic loads under laboratory conditions was developed, and the implementation and verification on three-story full-scale reinforced masonry shear walls was discussed. The new test method allows realistic seismic input simulation and trace of higher mode effects, even in the initial undamaged state of the structure. Problems typically associated with the stiff coupling between servo-controlled actuators in a multi-degree of freedom system were overcome with the introduction of elastomeric loading pads, which act as displacement amplifiers in the loading system. Advances in the actuator control loop also allowed testing without numerical damping in the time integration scheme, thus permitting the tested three-degree of freedom masonry shear walls to respond with lateral load distribution patterns consistent with the degree of structural stiffness deterioration.

With selected seismic ground motion input segments, stiff multi-degree of freedom structures can now be tested under realistic seismic loads to any predetermined critical design limit state. The Generated Sequential Displacement testing technique will now be applied in the first U.S. full-scale building test on a five-story reinforced concrete masonry building.

REFERENCES

- [1] Okamoto, S. and Noland, J. (1986) "U.S.-Japan Coordinated Program on Masonry Research", Dynamic Response of Structures, Proc. 3rd ASCE Conf., University of California, Los Angeles.
- [2] Seible, F. and LaRovere, H.L. (1987) "Summary on Pseudodynamic Testing", SSRP-87/01, Department of AMES, University of California, San Diego.
- [3] Takanashi, K. and Nakashima, M. (1986) "A State of the Art: Japanese Activities on On-Line Computer Test Control Method", Report of the Inst. of Industrial Science, The University of Tokyo, Vol. 32, No.3.
- [4] Shing, P.B. and Mahin, S.A. (1984) "Pseudodynamic Test Method for Seismic Performance Evaluation: Theory and Implementation", UCB/EERC-84/01, College of Engineering, University of California, Berkeley.
- [5] Mahin, S.A. and Shing, P.B. (1985) "Pseudodynamic Method for Seismic Testing", Journal of Structural Engineering, ASCE, 111(7), pp. 1482-1503.
- [6] Nakashima, M. (1987) "Summary of BRI Works on Developing Pseudo Dynamic Testing Techniques", 7th JTCC Meeting of US-Japan Cooperative Research Program Utilizing Large Scale Testing Facilities.
- [7] Thewalt, C.R. and Mahin, S.A. (1987) "Hybrid Solution Techniques for Generalized Pseudodynamic Testing", UCB/EERC-87/09, Engineering Research Center, University of California, Berkeley.
- [8] Shing, P.B. and Manivannan, T. (1990) "Implicit Time Integration for Pseudodynamic Testing", Journal of Earthquake Engineering & Structural Dynamics.

ASSESSMENT AND EXPERIMENTAL RESEARCH OF EXISTING WALLS INTENSITY

Lou Yong Lin¹

ABSTRACT

The question that is usually met in the design of evaluation and strengthening of earthquake capacity for existing the buildings whose loads carried by the walls is how to know the existing walls intensity. Based on the analysis comparison and experimental research, this paper suggests a method for assessing the existing walls intensity with simple tools to actually determine the shearing strength.

PREFACE

When strengthening the buildings without seismic design, increasing the existing middle-storey and lower-storey buildings or finding the quality of masonry walls construction which fails to meet the designing demand, we should measure the mortar intensity of existing walls. To check compressive strength and seismic intensity of walls, we could know compressive strength and shearing strength of masonry walls. Between two of them, the check of seismic intensity is of control effect. Table 1 shows the consequences of a certain residential building's mortar index appraisal and checking of vertical-horizontal walls compressive and shearing strength. The seismic intensity is obviously not enough. Determination of shearing strength is the main content of the wall intensity measuring.

Besides grade of brick, material and proportioning of masonry mortar, the factors influencing walls intensity are also connected with the construction method.

SITE MEASURING OF EXISTING WALLS INTENSITY

We often separate a block of brick wall at the worksite to measure existing wall intensity and to imitate the brick pillar to be pressed on indoor press to determine compressive strength. In the method, the masonry is easily damaged in the processes of separating, moving and repairing, especially when the grade of determined wall is too low. This kind of

1. Building science research institute of LiaoNing Province, Office Director, Senior Engineer

Table 1 Wall intensity assessment of a certain residential building in Tie Ling city.

Liao Ning province							
Item	Storey	1	2	3	4	5	6
Assessment of mortar index	compression	25#	10#	10#	10#	10#	10#
	shearing	10#	4#	4#	4#	4#	4#
K of compressive check		2.38	2.39	2.48	3.26	4.78	
Seismic check	K or horizontal wall	2.37	1.57	1.59	1.74	2.05	
	K or vertical wall	1.51	0.97	0.98	1.04	1.23	2.22

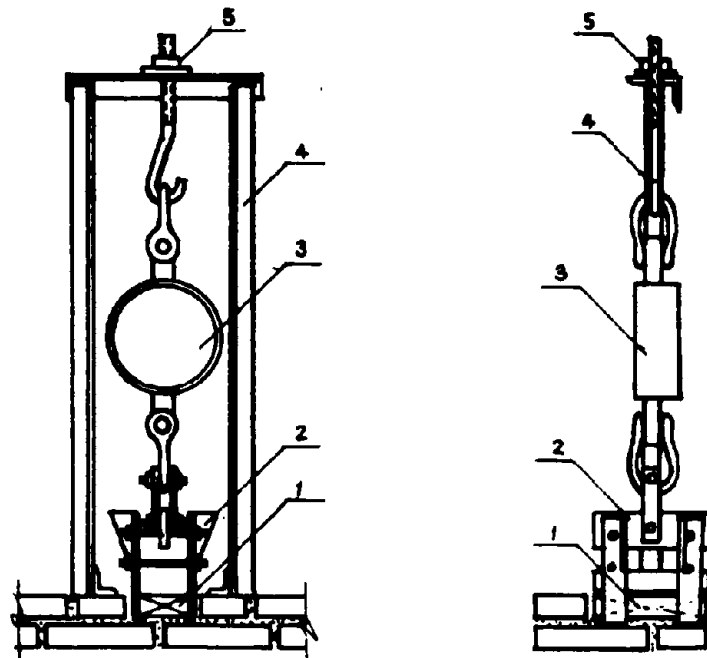
Note: 1) The compressive check requires $K = 2.3$ seismic check requires $k = 2.0$

2) Select the worst wall-section to take seismic check and compressive check

3) K of vertical seismic check has been enlarge $1/3$

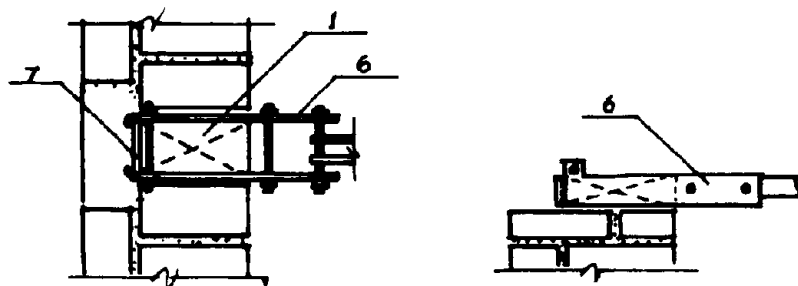
method can only be used in determining the compressive strength of wall, and hardly in shearing strength. Therefore, the method using resitiometer to determine the mortar intensity was put forward. Besides mortar intensity and hardness, the more important factor that determines the masonry shearing strength is viscosity between mortar and brick. It can't be determined by resitiometer. Referring to reference[2], we designed a field-tools used to measure shearing and tensile strength of existing building. See figure 1. The tools have been actually used in our institute building and people's procurato rate building.

Select unbearing-wall under window sill as determining part. Remove window sill board to expose masonry brick, and carefully dig out mortar in the surrounding joint of bricks. Then fasten the clipper (one of the measuring tools) on the brick.(Fasten clipper horizontally to measure T-brick shearing strength and vertically to measure joint tensile strength of horizon-brick). Tighten the screw to increase the pulling force until the joint ruined (To be translationed or pulled out). Measure the maximum pulling force with tensimeter. Divide the maximum pulling force by cross-section of brick to get shearing strength or tensile strength of existing wall. Select two or three positions in each storey and masure fifteen blocks of brick of each position. Take the average as shearing and tensile strength of each storey in the building.



a. apparatus for vertical loading

1—brick specimen; 2—vertical clamping apparatus;
3—dynamometer; 4—frame; 5—tension nut



b. loading apparatus for horizontal shear

6—horizontal clamp; 7—end bearing iron plate

Figure 1 equipment for determining strength of a in-situ brick wall

Having measured walls intensity of two buildings, we have found that it can't show the true shearing strength of existing walls only by observing composition and hardness of mortar in brick joint. E.g. Our office building was constructed in 1960. The mortar was mixture—mortar with more cement content. Its hardness was enough. It seemed have enough intensity. But the results of intensity measuring proved that the cementation between mortar and brick was very little. The main reason for it is the bad construction quality without enough mortar (The area pasted with mortar is only 20~30%). The brick might not be watered before laying and some of them might be constructed in winter. Therefore there had no cohesion between many bricks except that only few bricks had little cohesion.

It's assessed to be 10# mortar. The building of local procuratorate is an old building constructed in 1930s. Although the mortar is lime mortar, which contains very little cement and is not very hard, the quality of constructing and brick are very good and horizon-vertical joint mortar is enough. The coherence between bricks is very tight. The shearing strength has reached the index of 50# mortar.

EXPERIMENTAL RESEARCH ABOUT FIELD MEASURING INTENSITY OF EXISTING WALLS

To examine whether the field measuring intensity of existing walls are safty or reliable, we used three kinds of mortar and made mortar and brick test pieces for compressing, shearing and pulling tests and three pieces of 240mm brick walls. Having cured for a month, we did compressing, shearing and pulling experiments for mortar and masonry test pieces. For brick walls, we did T-brick horizon-shearing and vertical-pulling experiment. The results were shown in table 2.

Conclusions from table 2:

1. The shearing and tensile strength of masonry test pieces are smaller than that of mortar test pieces. It indicates that the cohesion between mortar and brick is smaller than that of mortar itself.
2. The shearing and tensile strength of brick walls are less than that of masonry test pieces. Beside different methods which cause partiality of measuring tools and influence of digging vibration, it also shows that the construction quality of brick walls was lower than that of test pieces was required to be 100 percent filled, but for brick walls only 80 percent are enough.
3. The vertical tensile strength of brick walls(similar to joint-curve-tensile strength) is smaller than the shearing strength.
4. The tooth-joint tensile strength measured from tensile pieces of 50# cement mortar masonry is smaller than that of 25# mixture mortar masonry. Its main reason probably is the influence of workability of mortar and the construction method. It makes the cohesion between cement mortar and brick smaller than that of test pieces built with mixture mortar.

Table 2 comparison of measured strength of walls

Type of specimens	Test classification	description of specimens	quantity of specimens of each group	measured strength of specimens of each group		
				10#	25#	50#
mortar	compressive strength $R_s(\text{kg/cm}^2)$	$70.7 \times 70.7 \times 70.7\text{mm}^3$ cub	9	7.70	15.90	48.30
	shearing strength $R_{sj}(\text{kg/cm}^2)$	Z-shaped, vertical shear plane $70.7 \times 70.7\text{mm}^2$	6	1.20	2.29	5.02
	tensile strength $R_{st}(\text{kg/cm}^2)$	8-susped, actual measurement of tension fracture plane	9	1.83	2.99	7.60
masonry	compressive strength $R(\text{kg/cm}^2)$	$250 \times 370 \times 750\text{mm}^3$ priz	3	18.40	20.00	21.10
	shearing strength of horizontal joint $R_{jm}(\text{kg/cm}^2)$	the bed of the brick pier is $490 \times 370 \times 120\text{mm}^3$, the upper part is $370 \times 370 \times 120$, and the middle part is the mortar joint to be measured	3	0.87	1.37	2.86
	tensile strength of step joint $R_t(\text{kg/cm}^2)$	masonry specimen, with I-shaped plane	3	0.90	1.56	1.26
brick wall	shearing strength of horizontal joint $R_{jm}(\text{kg/cm}^2)$	horizontal shear of one brick	15	0.66	1.35	2.05
	tensile strength of horizontal joint $R_{ww}(\text{kg/cm}^2)$	vertical pulling-out of one brick	15	0.425	0.565	0.800
	R_{jc} and R_{wc} are calculated from R_s according to the related specification			0.965	1.490	2.720
ratio	R_{jm} / R_{jc}			0.90	0.92	1.05
	R_{jw} / R_{jc}			0.90	0.92	0.75
	R_{ww} / R_{wc}			0.44	0.38	0.29

THE INFLUENCE OF CONSTRUCTION QUALITY TO THE WALL'S COMPRESSIVE AND SHEARING STRENGTH

The intensity index table and calculation formula of various masonry given out by "The standard of brick structure design" depend on grade of brick and masonry mortar. These are based on the correct construction operation in keeping with "standard of brick building construction and acceptance". The index of brick and masonry has different influence on compressive and strength of masonry brick when the construction operation isn't in keeping with the demands of the standard. For instance, if the mortar is not enough, it will decrease the compressive and shearing strength of masonry. When mortar has poor workability and brick is laid without water, the masonry compressive strength will be influenced very little, but the masonry shearing strength will be influenced very greatly. Because the mechanism of masonry being compressed to damage is that when the brick compressive

lateral deformation reach crack value and the mortar index is less than that of brick, the compressive crack has little reaction with the adhesion force between mortar and brick. This was proved by contrast experiment using compressive test pieces of brick masonry post immerred in oil. It showed that the compressive strength of immerred oil brick test pieces did not decrease. Certainly the shearing strength of masonry brick is mainly decided by adhesion between brick facing and bonding facing of mortar.

ASSESSING METHOD OF EXISTING WALLS INTENSITY INDEX

1. For buildings with few storeys and small area, determine the index of mortar by the method of observing material of mortar area of brick pasted with mortar, pinching and breaking the mortar block to estimate the intensity.

0# mortar: Mud or silt. Have no intensity by pinching.

4# mortar: Lime mud or lime fine sand. Have little intensity by pinching.

10# mortar: Lime middle__ coarse sand. Contain much lime or little cement. Have intensity but can be smashed by pinching.

25# mortar: Cement, lime middle__ coarse sand. Have great intensity by pinching. It's difficult to smash it by pinching. The piece of mortar can't be broken.

50# mortar: Much cement lime middle__ coarse sand. The mortar block can't be smashed and mortar piece is difficult to break.

Except for these, it also necessary to observe the adhesion area and intensity between brick and mortar. Sometimes the mortar block intensity is high, but the bad constructing operation quality made adhesion intensity between mortar and brick decrease. Therefore the masonry shearing strength should be lowered one grade. For masonry compressive strength, it should be considered by the area paved with mortar. When the area is large (reach 70~80 percent), the grade should not be lowered. When the area is small, the grade should be lowered one grade.

2. For the buildings that are important with large areas, it is better to use the tools shown in Figure 1 to measure shearing and tensile strength of masonry walls. To multi__storey buildings, we usually measure shearing strength only. Select the lower parts of windows or middle parts of long 240 walls as measuring spots. Get the shearing (horizon measure) or compressive (vertical measure) strength by dividing the maximum damage force with areas of bricks. In the same time, observe bricks areas stained with mortar and mortar material component. Measure 15 brick blocks in each position and 2~3 positions for one storey. Take the average as masonry shearing and tensile strength of construction in every storey. when construction of existing is normal (enough brick area stained with mortar and adhesion), read mortar index form "Brick construction design standard" (GBJ3__73) Table 5 in contrary direction at shearing strength to determine masonry compressive strength. When construction of existing wall is innormal (mortar block is too

hard, mortar surface is large but adhesion is small), increase masonry mortar index one grade and take it as masonry compressive strength.

REFERENCES

- [1] Edit group
«strengthening of earthquake capacity technical measures of industrial and civil buildings» 1986.
- [2] A.H.

RESEARCH OF VIBRATING PERIOD
CHARACTERISTICS OF R/C STRUCTURE

Wu Shiyang LiuZhenchang
Senior Engineer Engineer
The Institute of Earthquake Engineering,
China Academy of Building Research, BEIJING, CHINA

ABSTRACT

What is dealt with here is one of the subjects on R/C structure with one degree of freedom studied on a large scale shake table. Through surveying and analysing the structure under whole loading procedure, the authors suggested: natural period is the intrinsic characteristics of a structure; natural period changes with the stiffness of the structure which changes throughout the whole loading procedure; and in the structure under the action of cyclic dynamic load, there is an "instantaneously loaded period "(loaded period for short)property, which is the most crucial parameter for the estimation of the dynamic properties of the structure. This paper also covers a discussion on three different kinds of periods.

PREFACE

The natural period is an important parameter of dynamic property of structure especially when the structure is enduring the indirectly caused inertia response force which is related not only to the properties of the wave of ground movement but also to the property of structure itself. The problem of natural period, therefore, cannot be evaded in the research of the earthquake resistant countermeasures.

It is obviously unreasonable to suppose the structure as purely elastic because the material which the structure is made of is not purely elastic. Furthermore, it is also impossible to determine the elastic response for-

ce and the corresponding elastic inner force with the elastic period and then determine the steel area by the Design Code based on the ultimate equilibrium theory. Since from the beginning of undertaking the vibrating force to failure, the R/C structure is not elastic, so it becomes a prominent problem to estimate the influence of structure bearing capacity with elastic intrinsic period.

1. Basic Condition of Experiment

This experiment employed a normal R/C column which is fastened on a one-way horizontal vibrating table 3x3 meters in size with a lumped-mass weighed 1 ton on the top of the column to form the clear lumped-mass system.(see Fig.1).

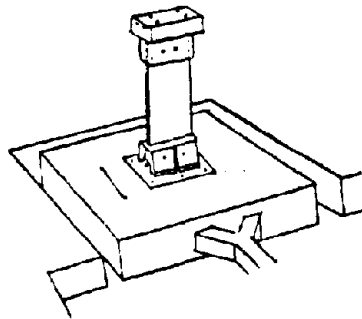


Fig.1

The test column has a rectangular cross section 60x15 cm in size; its concrete strength is $R=387 \text{ kg/cm}^2$; and it is reinforced by six grade I steel bars (10 mm diameter) with the yield strength $R=3610 \text{ kg/cm}^2$ (see Fig.3); grade I steel (6 mm diameter) is also used as hooks.

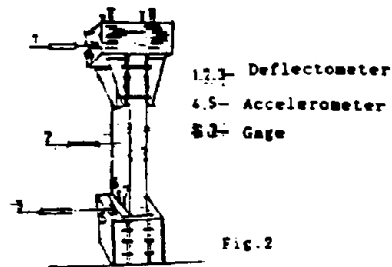


Fig.2

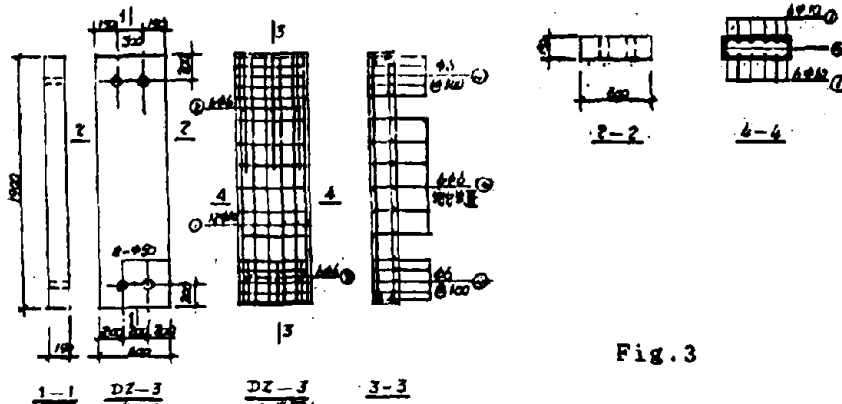


Fig. 3

The arrangement of testing instruments is shown in Fig. 2. Fixed acceleration and staged sine loading method are used to form the load wave in testing procedure for convenience sake.

2. Natural Period Determining Test

Before the dynamic load being put on the column, the common methods, pulse, strike and micro-shake methods, are used to find out the natural period of the column. The results are shown in Fig. 4.

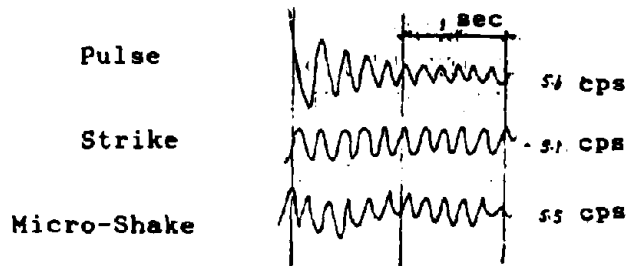


Fig. 4

The average value of this lumped-mass system's natural period T is found to be 0.185 sec. (5.4 cps) tested with the above methods.

According to the formula, however, the elastic natural period is:

$$T_0 = 2\pi\sqrt{W/k_0g} \dots\dots\dots(1)$$

Where, $K_0 = E J$

in this case, $W=1002 \text{ kg}$, $E_h = 32.7 \times 10^5 \text{ kg/cm}^2$

$J=0.00016875M^4$ $H=2.08 \text{ M}$

Substitute these values into eq.(1), it is obtained that:

$T=0.1472 \text{ sec.}$

$P=6.7 \text{ cps.}$

The calculation value and the results of the experiment fail to meet each other. It shows that it is much more rough to calculate natural period of the actual structure by the calculating formula considering that the simplified calculating model is very similar to the experiment installation.

Without doubt, the error relates to the synthetical elastic modulus of structure material used in the calculation. If real tangential modulus of elastic stage were substituted for secant modulus of concrete listed in the current "Design Code for R/C Structure", the calculating error of period would be decreased.

Increase the acceleration or change the loading frequency gradually after starting the shake table, and then cause the maximum curvature of the column and the column surface cracked by the inertia force yielded up to the damage of the column.

The rigidity of the column when cracking appears is different from that when the column is damaged. Stop the shake table and the changes of natural period in the two cases are detected by means of strike method(see Fig.5).

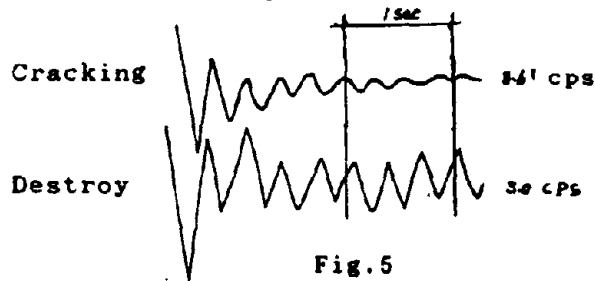


Fig.5

It is impossible to calculate accurately the response force by the elastic formula with these kinds of natural period because the system rigidity couldn't be decided accurately under these two kinds of conditions.

The testing of zero load period reveals that the natural period of structure during the loading procedure, is not a stable value which increases with the decrease of the rigidity of the structure, or with the damage of the structure step by step. It proves that the arithmetic reliability of R/C structure could be hardly estimated if only the elastic natural period or the converted period which multiplied by an artificial coefficient K was taken into account.

From the micro-shake condition of the shake table up to the damage of the column, the relationship between micro-shake natural period and the dynamic load $Q=MA$ (refer to Fig.6) shows that there must be periodic characters as long as the rigidity have not been exhausted, however, they are not constant ones.

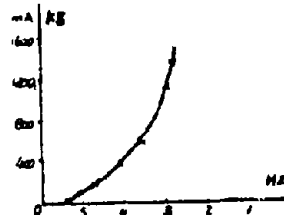


Fig.6

3. "Loaded period" of Structure

After the elastic natural period of the system having been detected, start the shake table, keep its acceleration as a constant $0.1g$ and change its frequency from 2 to 5 cps. If the R/C column can be assumed as elastic before cracking, its period should be no change, i.e., the system should resonate when its frequency increased to 5.4 cps. But the practically detected results are not as that assumed (see Fig.7). It shows that though no cracking appeared on the column surface after bearing the

shake with 0.1g as its acceleration only, there is a change of the column's vibration character, the frequency of which is smaller than its elastic natural frequency (see Fig.8).

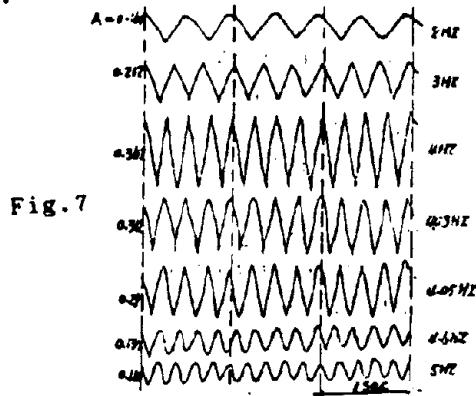


Fig.7

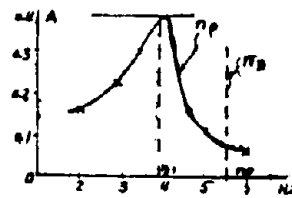


Fig.8

It is evident that if the response acceleration were deduced with the elastic natural period under this condition, it would be a wrong result with the error higher than tens or even more than hundreds per cent.

The natural period of the system increases to 0.33 sec. When cracking appears, the inertia response acceleration and the displacement of the column top are small while the acceleration of the shake table is 1.2g and the load frequency is 10 cps..

In opposite, resonant damage occurs when the acceleration is 0.142g and the load frequency is 2.5 cps.. The zero load natural frequency of the shake table is 2.0 cps., after the table stopped. This fact proves that there are frequency differences in characteristics between the conditions of dynamically loaded structures and that of free vibrating ones, it is the vibrating frequency of structure under shaking load that plays a vital role. Therefore, the instantaneous period of the structure under dynamic load is called "Loaded Period" by the authors.

4. Relationship between Loaded Period and Deformation

Fig.9 is the supposed diagram used to deduce the natural period of system with one degree of freedom.

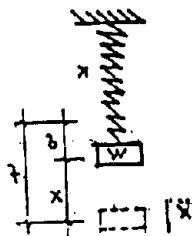


Fig.9

Weight W produces a vertical displacement. Let the block be displaced from its equilibrium position and released so that vibrations take place for the spring has rigidity k. Eq.(1) can be get according to this supposed diagram. It is known that the period of vibration depends only upon the magnitudes of the weight W and the rigidity of the system and is independent of the amount of displacement.

If the interfering force acted on the system doesn't vanish while the rigidity of the structure changes but not being exhausted, it is expected that the block vibrates about its equilibrium position under the actions of rigidity of the structure and the instantaneous changed external forces. Denote the displacement produced by interfering force by f, which equals to $x + \dots$, and regard the product of mass and acceleration as equivalent interfering force $Q = mA$, it is easy to get the formula similar to that of natural period as follows:

$$T_p = 2\pi \sqrt{Q_1 / K_1 g} \dots \dots \dots (2)$$

In the equation above, the synthetical parameter K of the building is very difficult to be figured out, especially in the case that there are many kinds of material used in buildings and the structure members are under loading conditions, so K is very hard to be put into actual calculation.

However, during loading procedure, the relationships between the displacement at the mass center of the column top and the acceleration and that between the displacement and vibration frequency were obtained by testing (see Fig.10).

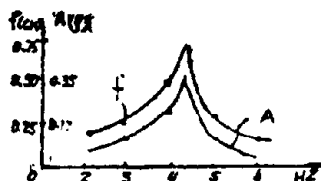


Fig.10

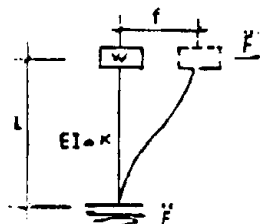


Fig.11

It is also known from Fig.11 that the moment of column under the inertial force f_m is

$$EIY'' = M \dots\dots\dots(3)$$

Where $E_k = Kp$, Y'' is a parameter which value is varying while the property of the structure changes from elasticity to plasticity under the action of inertial force.

When the structure system is at the pure elastic stage, it is known from common structural mechanics:

$$M = 3EI f / L^2 \dots\dots\dots(4)$$

Substitution of eq.(3) into eq.(4) yields:

$$EIY'' = 3EI f / L^2$$

$$f_e = 0.33Y''L^2$$

For reinforced concrete structures:

$$Y'' = 1/r = (\epsilon_L - \epsilon_h) / h$$

If the strain of tension zone is based on the tensile longitudinal bars:

$$Y'' = (\epsilon_h - \epsilon_g) / h_0 \dots\dots\dots(5)$$

The elastic of deformation of the cantilever column can expressed as following considering equation (5):

$$f_e = 0.33L^2 (\epsilon_h - \epsilon_g) / h_0 \dots\dots\dots(6)$$

When the material came into elastoplastic stage and till collapse, the cantilever might have appeared such kinds of curvature distributions as shown in Fig.12.

It is well known that :

$$f = \int (M_p M_1 / EI) dx \dots\dots\dots(7)$$

Substitute eq.(3) into (7), it is obtained that:

$$f = \int Y'' M dx$$

By using moment curve product method, the displacement at the column top under the three cases in Fig.12 can be determined:

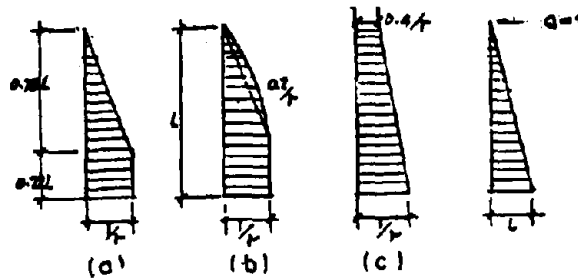


Fig.12

$$f_{ep} = 0.4LY'' = 0.4L^2(\epsilon_h - \epsilon_g)/h_0 \dots\dots\dots(8)$$

Where ϵ_h ---dynamical strain of concrete in the compressive zone of the section
 ϵ_g ---tensile strain of bars in the tensile zone of the section
 h_0 ---the effective depth of the section after cracking

It is known from eq.(6) and (8) that although there is no big difference between the parameters in the two equations, (one is 0.33, and another is 0.4), the meaning of curvature and strain are not the same. The test proved that there is no much error if equation (8) is used in the both cases before and after the column is cracked.

The testing values of the cantilever before and after cracking are shown in Table 1.

It is shown in Fig.13 that the testing values and the calculation values are almost the same.

After the dynamical deformation having been obtained, it is supposed that:

$$Q_1 = K_1 x f_d \text{ -----(9)}$$

Substitute eq.(9) into eq.(2), the period under the action of the load can be written as:

$$T_p = 2\pi \sqrt{f_d/g}$$

$$= 0.2 \sqrt{f_d} \text{ -----(10)}$$

The forced loaded period of the shake table is denoted by T_p and the loaded period of the structure is denoted by T_p . For the actual structure, the resonant period is 0.366sec while the calculation value of the loaded period is 0.368 sec. The relation curve of the period and the response value Q in the loading procedure is shown in Fig.14. The value of the collapse response force Q when response occurred is 1.24 ton.

Table 1 Testing values of Strain DZ 1-3

(CPS)	Q=Mf (T)	Compress Strain of Concrete x10 ⁶	Tensile Strain of Steel Bare x10 ⁶	Deforma- -tion f(cm)
4.12	0.12	243	222	0.64
4.30	0.31	191	180	0.54
4.30	0.27	176	162	0.46
4.48	0.25	153	148	0.44
4.55	0.22	133	133	0.42
4.58	0.20	119	120	0.36
5.00	0.17	98	98	0.33
6.00	0.12	58	63	0.22
4.13	0.44	268	232	0.72
4.10	0.47	288	248	0.72
4.12	0.42	255	225	0.68
3.96	0.60	293	270	0.78
4.08	0.41	231	225	0.64
3.96	0.45	289	275	0.68
4.16	0.38	235	208	0.54
3.18	0.69	619	1110	1.56
2.15	0.55	899	794	1.58
2.54	1.15	1727	1688	2.38
2.73	1.24	1953	2221	3.30
2.14	.06	1842	2253	2.94
2.14	0.76	1253	1750	2.31
2.97	0.42	610	634	1.17
2.67	1.35	2671	2593	4.62

5. Relationship between Several Kind of Period and the Inertial Response Force of One Degree of Freedom Column

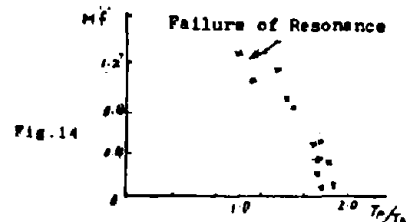
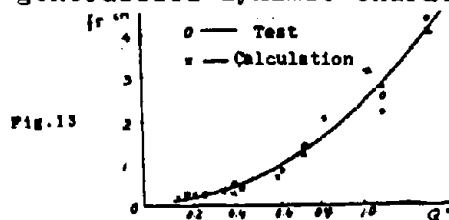
Ideal elastic one degree of freedom system possesses its natural period, the value of which can be determined by eq.(1). If the rigidity and the particle mass of the system keep constant, it will be invariable.

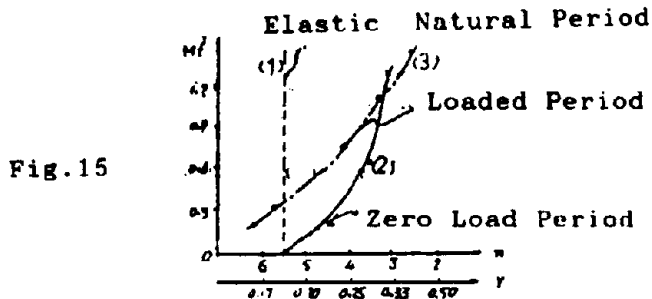
For lumped-mass reinforced concrete column, its rigidity, by the research throughout the whole procedure, gradually decreases in the process from cracking to collapse. If the shake table, in every stage, is stopped for testing the natural period, multiple period values will be obtained. The author call it zero load period. It is very hard to calculate the zero load period, because the elastoplastic rigidity of the column under zero load is very difficult to be calculated. However, the initial value of zero load period and the elastic natural period are the same (refer to curve (2) in Fig.15).

The zero load period is the testing value at the stage of micro-shake, but the rigidity of reinforced concrete members is varying with the changes of load. Therefore, the zero load period can not describe the properties of the structure under the action of vibrating load. So, the authors propose a concept of "loaded period".

The concept "loaded period" is proposed corresponding with that of the natural period. The prerequisite of its existence is that the structure itself is not really ideal elastic system, the rigidity EI of which is varying with change of the dynamic load.

When the action of dynamic load is very small, the "loaded period" may be equal to the natural period (see Fig.15(3)). However, the "loaded period" can describe the properties of the structure throughout the whole procedure (from vibrated to collapse). Therefore, it is a generalized dynamic characteristic value.





6. Suggestions on the Period

- 1) There are some current methods for testing the natural period: pulse, strike and micro-shake methods, all of these methods are to calculate the free vibration characteristics of the structure under the dynamic load. Such value of period can only represent the properties of the structure under the condition of small displacement (micro-shake), but can not represent the actual ones of the structure under the action of strong earthquake force.
- 2) The value of the period of a practically designed building calculated under the condition of some simplified assumptions is generally quite different from that of the period tested by micro-shake method, especially in the case that the structure of the building is considerably complex.
- 3) The elastic natural period of lumped-massed system is the smallest period of the system. With the increase of the load acting on the structure, this property will change. It will increase with the decrease of the rigidity of the structure.
- 4) If the material of the reinforced concrete structure comes into elastoplastic stage, the initial natural period will not represent the properties of the vibration in this stage. At this time, what directly relates to the vibration is the instantaneous period. Hence, in the practical calculation, the "loaded period" is much accordant with the actual situation.
- 5) If a structure after an earthquake is in the stage of severely cracking, it may collapse after a certain time. It is commonly thought that this is the effect of the time. If the concept "loaded period" is used, the phe-

nomenon can be correctly estimated. After research the authors suggest that the reason for this be not the effect of the time but the residual seismic period being close or equal to the period of the structure in the stage of severely cracking.

REFERENCES

1. Aseismic Design Code for Civil & Industrial Buildings (TJ11-89), Civil Engineering Press, 1989.
2. Research Group of Dynamic Deformation of R/C Column, Test Report on Property of R/C Column on Shake-table, Reference Material of the Institute of Earthquake Engineering, 1986.
3. Wu Shiyong and Liu Zhenchang, Research of Dynamic Strain of R/C Column on Shake-table, Reference Material of the Institute of Earthquake Engineering, 1986.
4. Zhu Keshan, Wu Shiyong and Liu Xila, Research of Nonlinear R/C Column, Reference Material of the Institute of Architecture of Sichuan Province, 1977.
5. Wu Shiyong, Calculation of Strength and Deformation of R/C Frame Column under Earthquake Shear Force, Thesis of Earthquake Engineering Conference, Mar., 1984.
6. R.W.Clough and J.Penzien, Dynamics of Structures, 1975.
7. Wu shiyong, and Liu zhenchang, A Study on the Sudden-Crack-Change of R/C Column under Dynamic Vibration-Strength and Deformation, Building Science 3 rd Quarter, 1990.

EXPERIMENTAL VERIFICATION of ACTIVE/PASSIVE CONTROL SYSTEMS

Robert D. Hanson
The University of Michigan
Dept. of Civil and Environmental Engineering
2340 GG Brown Building
Ann Arbor, Michigan 48109-2125, USA

INTRODUCTION

The creation and initial development of innovative active/passive control systems for enhancing the earthquake performance of buildings and other structures during earthquakes occurs first in the mind and then in the laboratory. However, before specific active/passive systems will be accepted by design professionals and the construction industry their theoretical and laboratory scale performance characteristics must be substantiated for realistic field conditions.

Base isolators and supplemental damping devices should be categorized as passive systems unless their characteristics are controllable on command during the seismic event. Then they become part of the active system. Similarly tuned mass dampers should be classified as passive systems unless their properties are actively controlled. As a consequence of this all elements whose properties are variable by external command during the seismic event (such as active mass drivers, gas jets, and active tendons) are classified as active systems.

Recent research and development efforts in active control have suggested that combinations of passive systems with active systems results in better building and bridge performance. These combinations have been called hybrid systems. Experimental verification of the performance of hybrid systems should not be much more difficult to assess than either the passive or active system alone.

In some cases the control system itself can be used to help verify its characteristics. In other cases the material characteristics are so well known that extrapolation to larger sizes and/or different

loading speeds can be accepted without full size - full speed verifications. In those cases where the control system is not capable of self excitation and the materials or control system are not well known verifications will be the most difficult. A brief discussion of current experimental techniques used for active and passive device tests will lead to a discussion of needed experimental techniques for active/passive control acceptance.

CURRENT EXPERIMENTAL TECHNIQUES

Static Cyclic or Pseudo-dynamic Tests.

Some base isolators have been made of rubber and steel plates with lead or other material to improve the device damping characteristics, Fig. 1. Each device is small enough so that full size - real time

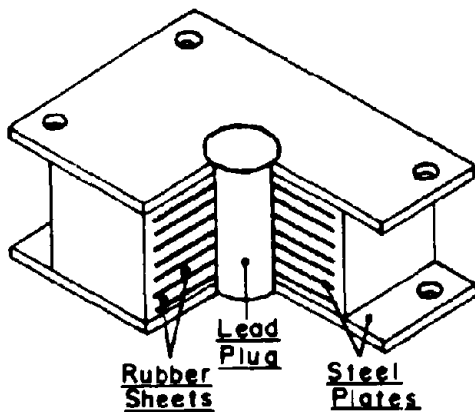
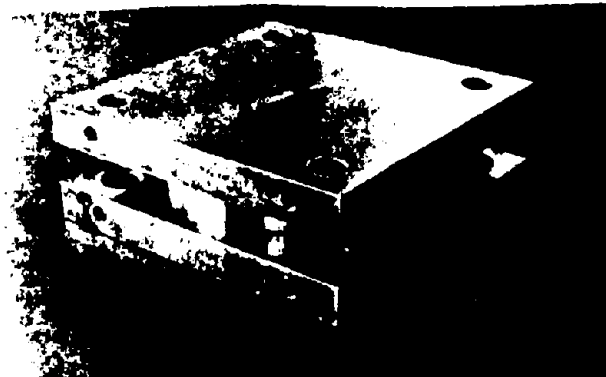
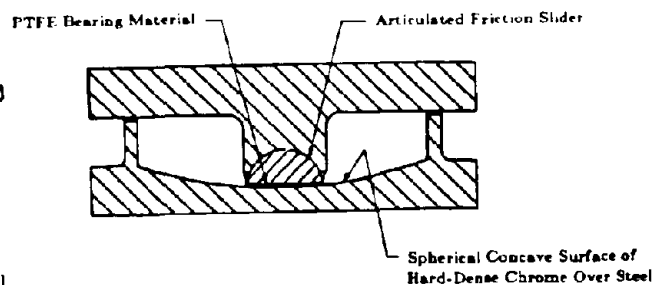


Fig. 1. Lead-Rubber Bearing [1]



Photograph of FPS



Section View of FPS

Fig. 2. Friction Pendulum Isolator [2]

laboratory experiments on a representative number of the manufactured devices can be performed. Other isolation systems such as friction pads and spherical heads, Fig. 2, have also been

tested at slow speeds in a cyclic manner. In all of these cases small scale shaking table tests have been performed to establish the rate of loading effect on device performance. Although individual devices have been laboratory tested, tests after installation in their operational state have not been done.

Metallic yield supplemental damping devices typically use materials whose strain rate effects are well documented, Fig. 3. Thus, static or pseudo-dynamic tests of full size devices are reliable and practical. Although individual devices have been laboratory tested, tests after installation in their operational state have not been done.

Friction and viscoelastic supplemental damping devices have strain rate and size effects which are difficult to separate. Small friction and viscoelastic devices have been tested at real speeds, Figs. 4 and 5, but full size devices as would be used in

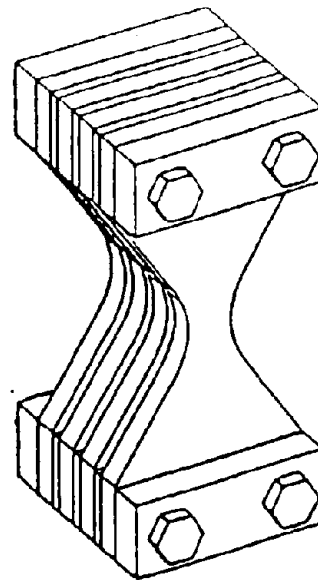


Fig. 3. ADAS Damping Device [3]

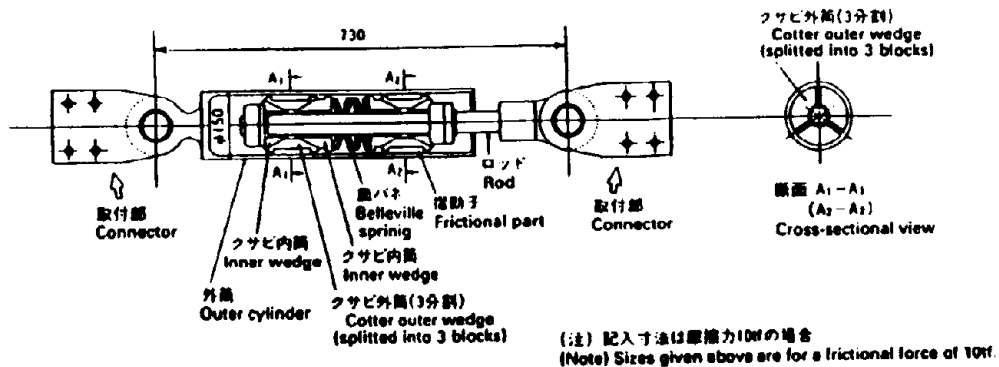


Fig. 4. Cylindrical Sumitomo Friction Damper [3]

buildings and bridges have not been tested at real strain rates. Some of the changes in device characteristics with strain rate is caused by temperature rise resulting from energy dissipation. Although some friction devices are manufactured to accommodate geometrical changes caused by temperature increases others do not. Most of the viscoelastic devices have not considered the temperature effect caused earthquake energy dissipation on thick sections of viscoelastic material. Static or pseudo-dynamic tests are not adequate to resolve these size and strain rate effect issues.

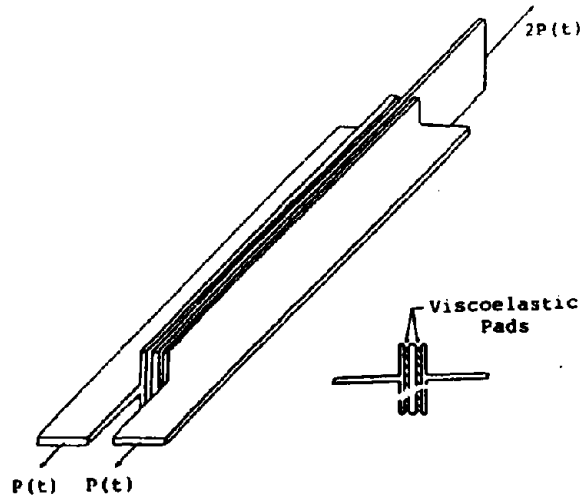


Fig. 5. Viscoelastic Damper [3]

The overall stiffness characteristics of active members which utilize electro-rheological materials can be obtained by static or pseudo-dynamic tests but their damping characteristics seem to require real time testing. Active tendon capacities and associated stiffnesses can be established and verified using static test techniques. Dynamic performance characteristics will require dynamic testing in some form. Active mass drivers and gas jets cannot be tested by static or pseudo-dynamic methods.

Shaking Table Tests.

Shaking tables in most countries have very limited capacities in terms of the size of test specimens which can be excited. This usually means that the structure and device must be at a smaller than normal size and the tributary mass is usually increased above its proportionate amount to keep the excitation frequencies closer to real frequencies. Thus it may be possible to maintain the correct strain rates, but the device dimensions will be smaller than full size.

Shaking table tests have been used to verify analytical characteristics of structures and devices which were established with static or pseudo-dynamic test results. This seems to be one of the most promising techniques for systems which are not both size and strain rate dependent. If the system has only size dependency, the system can be tested at shaking table size and full size using static or pseudo-dynamic techniques. Subsequent shaking table dynamic results can be extrapolated to full size dynamic results. If the system has only strain rate dependency, shaking table results can be compared with static results at different speeds to establish strain rate factors.

Using Active Control Systems as Testing Forces.

Active mass drivers (AMD), gas jets and active tendons can be used to excite the structure in which they are placed to control, Fig. 6. Their active driving of the structure can be used to assure proper performance of the control devices by inversion of the control operation to cause structural motion. This can be used to establish the physical performance characteristics of the system, but does not necessarily assure that adequate, timely control decisions will be made. The control algorithm and implementation can be verified with shaking table tests but size effects for physical implementation of the control decisions needs to be performed with the system installation. The final verification probably will be accomplished only through real event data acquisition and evaluation.

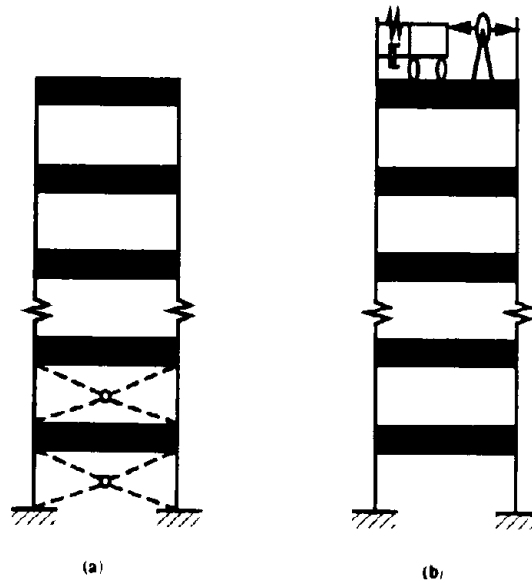


Fig. 6. Structural Model with Active Control (a) Active Tendon (b) AMD [4]

NEEDED EXPERIMENTAL TECHNIQUES

The systems which cannot be easily tested are those with both size and strain rate dependency. As noted above these include friction and viscoelastic dampers, and electro-rheological active members along with others. For these types of systems it is important to establish an acceptable experimental technique which can be used to satisfy the needs of the design profession for accurate performance characteristics and system reliability.

It is beyond the goal of this paper to recommend such techniques for acceptance by this workshop. However, a framework upon which discussions of possible techniques can be initiated will be suggested. In its simplest form:

1. Establish a procedure whereby the system's size effects can be characterized in manner which allows accurate analytical predictions of system performance at full size from acceptable reduced size test specimens.
2. Establish a procedure whereby the system's strain rate effects can be characterized in a manner which allows accurate analytical predictions of system performance at real time responses from "slower" tested specimens.
3. Establish a procedure whereby the system's size and strain rate effects can be characterized in a manner which allows accurate analytical predictions of system performance at full size in real time responses from smaller and "slower" tested specimens.
4. Establish a standard for field testing and real event data acquisition to provide a means for evaluation of real size, real time performance of the system.

CONCLUSION

It is important for the research community to establish experimental procedures for realistic characterization of real size and real time performance of active/passive control systems. Efforts to start this process should begin now.

ACKNOWLEDGMENTS

I wish to thank the organizers of this Workshop for the opportunity to discuss these important issues for the development of active and passive structural response control systems. Financial support from the USA National Science Foundation for travel to this Workshop and for support of Supplemental Damping research at the University of Michigan (NSF BCS-9114755) is gratefully acknowledged. The opinions expressed in this paper are those of the author and do not necessarily represent the views of the NSF.

The following sources were used to illustrate several devices:

1. Filiatrault, A., Sheldon Cherry, and P.M. Byrne, "The Influence of Mexico City Soils on the Seismic Performance of Friction Damped and Base Isolated Structures," **Earthquake Spectra**, EERI, Vol. 6, No. 2, May, 1990, pp. 335-352.
2. Zayas, Victor A., Stanley S. Low and Stephen A. Mahin, "A Simple Pendulum Technique for Achieving Seismic Isolation," **Earthquake Spectra**, EERI, Vol. 6, No. 2, May, 1990, pp. 317-333.
3. Hanson, Robert D., "Energy Dissipation Systems," Proceedings of the SEAOC Convention, October, 1988, Kona, Hawaii.
4. Yang, J.N., Z. Li and A. Danielians, "Hybrid Control of Seismic-Excited Nonlinear and Inelastic Structural Systems," Univ. of California at Irvine, Technical Report NCEER-91-0020, August, 1991.

ADVANCES IN SENSOR AND DATA ACQUISITION TECHNOLOGY

K.D. Bennett
Department of
Electrical Engineering
Lafayette College
Easton, PA 18042

Le-Wu Lu
Department of
Civil Engineering
Lehigh University
Bethlehem, PA 18015

Weiping Li
Department of
Electrical Engineering
Lehigh University
Bethlehem, PA 18015

Introduction

Sensor and data acquisition technology is an integral part of any structural performance monitoring work, either in a laboratory environment or in the field. In earthquake structural engineering, the objectives of such a monitoring program may include: 1) determination of the forces acting locally or globally on the structures, 2) evaluation of the structural responses to these forces, and 3) assessment of damage caused by the earthquake ground motion. There is also the special case of monitoring involving the use of sensor inputs to modify or control the dynamic structural response [1]. The results of a monitoring scheme can be used to develop rational methods to estimate the magnitude and distribution of forces that similar structures must be designed to withstand, to establish the validity of the analytical methodologies that are used in the design of the structures (often based on simplifying assumptions and idealizations), to evaluate the degree of damage and remaining life of the structures, and to develop repair and retrofit strategies [2,3,4]. Structural monitoring has been carried out, with varying degrees of success, to study the dynamic responses of buildings, bridges, offshore platforms, and transmission towers.

Many different types of sensor and data acquisition techniques have been developed and employed in structural monitoring [2,4]; some are highly specialized and have unique capabilities. One of the basic functions of a sensor is to detect or measure the change of a physical quantity and convert it to an electrical signal that can be conveniently transmitted through a medium to a recording instrument. The availability of certain "advanced" sensor and data acquisition techniques makes it possible to carry out some of the more promising structural monitoring programs currently underway.

The present authors are all associated with the NSF-supported Engineering Research Center for Advanced Technology for Large Structural Systems (ATLSS) at Lehigh University, which maintains a major research thrust in the area of "Sensing and Infrastructure Assessment." K.D. Bennett is engaged in optical fiber sensor research for application to structural systems, while W.P. Li directs a program to develop a reliable structural monitoring system using advanced signal processing techniques and very large scale integration (VLSI) technology. L.W. Lu provides structural engineering input to both of these efforts. This paper is a brief summary of some recent advances made in two areas: fiber

optic sensing, and signal processing and data acquisition; both are considered to have high potential for application to seismic research. The technology discussed however, is not restricted to seismic monitoring applications.

Structural Evaluation and Performance Monitoring Using Optical Fiber Sensors

The result of designing more elaborate structures, using new materials for an expanding variety of applications, and making more demands on those structures in terms of performance, efficiency, and reliability, has been to create a need for a new generation of measurement tools. Although headway is being made in acoustic, electromagnetic, thermographic, holographic, and other sensing techniques, few are well suited to dynamic, in-situ, or internal measurements. An important new technology emerging in the monitoring and nondestructive evaluation of structures involves the use of fiber optic sensors to address many of these needs.

Advantages of Fiber Optic Sensors

Optical fibers offer the same advantages to sensing systems as they do to telecommunications. First, extremely high signal bandwidth and low attenuation are achievable with fiber optic sensors. Second, the dielectric nature of optical waveguides inherently renders them insensitive to electrical noise. Third, their chemical structure makes these sensors safe for certain types of corrosive or high temperature environments which conventional sensors cannot tolerate. Also, optical fibers can be made responsive to any number of parameters: electric, magnetic, or acoustic fields, mechanical displacement, velocity, acceleration, pressure, strain, chemical concentration, or temperature, to name just a few [5,6]. Furthermore, because of their small size, and more particularly because of the small wavelength of light, optical sensors can demonstrate extremely high sensitivity and dynamic range.

Other benefits of fiber optic sensors stem from their geometric versatility. Glass fibers are thin and light, can be made flexible yet rugged, and can be incorporated into an endless variety of sensor configurations. This can include extrinsic designs, where light signals are captured by the fiber and are guided along its path to a photodetector, or intrinsic designs, where the signal light stays inside the fiber over its entire length until it exits at the photodetector; the transmission characteristics of the light within the fiber are changed by the parameter to be measured. Moreover, because of their common components, fiber sensors and fiber communications systems are highly compatible. Thus in many cases the same fiber which performs the structural sensing may also be used as the medium over which the sensing data is relayed back to a control station. In addition, compatibility means that advances in communications technology, such as in the development of new fibers and integrated optical components, often translate into enhanced capabilities in the sensor field.

When considering the measurement requirements for engineering structures, the inherent advantages and sensing capabilities of optical fibers make them an ideal candidate for use in real time monitoring. As attached sensors, fibers can readily be laid singly or in arrays to detect surface conditions or monitor the environment external to the structure. Furthermore, optical fibers may be embedded in many structural materials without introducing significant degradation in material properties [7]. Thus, rather than relying entirely on external measurements, internal inspection of the structure is enabled where damage is most likely to occur or where measurements are most critical.

Attached and embedded optical fibers also offer the possibility of providing for cradle-to-grave structural health monitoring, as embodied in the relatively new concept of "smart structures." Fibers placed in an uncured concrete component or composite laminate may sense internal conditions such as pressure, temperature, and density during cure, implying that more accurate processing control and therefore more structurally sound materials may be achieved efficiently [8,9]. Once in service, components containing optical fibers may be continuously monitored, and controls put in place which are aimed at keeping the structure from experiencing dangerous load levels. Finally, if structural damage does occur, either because those levels are unavoidably crossed, or because material degradation such as corrosion occurs, then the same fibers could be used to detect and quantify the damage. Although a number of developmental steps must be taken before they can be widely deployed, the broad range of fiber optic sensor types and configurations offer to measurement science a new class of tools for use in structural monitoring.

Fiber Optic Transduction Mechanisms for In-Service Monitoring

In the now nearly fifteen years since research into fiber optic sensors began in earnest, workers have reported monitoring a host of mechanical and environmental observables by causing the observable to interact with one of the fundamental parameters of the light inside a fiber. These parameters can be understood by examining the simplified equation of an electromagnetic wave propagating within an optical waveguide. If we assume without loss of generality that the fiber is aligned along the z-axis and that the light is polarized in the x direction, the total electric field may be written as

$$\vec{E}(\vec{r}, t) = E_0(\vec{r}) \cos(\omega t - \beta z + \psi) \vec{a}_x . \quad (1)$$

In the output field, the total intensity as a function of position \vec{r} is given as proportional to the square of the wave amplitude E_0 , while the phase of the optical wave is a function of the optical frequency ω , of the propagation constant β , and of the initial phase ψ . Thus if the optical intensity or phase may be determined, than any physical mechanism which alters these can also be monitored. By the same reasoning, observables may be interrogated by monitoring changes in the spectral content of the light (note that the

optical wavelength is related to the frequency and the speed of light in the material), the polarization state, the propagation time t , or the modal power distribution (giving rise to changes in β and therefore the intensity at each position in the output).

On the structural side, the observable which has received the most attention is strain. This may be mechanically induced by loading, or thermally induced by temperature cycling. In the paragraphs that follow, three important techniques for measuring strain will be reviewed, and a few of the many existing examples of both quasi-static and dynamic strain measurements in structures will be presented.

Single Mode Fiber Interferometry

The earliest strain monitors employing optical fiber sensors were interferometric in nature, appearing after the original paper on the subject by Butter and Hocker was published in 1978 [10]. Not long after, fiber optic interferometers were extended specifically to sensing applications in graphite/epoxy composites, with sensitivities several orders of magnitude better than obtainable using conventional strain gages [11-13]. In addition to strain due to mechanical loading, absolute and differential fiber interferometry has been used to monitor both thermally and acoustically induced strain, again achieving similar high levels of sensitivity [14].

Single mode fiber interferometers may take one of several forms, including the Mach-Zehnder, Fabry-Perot, Michelson, and Sagnac interferometers. Because of its relative ease in application, the Mach-Zehnder, shown in simple form in Figure 1, is often used to investigate strain in structures. As in conventional interferometry, light from a coherent source is split into two paths, in this case generally using a single mode fiber optic coupler. One arm of the interferometer is bonded onto or embedded in the structural component, while the other arm is held stable as a reference. The light from each arm is then recombined in a second fiber coupler, and optical interference is created. When the component is strained, the path length of the sensor fiber changes accordingly, and the resulting phase change modulates the interference output. Also shown in Figure 1 is the theoretical output of such a sensor; its nonlinear characteristic is typical of all interferometers. Optical fiber interferometers have been shown to be theoretically capable of measuring stress-induced strain on the order of 10^{-12} per centimeter of gage length, while reported experimental values range to within a few orders of magnitude of theoretical [15-17].

By now the number of authors reporting the use of Mach Zehnder, Michelson, and Fabry-Perot interferometers for strain sensing is enormous. More and more researchers with a largely mechanical engineering background are beginning to apply fiber optic sensor methods, and specifically the single mode interferometer, to the problem of on-line strain measurement in structural elements. In one example, a Mach-Zehnder configuration has been employed to accurately isolate strain in one dimension under the case of biaxial loading [18], while the case of arbitrary loading of both surface-mounted and embedded fibers has also been treated

[19,20]. Practical concerns arise with these sensors in that they suffer from the general inability to make distributed measurements. As a result, certain sections of the fiber must be made insensitive to environmental fluctuations, while the sensing portion must be exposed to the observable. Often this approach is not highly effective, leading to relatively low signal to noise ratios, and is at best complicated to implement.

Time Domain Techniques

One of the earliest routes taken towards single fiber distributed measurements made use of optical time domain reflectometry (OTDR) techniques. Light generated by a pulsed optical source is coupled into the fiber and propagates as one or more guided modes. As the light travels along the fiber, it is partially backscattered by anomalies in the waveguide structure. In otherwise unperturbed fibers, uniform Rayleigh backscatter caused by the intrinsic molecular structure of the component glasses results in an exponential decrease in optical power received at the front end as a function of time. Deviations from this anticipated baseline return signal may be interpreted as being caused by regions of local fiber perturbation, specifically local variations in fiber geometry or index of refraction or both. The location of such regions along the length of the fiber may be determined by measuring the round trip time of flight of an optical pulse from the source to the backscatter site and back to the detector.

In what appears to be the first application of OTDR to fibers embedded in materials, Claus, *et. al.* demonstrated the ability to locate and monitor regions of stress concentration arising from loads applied to host graphite/epoxy panels [21]. In this work, measurements were performed using a communications OTDR unit having a spatial resolution (related to the temporal width of the excitation pulse) of 16 cm; the experimental setup and representative results are shown in Figure 2. Since then, refinements in commercially available OTDR instrumentation have increased the possible position resolution to nearly 100 μm , enabling distinctions to be made between strain levels which elongate the fiber such small distances. Employing such a unit, quasi-distributed strain was measured using in-line air gap splices as time (and therefore position) markers [22,23]. More recent advances take advantage of re-entrant loop techniques, and may better the resolution limit by as much as two orders of magnitude [24].

Modal Domain Sensors

The interferometers described above are characterized by several distinct features. For one, they are extremely sensitive; this is an advantage in some circumstances, and a disadvantage in others where some sensitivity can be traded off for stability. For another, they are somewhat cumbersome to construct, requiring beamsplitting optics, two single mode fiber paths, and a means to recombine their exit beams. Another feature, already mentioned, is their non-linear signal output. In an alternate method, herein referred to as modal domain sensing (MDS), structural monitoring is performed by causing the perturbation of interest

to interact with a fiber which propagates more than one optical mode. In general, any two nondegenerate modes are affected differently since their phase velocities and path lengths differ; the phase difference between modes is employed to infer the amount of physical disturbance.

The most basic modal domain sensor consists of a single mode fiber operated slightly below its cut-off wavelength, such that only the two lowest order modes propagate. For ordinary communications-grade fiber with a core of radius a and index of refraction n_1 , a cladding of index n_2 , and propagating light of wavelength λ , this implies that the LP_{01} and LP_{11} modes are employed, generally resulting in a two lobe interference pattern in the output. The intensity of this output pattern radiating from the core can be calculated as

$$I(r, \phi) = \frac{Y}{2} \left[A_0^2 \frac{J_0^2(u_0 r/a)}{J_0^2(u_0)} + A_1^2 \frac{J_1^2(u_1 r/a)}{J_1^2(u_1)} \cos^2 \phi \right. \\ \left. + 2 A_0 A_1 \frac{J_0(u_0 r/a)}{J_0(u_0)} \frac{J_1(u_1 r/a)}{J_1(u_1)} \cos \phi \cos(\tilde{\beta}z - \tilde{\psi}) \right]. \quad (2)$$

In this expression, Y is the admittance of the waveguide, and A_0 and A_1 are the initial wave amplitudes of the LP_{01} and LP_{11} modes, respectively. The core radial propagation constants u_0 and u_1 are fixed for a given unstrained fiber, and are given as

$$u_0 = k_0 a \sqrt{n_1^2 - (\beta_{01}/k_0)^2} ; \quad u_1 = k_0 a \sqrt{n_1^2 - (\beta_{11}/k_0)^2} . \quad (3)$$

The factor k_0 refers to the free space wave number $2\pi/\lambda$, while β_{01} and β_{11} are the respective mode propagation constants. In addition, the Bessel functions J_0 and J_1 are a function of the radius r from the center of the fiber, normalized with respect to a . The tildas in (2) refer to the difference in propagation constants and initial phases of the two modes.

The terms in equation (2) can be thought of as the two self-interference terms of the constituent modes, plus a third cross term. The self-interference terms are nominally static with strain and therefore considered as background, while the cross term changes with z , the fiber length. Plotting this expression, one sees an asymmetric pattern consisting of a lobe of intensity which periodically shifts from one side of the output to the other with the application of axial strain [25-27]. That is, a dual mode fiber can act as a strain sensor by monitoring the intensity of the output lobes. Signal recovery is most often accomplished by imaging a single lobe, or part of a lobe, onto a photodiode through an aperture.

Highly multimode fibers may also be employed as modal sensors. Assuming the fiber is excited with coherent radiation, the output will consist of a complex pattern formed by the interference of all modes, commonly referred to as a speckle pattern. Disturbances on the fiber

translate to local changes in refractive index and geometry, which alter the differential phase of the modes and thus modulate the speckle pattern. With multimode fibers, it is usually the average modulation of several speckles that is detected to infer perturbations.

The operation of MDS systems has been investigated in detail for the monitoring of structural vibration modes. The first known application, developed by Kush and Meffe, used the interference between modes in a multimode fiber to infer structural mode shape amplitudes [28]. This basic idea was implemented in a number of configurations by Bennett, Ehrenfeuchter, and co-workers, using primarily few-mode fibers [29,30]. In their first modal domain fiber sensor, the optical output was interrogated and processed to yield the dynamic Fourier coefficients of the mechanical vibrational modes. A typical set-up and results of such a measurement are depicted in Figure 3.

A number of other applications of modal domain sensors to structures have been reported in the literature. Subsurface ground vibrations due to activity on the surface have been detected, with the possible extension to earthquake monitoring [31,32]. These sensors have also been used to monitor and quantify acoustic shock waves and subsequent mechanical ringdown which arise from impacts to both metallic and composite structures [33,34]. Higher frequency acoustic emissions have been sensed using few mode fibers embedded in composite coupons [35]. In all cases, a single sensor may be laid throughout a structure as a general listening device, though it may be possible to apply individual point-like sensors and use triangulation to locate signal sources. Dual mode, few mode, and highly multimode fibers have all been employed successfully.

The use of modal domain sensors in monitoring the slewing and vibration of large, flexible structures has led to the analysis of possible control system architectures that utilize the inherent and fundamentally different nature of fiber sensor output signals in feedback control systems. Conventional control systems accomplish such slewing tasks through the use of "point" sensors, that is, resistive strain gages which are much smaller in size than the structure to be controlled, that are generally attached at predetermined vibrational anti-nodes. However, since the fiber strain sensors yield the strain integrated along the fiber path rather than strain at a point, control algorithms must be modified. The situation is further complicated by the fact that for fiber elongations longer than the beat length between the participating modes, often as small as 100 μm , the signal output takes on the oscillatory nature characteristic of interferometers. However, it has been shown that this nonlinear sensor output will not lead to instabilities in the control system if the latter is appropriately designed [36].

Advanced Monitoring and Data Acquisition System

Structural experiments always involve data collection and processing. The technology for collecting and processing such experimental data determines how much and how well we are able to observe the behavior of the test structures either in a laboratory setting or in the field. Research

currently being carried out at the ATLSS Center will have an impact on this technology. The goal of the work is to develop remotely accessible, economically affordable, and highly reliable monitoring systems which will enhance the capability of assessing performance of structures.

Figure 4 illustrates the idea of such a monitoring system. The entire system consists of sensors and processor modules distributed on a structure (a bridge in this case) powered by small batteries, a radio repeater near the structure powered by a larger battery, and a radio receiver and process computer at a central facility. The sensors and processor modules are capable of collecting and processing data on site in real time. Processed data from each individual sensor and processor module are transmitted to the radio repeater. The repeater transmits multiplexed data from all sensors and processor modules on the structure to the central facility. The computer at the central facility displays the processed data in various forms. Every sensor and processor module has a unique identification number indicating the type of sensor, the type of processing, and the location of the sensor and processor module.

The sensors and processor modules can be set up to perform continuous monitoring, event triggered processing, or remote controlled data collection. The continuous monitoring mode is used with structures in which damage would critically impair human safety. In this mode, processed data are sent back continuously and compared with a critical threshold template by the computer at the central facility. An alarm signal will be triggered when the processed data indicate a problem with the structure. The event triggered processing mode is used for structures such as bridges with low traffic load. The data processing and transmission units will be triggered to operate only when a vehicle is passing the bridge. This will lower unnecessary power consumption of the processor modules on the structure. The remote controlled data collection can be activated by an operator at the central facility through dialing the identification numbers of the sensor and processor modules. Issues which must be considered in such a monitoring system include determining the optimal number, location, and type of sensors to be used, and the kind of processing that should be performed on site in real time. It is also necessary to identify the best means to transmit the processed data to the central office and the power requirements for both on-site processing and transmission. Once the processed data reaches the central computer, efficient ways to display the information contained within the data must be ascertained, and methods for identifying the proper threshold template established.

The system currently under development is primarily intended for fatigue damage monitoring of bridges since fatigue damage assessment has been an important issue in bridge inspection and evaluation [37,38]. The algorithm used for estimating fatigue damage requires rainflow counting, stress histogram generation, and equivalent stress range calculation. Using the calculated equivalent stress range and the appropriate AASHTO fatigue design curve, the total number of fatigue cycles can be estimated. The remaining fatigue life of the monitored bridge member can then be obtained by subtracting the number of used fatigue cycles from the total number of fatigue cycles.

As shown in Figure 5, the signal processing module consists of a signal conditioning unit, an analog to digital conversion unit, a digital filter unit, a rainflow counting unit, and a histogram generation unit. In the signal conditioning unit, a low-pass analog anti-aliasing filter with a cutoff frequency of about 1 kHz is used. Although most useful strain gage signals have much lower frequencies than 1 kHz, this cutoff frequency was chosen because it is difficult to implement an anti-aliasing filter with a very low cutoff frequency in a small analog integrated circuit. A sampling frequency between 2 kHz and 3 kHz is used for the analog to digital conversion. A digital low-pass filter is used to reduce the signal bandwidth further. The frequency response of an ideal low-pass filter equals 1 from $-\theta_c$ to θ_c and 0 otherwise, where θ_c is the digital cutoff frequency related to the analog cutoff frequency f_c through the sampling frequency f_s as follows:

$$\theta_c = 2\pi \frac{f_c}{f_s} . \quad (4)$$

For example, if the sampling frequency is $f_s = 3$ kHz and the analog cutoff frequency is $f_c = 100$ Hz, then the digital cutoff frequency is $\theta_c = \frac{\pi}{15}$.

Once the digital cutoff frequency is determined, the impulse response of the ideal low-pass filter can be determined by taking the inverse discrete-time Fourier transform of the frequency response as follows:

$$h_d(n) = \frac{1}{2\pi} \int_{-\pi}^{\pi} H_d(\omega) e^{j\omega n} d\omega = \frac{1}{2\pi} \int_{-\theta_c}^{\theta_c} e^{j\omega n} d\omega = \frac{\sin(\theta_c n)}{\pi n} \quad (5)$$

Because we want a finite impulse response (FIR) filter, the ideal impulse response is weighted by a finite length window sequence $w(n)$ as follows:

$$h(n) = w(n) h_d(n) . \quad (6)$$

To implement the FIR filter, we use distributed arithmetic. Let $x(n)$ and $y(n)$ be the input and output of the FIR filter respectively. The output is obtained by convolving the impulse response $h(n)$ and the input, that is:

$$y(n) = \sum_{i=0}^{N-1} h(i) x(n-i) . \quad (7)$$

Assuming the input is quantized using B bits according to the algorithm

$$x(n) = \sum_{b=0}^{B-1} x_b(n) 2^{-b} , \quad (8)$$

then we can re-write the convolution operation as

$$y(n) = \sum_{i=0}^{N-1} h(i) \sum_{b=0}^{B-1} x_b(n-i) 2^{-b} = \sum_{b=0}^{B-1} \left(\sum_{i=0}^{N-1} h(i) x_b(n-i) \right) 2^{-b}. \quad (9)$$

Because the impulse response $h(n)$ is known once the filter is designed, we can pre-calculate all possible combinations of $h(n)$ and store them into a memory. The input data will be used as addresses to read out appropriate combinations from the memory at the time of operation. Thus no multipliers are needed in the FIR filter.

Because the data rate is several orders of magnitude lower than the processor clock rate, a fully serial architecture is adopted for the digital low-pass filter, the rainflow counting unit, and the histogram generation unit. The fully serial architecture minimizes the number of transistors and consequently reduces the chip size and increases the chip reliability.

Summary

The desire for greater performance and higher reliability in advanced engineering structures targeted for use in the civil environment has created a growing demand for techniques to monitor and assess structural fatigue and damage. This is increasingly true where the information from in-service, real time monitors may be processed to make decisions critical to human safety. A goal in present sensor research is to develop transducers which can interrogate the interior of structural components to determine areas where damage is most likely to form. This is especially true for structural elements formed from complex layered media, such as steel reinforced concrete and advanced composites, where internal interface conditions may vary from place to place. The inhomogeneous and anisotropic structure of these materials presents new challenges to traditional structural monitoring techniques. In addition to catastrophic damage, modern control systems are also demanding that sensors provide real-time measurements of the forces external to the structure, as well as its responses to those forces.

While sensors are vital to any monitoring program, equally important is a means to make it practically and economically feasible to deploy the large number of sensors necessary to adequately monitor even a simple civil structure. Sensors need to be powered, and their outputs individually tracked. Also, in order to be eventually useable to a human operator, the vast amounts of data collected must be at least partially processed, and must be transferred to a remote central control location. To be viable, the sensors, the signal processors, and transfer components must be rugged and reliable, while at the same time cost-effective. As discussed in this paper, fiber optic technology promises to help meet the sensing needs of advanced structural monitoring, while the monitoring and data acquisition program described takes a first step towards practical, long term field deployment of sensing systems.

References

1. R. Roberts, W. Li, and K. Bennett, "Sensors and Signal Processing for Structural Control," Report of NSF Workshop (Washington, D.C.), Feb. 25-26, 1991.
2. R.D. Marshall, "Sensors and Measurement Techniques for Assessing Structural Performance," Proceedings of an International Workshop (Gaithersburg, MD), Sept. 8-9, 1989.
3. F. K. Garas, J.L. Clarke, G.S.T. Armer, eds., *Structural Assessment: The Use of Full and Large Scale Testing*, Butterworths, 1987.
4. M.S. Agbabian and S. F. Masri, eds., *Proceedings of the International Workshop on Nondestructive Evaluation for Performance of Civil Structures*, University of Southern California, Feb. 1988.
5. T.G. Giallorenzi, J.A. Bucaro, A. Dandridge, G.H. Sigel, J.H. Cole, S.C. Rashleigh, and R.G. Priest, "Optical Fiber Sensor Technology," *IEEE J. Quantum Electronics*, QE-18, pp. 626-664, 1982.
6. C.M. Davis, "Fiber Optic Sensors: An Overview," *Optical Engineering*, Vol. 24, No. 2, p. 347, 1985.
7. R.O. Claus, K.D. Bennett, A.M. Vengsarkar, and K.A. Murphy, "Embedded Optical Fiber Sensors for Materials Evaluation," (invited), *Journal of Nondestructive Evaluation*, Vol 8., No. 2, pp. 371-381, 1989.
8. F. Ansari and Q.Y. Chen, "Fiber-optic refractive-index sensor for use in fresh concrete," *Applied Optics*, Vol. 30, No. 28, p. 4056, 1991.
9. M.A. Aframowitz, "Fiber Optic Polymer Cure Sensor," *J. Lightwave Technology*, Vol. 6, No. 10, pg. 1591, 1988.
10. C.D. Butter and G.B. Hocker, "Fiber optics strain gage," *Applied Optics*, Vol. 17, No. 18, p. 2867, 1978.
11. R.O. Claus and J.H. Cantrell, "Detection of ultrasonic waves in solids by an optical fiber interferometer," *Proc. IEEE Ultrasonics Symposium* (Boston, MA), October 1980.
12. J.C. Wade and R.O. Claus, "Interferometric techniques using embedded optical fibers for the quantitative NDE of composites," *Proc. Rev. of Progress in Quantitative NDE* (La Jolla, CA), August 1982.
13. A.O. Garg and R.O. Claus, "Application of Optical Fibers to Wideband Differential Interferometry," *Materials Evaluation*, Vol. 41, p. 106, 1983.
14. M. Reddy, K.D. Bennett, and R.O. Claus, "Imbedded optical fiber sensor of differential strain in composites," *Proc. Rev. of Progress in Quantitative NDE* (La Jolla, CA), August 1986.
15. R.O. Claus, K.D. Bennett, and K.T. Srinivas, "Interferometric optical fiber measurements of internal strain in adhesive joints," *Proc. 2nd International Symposium on the Nondestructive Characterization of Materials* (Montreal, Canada), July 1986.
16. D.A. Jackson, A. Dandridge, and S.K. Sheen, "Measurement of small phase shifts using a single-mode optical interferometer," *Optics Letters*, Vol. 5, p. 139, 1980.
17. J.D. Weiss, "Fiber-Optic Strain Gauge," *J. Lightwave Technology*, Vol. 7, No. 9, 1989.
18. J.S. Sirkis, "Interferometric optical fiber strain sensor under biaxial loading," *Proc. 5th Conf. on Optical Fiber Sensors* (New Orleans, LA), p. 203, January 1988.
19. J.S. Sirkis and H.W. Haslach, "Interferometric Strain Measurement by Arbitrarily Configured, Surface-Mounted, Optical Fibers," *J. Lightwave Technology*, Vol. 8, No. 10, p. 1497, October 1990.

20. J.S. Sirkis and H.W. Haslach, "Complete Phase-Strain Model for Structurally Embedded Interferometric Optical Fiber Sensors," *J. of Intelligent Material Systems and Structures*, Vol. 2, p. 3, January 1991.
21. R.O. Claus, K.D. Bennett, and B.S. Jackson, "NDE of composite materials by pulsed optical time domain methods in embedded optical fibers," *Proc. of Review of Progress in Quantitative NDE* (Williamsburg, VA), June 1985 (invited).
22. R.O. Claus, S. Sudeora, K.A. Murphy, and K.D. Bennett, "Low profile optical time domain fiber sensors for materials evaluation," *Proc. Rev. of Progress in Quantitative NDE* (La Jolla, CA), Vol. 8B, p. 1437 August 1988.
23. B.D. Zimmermann, K.A. Murphy, and R.O. Claus, "Local strain measurements using fiber splices and time domain reflectometry," *Proc. Rev of Progress in Quantitative NDE* (Williamsburg, VA), June 1987.
24. B.D. Zimmermann, R.O. Claus, D.A. Kapp, K.A. Murphy, "Optical time domain reflectometry for local strain measurements," *Proc. SPIE O/E Fiber Lase* (Boston, MA), Vol. 986, September 1989.
25. M.R. Layton and J.A. Bucaro, "Optical fiber acoustic sensor utilizing mode-mode interference," *Applied Optics*, Vol. 18, No. 5, p. 666, March 1979.
26. A. Safaai-Jazi and J.C. McKeeman, "Synthesis of Intensity Patterns in Few-Mode Optical Fibers," *J. Lightwave Technology*, Vol. 9, No. 9, p. 1047, 1991.
27. K.D. Bennett and N.F. O'Brien, "Optimal Detection Schemes for Dual Mode Fiber Sensor Signals," *Proc. of the Fiber Optic Sensor-Based Smart Materials and Structures Workshop* (Blacksburg, VA), April 15-16, 1992.
28. S.T. Kush and M.E. Meffe, "Fiber Optic Vibration Modal Sensor," U.S. Patent No. 4,525,626, June 1985.
29. K.D. Bennett and R.O. Claus, "Analysis of composite structures using optical fiber modal sensing techniques," *IEEE Region 3 Conference* (Richmond, VA), March 1986.
30. P.A. Ehrenfeuchter and R.O. Claus. "Optical fiber waveguide methods for advanced materials," *Proc. Intl. Metallagraphic Soc. Conf.* (Monterey, CA), July 1987.
31. C. Leung, I. Chang, and S. Hsu, "Fiber optic line-sensing system for perimeter protection against intrusion," *Technical Digest, Fourth International Conference on Optical Fiber Sensors* (Tokyo, Japan), 1986, p. 113.
32. W.B. Spillman, B.R. Kline, L.B. Maurice, and P.L. Fuhr, "Statistical-mode sensor for fiber optic vibration sensing uses," *Applied Optics*, Vol. 23, No. 15, August 1989.
33. K.D. Bennett, R.O. Claus, and M.D. Dumais, "Impact characterization by optical fiber ultrasonic sensors," *IEEE Ultrasonics Symp.* (Chicago, IL), October 1988.
34. K.D. Bennett, R.O. Claus, and D.A. Kapp, "Characterization of optical fiber impact sensors for composite materials," *Proc. ASNT Meeting on NDE for Life Extension* (Charlotte, NC), March 1989.
35. K.D. Bennett, R.O. Claus and M.J. Pindera, "Internal monitoring of acoustic emission in graphite epoxy composites using embedded optical fiber," *Proc. Rev of Progress in Quantitative NDE* (La Jolla, CA), August 1986.
36. D. Cox, D. Thomas, K. Reichard, D. Lindner, and R.O. Claus, "Modal domain fiber optic sensor for closed loop vibration control of a flexible beam," *Proc. SPIE O/E Fiber Lase* (Boston, MA), September 1989.
37. B.T. Yen, D. Moser, H.R. Hsieh, and J.W. Fisher, "Examination of Fatigue Cracking and Response of I24 Tied-Arch Bridges Near Paducah, Ky." Fritz Engineering Laboratory Report No. 200.88.479E1, Lehigh University, March 1988.
38. B.T. Yen, *et. al.*, "Manual for Inspecting Bridges for Fatigue Damage Conditions," FHWA-PA-89-022+85-02, Jan. 1990.

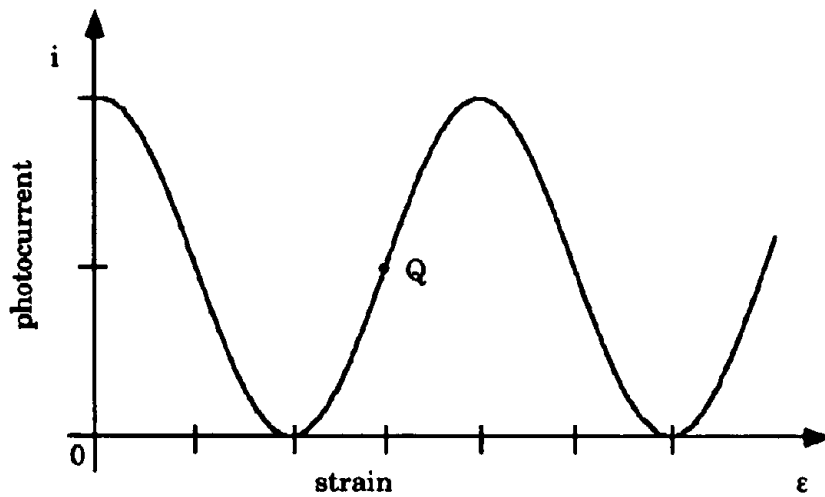
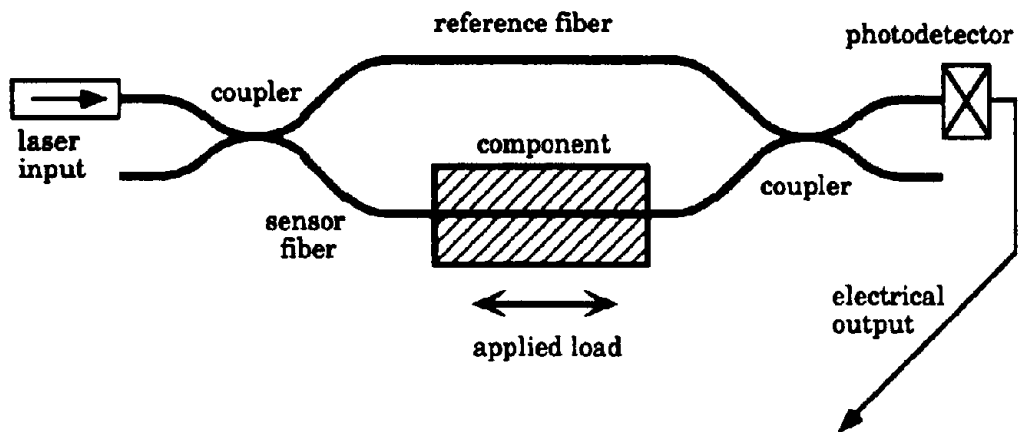


Figure 1. A simplified Mach-Zehnder fiber optic interferometer arrangement, and the theoretical output as a function of strain on the structural component to which the sensing fiber is attached.

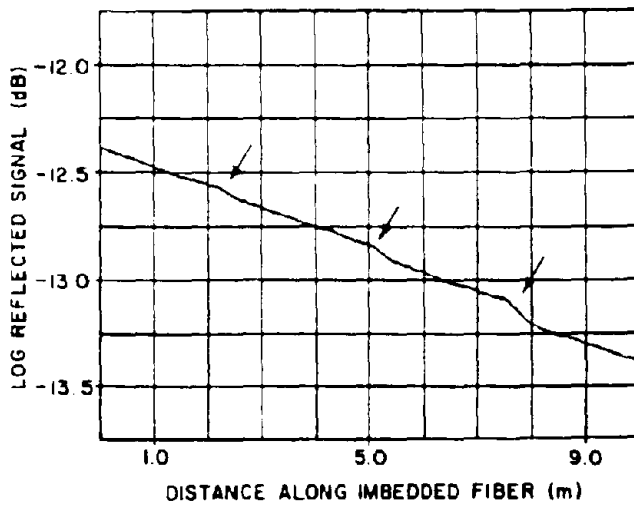
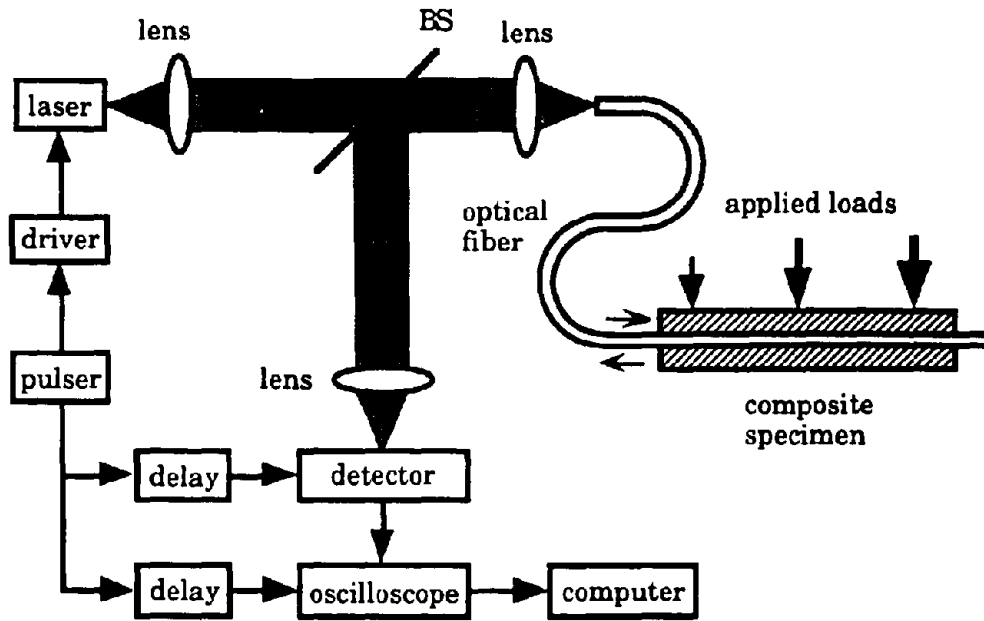
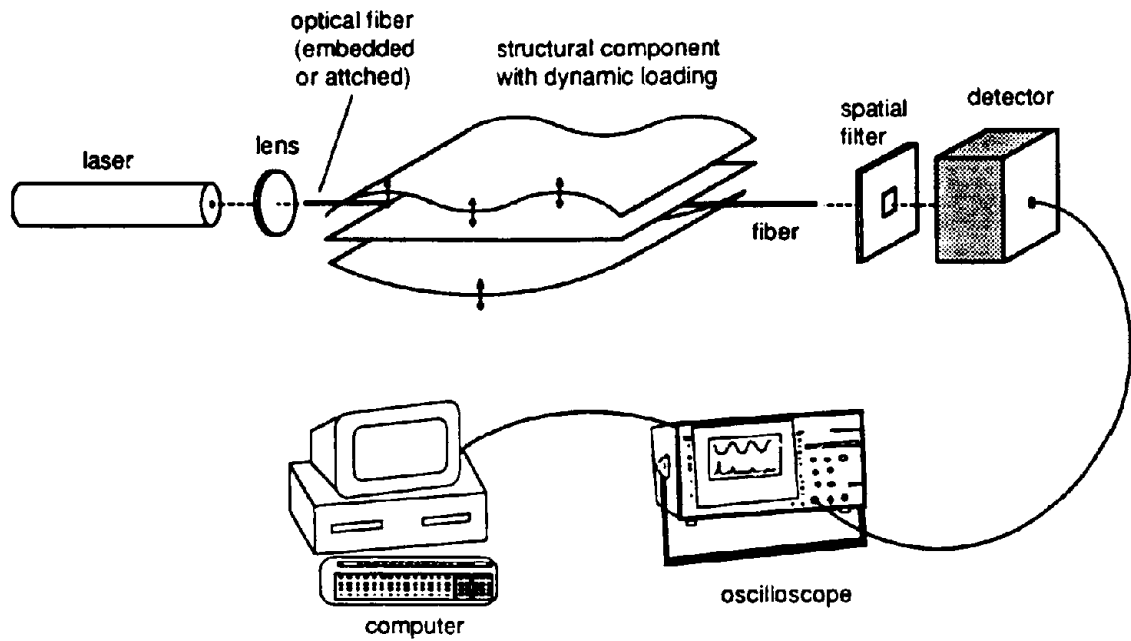
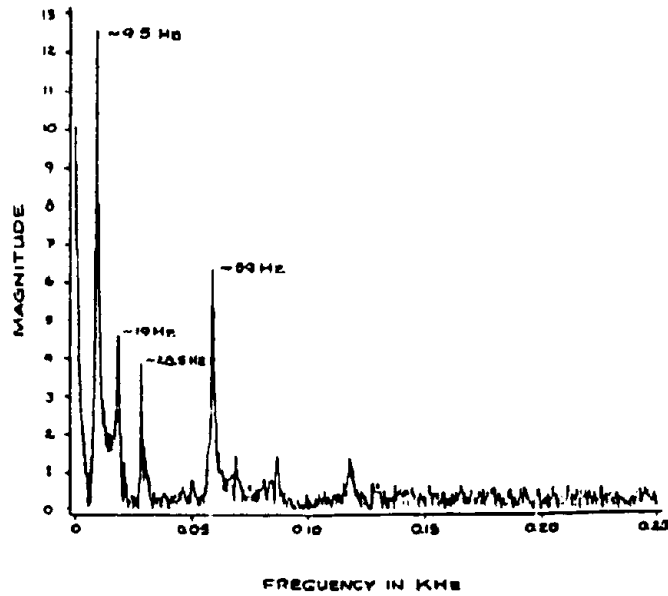


Figure 2. Basic OTDR system used to measure strain in a composite specimen loaded at three locations along the fiber, and the digitally averaged resulting signal. Slope changes proportional to the respective loads (350, 700, and 1050 kPa) are observable at 2.2, 5.1, and 7.8 meters [17].



a.



b.

Figure 3. a. Experimental set-up for optical fiber modal domain sensing of mechanical vibrations [24]. b. Frequency spectrum of a modal domain sensor attached to a long flexible beam [25].

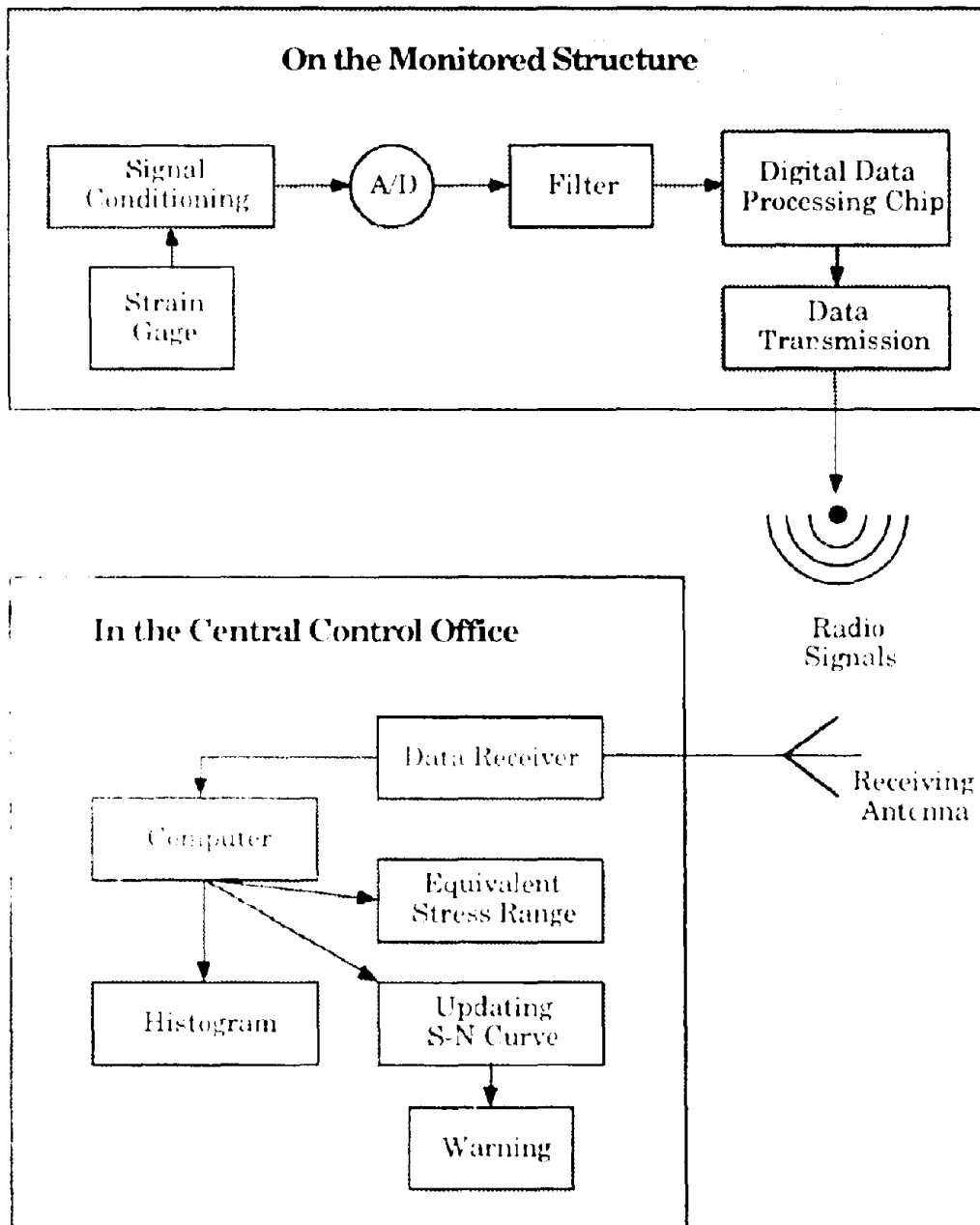


Figure 4. System diagram for structural monitoring and data acquisition.

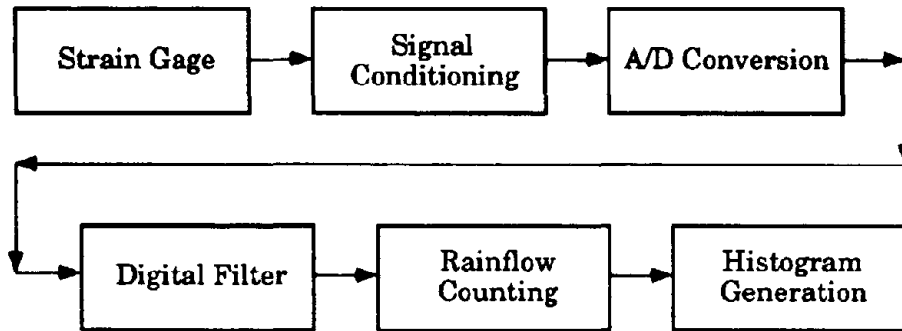


Figure 5. Block diagram of the signal processing module.

New Developments in Strong Motion Accelerographs

J.G. Diehl
Kinemetrics, Inc., Pasadena, California

ABSTRACT: Modern accelerographs benefit from new technologies in instrumentation. Twenty-five strong motion accelerographs from eight instrument companies are reviewed. The results presented by feature, and by application in tabular form. Improvements are discussed and needs for new research are presented.

INTRODUCTION

The earthquake engineering community has historically used strong motion earthquake data for regional seismicity research, ground motion studies, and structural response analysis. Recent interest in site response and microzonation studies requires increasingly accurate strong motion data as one ingredient for the prediction of ground motions. In the paper introduced at the 10th World Conference on Earthquake Engineering, Diehl and Iwan presented the results of a worldwide survey of strong-motion instruments.

The purpose of this paper is to review these results from the standpoint of new developments in technology, and the implications for experimental earthquake engineering.

METHOD

The data gathering method reported by Diehl and Iwan is repeated here. Eighteen seismic instrument manufacturers were given the opportunity to supply information on the features and capabilities of their strong motion accelerographs. A survey form (Diehl, *SURVEY*) was provided with a standard set of definitions for each feature,

such as dynamic range, in order to facilitate comparison. The definition of applications are presented in the next section.

Manufacturers were allowed to categorize their own instruments according to the guidelines. In addition, each had the opportunity to indicate any special features of their instruments.

In order to qualify for comparison, an accelerograph had to meet the minimum standards for a stand-alone, autonomous station. This meant that a manufacturer combining a recorder with an external sensor package must be willing to sell both units as a system, including all necessary software and cabling. Finally, manufacturers were asked to not provide any information about instruments they did not intend to manufacture for at least the next two years.

APPLICATIONS

Several workshops have been held, and papers written defining the characteristics of various instrumental arrays (Iwan, Spudich). Diehl and Iwan use the following categories:

- autonomous stations
- regional networks
- structural arrays
- fixed surface arrays

dense three-dimensional arrays mobile arrays

The basic requirements for each application are presented in the Legend of Table 1 (page 6). The Autonomous Station describes an instrument which may not be designed to connect to any other instruments, and also represents the minimum standard for defining an accelerograph. A Regional Network is a group of accelerographs installed in a geographic region for the purpose of collecting strong motion data, and not connected to one another. The dominant requirement is accurate time.

A Fixed Dense Surface Array is primarily two dimensional, and designed to study source mechanism and wave propagation phenomenon. The controlling features in this case are high dynamic range, broad bandwidth, and common time. The 3-dimensional Dense Array differs from Fixed Surface Arrays in that they are three dimensional, adding necessary features of downhole sensing. Mobile Arrays are similar to dense arrays, but must be capable of mobility and autonomy.

Finally, Structural Arrays are dense local arrays which have the capability for central recording.

RESULTS

All data submitted by the manufacturers for accelerographs which meet minimum requirements (see definitions) are presented in the accompanying Table 1 (Diehl and Iwan). Table 2 presents the results by application.

DISCUSSION

Table 3 illustrates the advances in modern accelerograph technology over film recording systems. Clearly, the technological improvements of digital accelerographs over their analog predecessors cover all aspects of

the accelerograph system, including bandwidth, dynamic range, accuracy, recording capacity, triggering, and pre-event memory. Also, as indicated in Table 2, modern instruments can serve in multiple capacities for different experiments and applications. Equally important, in 1970 dollars, the cost of these accelerographs has improved dramatically, generally following the revolution in electronics. As reported by Merrill and Reyes, network operation costs are also less than analog accelerographs in most cases.

The future of technology is even brighter. For regional networks and structural arrays, the combination of low cost 12-bit digital recording and silicon sensors, and application of digital communications should produce ever more reliable and cost effective accelerograph systems. FLASH memory card systems offer the advantages of digital recording, with even greater convenience than film magazines. Kinematics has already announced a retrofit for its SSA-2 product which provides FLASH memory card recording. The new option allows users to retrieve data and rapidly set instrument parameters in the field just by removing and replacing the FLASH card. Early memory card systems relied on internal batteries, and were limited in usefulness due to a proprietary interface. The new flash memory card system offers lower cost memory, and is interchangeable with other PCMCIA memory card systems because of a common form factor, input/output, execution software, and power specs, and the data are nonvolatile - without dependence on batteries.

For research arrays, 16-bit systems are already here with the promise of 20- and 24-bit systems on the horizon. FLASH memory cards already offer 20 Mbyte capacities, and low power 2.5 inch hard disks provide capacities over 100 Mbyte. Several accelerograph manufacturers already offer GPS time code and location receiver systems, and this technology has rapidly become the system of choice, both for accuracy

(measured in nanoseconds) and cost effectiveness. Portable broad band sensors provide very high dynamic range (better than 140 dB) in bandwidths from 30 seconds to 100 Hz. Interconnect systems allow concurrent, synchronous sampling of all data channels for perfect preservation of channel-to-channel motion phase relationships. New battery technologies are emerging, driven by the demand for portable PCs with ever increasing autonomy. Finally, powerful microcomputers allow a level of strong motion data analysis, including multichannel cross-spectral studies, heretofore unavailable except on minicomputers and mainframes.

RESEARCH NEEDS

While many researchers continue to develop better approaches to the processing of analog film recording data, little has been done in the development and validation of new software to take advantage of the new features offered in digital accelerographs, such as pre-event memory and broader bandwidth. Figure 1 illustrates the results of a simple experiment where an accelerograph was moved horizontally on a table top (Graizer). The acceleration was double-integrated without the usual band-pass filtering, the results corroborated the physical test within 5%.

The seismic risk assessment of long-span bridges and base-isolated structures requires more accurate data on long period and residual displacements. More research is needed to evaluate these new integration approaches, and provide the community with acceptable software.

CONCLUSIONS

Modern accelerographs offer dramatic improvements in strong motion data acquisition. New technologies should provide increasing performance at competitive prices. However, more research is needed to develop internationally

accepted, proven methods for processing digital accelerograms with long period information.

REFERENCES

- Diehl, J.G., and Iwan, W.D., *A Technical Review of Modern Strong Motion Accelerographs*, 10th World Conference on Earthquake Engineering, July 1992, Madrid, Spain
- Diehl, J.G., and Iwan, W.D., *SURVEY FORM: A Technical Review.....*, Jan 28, 1992, available from ISMAC/W.D. Iwan
- Graizer, V., *A Simple Low-Frequency Test of Digital Strong-Motion Accelerographs*, Institut de Physique du Globe, Strasbourg, France, 1991
- Iwan, W.D., *Strong Motion Earthquake Instrument Arrays*, Proc. International Workshop on Strong-Motion Earthquake Instrument Arrays, Honolulu, 1978
- Iwan, W.D., *U.S. Strong-Motion Earthquake Instrumentation*, Proc. of the U.S. National Workshop on Strong-Motion Earthquake Instrumentation, April 1981
- Merrill, R.A., and Reyes, A., *A Performance Review of Digital Solid State Accelerographs vs Analog Film Recording Accelerographs*, 10th World Conference on Earthquake Engineering, July 1992, Madrid, Spain
- Spudich, P., and Boore, D.M. et al, *National Plan to Record Earthquake Motions on the Ground and in Man-Made Structures*, DRAFT USGS Open File Report, Aug 1985

SURVEY OF STRONG MOTION ACCELEROGRAPHS					
Table 1					Page 1
DESIGN FEATURE	KINEMATICS SSA-2	KINEMATICS SSA-18	KINEMATICS SSA-3	KINEMATICS SSP-1 with FBA-23	KINEMATICS SMA-1
Price	\$3,850	\$7,250	\$18,285	\$12,500	\$3,920
Suitable Applications	A.N.S.	A.N.S.D.3D	S	A.D.3D	A.N.
No. of Channels	3	3	6	3	3
Optional			24,3	6	
Sample rate (sps)	200	200	200	200	*
Dynamic Range (dB)	66dB	90dB	66	90	45
Sensor Type	VC, EMF	VC, EMF	VC, EMF	VC, EMF	O
Internal/External	I	I	I	I	I
Optional	E	E	E	E	
Natural Frequency (Hz)	50 Hz	50	50	50	25
Sensitivity (g)	2	2	2	2	1
Optional	1, .5, .25, .1	1, .5, .25, .1	1, .5, .25, .1	1, .5, .25, .1	.5
Damping (%critical)	.70	.70	.70	.70	.65
Resolution	12 bits	16 bits	12 bits	16 bits	0.006
Bandwidth	DC to 50 Hz	DC to 50 Hz	DC to 50 Hz	DC to 50 Hz	DC to 25
Low-pass filter	2-pole, 50 Hz	2-pole, 50 Hz	2-pole, 50 Hz	-48	-12
character	Butterworth,	Butterworth,	Butterworth,	Butterworth,	Butterworth,
Preamp (dB)				0-60,20	
Noise (g)	LSB 0.00098	LSB 0.00061	LSB 0.00098	LSB 0.00061	<0.005
Int.System F.Test	SU	SU	SU	SU	SU
Sensor Interface	SE, 100k, +/-12,3	SE, 100k, +/-12,3	SE, 100k, +/-12,3	D, 100k, +/-12,3 or 6	
External Indicators	P,E	P,E	P,E	P,E,T	P,E
Interconnect	M,S,C,T,D	M,S,C,T,D	M,S,C,T,D	M,S,C,T,D	M,S,C,T
Trigger Modes					
character	Threshold	Threshold	Threshold	Threshold, STA/LTA	Threshold
bandwidth	.1 to 12 Hz	.1 to 12 Hz	.1 to 12 Hz	.1 to 12 Hz	1 to 10 Hz
range	.002-.2/.002	.002-.2/.002	.002-.2/.002	.002-.2/.002	0.005 to 0.025
Pre-event memory (sec)	0, 1.25, 2.5, 5, 10, 15	0, 1.25, 2.5, 5, 10, 15	0, 1.25, 2.5, 5, 10, 15	0, 1.25, 2.5, 5, 10, 15	0
3 ch, 200 sps	10, 15, 30, 60, 90	10, 15, 30, 60, 90	10, 15, 30, 60, 90	10, 15, 30, 60, 90	7 to 20 min
Post-event hold (sec)					
Recording medium	CSRAM	CSRAM	CSRAM	CSRAM	film RAR2494, 70mm
std				Hard Disk	
OPTIONAL				Lithium	
Mem.Backup Battery (type)	Lithium	Lithium	Lithium	Lithium	25min, full
Recording capacity (min)	9 DC2	18 DC2	25 DC2	14	
OPTIONAL					
	72,9	108,18	430,18	84,14 RAM, 2800 HD	
Playback hardware	IBM Compatible PC	IBM Compatible PC	IBM Compatible PC	IBM Compatible PC	Dark Room
Comm Software	QuickTalk(TM)	QuickTalk(TM)	QuickTalk(TM)	QuickTalk(TM)	
OPTIONAL	any XMODEM	any XMODEM	any XMODEM	any XMODEM	M
Retrieval Method	T	T	T	T	
OPTIONAL				H	
Transfer Rate (baud)	38400	115200	38400	115200	
Clock stability					
standard (accuracy,	1x10E-4, -20to65C	1x10E-4, -20to65C	1x10E-4, -20to65C	+/-2x10-7, -20-70C	+/-2x10-3, -20to55C
temperature range)				aging 5x10-7	
OPTIONAL	3x10E-7, 0 to +50C	+/-2x10-7, -20to70C	3x10E-7, 0 to +50C		3x10E-7, 0 to +50C
		aging 5x10-7			
Synchronization	M,AR	M,AR	M,AR	M,A,AS,AR	AS
optional	M,A,AS	M,A,AS,AR	M,A,AS		
Receivers	G,W,M,D	G,W,M,D	G,W,M,D	G,W,M,D	W,M,D
Power supply					
std (#batts, volts, cap)	1, 12VDC, 6.5Ah	2, 12VDC, 6.5Ah	2, 12VDC, 6.5Ah	2, 12VDC, 6.5Ah	2, 2.5Ah, 6V
external	+12 VDC	+12 VDC	+12 VDC	+12 VDC	+12 VDC
Current Drain (milliamps)	approx 75 ma	approx 140 ma	approx 75 ma	approx 140 ma	0.15mA
Capacity (days)	4 days	4 days	4 days	4 days	>90
Physical					
Size (LxWxH in cm)	27x10x38	40x41x20	19" rack mount	23x41x43 + 13x13x6	20x35.5x20
Weight (Kg)	12	18	depends # ch	17 + 2.3	11
Housing	sealed aluminum	sealed aluminum	sealed aluminum	sealed aluminum	sealed aluminum
Operating Temp (C)	-20C to +65C	-20C to +65C	-20C to +65C	-20C to +65C	-20C to +55C
Humidity	100%	100%	100%	100%	100%
Data Reduction					
Software Available	D,P	D,P	D,P	D,P	D,P
OPTIONAL	DSP,VOL,I	DSP,VOL,I	DSP,VOL,I	DSP,VOL,I	DSP,VOL
Company Notes	* With 300 dpi scanner, SMA-1 equivalent digital performance is: sample rate = 160 sps dynamic range = 55dB resolution = .0035g bandwidth = 1 to 50 Hz				

Table 1

SURVEY OF STRONG MOTION ACCELEROGRAPHS

Page 2

DESIGN FEATURE	MARK RAND CO. DACS-omega SM16 Super	MARK RAND CO. DACS-omega ME-16	OFITECO ACD-3E	REFRACTION TECH 72A-06/C (Columbia Accel)	REFRACTION TECH 72A-06/G (Gurain Accel)
Price	US \$30,000	US \$41,200	US \$8,000	\$11,215	\$12,625
Suitable Applications	A,N,D,M,S	A,N,D,M,S	A,N,S	M,D,3D,S,N,A	M,D,3D,S,N,A
No. of Channels	3	3	3	3/6	3 (with dual gain) 6 (w/o dual gain)
Optional					
Sample rate (sps)	100,200	100,200,500,1000	100,200	500,250,200,125,100 50 sps	500,250,200,125,100 50 sps
Dynamic Range (dB)	96 + 18dB (gain range)	96 + 80dB (gain range)	66	90 dB	90dB(140dB dual gain)
Sensor Type	S	S	S	S	S
Internal/External	E	E	E	E	E
Optional					
Natural Frequency (Hz)			N/A	150	50-100 Hz
Sensitivity (g)	2	2	2g	2	2g
Optional					
Damping (%critical)	5, 10	0.5, 1.5	0.5, 0.25, 1, 5 g	1, 0.5, 0.25 SEE NOTE 1	1, 0.5, 0.1
Resolution	<10-4 g	<10-6 g	0.001 g	7x10-5G	7x10-5G SEE NOTE 3
Bandwidth	0.08 to 25.50HZ	0.08-25.50,125-250HZ	Dc-30 Hz	DC to 40% of S.R.	DC to 40% of S.R.
Low-pass filter	-72	-72	Butterworth	FIR (digital filter)	FIR (digital filter)
character			n/a	0dB	0dB and 54dB
Preamp (dB)	0 to 18dB,6dB steps	0 to 80dB, 10 dB steps	0.001	0 (step)	0 (step)
Noise (g)	<30 uV	<0.2 uV	P	D, 2 Meg, +12V, 3/6	D, 2 Meg, +12V, 3/6
Int.System F. Test	SU	SU	SE, +12V, 3		
Sensor Interface	100K, +/-15 VDC	100K, +/-15 VDC	P,E,T,H, Low Batt		
External Indicators	P,E,T,H *1	P,E,T,H *1	M,S,C,T	M,S,C,T,D	M,S,C,T,D
Interconnect					
Trigger Modes	thrsh,ext,STA/LTA rat.	thrsh,ext,STA/LTA rat.	Threshold	LEVEL, STA/LTA	LEVEL, STA/LTA
character	0.1 TO 5 Hz *2	0.1 TO 20 Hz *2	1 TO 512 s.	External, Time	External, Time
bandwidth	1 LSB step 19uV-5v	1 LSB step 19uV-5v	0.1 TO 10% Range	same as instrument	same as instrument
range				Level 1-37,768 cnts	Level 1-37,768 cnts
				(2G to 7x10-5G)	(2G to 7x10-5G)
Pre-event memory (sec)	0-3000 samp, sel. *3	0-3000 samp, sel. *3	1 to 256 s	0-150s,0.001s incr	0-150s,0.001s incr
3 ch, 200 sps	1-999, 1 sec incr	1-999, 1 sec incr	1 to 512 s.	0-99.999s;0.001s incr	0-99.999s;0.001s incr
Post-event hold (sec)					
Recording medium	memory card	memory card	CSRAM	HD,234MB,FORMATTED	HD,234MB,FORMATTED
std					
OPTIONAL					
Mem.Backup Battery (type)	dry battery (intrnl)	dry battery (intrnl)	Lithium	N/A	N/A
Recording capacity (min)	15	15	7 m.	1500 min (25hrs)	1500min dual gain
OPTIONAL	45,15	45,15		dual gain	
				3000 min (50hrs	3000 min (50hrs
				w/o dual gain	w/o dual gain
Playback hardware	Display,prnter,atchd	Display,prnter,atchd	Rampack reader	PC, SUN WORKSTATION	PC, SUN WORKSTATION
Conn Software			Accl	PASCAL S/W, FSC *2	PASCAL S/W, FSC *2
OPTIONAL	Analog playback	Analog playback	M	Pitaa, DaDisp, Matlab	Pitaa, DaDisp, Matlab
Retrieval Method	M, T (9600 bps)	M, T (9600 bps)		T(SCSI) TO TAPE,DISK	PC OR SUN
OPTIONAL	data transmission	data transmission		T (XMODEM) TO PC	(XMODEM) TO PC
Transfer Rate (baud)	software (modem dir.)	software (modem dir.)		58 Kbytes/sec (SCSI)	58 Kbytes/sec (SCSI)
	*4	*4			
Clock stability	5x10-8	5x10-8	+/- 2x10e-3;0-50C	5X10e-7 (0-50 C)	5X10e-7 (0-50 C)
standard (accuracy,			+/- 5x10e-6;0-50C	3X10e-7 (0-50 C)	3X10e-7 (0-50 C)
temperature range)					
OPTIONAL					
Synchronization	A	A	AS	A, AS	A, AS
optional					
Receivers	W,M, J	W,M, J	W,M,D,MSF	G,M(or any TrueTime	G,M(or any TrueTime
				rec'r with serial output)	rec'r with serial output)
Power supply	100V AC	100V AC	1,6.8Ah, +12 Vdc	72A-04 aux. pwr sply	72A-04 aux. pwr sply
std (#batts,volts,cap)			+12 Vdc	(EXT), two powersonic	(EXT), two powersonic
external				ps-1265, 6.5 AH each	ps-1265, 6.5 AH each
Current Drain (milliamps)	18.4 w	18.4 w	150 mA max.	+12Vdc	+12Vdc
Capacity (days)			2 days	250ma	250ma
Physical				2.0 days	2.0 days
Size (LxWxH in cm)	30x36.5x27	30x36.5x27	36x22x31	32x21x19+32x21x12+sens	32x21x19+32x21x12+sens
Weight (Kg)	9.5	9.5	12	11 kg + sensor	11 kg + sensor
Housing	glass fiber case	glass fiber case	Aluminum	polyethylene, sealed	polyethylene, sealed
Operating Temp (C)	-5 to +50	-5 to +50	-5 to 65 C	-20 to +60 C	-20 to +60 C
Humidity	95% noncondensing	95% noncondensing	100%	sealed (air 2.5 psi)	sealed (air 2.5 psi)
Data Reduction			D, P	D	D
Software Available	D,P,DSP	D,P,DSP		DSP,P,VOLI,PITSA	DSP,P,VOLI,PITSA
OPTIONAL					
Company Notes	*1 memory remaining, amplifier gain, trigger level			NOTE *1 150Hz(2G), 125(1G), 100(5G), 75(25G)	
	*2 user specify			*2 Field parameters setup for PC	
	*3 @ 100 sps 0-30sec in 1sec increments			*3 2x10-7 high gain	
	*4 Software used on PC computer. Serial port is standard at DACS-omega				

DESIGN FEATURE	REFRACTION TECH 72A-08/GDH (Gurain DH Accel)	SYSCOM MR 2002	TELEDYNE A-800	TELEDYNE A-800	TERHATECH IDS-3602S
Price	\$18,200	\$16,427.00	\$6,960.00	\$9,565	\$9,975
Suitable Applications	3D	A.N.S	A.N	A.N	A.N.D
No. of Channels	3 (with dual gain)	3	3	3	3
Optional	6 (w/o dual gain)		0	0	
Sample rate (sps)	500,250,200,125,100 50 sps	200 SPS	200	200	1000 NOTE 3
Dynamic Range (dB)	80dB(140dB dual gain)	66	66	90	126 NOTE 4
Sensor Type	S	VC	PE, S	PE, S	S
Internal/External	E	E	I	I	Internal
Optional		I	E	E	
Natural Frequency (Hz)	50-100 Hz	850 Hz	1250 Hz	200 Hz	70Hz
Sensitivity (g)	2g	2g	+/-2	+/-2	2
Optional	1, 0.5, 0.1	1, 0.5, 0.25			1, .5, .25, .1
Damping (%critical)	0.8	0.7	95%	70%	70%
Resolution	7x10-5G SEE NOTE 3	12 bits	12 bits	16 bits	.95 X 10-6
Bandwidth	DC to 40% of S.R.	DC-50 Hz	0.1 to 50 HZ	DC to 50 HZ	70 NOTE 1
Low-pass filter	-90dB	6-pole, 50 Hz	-48	-60	90 NOTE 2
character	FIR (digital filter)	Butterworth	Butterworth	Butterworth	butterworth
Preamp (dB)	0dB and 54dB	0dB	0.6, 12, 18	0.6, 12, 18	12, 24, 36
Noise (g)		<0.0001	0.0005	0.000044	.47X 10-6
Int. System F. Test	0 (step)	SU	SU, P, O*	SU, P, O*	P
Sensor Interface	D, 2 Meg, +12V, 3/6	SE, 100K, OV, 6.5V	D, >1M, +15, 3	D, >1M, +15, 3	
External Indicators		P.E.H 0: run/mem used	P.E.T, O**	P.E.T, O**	E.T.H
Interconnect	M.S.C.T.D	M.S.C.T.D. NOTE 1	M.S.C.T	M.S.C.T	M.S.C.T.D
Trigger Modes	LEVEL, STA/LTA				
character	External, Time	filtered threshold	Threshold, external	Threshold, external	Threshold, STA/LTA
bandwidth	same as instrument	0.5-15Hz	0.1-12	0.1-12	.1-12
range	Level 1-37,768 cnts (2G to 7x10-5G)	0.1-5% full scale	0.002-1.998/0.002	0.002-1.998/0.002	0.002-1.998/0.002
Pre-event memory (sec)	3 ch, 200 sps				
Post-event hold (sec)	0-150s, 0.001s incr	1-17 sec 1 sec incr	1-40/1	1-40/1	1-99/1
Recording medium	0-99.999s; 0.001s incr	1-30 sec 1 sec incr	1-10000/1	1-10000/1	1-99/1
Optional					
Mem. Backup Battery (type)	HD, 234MB, FORMATTED	CS RAM	CSRAM	CSRAM	CRSRAM
Recording capacity (min)	MEM CARD (JEIDA)	LITHIUM	None	None	Lithium
OPTIONAL	1500min dual gain	15 DC 2.5	Lithium	Lithium	22 DC 2.5
			15.0	28.0	
	3000 min (50hrs w/o dual gain)	240 IN 4	120, 15	112, 14	132/22
Playback hardware	PC, SUN WORKSTATION	PC, OR MODEM + PC	IBM Compatible PC	IBM Compatible PC	IBM PC Compatible
Comm Software	PASCAL, S/W, FSC *2	LINK, PREVIEW	None	None	Terra SDRA
OPTIONAL	Ptisa, DaDiap, Matlab	VIEW 2002	ASET, Crosstalk	ASET, Crosstalk	
Retrieval Method	* SEE PRIOR	T	T	T	T
OPTIONAL	T (XMODEM) TO PC	M			
Transfer Rate (baud)	58 Kbytes/sec (SCSI)	38400	38400	38400	115,200
Clock stability					
standard (accuracy, temperature range)	5X10e-7 (0-50 C)	+/- 2X10-5	+1 x 10-4 from	+1 x 10-4 from	+/-1X10-6, 0to50C
OPTIONAL	3X10e-7 (0-50 C)	FROM -20..65 C	-20to 70 deg. C	-20to 70 deg. C	1X10-6 AGING
Synchronization	A, AS	+/- 1x10-7, -15to75C	+5 X 10-7 from	+5 X 10-7 from	+/-3X10-7, -20to70C
optional		5x10-7 aging	-20 to 75 deg. C	-20 to 75 deg. C	1X10-6 AGING
Receivers	G, M (or any TrueTime rec'r with serial output)	M, A	M, AR	M, AR	M, A, AS
		AS	M, A, AR	M, A, AR	
		D, M, W	G, W, M, E, D	G, W, M, E, D	W, M, O- Any IRIGE
Power supply					
std (#batts, volts, cap)	72A-04 aux. pwr aply (EXT), two power sonic pa-1265, 6.5 AH each	ONE 12vdc 6.5 Ah	2, +12 Vdc, 5AH	1, +12 Vdc, 17AH	1, +12V, 24 Ah
external	+12Vdc	12vdc	11-14 Vdc	11-14 Vdc	
Current Drain (milliamps)	250ma	125 mA	265 at 12 Vdc	225 at 12 Vdc	125 mA
Capacity (days)	2.0 days	2.4 days	1.5 days	3.0 days	4.0
Physical					
Size (LxWxH in cm)	32x21x19+32x21x12+sens	20x23x11	33x27.9x22.8	33x27.9x22.8	35.6X30.5X20.3
Weight (Kg)	1.1 kg + sensor	6.9 kg	20.5	24	21.4
Housing	polyethylene, sealed	sealed cast aluminum	Base cover of cast aluminum-crushproof	Base cover of cast aluminum-crushproof	Std. Steel IP65
Operating Temp (C)	-20 to + 60 C	-20 to 65	-20 to +65 deg. C	-20 to +65 deg. C	OPT. Stainless IP67
Humidity	sealed (air 2.5 psi)	100%	0-100% non-condens	0-100% non-condens	-25 to + 70 C
Data Reduction					
Software Available	D	D, P	None	None	D, P, DSP, VOL
OPTIONAL	DSP, P, VOL, I, PTISA	DSP	D, P	D, P	
Company Notes		*1 Data Transfer, Parameter setup	*1 Sinewave **2 Low Battery		

DESIGN FEATURE	TERRATECH IDS-3602SX	TERRATECH IDS-3602F	TERRATECH IDS-3602D	TERRATECH DCA 333R	TERRATECH DCA 300R
Price	\$7,875.00	\$9,775.00	\$11,900.00	\$8,750.00	\$18,900.00
Suitable Applications	A,N,D,3D	M	S	A,N	S
No. of Channels std	3	3	3	3	6
Optional Sample rate (sps)	1000 NOTE 3	1000 NOTE 3	1000 NOTE 3	100	12/3 100 or 200
Dynamic Range (dB)	126 NOTE 4	126 NOTE 4	126 NOTE 4	66	66
Sensor Type	S,O Accepts Sensor	S,O Accepts Sensor	S,O Accepts Sensor	S	S
Internal/External	E	E	E	I	E
Optional				E	
Natural Frequency (Hz)	70Hz	70Hz	70Hz	30	30,50
Sensitivity (g)	2	2	2	1	1
Optional	1,.5,.25,.1	1,.5,.25,.1	1,.5,.25,.1	2,.5,.25	2,.5,.25
Damping (%critical)	70%	70%	70%	70%	70%
Resolution	.95 X 10-6	.95 X 10-6	.95 X 10-6	.0005	.0005
Bandwidth	70 NOTE 1	70 NOTE 1	70 NOTE 1	30	30 or 50
Low-pass filter	90 NOTE 2	90 NOTE 2	90 NOTE 2	30	30
character	Butterworth	Butterworth	Butterworth	Butterworth	Butterworth
Preamp (dB)	12,24,36	12,24,36	12,24,36		
Noise (g)	.47 X 10-6	.47 X 10-6	.47 X 10-6	2.4 x 10-4	2.4 x 10-4
Int.System F. Test	P	P	P	P	P
Sensor Interface	SE,>35K, +/-12,3	SE,>35K, +/-12,3	SE,>35K, +/-12,3	SE,>10K, +/-12,3	SE, >10K, +/-12,12
External Indicators	E,T,H	E,T,H	E,T,H	E,T,O Led Indicator	E,T,O Led Indicator
Interconnect	M,S,C,I,D	M,S,C,I,D	M,S,C,I,D	M,S,C,I,D	M,S,C,I,D
Trigger Modes	Threshold,STA/LTA	Threshold,STA/LTA	Threshold,STA/LTA	Threshold	Threshold
character	.1-12	.1-10	.1-10	.1-10	.1-10
bandwidth	0.002-1.998/0.002	0.002-1.998/0.002	0.002-1.998/0.002	.001-.1/001	.001-.1/001
range					
Pre-event memory (sec)	1-99/1	1-99/1	1-99/1	4 @ 100 sps only	.64-3.2/.64
3 ch, 200 sps				15	15
Post-event hold (sec)	1-99/1	1-99/1	1-99/1		
Recording medium	CSRAM	CSRAM	CSRAM	CSRAM	CSRAM
std				Digital Cassette	Digital Cassette
OPTIONAL				Dual Lithium	Dual Lithium
Mem.Backup Battery (type)	Lithium	Lithium	Lithium	32 DC 1.5 @ 100 SPS	16 DC 1.5
Recording capacity (min)	22 DC 2.5	22 DC 2.5	22 DC 2.5		
OPTIONAL	132/22	132/22	132/22	96/32	48/16
Playback hardware	IBM PC Compatible	IBM PC COMPATIBLE	IBM COMPATIBLE	IBM PC Compatible	IBM PC Compatible
Comm Software	Terra SDR4	Terra SDR4	Terra SDR4	Terra TRAP	Terra TRAP
OPTIONAL					
Retrieval Method	T	T	T	T	T
OPTIONAL					
Transfer Rate (baud)	115,200	115,200	115,200	9600	9600
Clock stability	+/-1X10-6, 0to50C	+/-1X10-6, 0to50C	+/-1X10-6, 0to50C	5X10-6, 0 to 50C	5X10-6, 0 to 50C
standard (accuracy,	1X10-6 AGING	1X10-6 AGING	1X10-6 AGING	5X10-6 Aging	5X10-6 Aging
temperature range)	+/-3X10-7, -20to70C	+/-3X10-7, -20to70C	+/-3X10-7, -20to70C	5x10-7, .25to50C	5x10-7, .25to50C
OPTIONAL	1X10-6 AGING	1X10-6 AGING	1X10-6 AGING	5X10-7 Aging	5X10-7 Aging
Synchronization	M,A, AS	M,A, AS	M,A, AS	M,AR	M,AR
optional					
Receivers	W,M,O- Any IRIGE	W,M,O- Any IRIGE	W,M,O- Any IRIGE	W,M	W,M
Power supply	1, +12V, 24 Ah	3, +/-12&6, 18 Ah tot.		2,6V,8Ah	
std (#batts,volts,cap)					
external			+12V		+/-12V
Current Drain (milliamps)	125 mA	100 mA	125 mA	60	205
Capacity (days)	4.0	3.5	Supply Dependant	5	
Physical					
Size (LxWxD in cm)	35.6X30.5X20.3	38 X 25 X 18	45X48X30	30X30X15	
Weight (Kg)	20.2	8.6	19	10	
Housing	Std, Steel IP65	Formed ABS Plastic	Rack Mount, Steel	Std, Steel, IP65	Std, Steel, IP65
Operating Temp (C)	OPT, Stainless IP67	W/Remov Battery Pac	Panel (19")	OPT Steel, IP 67	OPT Steel, IP 67
Humidity	-25 to +70 C	-25 to +70 C	-25 to +70 C	-23 to +60C	-30 to 65 C
	100% (Non Condens)	100% (Non Condens)	100% (Non Condens)	Std. Housing 85%	100%
				OPT Housing 100%	
Data Reduction	D,P, DSP, VOL	D,P, DSP, VOL	D,P, DSP, VOL	D,P	D,P
Software Available				DSP,VOL	DSP,VOL
OPTIONAL					
Company Notes	NOTE 1 Bandwidth Selectable in 10 Hz steps 2 Digital filter at 48dB per octave below 70 Hz. 3 1000 sps per channel is digitally filtered 4 With gain range, 90dB at fixed gain				

Table 1

SURVEY OF STRONG MOTION ACCELEROGRAPHS

Page 5

DESIGN FEATURE	TOKYO SOKUSHIN CV - 601	TOKYO SOKUSHIN CV - 701	TOKYO SOKUSHIN CV - 901	TOKYO SOKUSHI SAMTAC-15X	TOKYO SOKUSHIN SPC-35
Price	Y 1,400,000.	Y 1,500,000.	Y 2,200,000.	Y 4,800,000.	Y 2,950,000.
Suitable Applications	N.S.	N.S.	N.S.	3D	M
No. of Channels std	3	3	3	16	3
Optional Sample rate (sps)	100	100	8 50,100,200	50,100,200	6 OR 8 1-1000 (1,2,5 steps)
Dynamic Range (dB)	96	96	96	120	96
Sensor Type	S	S	S	S	S
Internal/External	I	I	I	I	E
Optional	E	E	E	E	
Natural Frequency (Hz)	100	100	100	100	100
Sensitivity (g)	1.02	1.02	1.02	1.02	1.02
Optional	0.5, 2	0.5, 2	0.5, 2	0.5, 2	2
Damping (%critical)	64to70	64to70	64to70	64to70	64to70
Resolution	3X10-5	3X10-5	3X10-5	2X10-6	3x10-5
Bandwidth	DC-47	DC-47	DC-47	DC-50	DC-1/3 sample Hz
Low-pass filter character	-12 Butterworth	-12 Butterworth	-12 Butterworth	-12 Butterworth	-12 Digital filter
Preamplifier (dB)	6	6	6	6	6
Noise (g)	3X10-5	3X10-5	3X10-5	2X10-6	3x10-5
Int. System F Test	O NOTE 1	O NOTE 1	O NOTE 1	N	N
Sensor Interface	SE, 100k, +/-15v,3	SE, 100k, +/-15v,3	SE, 100k, +/-15v,3	SE, 100K, +/-15V,1	SE, 100K, +/-15V,3
External Indicators	P,E,T,O	P,E,T,O	P,E,T,O	P,E,T,O	P,E,T,O
Interconnect	M,S,C,T	M,S,C,T	M,S,C,T	M,S,C,T	M,S,C,T
Trigger Modes character bandwidth range	filtered threshold 0.07-7 0.0002-0.01	filtered threshold 0.07-7 0.0002-0.01	filtered threshold 0.07-7 0.0005-0.1275	filtered threshold 0.07-7 0.0005-0.1275	threshold 0.07-7 0.001-0.5
Pre-event memory (sec) 3 ch, 200 sps	5 (100 sps)	5 (100 sps)	5 - 20 0 - 30	2.5-15 0-30	0-25 0-60
Post-event hold (sec)	54 sec/event	54 sec/event	IC CARD	IC CARD	IC CARD
Recording medium std	IC CARD MAXELL ML-128PC	IC CARD MAXELL ML-256PC	MAXELL ML-1024PC	MAXELL ML-1024	FD, HD
OPTIONAL					
Mem. Backup Battery (type)	Mercury cell	Mercury cell	Mercury cell	Mercury cell	
Recording capacity (min)	128 Kbyte x 2 7.2 (100 sps)	256 Kbytes x 2 14.4 (100 sps) *	1 Mbyte x 4 116 *	1 Mbyte x 4 30 *	16 (F,D), 540(H,D)
OPTIONAL					
Playback hardware	DAC-100	DAC-100	DAC-16X	DAC-15X	
Comm Software					MS. DOS
OPTIONAL					
Retrieval Method	M,O NOTE 2	M,O NOTE 2	M,O NOTE 2	M,O NOTE 2	M,O NOTE 2
OPTIONAL					
Transfer Rate (baud)					
Clock stability standard (accuracy, temperature range)	1x10-6, 0-40C	1x10-6, 0-40C	1X10-6, -10-50C	1X10-6, -10-50C	1x10-6, 0-40C
OPTIONAL	1x10-7, -20-50C	1x10-7, -20-50C	1x10-7, -20-50C	1x10-7, -20-50C	
Synchronization	A	A	A	A	A
optional					
Receivers	O, NHK	O, NHK	O, NHK	O, NHK	O, NHK
Power supply std (#batts, volts, cap)	one, 12v	one, 12v	one, 12v	one, 12v	one 12v DC
external					
Current Drain (milliamps)	100vac, 12vdc 500mA DC	100vac, 12vdc 500mA DC	100vac, 12vdc 700mA DC	100vac, 12vdc 550mA DC	90-240VDC 380mA DC
Capacity (days)	1 hours	1 hours	3 hours		2 hours
Physical Size (LxWxD in cm)	24.7x35x31	24.7x35x31	34x42x27	33X47.5X15.2	33x46x17
Weight (Kg)	16	16	24	8	10
Housing	cast aluminum case	cast aluminum case	cast aluminum case	cast aluminum cas	aluminum attache cas
Operating Temp (C)	-10-50	-10-50	-10-50	-10-50	0-40
Humidity	100%	100%	100%	100%	80%
Data Reduction Software Available	D, P	D, P	D, P	D, P	D, P
OPTIONAL	DSP VOL	DSP VOL	DSP VOL	DSP VOL	DSP VOL
Company Notes		NOTE 1 Calibration Coil NOTE 2 Telemetry Interface			
		* Editorial ability, strong 16 data are selected and saved automatically (NOTE: Strong A for CV-601)			

Applications with preferred features:

A - Autonomous Stations

- Minimum accelerograph with:
 - a. triaxial, orthogonal accelerometer
 - b. discriminating, adjustable trigger
 - c. timing system
 - d. time history recorder
 - e. uninterruptible power supply
 - f. environmental housing

N - Regional Networks

- bandwidth .1 to 30 Hz
- pre-event memory
- trigger range 0.01 to 0.02g
- dynamic range 60dB
- high clock stability
- extended power capacity
- 2g sensors
- common time

D - Dense Surface Arrays, Fixed

- bandwidth .1 to 50 Hz
- dynamic range 120dB
- common time
- 45 min storage capacity
- min preevent memory 2 sec
- smart trigger
- adjustable preamp

3D - Dense 3D Arrays

- as in "D" plus downhole sensor
- borehole package
- means of orientation
- means of recovery
- downhole cabling

M - Mobile Arrays

- as in "D" plus
- very high recording capacity
- common time
- common start
- low size and weight
- ruggedness

S - Structural Arrays

- capability of remote sensors
- capability of more than 3 channels
- bandwidth min .1 to 30Hz
- common start, common time,
- common sampling

Dynamic Range = $DR = 20\log_{10}(x_{max}/x_{min})$

where x_{max} is the maximum instantaneous value of the signal that can be transmitted by the system without distortion

and x_{min} is the minimum detectable value of the signal generated by the transducer at the output display units are dB

Noise = RMS value of background system noise, in g's

Time synchronization

- M - manual, by depressing key or switch
- A - completely automatic, simply feed a time code
- AS - so called "arm and synch"
- AR - set manually, and then advance and retard to synchronize while watching indicator

Time Stability is usually expressed as an accuracy over a temperature range.

NOTE: Generally, feature capacities can be expressed as $x.n$ where x is the maximum value and n is the increment. Example: optional memory expressed as 72.9 means that a maximum capacity of 72 minutes is available in 9 minute steps.

Price

Domestic price for manufacturer's country.
Export prices usually higher to cover warranty, sales costs

External Indicators

- P - AC power applied
- E - event trigger
- T - time indicator
- H - state of health
- O - other, explain below

Accelerograph Interconnect

- M - master start
- S - slave start
- C - common start, any instrument
- T - common time shared by all
- D - common sampling
- O - other, explain

Retrieval Method

- M - remove and replace media (card, cassette)
- H - remove and replace hard disk
- T - transfer binary data
- A - transfer ASCII data
- O - other, explain

Sensor Type

- PE - piezoelectric element
- VC - variable capacitance element
- S - servo
- EMF - electromagnetic feedback

Internal System Functional Test

- SU - step, undamp, Kinematics style
- P - single cal pulse
- O - other, explain below

Sensor interface (External)

- SE - single ended
- D - differential
- ohms input impedance
- power supply available in volts
- number of channels

Recording Capacity: DCx indicates data compression where x is approximate compression ratio

Data Reduction Software

- D - display software, for use with "playback hardware"
- P - waveform printing software
- DSP - digital signal processing software
- VOL - baseline and instrument correction, and double integration software
- I - IASPEI software: SUDS format conversion or compatibility with available IASPEI software
- PIT - PITSA seismic waveform analysis software

Receivers

- G - GPS
- W - WWVB
- M - OMEGA
- E - GOES
- D - DCF77
- J - JJY
- O - other, explain

Table 2

ACCELEROGRAPHS BY APPLICATION

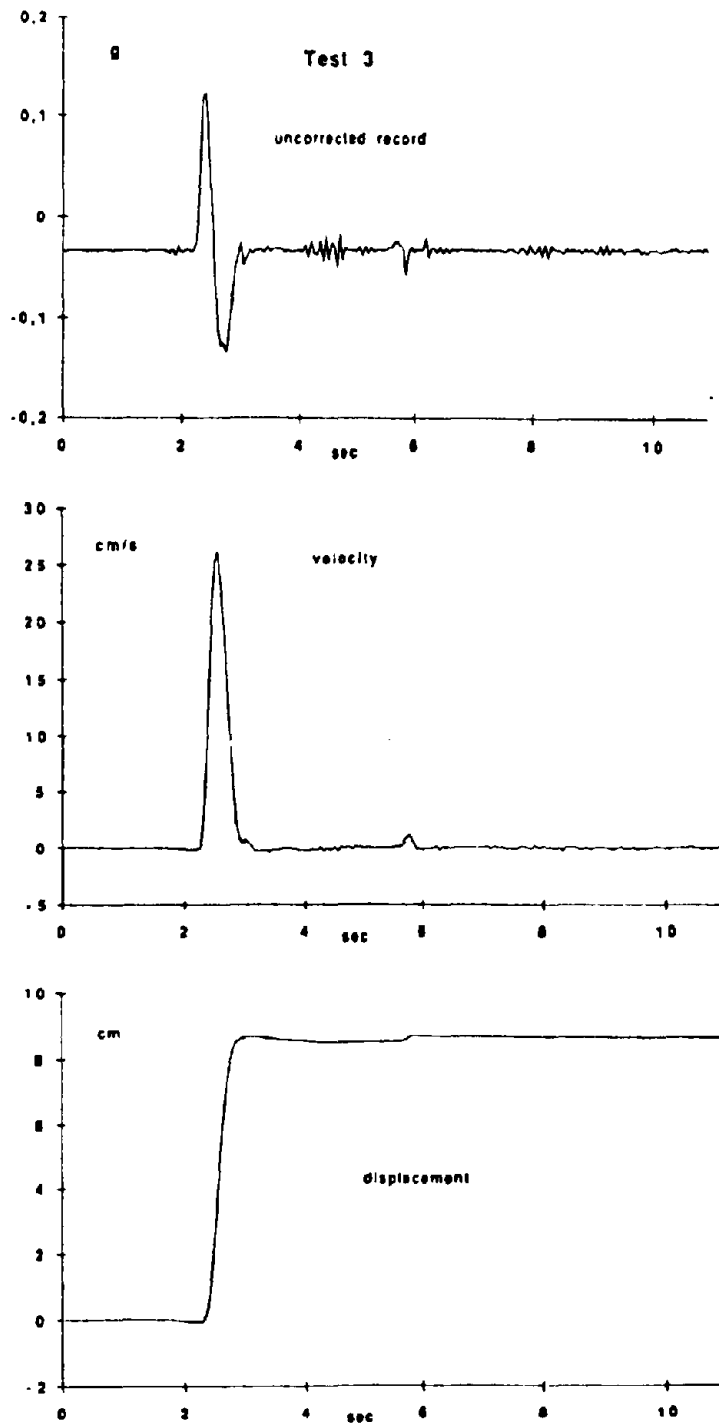
APPLICATION	KINEMATRICS	MARK RAND	OFITECO	REFTEK	SYSKOM	TELEDYNE	TERRATECH	TOKYO SOKUSHIN
Regional Networks	SSA-2,SSA-16, SMA-1	SM-16, ME-16	ACD-3E	72A-06	MR2002	A-800,A-900	IDS-3602S, IDS-3602SX, DCA333R	CV-601, CV-701, CV-901
Dense Surface Arrays	SSA-16,SSR-1	SM-16, ME-16		72A-06			IDS-3602S, -SX	
Dense 3-D Arrays	SSA-16,SSR-1			72A-06			IDS-3602SX	SAMTAC-15X
Mobile Arrays	SSR-1	SM-16, ME-16		72A-06			IDS-3602F	SPC-35
Structural Arrays	SSA-2,SSA-16, SSA-3	SM-16, ME-16	ACD-3E	72A-06	MR2002		IDS-3602D, DCA300R	CV-601, CV-701, CV-901

Table 3

ADVANCES OF MODERN ACCELEROGRAPHS

FEATURE	FILM RECORDER (SMA-1)	DIGITAL ACCELEROGRAPH (SSA-2)
Recorder	Optical	Digital
Recording Media	Film	FLASH memory
Playback	Darkroom	PC compatible
Bandwidth	.1 to 25 Hz	DC to 50 Hz
Dynamic Range	100:1*	2000:1
Capacity	25 min (full magazine)	9 min, expandable to 72 min
Pre-event Memory	-100 milliseconds	0 to 15 sec
Power Supply	single +12VDC supply	single +12VDC supply
Trigger	Verticle, 0.005 to .025g	Triaxial, weighted, .1 to 10% of full scale
Data Retrieval Compatibility	Any darkroom	XMODEM protocol
Phase Between Records	IF Common Time, about +/-20 msec, otherwise none	Interconnect for common sampling
Auto Documentation	None (manual only)	More than 60 parameters automatically recorded
* 1000:1 with digital processing		

Figure 1
SSA-2 DISPLACEMENT EXPERIMENT



Shaking Table Waveform Correction Based on Least Square System Identification

Yin Jianhui

Department of Electrical Engineering
Shanghai Institute of Railway Technology

Bao Zhiwen

Department of Civil Engineering
Tsinghua University, Beijing

ABSTRACT

Dynamic of load analysis for structure models often requires the reappearance of original waveform on shaking table. Traditional waveform correction method is an analogous one. In this paper, a method of reversed system prefiltering based on least square system identification is proposed. An FIR model is used to simulate the system between the signal input point of shaking table and response output point of shaking table. A set of least square equation to be solved for FIR system coefficients can be obtained by minimizing the square error between the measured system output and an estimation from the FIR system output. An efficient algorithmic solution for the normal equations has been developed. If the assumed FIR system is of duration M samples, the solution requires a number of computational operations proportional to M^2 and storage of normal equation coefficients proportional to M . So, it is possible to use a microcomputer to do it.

The results obtained by the method above and those of other waveform correction methods such as sine dwell method, estimation in frequency domain based on Fourier Transform are compared. It is proved that waveform correction method based on least square system identification is effective in dispelling the influence of load mass.

INTRODUCTION

In simulating seismic experiment of structure models, an obvious characteristic is that the model is heavier than the table, even times than the table. Because of the reaction force between model and table, the system feature is seriously influenced. The heavier the load mass is, the narrower the system dynamic range is, especially in a destroyed experiment. It is not available to regard the aluminium table and table diameter as rigid body in great acceleration. This means that the system transfer function is time-varying with model from

elasticity to destroyed. This is the primary factor that accounts for the distortion of shaking table response waveform.

It is necessary to correct the feature of shaking table for the reappearance of original seismic waveform on shaking table. First of all it is to determine the standard of simulating seismic surrounding. Usually, there are two different standards of simulating seismic surrounding.

1. Power Spectral Density (PSD)
2. Seismic Waveform Time-process (SWT)

For the former, the energy distribution of frequencies is considered important. There are many different time-process to corresponding same power spectral density. So, the time-process of waveform is not a sole one.

The latter, also called standard of Fourier Frequency Spectrum, presents seismic waveform time-process with information in frequency domain. The amplitude and the phase of frequency is determined by Fourier Transform's one to one transformation.

Here, we choose the time-process as standard of simulating seismic surrounding.

WAVEFORM CORRECTION METHOD WITH COMPUTER

Fig.1 is an idealized shaking table block diagram. $H(j\omega)$ is the transfer function between the signal input point of shaking table. $x(t)$ is a driving signal. $y(t)$ is response acceleration signal on shaking table. Here, we assume $H(j\omega)$ as linear system and $H(j\omega)$ does not change too much during adjacent test which has close energy level of driving signal. So, we can use the transfer function obtained from the above test to calculate the

Fig.1 Idealized shaking table block diagram

Fig.2 Inversed system pre-filter block diagram

iterative control. If we can get the transfer function $H(j\omega)$ exactly, according to Fig.2 we can expect to get exact original seismic waveform on shaking table. This thought is called reversed system pre-filtering. Because correction is not on-line, the reversed system $H(j\omega)$ must be stabilized and exist. Usually, the way of getting system transfer function as follows:

- * Sine dwell method.
- * Estimation in frequency domain based on Fourier Transform.
- * Parameter estimation and system identification in time domain.

1. Sine dwell method

This method is still widely used in structural dynamic test though it is not sophisticated.

It is noticed that:

(1) Amplitude measurement is preciser than phase measurement due to the error caused by measure instrument and record instrument in phase measurement.

(2) Measurement-system must have property with level amplitude-frequency characteristic and phase-frequency characteristic proportional to frequency.

(3) Driving signal's amplitude must be considered carefully because of the non-linear factors in real system. The system output will saturate when input signal is too big and have nothing when input signal is too small.

2. Estimation in frequency domain based on Fourier Transform.

This kind of method is based on Fourier Transform of structural vibration response random or transient excitation.

The frequency domain analysis methods suffer from two primary sources of error, excluding any non-linear response effects. These are the signal-to-noise (SNR) error or dynamic range error and the smoothing error rate. The signal-to-noise rate error is statistical in nature and can be reduced by averaging the analyzed data over a number of ensembles. So, this method can obtain transfer function in low SNR. The smoothing, resolution, however, dependent on the modal parameter of model such as the resonent frequency and modal damping. For a time interval, the finite length data samples are, generally, nonperiodic. Leakage is introduced into the structural response spectrum when the periodic Fourier Transform is used to analyze such nonperiodic data. All kinds of smoothing functions can be used to suppress the spurious side lobes but only at the expense of increasing the resolution error.

So far as the transfer function $H(j\omega)$ is concerned, low-as-possible resolution error is required. For this purpose, long length data samples is often required because low frequency component is the main component in seismic wave. Sometimes, it is not easy to do. The precise of $H(j\omega)$ is determined by:

- 1) The number of averaged ensembles
- 2) The SNR in measurement.

It is noticed that the error of the number near zero in Fourier frequency spectrum of input signal will cause an error in $H(j\omega)$, even make $H(j\omega)$ false. The frequency response function $H(j\omega)$ which is not smoothed or is smoothed well will cause a spurious sine component in impulse response function $h(t)$.

The results of computer simulation and real seismic experiment by this kind of method is given in Fig.4 to Fig.5.

3. Parameter estimation and system identification

Fig.3 is a block diagram of a finite impulse response (FIR) system identification model.

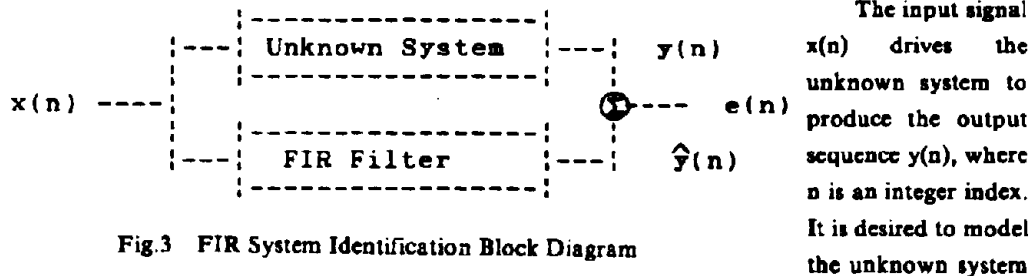


Fig.3 FIR System Identification Block Diagram

as an FIR filter, assumed to be of duration $M+1$ samples. So that impulse response $h(n) = 0$ for $n < 0$ and $n > M$. If the unknown system is actually an FIR system, then the modeling procedures provided here can be exact. If the unknown system is not an FIR filter, the order of the FIR filter model is chosen to make a reasonable approximation of the unknown system. The order of FIR system is defined here as the highest index for which $h(n) \neq 0$. For the case above, the order is M .

The approach used here is to determine the coefficients $h(n)$ of the FIR system model and the order M that:

- 1) minimize the mean square error (MMSE) between $y(n)$ and FIR filter output $\hat{y}(n)$ in the case of known statistics for the process $x(n)$ and $y(n)$, or by that:
- 2) produce the least square error (LSE) in the case when only a finite number of measurements of $x(n)$ and $y(n)$ is available.

The latter case is the one of primary interest. An efficient recursive algorithm is available when the autocorrelation and cross correlation functions of process $x(n)$ and $y(n)$ are known. The algorithm is based on the Toeplitz structure of the matrix equation solution [6]. The least square solution produces a matrix equation similar in structure to the Wiener solution; However, the matrix in this case is not toplice. But, the least square matrix equation has additional structure that can be exploited to yield an efficient recursive algorithm, which incorporates the fact that the solution to the FIR system identification problem can be embedded in the solution of the linear prediction problem for which an efficient solution has already been developed [3][4][5].

Compared with the classical least square system identification which requires a number of computational operations proportional to M and storage of normal equation coefficients proportional to M , the algorithm in our test requires a number of computational operations proportional to M and storage of normal equation coefficients proportional to M . Thus, this makes it possible to use microcomputer to do it.

COMPUTER NUMERICAL SIMULATION AND EXPERIMENT

1. Computer Numerical Simulation

A quadratic difference equation simulation was run using waveform correction methods based on least square system identification and based on estimation in frequency domain. The difference equation as follows:

$$y(n) - 1.5y(n-1) + 0.7y(n-2) = x(n-1) + 0.5x(n-2) + e(n) \quad (3-1)$$

where

$x(n)$ is excitation sequence (El-centro NS wave or White noise).

$y(n)$ is model response sequence.

$e(n)$ is normal distribution white noise with mean 0 and variance σ . σ can be adjusted.

$e(n)$ is generated by formulation follow:

$$e(n) = \sigma \left\{ \sum_{k=1}^{12} w(k) - 6 \right\} \quad (3-2)$$

where

$w(k)$ is uniform (0,1) distribution random number generated by computer internal function.

The simulation results are given in Fig.1 to Fig.5.

From table 1 and table 2, we can see that the method based on least square system identification is stronger than method based on Fourier transform in bearing noise.

2. Experiment

We have made waveform correction experiment for offshore platform with a 1500kg force electromagnet excitation shaking table. The excitation signal is El-centro NS wave and Mexico seismic wave. The waveform incorrected and waveform corrected by least square system identification are given in Fig.6 to Fig.8.

It has been proved through the simulating seismic experiment of structural model that the method based on least square system identification is effective in dispelling the influence of load mass.

DISCUSSION ON FIR SYSTEM ORDER M

In computer simulation, the model order M is known. But in real model experiment, the system order is unknown. We choose an FIR filter model to make a reasonable approximation of the real system. Theoretically, we can define the highest index for which $h(n) \neq 0$ as system order. Actually there is not $h(n) = 0$ due to exist of noise. The accuracy of system order M is associated with the accuracy of waveform. A method is effective in determining the real system order. That is to check the energy of least square error (LSE) between real output measurements and output of FIR model with order M . LSE is monotone decreasing as order M rises (See Fig.9). When model order M is greater than the order of real system, LSE drops slowly. This phenomenon can be used to determine the real system order directly. But this method requires enormous computational operations because it is not recursive. The better method is to judge the model order M with certain criterion in

recursive. When optimal order M_{opt} is reached, recursive process ends. There are two kinds of common criterions as follows:

1. Final Predictions Error Criterion (FPE)

For an model with order M

$$FPE(m) = \frac{N + M - 1}{N - M - 1} P(m) \quad (4 - 1)$$

Where N is data samples. $P(m)$ is to mean square error at order M . M_{opt} is the M which makes $FPE(m)$ reach minimize.

2. Information Theoretic Criterion (AIC)

$$AIC(m) = \frac{2m}{N} + \ln P(m) \quad (4 - 2)$$

It can be proved:

$$\lim_{N \rightarrow \infty} \{\ln FPE(m)\} = AIC(m) \quad (4 - 3)$$

Applying the above criterions to real model experiment, the M_{opt} obtained by FPE is near or equal to the M_{opt} obtained by AIC. Both M_{opt} s are greater than the M_{opt} obtained by LSE.

CONCLUSION

In conclusion, the waveform correction method based on least square system identification identifies the weight sequence of structural model based on its physics property. It has the advantage of directness and preciseness. This method is effective in dispelling the influence of load mass.

Compared with the method of estimation in frequency domain based on Fourier Transform (FFTM), the method based on least square system identification (ELSM) can be obtained $H(j\omega)$ in lower SNR than the former. Impulse error in measurement has no effect on ELSM but obviously on FFTM. ELSM is stronger than FFTM in bearing numerical error and provide a flag quantity to determine the real system order accurately.

Table 1 Noise-Level, Model Order, Error Energy in ELSM Method

noise level	model order	estimation error energy
$\sigma = 0.0$	$m = 24$	0.E+00
$\sigma = 0.1$	$m = 24$	1.16222E-07
$\sigma = 0.5$	$m = 24$	5.43071E-07
$\sigma = 1.0$	$m = 24$	1.95163E-06
$\sigma = 5.0$	$m = 100$	2.45788E-02

Table 2 Noise-Level, Model Order, Error Energy in FFTM Method

noise level	model order	estimation error energy
$\sigma = 0.0$	m = 100	3.3533E-02
$\sigma = 0.1$	m = 100	4.80504E-02
$\sigma = 0.5$	m = 100	0.21671
$\sigma = 1.0$	m = 100	0.676411
$\sigma = 5.0$	m = 100	14.31

REFERENCES

- (1) Huan Haohua, Xu Wende, Shong Xueyun "Seismic Simulating Shaking Table Controlled by Acceleration Signal" The RP of Academy of Sciences of China, Feb 1982.
- (2) Lu Yongcan, Gao Yiming, Zhang Weilin: Microcomputer Iterative Control Application in Shaking Table Earthquake and Vibration September 1985.
- (3) L.D.T.Morf, Friedlander: Recursive Least Squares Latter Estimation Algorithm IEEE CAS-28 n6 Jun 1981.
- (4) Marple.J.R "Efficient Least Square FIR System Identification" IEEE ASSP-29 Feb 1981.
- (5) Marple.J.R "Fast Algorithm for Linear Prediction and System Identification Filter with Linear Phase" IEEE ASSP-30 Dec 1982.
- (6) B.Porat and T.Kaikth "Normalized Lattice Algorithm for Least Square FIR System Identification" IEEE ASSP-31 Feb 1983.
- (7) Coppolino, R.N. "A Simultaneous Frequency Domain Technique for Estimation of Modal Parameters for Measured Data" SAE 811046, October 1981.
- (8) Ibrahim, S.R. and E.C.Mikulick "A Method for the Direct Identification of Vibration Parameters from the Free Response" Shock and Vibration Bulltin, Bulltin 47, Part 4 September 1977 pp183-198.
- (9) Vold, H., et al., "A Muti-input Modal Estimation Algorithm for Mini-Computers" SAE 820194, February 1982.
- (10) Hunt, D.L., J.Matthews, R.Willams "An Automated Tuning and Data Collection System for Sine Dwell Modal Testing" AIAA 25th Structural Dynamics, and Materials Conference, May 1984.

BIBLIOGRAPHY

Yin Jianhui born in Hunan, China in 1964. He received B.S degree of Automation Engineering and M.S degree of Civil Engineering in Tsinghua University, Beijing, 1985, 1988 respectively. His current research interests are

structural dynamic testing & analysis, computer control system, digital signal processing.

Bao Zhiwen born in Shanghai, China. She graduated from Tsinghua University, Beijing in 1962. Now she has been employed in RISE (Research Institute of Structural Engineering), Tsinghua University. She has been engaged in the study of safety inspection and parameter evaluation of structures, measurement and analysis of dynamic characteristics of high-rise building and other structures, vibration tests of prototype and model structures, technique of shaking table tests and data processing, pseudo-dynamic tests.

Fig.1 The Time-Process of $h(t)$ for Equation 3-1 by ELSM Method and FFTM method

Fig.2 The FFTM Simulation Result for Equation 3-1 by Exciting of El-Centro NS Wave ($\sigma = 1.0$)

Fig.3 The FFTM Simulation Result for Equation 3-1 by Exciting of El-Centro NS Wave ($\sigma = 5.0$)

Fig.4 The ELSM Simulation Result for Equation 3-1 by Exciting of El-Centro NS Wave ($\sigma = 1.0$)

Fig.5 The ELSM Simulation Result for Equation 3-1 by Exciting of El-Centro NS Wave ($\sigma = 5.0$)

Fig.6 The Waveform in Experiment (Uncorrected) by Exciting of El-Centro NS Wave

Fig.7 The Waveform in Experiment (Corrected) by Exciting of El-Centro NS Wave

Fig.8 The Waveform in Experiment (Corrected) by Exciting of Mexico EW Wave

Fig.9 The Relationship of Error Energy P and Model Order M (El-Centro Exciting)

FFTM in bearing numerical error and provide a flag quantity to determine the real system order accurately.

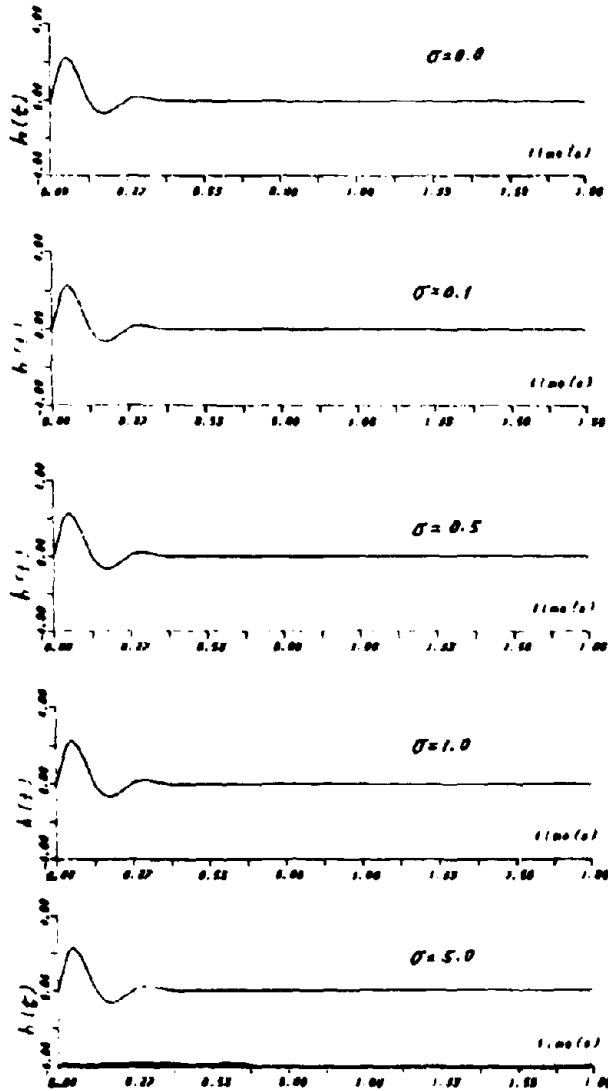
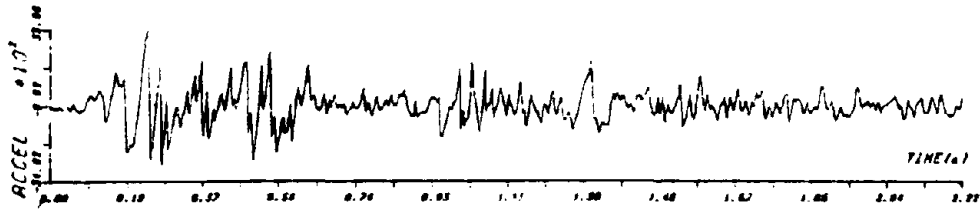
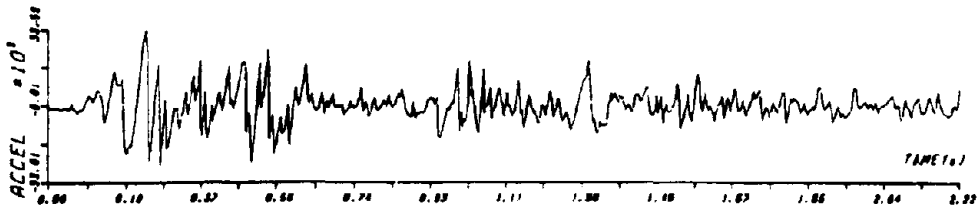


Fig. 1 The Time-Process of $h(t)$ for Equation 3-1 by ELSM Method and FFTM method



Model Seismic Input Waveform Time-Process

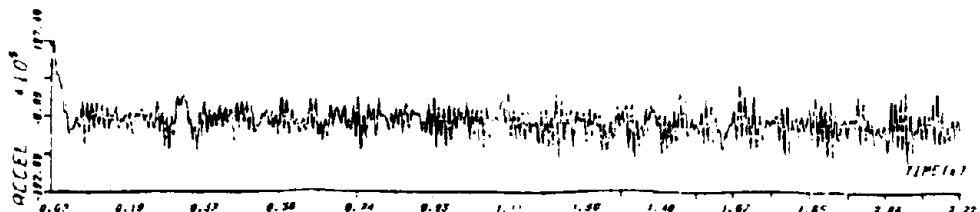


Corrected Waveform Time-Process (Simulation)

Fig. 2 The FFTM Simulation Result for Equation 3-1 by Exciting of El-Centro NS Wave ($\sigma=1.0$)

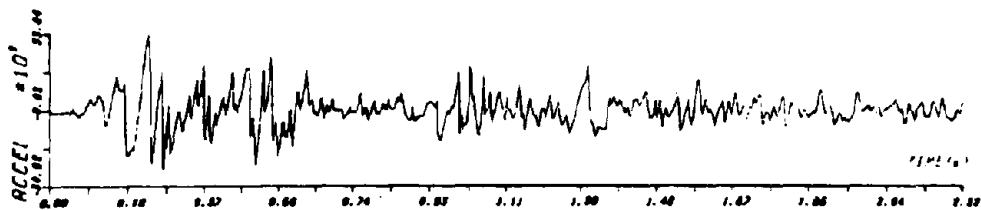


Model Seismic Input Waveform Time-Process



Corrected waveform Time-Process (Simulation)

Fig. 3 The FFTM Simulation Result for Equation 3-1 by Exciting of El-Centro NS Wave ($\sigma=5.0$)

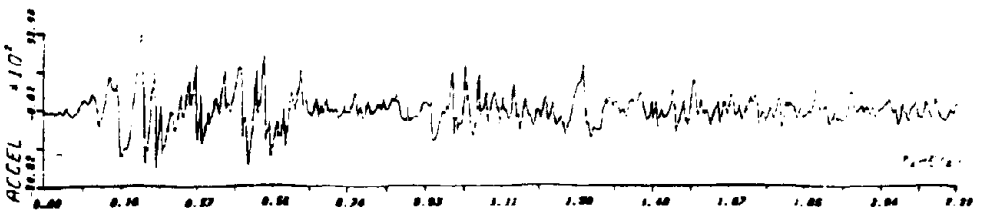


Model Input Seismic Waveform Time-Process

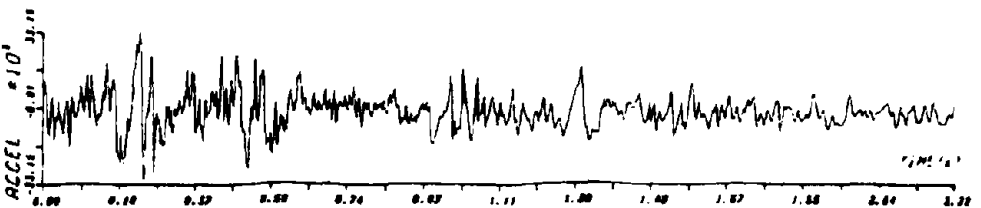


Corrected Seismic Time-Process (Simulation)

Fig. 4 The ELSM Simulation Result for Equation 3-1 by Exciting of El-Centro NS Wave ($\sigma=1.0$)

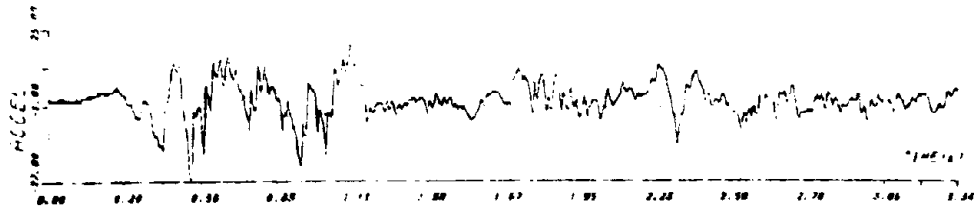


Model Input Seismic Waveform Time-Process



Corrected Seismic Time-Process (Simulation)

Fig. 5 The ELSM Simulation Result for Equation 3-1 by Exciting of El-Centro NS Wave ($\sigma=5.0$)

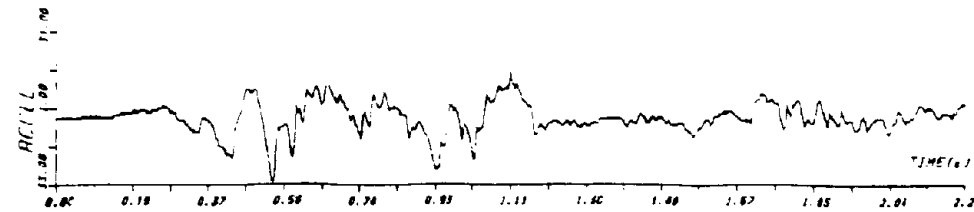


Shocker Table Input Waveform Time-Process

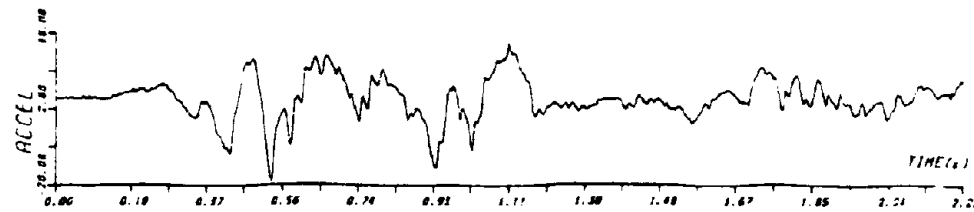


Response Time-Process on Shocker Table.

Fig. 6 The Waveform in Experiment (Uncorrected) by Exciting of EL-Centro NS Wave

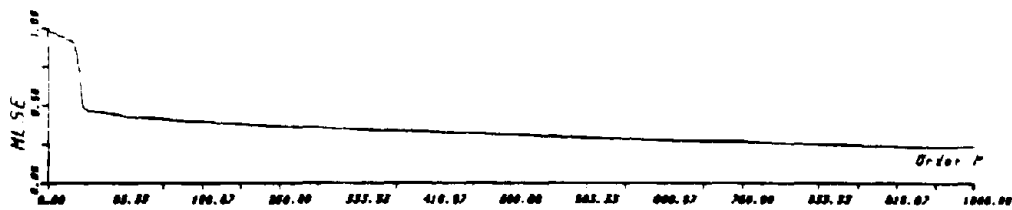


Shocker Input Seismic Waveform Time-Process

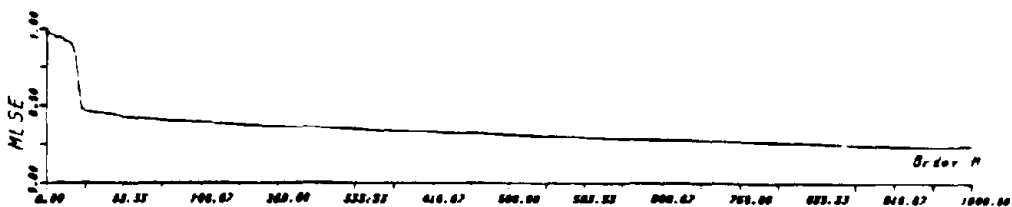


Corrected Waveform Time-Process (Experiment)

Fig. 7 The Waveform in Experiment (Corrected) by Exciting of EL-Centro NS Wave



The Minimum Least Squares Error Curve



The Minimum Least Squares Error Curve

Fig. 8 The Relationship of Error Energy P and Model Order M (EL-Centro Exciting)

noise level	model order	estimation error energy
$\sigma = 0.0$	m=24	0.E+00
$\sigma = 0.1$	m=24	1.16222E-07
$\sigma = 0.5$	m=24	5.43071E-07
$\sigma = 1.0$	m=24	1.95163E-06
$\sigma = 5.0$	m=100	2.45788E-02

Table 1 Noise-Level, Model Order, Error Energy in ELSM Method

noise level	model order	estimation error energy
$\sigma = 0.0$	m=100	3.3533E-02
$\sigma = 0.1$	m=100	4.80504E-02
$\sigma = 0.5$	m=100	0.21671
$\sigma = 1.0$	m=100	0.676411
$\sigma = 5.0$	m=100	14.31

Table 2 Noise-Level, Model Order, Error Energy in FFTM Method

The Parameter Identification of Seven Story Building Model made of CSGCB

Zhao Wei*

SUMMARY

The buildings made of coal-slag-gas-concrete block (CSGCB) have been built up in some cities in China, and will be built expansively. One of important problems is the dynamic characteristics of this kind of structure. A earthquake simulation testing was made for the building model with 1/6 scale ratio. The basic principle of physical parameters identification and estimated results are introduced in this paper.

INTRODUCTION

The coal slag is trash of power station, it can be used to make coal slag gas concrete block which has a good feature of heat isolation and light weighting. One of important problems is the ability of resistant earthquake for the buildings made of CSGCB. A earthquake simulation testing of building model whose scale ratio is 1/6 was made on a 5"×5" shaking table to study its dynamic characteristics. The model structure is shown in Fig.1.1, and Fig.1.2. The direction of input excitation is coincided with short axis of building model. The model is made of reinconcrete column and CSGCB. The mass of each DOF is assumed to be known and the model is considered as shear building

*professor, Institute of Engineering Mechanics SSB, China

when we identify the model parameters.

Many testings were made, but only a few groups of typical data were taken for parameter identification under condition of basement input motion. The direct fitting method of physical parameter identification are used in the paper.

PARAMETER IDENTIFICATION PROCEDURE

The building model is considered as a system with seven DOF, when we study the dynamic characteristics of model structure. Its equation of motion is that

$$M\ddot{X} + C\dot{X} + R(x, \beta; t) = -M\ddot{X}_b \quad (2.1)$$

where M and C are mass and damping matrix respectively. The mass matrix is a diagonal. Each diagonal element corresponds with the summation of corresponding roof mass, auxiliary lead block mass and the mass of wall and column. 1 is a unit vector. The spring restoring force $R(x, \beta; t)$ is a function of relative displacement between two stories, model parameters and time. If the restoring force model is linear, then

$$R(x, \beta; t) = kx \quad (2.2)$$

where k is stiffness matrix, x is a displacement vector, \ddot{X}_b is basement input acceleration. The mass matrix is presumed to be known, damping matrix can be expressed as Rayleigh damping

$$C = aM + b k \quad (2.3)$$

The constants a and b may be given by following expression''

$$\xi_i = \frac{a+b\omega_i^2}{2\omega_i} \quad i=1,2 \quad (2.4)$$

The damping factors ξ_1 and ξ_2 can be obtained from modal testing. The parameter estimated is the model parameter vector β of restoring force.

The mathematical model which describes the relationship between input and output is expressed in Eq.(2.1). The responses of structure would be determined by solving a equation system when the parameters of system and force applied on the structure are known. The main problem of identification is to give the restoring force model and its parameters. Suppose that absolute displacement $y_i = x_i + x_0$. Eq.(2.1) may be given in following form

$$\begin{aligned} m_n \ddot{y}_n + c_n (\dot{y}_n - \dot{y}_{n-1}) + G_n (y_n, y_{n-1}; \beta) &= 0 \\ m_{n-1} \ddot{y}_{n-1} + c_{n-1} (\dot{y}_{n-1} - \dot{y}_{n-2}) + G_{n-1} (y_{n-1}, y_{n-2}; \beta) \\ &\quad - C_n (\dot{y}_n - \dot{y}_{n-1}) - G_n (y_n, y_n; \beta) = 0 \\ \dots \dots \\ m_1 \ddot{y}_1 + c_1 (\dot{y}_1 - \dot{y}_0) + G_1 (y_1, y_0; \beta) \\ &\quad - C_1 (\dot{y}_1 - \dot{y}_0) - G_1 (y_1, y_1; \beta) = 0 \\ m_0 \ddot{y}_0 + c_0 (\dot{y}_0 - \dot{y}_0) + G_0 (y_0, y_0; \beta) \\ &\quad - C_0 (\dot{y}_0 - \dot{y}_0) - G_0 (y_0, y_0; \beta) = 0 \end{aligned} \quad (2.5)$$

It can be given from Eq.(2.5)

$$m_i \ddot{y}_i + C_i (\dot{y}_i - \dot{y}_{i-1}) + G_i (y_i, y_{i-1}; \beta) = - \sum_{\substack{l=i+1 \\ l \neq N}}^N m_l \ddot{y}_l \quad (2.6)$$

in which m_i and C_i are mass and damping factor of i^{th} DOF, respectively. y_i , \dot{y}_i and \ddot{y}_i are absolute displacement, velocity and acceleration of i^{th} roof, respectively. $i=0$ means basement motion. The spring restoring force $G_i (y_i, y_{i-1}; \beta)$ is a function of relative displacement

and model parameter vector β . For a linear system, the spring restoring force is that

$$G_i(y_i, y_{i-1}; \beta) = k_i \Delta y_i \quad (2.7)$$

where $\Delta y_i = y_i - y_{i-1}$ is relative displacement between two stories, k_i is the stiffness of i^{th} DOF.

If a system is described by a bilinear model, the model parameter vector β is expressed as

$$\beta = (S_i, RT, S_p, S_r)^T \quad (2.8)$$

in which S_i = initial stiffness

RT = yield force

S_p = hardening stiffness

S_r = retrograde stiffness

The elements of parameter vector β are quite different for different models of restoring force.

Suppose that the mass m_i ($i=1, 2, \dots, N$) is already known, then Eq. (2.6) can be expressed as

$$G_i(y_i, y_{i-1}; \beta) = - \sum_{i=1}^N m_i \ddot{y}_i - C_i (\dot{y}_i - \dot{y}_{i-1}) \quad (2.9)$$

Assuming $C_i = 0$, then the relationship between relative displacement and restoring force may be displayed on a coordinate plane. The model parameters can be estimated by curve fitting method. The natural frequencies would be computed from estimated parameters. The damping matrix is obtained from Eq. (2.3) and damping factors ξ_1 and ξ_2 which were given by modal testing. Therefore the nearly corresponding damping C_i ($i=1, 2, \dots, N$) is obtained, then the spring restoring force considered the effect of damping force is given. Above iterative process is

repeated until the satisfactory result is met.

In fact, each element of Rayleigh damping matrix does not precisely correspond to the damping factor of each DOF. In order to consider the effect of damping force on the estimation parameters, Eq.(2.5) can be expressed as

$$\begin{aligned}
 G_n(y_n, y_{n-1}; \beta) &= -m_n \ddot{y}_n - D_n(t) \\
 G_{n-1}(y_{n-1}, y_{n-2}; \beta) &= G_n(y_n, y_{n-1}; \beta) \\
 &= -m_{n-1} \ddot{y}_{n-1} - D_{n-1}(t) + D_n(t) \\
 \dots \dots \\
 G_2(y_2, y_1; \beta) &= G_3(y_3, y_2; \beta) \\
 &= -m_2 \ddot{y}_2 - D_2(t) + D_3(t) \\
 G_1(y_1, y_0; \beta) &= G_2(y_2, y_1; \beta) \\
 &= -m_1 \ddot{y}_1 - D_1(t) + D_2(t)
 \end{aligned} \tag{2.10}$$

Eq.(2.10) can be expressed as following matrix

$$G = -M\ddot{Y} - D \tag{2.11}$$

where

$$\begin{aligned}
 G &= \begin{vmatrix} G_n \\ G_{n-1} - G_n \\ \dots \dots \\ G_2 - G_3 \end{vmatrix} \\
 D &= \begin{vmatrix} D_n \\ D_{n-1} - D_n \\ : \\ D_2 - D_3 \end{vmatrix} = C\dot{X} \\
 \ddot{Y} &= \begin{vmatrix} \ddot{y}_n \\ \ddot{y}_{n-1} \\ : \\ \ddot{y}_1 \end{vmatrix}
 \end{aligned} \tag{2.12}$$

in which

$$X = \ddot{y} - \ddot{y}_g \quad (2.13)$$

The spring restoring force considered the effect of damping force is given by solving Eq.(2.11)

It is convenient to show the model type of restoring force by displaying the relationship between relative displacement and restoring force on a coordinate plane. It is easy to give the model parameters of model by curve fitting. This is a simple and obvious identification method.

THE RESULTS OF PARAMETER IDENTIFICATION

For the system with seven DOF, the mass of each DOF is as following

$$\begin{aligned} m_i &= 2.2745 \text{ kg} \cdot \text{s}^2 / \text{cm} & i=1, 2, \dots, 6 \\ m_7 &= 1.825 \text{ kg} \cdot \text{s}^2 / \text{cm} \\ \xi_{1,2} &= 0.03 \quad \text{and} \quad \xi_{3,4} = 0.02 \end{aligned}$$

The excitation of shaking table is Ning He earthquake. The identification of building model will be given for different input excitations.

The maximum values of base acceleration are 57.8gal, 132.8gal, 240.6 gal and 498.6gal, respectively. The relationship between relative displacement and restoring force may be gotten and the model parameters would be obtained from it. The the relationship between relative displacement and restoring force is shown on a coordinate plane, the math model of restoring force is taken as

$$F = f(DL, \beta) \quad (3.1)$$

For linear system

$$F = S \cdot DL$$

in which F is restoring force, β is model parameter vector. DL is relative displacement. The objective function is defined as

$$J(\beta, T) = \int_{t_1}^{t_2} [G(t) - f(DL, \beta)] W [G(t) - f(DL, \beta)] dt \quad (3.2)$$

where W is a weight function. The optimal estimator β^* can be given by minimizing the objective function by Powell method. In order to check the reliability of identified parameters, after the responses of building model is computed by Wilson- θ method, comparing it with measured response should be made

The identification results are shown in table 3.1. It can be seen that the effect of damping force on estimation parameters can be neglected. The comparison of results measured and computed from identified parameters is presented in table 3.2.

CONCLUSION

The identification results will be discussed in this chapter to give a proper explanation.

4.1 Stiffness Between Stories

The stiffness between stories is an important problem for investigation of earthquake resistance of structure. A lot of mechanics property tests for wall block, beam and column has been made. But the special attention is paid to how to calculate the stiffness of structure made of wall and column. The stiffness can be identified by measured data from earthquake simulation testing of model structure. It can be seen from table 3.1 that the stiffness is the greatest for 1st story, greater for 2nd story, nearly same stiffness for 3rd, 4th and 5th

story, less for 6th story and least for 7th story. The reason is that the walls and columns of low story are subjected to more pressure. Besides, the roofs of high stories would be shaken, which makes model structure far from the assumption of shear building, the end condition of column and wall is not fixed completely, so that the stiffness is certainly descended.

The small crack on the wall at 1st and 2nd story occurred when the maximum value of basement acceleration is 132.2 gal, but stiffness between stories is not changed obviously. Its natural frequencies are not obviously changed. More cracks took place when the maximum value of basement acceleration is 240.6 gal. The result of parameter identification shows that the stiffness of 1st and 2nd story is changed lightly and is not changed for other story, the natural frequency of first mode is descended by 7%.

When the maximum value of basement acceleration is 498.6 gal, except the 7th story, the stiffness is obviously descended for other stories, specially for 2nd story. The first natural frequency is descended by 35%.

4.2 The Description of Nontlinear State

Identifying stiffness of stories, the fitting curve of restoring force is taken as

$$F = S \cdot DL \quad (4.1)$$

The integrating range of objective function is taken as $t_1 = 3.66$ sec. and $t_2 = 5.05$ sec. The maximum values of restoring force and relative displacement occur in this range. The average stiffness in this range is given by minimization of objective function. Typical relationship of relative displacement vs restoring force and estimated results are shown in Fig. 4.1.

When basement acceleration is increased, the relationship between restoring force and relative displacement is obvious nonlinear for

1st, 2nd and 3rd story, but still linear for other story.

The relationship between restoring force and relative displacement in the range of maximum restoring force is shown in Fig.4.2 for 1st and 2nd story, it is hysteretic curve likely. The stiffness of each segment is displayed and remarked on the figures. The fitting model is taken as

$$F = C + S DL \quad (4.2)$$

Its stiffness of equivalent linearization is presented in table 4.1-1.

The relationship between restoring force and relative displacement in the range of maximum relative displacement is shown in Fig 4.3 for 1st and 2nd story. The hysteretic curve is much like a relationship of force and deformation of plastic hinge of reinforced concrete components.

The fitting results are presented in table 4.1-2. There are one or two segments of negative stiffness, it shows that the damage occurs in this range.

ACKNOWLEDGEMENT

This study was supported by National Natural Science Foundation of China, thanks are given to NNSF and Professor Xia Jingqian for her helps.

References

- [1] N.E. Agabin, Bull of Int. Insti. Seismol. and Earth. Engr. Vol.8, 1971.
- [2] Zhao Wei, J. of Vibration Engineering Vol.1, No.4 Nov. 1988. (in Chinese).

table 3.1 Identified stiffness(kg/cm)between stories

position	57.8gal		132.8gal	240.6gal	498.6gal
	damping	No damping			
1	196744.4	392970.6	407830.4	376119.3	166854.3
2	349712.5	346840.0	333679.4	305896.6	100166.8
3	244329.8	242824.9	241860.4	236127.5	108260.3
4	258310.0	256399.5	261939.5	262791.4	138855.9
5	250535.6	249065.6	241389.5	227124.4	132094.3
6	205823.3	203813.0	198154.3	218121.2	115047.3
7	111500.2	111157.0	107046.2	138186.2	127742.7

table 3.2 Comparison of maximum relative displacement(cm)

Position	57.8gal		132.8gal		240.6gal	
	measured	computed	measured	computed	measured	computed
1	0.00215	0.00290	0.00539	0.00616	0.0128	0.0115
2	0.00264	0.00316	0.00633	0.00702	0.0139	0.0124
3	0.00315	0.00364	0.00764	0.00874	0.0151	0.0133
4	0.00215	0.00265	0.00612	0.00730	0.0106	0.0096
5	0.00227	0.00287	0.00508	0.00601	0.0083	0.0089
6	0.00227	0.00252	0.00386	0.00424	0.0059	0.0071
7	0.00116	0.00153	0.00228	0.00318	0.0041	0.0052

table 4.1-1 estimated parameters

position	S_1	S_2	S_3	S_4	S_5
1 st story	223167.2	242304.4	245270.8	113486.8	243823.4
2 nd story	155501.6	164842.8	146920.3	70942.6	144324.6

table 4.1-2 estimated parameters

position	S_1	S_2	S_3	S_4	S_5	S_6
1 st story	227884.5	-282685.5	126079.9	584791.0	87902.9	195737.9
2 nd story	13917.1	-136868.1	36539.9	111825.9	558701.6	123478.5

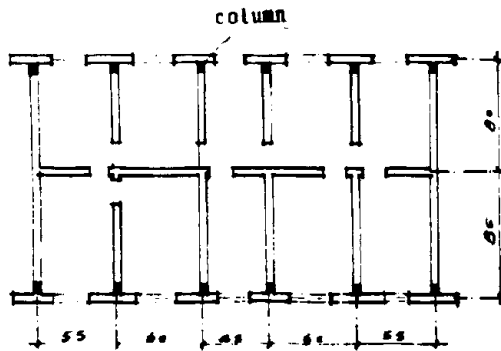


Fig. 1.1 Model structure plane 1,30

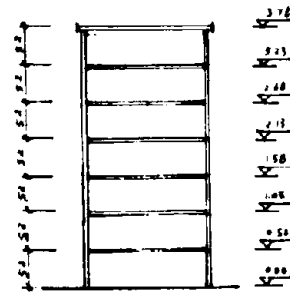


Fig. 1.2 Model structure section 1,60

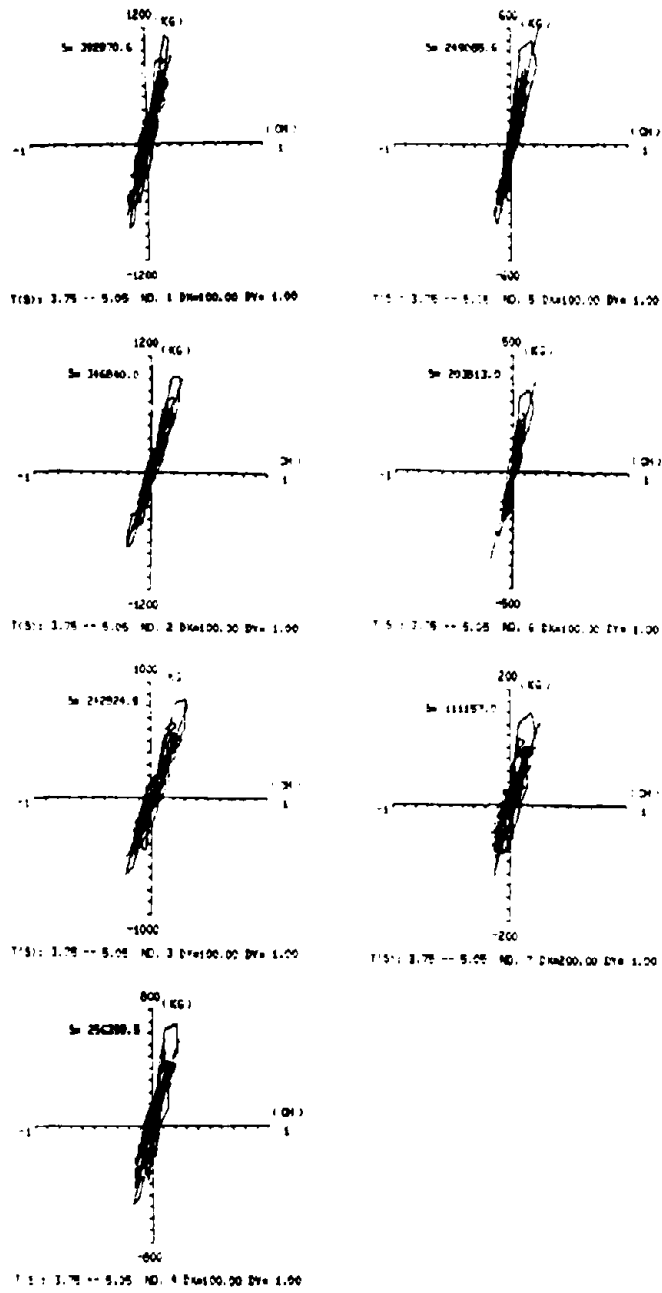
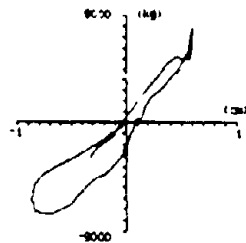
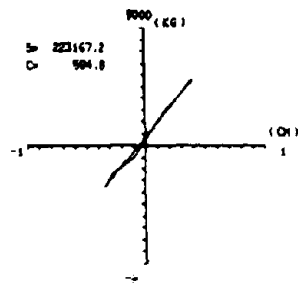


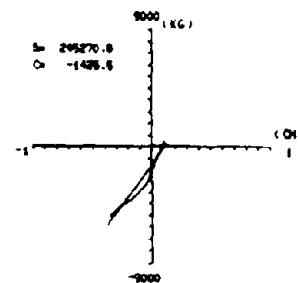
Fig. 4.1 relative displacement vs restoring force



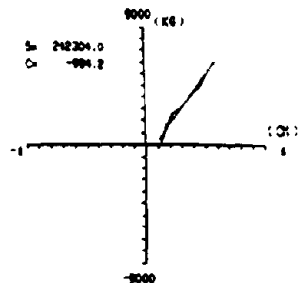
T(5): 3.78 -- 4.22 ND. 1 DM= 20.0 DY=1.000



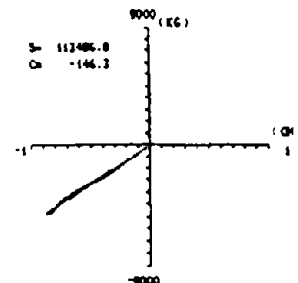
T(5): 3.78 -- 3.84 ND. 1 DM= 20.00 DY= 1.00



T(5): 4.07 -- 4.12 ND. 1 DM= 20.00 DY= 1.00



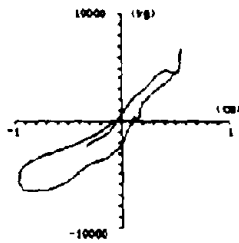
T(5): 3.93 -- 4.06 ND. 1 DM= 20.00 DY= 1.00



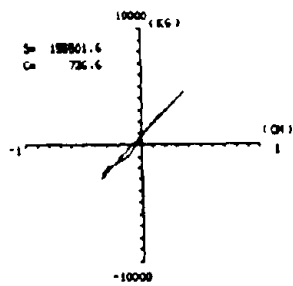
T(5): 4.17 -- 4.22 ND. 1 DM= 20.00 DY= 1.00

· 97 ·

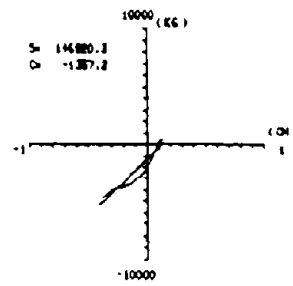
Fig.4.2-1 Maximum restoring force segment for 1st story



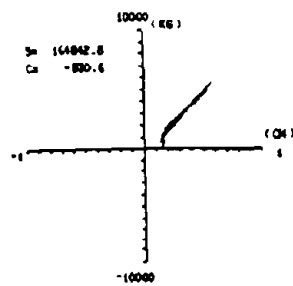
T(S): 3.78 -- 4.22 NO. 2 DX= 15.0 DY=1.000



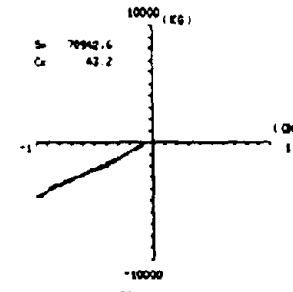
S= 189501.6
C= 726.6
T(S): 3.78 -- 3.84 NO. 2 DX= 15.00 DY= 1.00



S= 145880.3
C= -1.877.2
T(S): 4.07 -- 4.12 NO. 2 DX= 15.00 DY= 1.00



S= 164842.8
C= -830.6
T(S): 3.82 -- 4.06 NO. 2 DX= 15.00 DY= 1.00



S= 70942.6
C= 42.2
T(S): 4.17 -- 4.22 NO. 2 DX= 15.00 DY= 1.00

Fig.4.2-2 Maximum restoring force segment for 2nd story

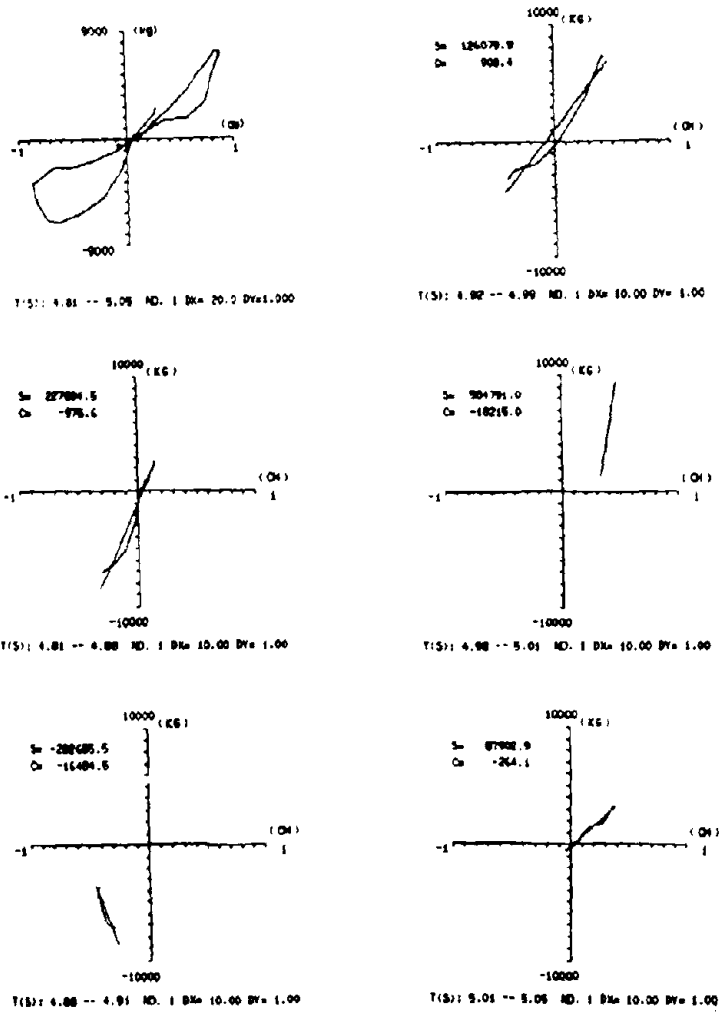


Fig.4.3-1 Maximum restive displacement segment for 1st story

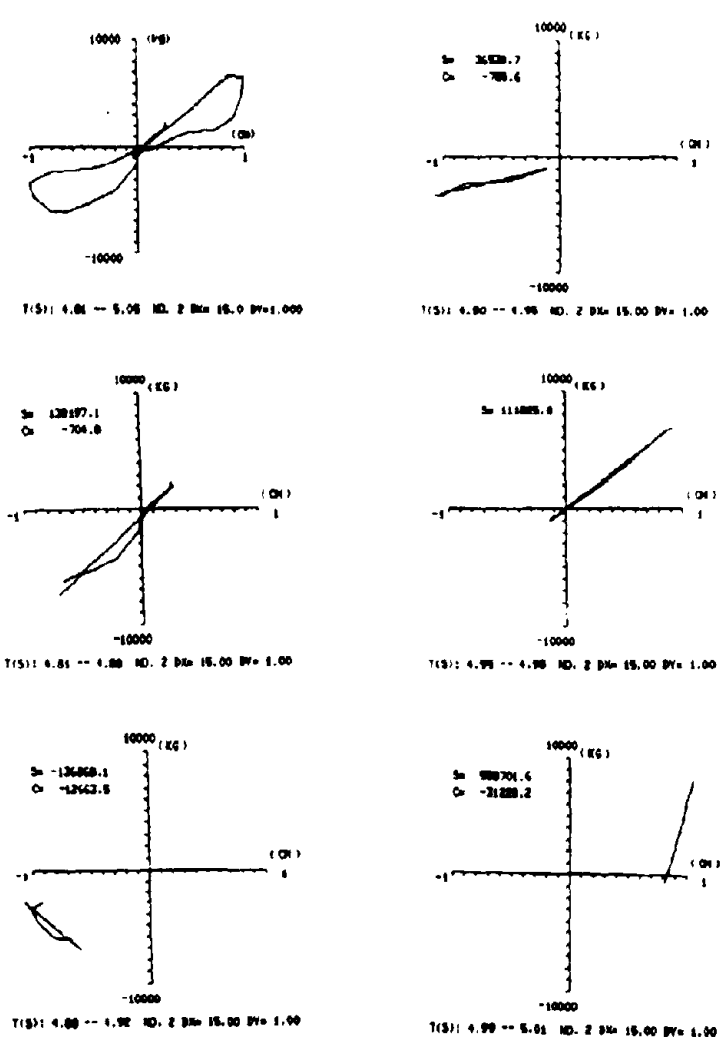


Fig.4.3-2 Maximum restive displacement segment for 2nd story

APPLICATION OF CURVE FITTING METHODS IN CONSTRUCTIONAL ENGINEERING DYNAMIC PARAMETER IDENTIFICATION

Liu Lihua*

ABSTRACT

In this paper, the theory of curve fitting by fitting circle and transfer function methods have been reviewed. Relevant methods of curve fitting in modal parameter identification are also described. Examples based on the testing data for suspended cable structures and grain storage silos are presented. Fundamental dynamic parameter for frequency, modal shape and damping are obtained for earthquake resistance analysis. Advantages, disadvantages and applicational range of the curve fitting methods are also pointed out.

I. INTRODUCTION

In order to design aseismic structures for optimal performance, we must solve the problem of dynamic behaviour of structures. Since the development of electronic technique, there appear installations of structural response measurements, providing the solution of many structural dynamic problems. The measurement of frequency response is the heart of structural analysis. The frequency response, $H(\omega)$, is defined in terms of the single input/single output system (shown in Fig. 1) as the ratio of the Fourier transform of the system output, $y(t)$, to the Fourier transform of the system input, $x(t)$.

$$H(\omega) = \frac{Y(\omega)}{X(\omega)}$$

where

$Y(\omega)$ is the Fourier transform of system output, $y(t)$;
 $X(\omega)$ is the Fourier transform of system input, $x(t)$.

The frequency response function otherwise called the transfer function is a complex quantity. That is, it has been associated with both magnitude and phase as its real and imaginary part. To adopt Digital Signal Analyzer or Structural Dynamic Analyzer, we utilize sampled data techniques to perform power spectrum and transfer function analysis. Through modal parameter identification, we can obtain the dynamic behaviour of structures.

In model parameter identification technique, we can use different

*Laboratory of the Institute of Earthquake Engineering, China Academy of Building Research.

forming formulae of transfer function, correspondingly, we can draw different forming curves. Specific formula of transfer function can be selected in accordance with testing scheme, data format and desired dynamic parameters of structures.

In this paper, curve fitting method has been presented by means of formula with real and imaginary parts in the form of complex polynomials of the transfer function. Curve fitting methods are effective in structural modal parameter identification. It is the application of weight residual method in hardware equipment.

II. FOUNDATION OF THE THEORY

We can use the frequency response function obtained from Structural Dynamic Analyzer or Digital Signal Analyzer in structural response measurements for the determination of frequency, modal shapes and damping of the system measured, that is, for the determination of modal parameters of the system measured.

Process of curve fitting can be carried out between curve of frequency response function from testing and curve of response function of theoretical regeneration. It is by so doing that reliability of dynamic parameters of structures can be advanced.

Transfer function of system can be written as follows[1][2]:

$$H(s) = \sum_{k=1}^{2n} \frac{a_k}{s - p_k}$$

where

- n is number of degrees of freedom;
- p_k is root of determinant of $B(s)$ matrix;
- $B(s)$ is system matrix;
- a_k is residue of k th root.

p_k can be called pole of transfer function. The pole p_k is complex and pole p_k^* is its conjugate. It can be written as follows:

$$p_k = -\sigma_k + j\omega_k$$

$$p_k^* = -\sigma_k - j\omega_k$$

where

- σ_k is coefficient of modal damping;
- ω_k is the natural frequency.

Relationship between σ_k and ω_k can be represented by graphics.

According to the symmetry of the transfer matrix, the residue of any row or column of $H(s)$ matrix is used to determine the natural frequency, modal shape and damping of the system. For single modal of system, the transfer function can be written as follows:

$$H_k(s) = \frac{A_k}{s-p_k} + \frac{A_k^*}{s-p_k^*}$$

where

A_k is $N \times N$ complex matrix;
 p_k is pole of k th modal.

Components of $H(s)$ can be written as follows[3][4]:

$$H(s) = \frac{r_k}{2j(s-p_k)} - \frac{r_k^*}{2j(s-p_k^*)}$$

where

s is laplace argument, $p_k = \sigma_k + j\omega_k$, σ_k being coefficient of damping, ω_k being the natural frequency, r_k being the residue and $r_k/2j$ being the complex residue of k th model.

To use curve of real and imaginary parts of transfer function, for the determination of natural frequency of structures, after having obtained the natural frequency, estimate the damping of the structures by curve fitting methods. In curve fitting process, calculate k th value of residue, and then calculate coefficient of the modal shape.

In order to minimize mathematically the error between measured curve and fitting curve, we usually adopt the least square method. The Hp-5423A Structural Dynamic Analyzer uses the formula as follows[5]:

$$E = \sum_{i=1}^n |h_i - H(j\omega_i)|^2$$

where

h_i are values of measurable data;
 $H(j\omega_i)$ are the fitting function of frequency.

III. ENGINEERING EXAMPLES

We apply Hp-5423A to utilize sampled data techniques to perform a wide variety of single and dual channel measurements which include time record average, auto and cross spectrum, impulse response, and frequency response. We can perform a wide variety of analysis for the dynamical features of building structures, and supply dynamical parameters of engineering design, for obtaining the dynamic parameter identification of

Various model structures.

(1) Dynamic parameter identification of suspended cable structural model.

For the suspended cable structural model as shown in Fig. 2, it consists of 5 beams and 7 cables, when model testing, by using of the hammer method. 3 response points were measured through 35 points of hammer points of the system. In Fig. 2, symbol Δ represent response points, that is, positions of the installation of velocity transducers by multi-point measurement and single-point excitation. Adopt transfer function fitting method, when it is going to perform measured data analysis. The steps for the process are as follows:

1. To determine frequency of structural model by transfer function fitting method.

In a light modal coupling case, the measurement data in the vicinity of a modal resonance peak is predominantly due to that mode, and the influence of the other modes is negligible. In this case, a single modal curve fitting method can give accurate results of the frequencies of the model structures.

In a heavy modal coupling case, the influence of the tails of other modes is not negligible, so a single modal method cannot correctly identify the modal parameters. In order to improve the accuracy of modal parameter identification, we still need to perform the analysis of auto spectrum and real and imaginary frequency curve of the transfer function, to help the exact finding frequency values of structural modes.

By the above mentioned steps, in order to determine the frequency values of suspended cable structural model, we find three peaks from Fig. 3, then we can use the x cursor to find the frequency values of the three peaks. Then we should perform statistical estimation algorithms, which will use large amounts of measurement data, we should also estimate the modal parameters, through comparison and synthesis to finally determine the frequency values of the model structure as shown in Table 1.

2. To estimate damping of model structure by transfer function fitting method.

After having determined the frequency values of model structure, we need to replicate selected fitting bandwidth and then to perform replicated fitting of measured transfer function curve by regeneration theory of transfer function curve. That is, when two transfer function curves overlap, they must satisfy the minimized error condition. At this moment, we can obtain the damping values and estimated mode value of the model structure as shown in Table 1.

Practical examples demonstrate that, the conditions and the variety of range of application for transfer function are better as compared with fitting circle method. Higher modal shapes can be identified by the transfer function method, but only single degree of freedom or light coupling modal of multi-degree of freedom can be used by the fitting circle method.

IV. CONCLUSION

Examples of engineering testing data analysis have proved that the curve fitting method is quite useful in modal parameter identification of structural dynamic analysis. Advantages, disadvantages, feature and range of application by different curve fitting methods are also given in the paper.

Our conclusion can be summarized as follows:

1. Fitting circle method is useful for single degree of freedom system. According to phase response directly obtained from measurements, the feature of resonant peak is in the neighbourhood of the frequency response function.

2. Effects of structural nonlinearity can be neglected in modal parameter identification.

3. Disadvantages of the fitting circle method are as follows:

- (1) The condition of using the fitting circle method is relatively strict. It can be applied only for parameter identification of a single degree of freedom system.

- (2) In terms of graphical procedure for the determination of modal parameters, the calculation accuracy depends upon the graphical accuracy.

- (3) Error will be increased, when there happens modal shapes coupling in the system.

4. Advantages of the transfer function curve fitting method are as follows:

- (1) Range of application can be widened to multi-degree of freedom system for modal parameter identification, besides single degree of freedom system. From the inherent conditions of supposition view point, it can reduce the requirement for using the transfer function as compared with that of the fitting circle method.

- (2) Improvement the accuracy of the modal parameter identification

3. To calculate coefficients of the modal shapes by transfer function fitting method

After determining the frequency and damping of the modal structure, we can use the residue of curve fitting process to determine the coefficients of the modal shapes. We can find the transfer function curves of measured and theoretical regeneration in Fig. 4, the transfer function fitting curve in Fig. 5 and the three modes of suspended cable structural model in Figure 6,7,8.

(2) Dynamic parameter identification for plexiglass model of the grain storage silo

The sketch of the plexiglass model of the grain storage silo is shown in Fig. 9. The height and diameter of the prototype model for the grain storage silo are 38.0 M and 8.7 M. The ratio between model and prototype model is 1:28. The height and diameter of model for plexiglass are respectively 1.38 M and 0.31 M. Testing methods of the model consist of hammer, shaker and traction-release. Zero, half and full loading can be performed respectively for testing. In this paper, for zero loading testing results of model under hammer for a single grain storage silo are presented. To perform dynamic parameter identification for a single silo model under zero loading, use curve fitting methods of transfer function and fitting circle. We can identify dynamic parameter of first two modal shapes only fitting circle method is to be used. The result of the first mode obtained by transfer function is compared with that by the fitting circle method. The specific steps are described as follows:

1. Identify dynamic parameter by transfer function fitting method

Transfer function curve from measured data of model is shown in Fig. 10. Theoretical regenerated transfer function curve is shown in Fig. 11. The fitting curve of the above mentioned transfer function is shown in Fig. 12. Because there is no coupling of frequencies at some peaks, therefore frequency, damping and modal shapes can be determined respectively as shown in Fig. 10 and Table 2.

2. Identify dynamic parameter by fitting circle for grain storage silo of plexiglass model

Fitting circle from measured data and theoretical regeneration curve are shown in Fig. 13. The graphic representation of the transfer function and the fitting circle are shown in Fig. 14. Frequencies and damping obtained of models through fitting circle method are shown in Table 2. The graphic representation of modal shapes is given in Fig. 18, solid line and dotted line represent respectively the results obtained by the transfer function and by the fitting circle method. The modes of model structures are shown in Fig. 15,16,17.

as compared with that of the fitting circle method.

Based upon the above mentioned facts, it is to be noted that for increasing the precision of the method, we should.

First determine the fitting circle, then evaluate the modal parameter by the graphic method. In order to find the natural frequency from centre of circle to resonant peaks in the circumference, draw lines in sequence and record the angles between two radii to determine the ratio of the change in arc, that is, to determine the natural frequency for the position of the maximum ratio of change in arc. Accuracy of natural frequency must be controlled within 10% of increment of frequency between data points.

Estimate damping by fitting circle method, calculate values of damping and then recalculate the average of the average values. In theory, for the case of heavy damping, it is required that the average values should be close to each other.

Calculation of the modal parameters by transfer function with measurements, using the displacement and acceleration transducers, to determine the frequencies. We can also use the imaginary part of the transfer function to determine the frequencies.

By selecting the appropriate bandwidth, we can directly determine the error of damping estimation and find the accuracy of the frequencies. If the points by the curve of modal shape from transfer function of measurement and the points by the curve of theoretical regeneration of transfer function coincide with each other, then excellent damping estimation and coefficient of modal shape can be realized.

The testing modal analysis technique comes from the basic theory of random vibration. To perform data process, we need to synthesize the analysis of some statistical parameter, such as natural frequency, auto-power-spectrum and coherent analysis. Furthermore, we can also use the real frequency curve and imaginary frequency curve to determine the natural frequencies. For the calculation of errors, we can use the optional consistent estimation error method. Practical engineering demonstrates that curve fitting method plays an important role in testing modal analysis technique. We can see in future wide application of the curve fitting method in many fields.

REFERENCES

- [1] Ramsey, K.A., "Effective Measurements of Structural Dynamics Testing," Sound and Vibration Magazine, Part I, Nov. 1975, pp. 24-25, Part II, April, 1976, pp. 18-31.

- [2] Halvorsen, W.G. and Brown, D.L., "Impulse Technique for Structural Frequency Response Testing", Sound and Vibration Magazine, Vol. 11, No. 11, November, 1977.
- [3] NATKE, H.G., "Identification of Vibrating Structures", pp. 162-167, pp. 170-175, 1982.
- [4] EWINS, D.J., "Modal Testing: Theory and Practice", 1984.
- [5] 5423A Structural Dynamics Analyzer, Use's Guide Introduction to Operation Vol. 1, HEWLETT PACKARD, 1979.

Table 1. Frequency and Damping of Model Structure

Parameter Mode Shapes	Frequency (HZ)	Damping
First Mode	4.26	0.81
Second Mode	4.57	1.21
Third Mode	5.32	1.28

Table 2. Frequency and Damping of Model

Method Parameter Mode Shape	Frequency (HZ)		Damping Ratio	
	1-Mode	2-Mode	1-Mode	2-Mode
Transfer Function	37.0	132.82	6.19	4.94
Fitting Circle	37.0	—	5.41	—

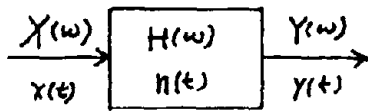


Fig. 1 Single Input/Single Output System

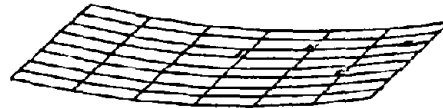


Fig. 2 Suspended Cable Structural Model

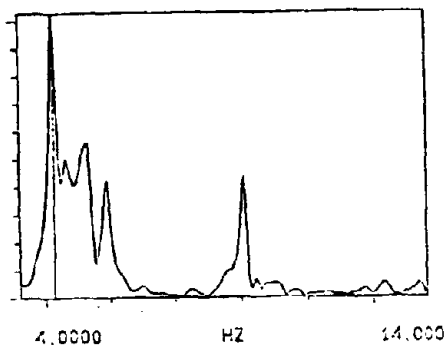


Fig. 3 Transfer Function Curve from Measured Data

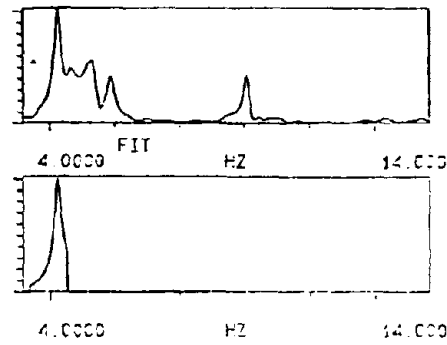


Fig. 4 Transfer Function Curves of Measured Date and Theoretical Regeneration

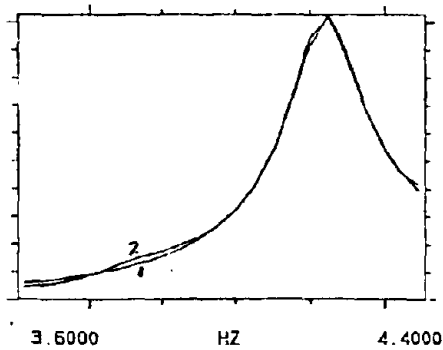


Fig. 5 Transfer Function Fitting Curve

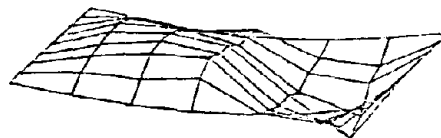


Fig. 6 First Mode of Suspended Cable Model

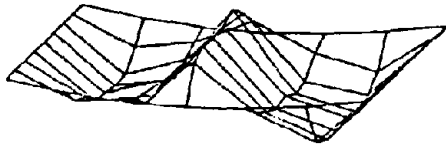


Fig. 7 Second Mode of Suspended Cable Model



Fig. 8 Third Mode of Suspended Cable Model

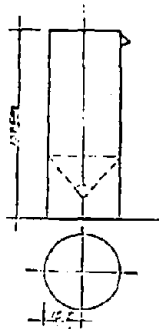


Fig. 9 Grain Storage Silo

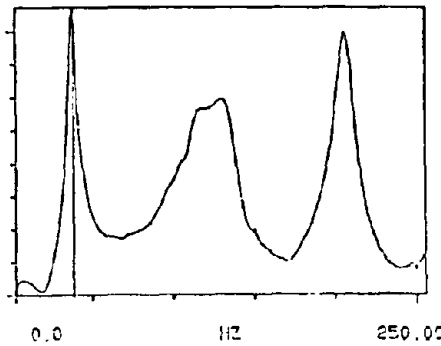


Fig. 10 Transfer Function Curve of Grain Storage Silo Model

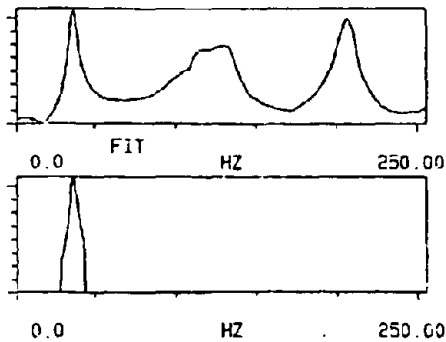


Fig. 11 Transfer Function from Measured Data and Theoretical Regeneration for Grain Storage Silo Model

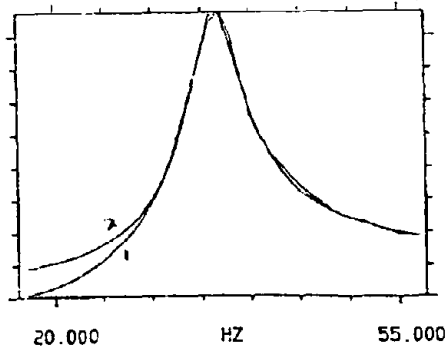


Fig. 12 Fitting Curve of Transfer Function Between Measured Data and Theoretical Regeneration

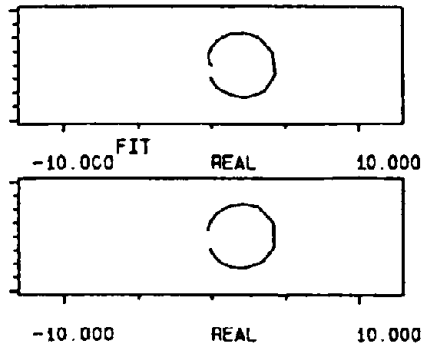


Fig. 13 Fitting Circle of Measured (upper) and Theoretical Regeneration (bottom)

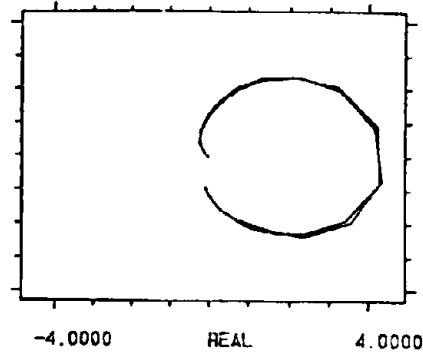


Fig. 14 Fitting Curves of Measured Data and Theoretical Regeneration

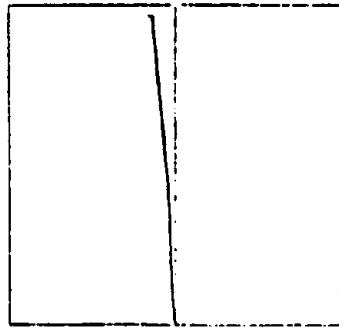


Fig. 15 First Mode by Transfer Function Curve Fitting Method

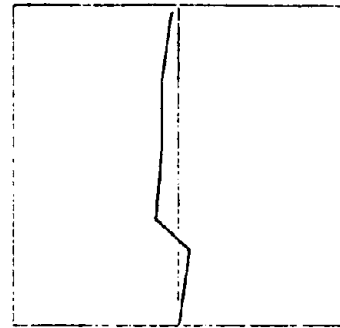


Fig. 16 Second Mode by Transfer Function Curve Fitting Method



Fig. 17 First Mode by Fitting Circle Method

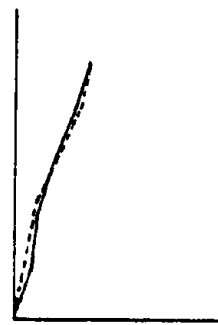


Fig. 18 Comparison of First Mode with that by Transfer Function and Fitting Circle Method